CRANFIELD INSTITUTE OF TECHNOLOGY

SCHOOL OF INDUSTRIAL AND MANUFACTURING SCIENCE

PhD THESIS

Academic Year 1991

C P SHAW

Polymeric Materials for Piezoelectricity and Second Harmonic Generation

Supervisor: Professor H.Block

September 1991

ABSTRACT

Studies have been undertaken to utilise the possible potential of the rodlike, helical structures associated with polyglutamates and polyisocyanates for piezoelectric (PE) and nonlinear optical (second harmonic generation (SHG)) applications.

Various techniques have been employed to form samples/films of these polymers containing oriented helices whose bulk structures are non-centrosymmetric, (an important criterium for the aforementioned applications).

Owing to the poor yields obtained for certain intermediates in the synthetic stages of these polymers, only poly(ɣ-benzyl-L-glutamate) (PBzLG) and poly(n-hexylisocyanate) (PHIC) were available for subsequent studies.

Piezoelectric work was limited to hydrostatic measurements (d_{3h}) made on electrically poled, composite (guest host), polymer samples. Phase separation was common in all the samples, but no piezoelectric response was observed. However, low concentration (not greater than 10% w/w) of active polymer (PBzLG or PHIC) and high conductivity during the poling stage, may have accounted for the lack of response.

Electrically poled, homopolymer samples of PBzLG and PHIC were achieved using a solvent evaporation technique. Nonlinear optical studies of these poled samples revealed threshold fields above which detectable levels of SHG could be observed, (i.e. PBzLG > 40 V/mm, PHIC > 150 V/mm). The

variation of SHG signal versus the angle of polarisation of the incident laser light (1064 nm) relative to the poling direction of the film, implied biaxial symmetry was present in the case of PBzLG, whereas the more conventional uniaxial symmetry was observed for PHIC. The variation in SHG signal observed for a fixed thickness was attributed to varying degrees of alignment, resulting from uneven poling.

Although PHIC and PBzLG showed low SHG activity (less than value for urea), little ageing of this activity occurred over the 6 month testing period.

Langmuir Blodgett studies carried out on chemically modified, low molecular weight PBzLG molecules showed poor transference of the monolayer to a quartz substrate once ten layers had been deposited. In addition, areas per molecule (or per residue) calculated from the pressure-area isotherms, proved inconclusive when deducing possible orientations for the PBzLG helices. No SHG signal was observed for the L.B. films.

Acknowledgement

I would like to thank Professor H. Block for all his help over the years, and I would like to thank him and Mr. C.I Pope for allowing me access to computer facilities for the production of this thesis. I would also like to thank SERC and the institute for funding the work.

Finally, love to Amanda for her patience and support.

CONTENTS

CONTENTS

FIGURES

NOTATION

PBzLG	poly(γ-benzyl-L-glutamate)
PHIC	poly(hexylisocyanate)
PBuLG	poly(n-butyl-L-glutamate)
γ-BzLG	γ-benzyl-L-glutamate
HMW	high molecular weight
LMW	low molecular weight
SHG	second harmonic generation
PE	piezoelectricity
L.B.	Langmuir Blodgett
M.W.	molecular weight
β	second order hyperpolarisability
n	refractive index
σ	stress
d_{ij}	piezoelectric or SHG coefficient
π_c	isotherm collapse pressure
A_o	area per molecule at zero pressure

INTRODUCTION

In general, the main physical requirement for materials to show piezoelectricity (PE) or second harmonic generating (SHG) effects, is their lack of symmetry at a molecular level. It is well documented (Atkins (1982)), that according to crystallography there exists 32 crystal classes among which, 20 classes are piezoelectric. Such non-symmetry, in inorganic PE and SHG crystals is illustrated by materials such as potassium dihydrogen phosphate (KDP), potassium titanium phosphate (KTP) and lithium niobate (Hon (1979)). In such cases, the non-symmetry is inherent in the way the molecules arrange themselves as they crystallise/form. No external alignment processing is required, although certain special conditions are needed to grow large defect free crystals.

Having understood the origins of the SHG, the organic chemist has set about designing molecules which in theory should show large nonlinear coefficients, e.g. asymmetric molecules involving strongly delocalised π-electronic systems. However, it is often found that the measured values of the coefficients of the bulk material are small, if not zero, the problem being that the crystal structure of the newly designed molecule is centrosymmetric. To overcome this problem, the next stage is usually a slight chemical modification to the molecule's structure, so that a non-centrosymmetric crystal structure is possibly generated, (i.e. 4-nitroaniline forms a centrosymmetric crystal, and a non-centrosymmetric structure is achieved by

forming the 2-methyl-4-aniline derivative).

The technique known as electric field induced second harmonic (EFISH) generation (Bethea (1975)), which is used to measure SHG of molecules in solution, highlights another approach to overcome the problem of centrosymmetry. This technique disturbs the random centrosymmetric arrangement of a solution by applying a pulse of electric field, allowing a measure of SHG efficiency to be made before the molecules relax to their centrosymmetric equilibrium state.

For the work carried out in this project, various physical/mechanical techniques of alignment have been employed to hopefully impose non-centrosymmetric structures in certain polymeric systems. In general, there have been three main stages to this approach.

1. As in the case of EFISH, a suitable solvent has been required for the polymer in question, to produce a system with free mobility (rotation, and translation) of the polymer molecules. Hence, an understanding of the properties of the polymer in solution (e.g. conformation, phase changes), was important.
2. Various alignment techniques were then tried to orientate the free-system, which can be summarised as follows:-

a) electric field;

b) magnetic field;

c) Langmuir film compression;

d) liquid crystal alignment;

e) mechanical alignment;

3. Unlike EFISH, the last stage involves moving from a solution state to a solid polymer film/disc, but maintaining the state of alignment within the film. The following categories summarise the various methods used to achieve this:-

a) polymerisation of solvent (vinyl monomer solvent);

b) evaporation of solvent (film casting);

c) Langmuir Blodgettry.

Note: in all these methods, the alignment force is maintained during the third stage.

CHAPTER 1

ACTIVE POLYMERS

As far as this work is concerned, two different classes of polymer have been studied, i.e. poly(glutamates) and Poly(alkylisocyanates). In the main, poly(γ-benzyl-L-glutamate) (PBzLG) and poly(hexylisocyanate) (PHIC) have been looked at owing to their ease of preparation and their ideal solution properties, although certain chemical modifications of PBzLG were attempted when required.

In common between these two classes of polymers is the long range order within the polymer chains which can exist in solution and the solid state. When such order exists, the molecules are often described as rodlike, because they form in a helical structure as illustrated by figure 1.1. It is this structure and the associated orientation of dipoles within the helix that are the main hope for them to show both PE and SHG.

1.1 PBzLG

1.1.1 Introduction

The general chemical formula for poly(α-amino acids) can be represented as follows:-

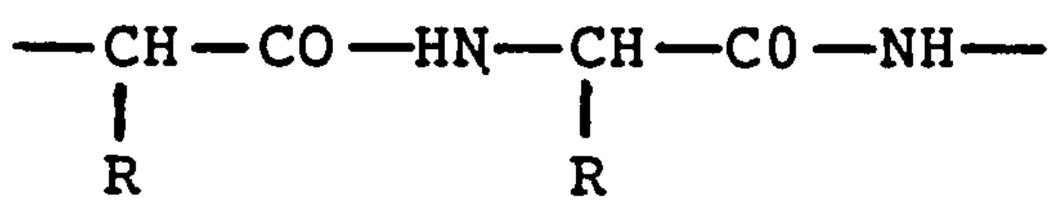

Block (1983) gives a comprehensive list of the derivatives associated with the various R groups.

For the specific case of PBzLG, the R group is -$(CH_2)_2$-CO_2-CH_2-Ph having been derived from the γ-benzyl-L-

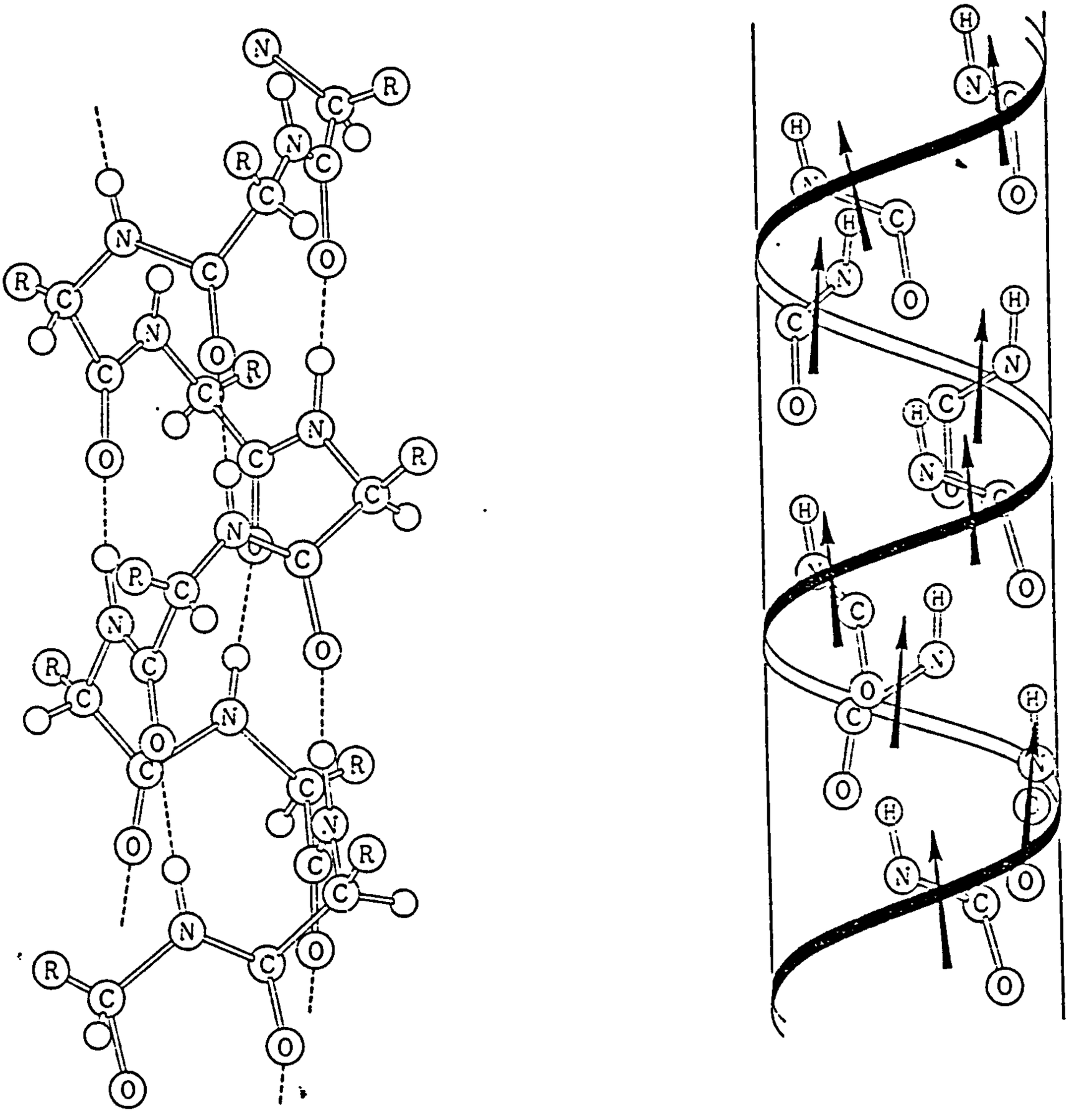

Figure 1.1 α-helix and associated main chain dipole moments.

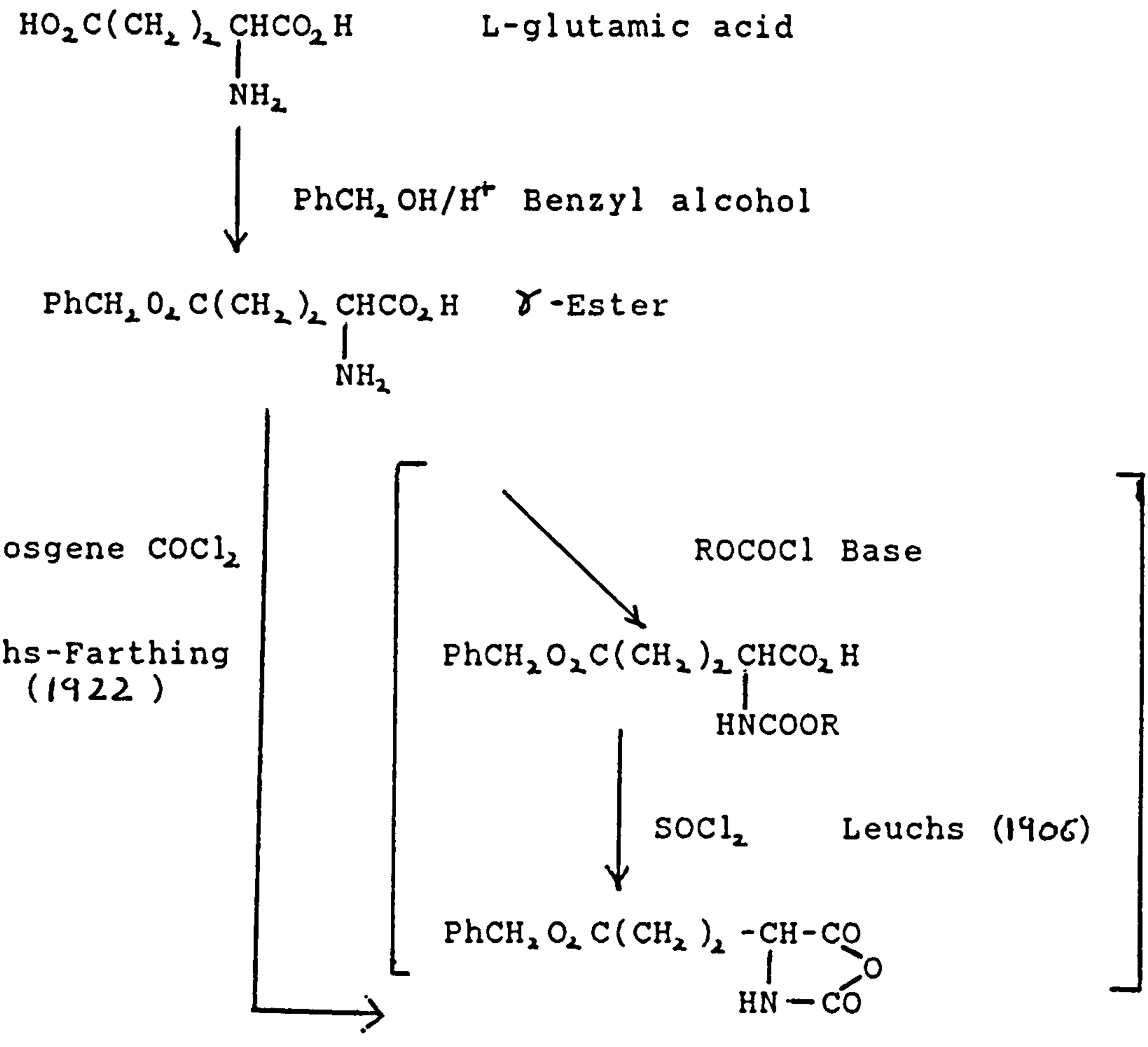

Polymerisation Step :

$$\delta\text{-benzyl NCA} \xrightarrow{\text{initiator}} \text{PBzLG}$$

Figure 1.2 Synthetic route for PBzLG.

glutamate. L-glutamic acid which is the parent acid of the γ-benzyl ester is made industrially as a food additive in the well known form of monosodium glutamate. It is therefore cheap and readily available, making the most easily manufactured polyglutamate PBzLG, readily available too.

1.1.2 Synthesis

Figure 1.2 shows the general scheme for the conversion of L-glutamic acid to PBzLG. Of the two routes shown for the conversion of ester to NCA, the Fuchs-Farthing method (Fuchs (1922)) is favoured as side products are readily removed.

Polymerisation and Initiators

The polymerisation step is usually performed in solution using base initiation, (in particular, primary, secondary or tertiary amines). Work in understanding the polymerisation mechanism of NCA is covered in reviews by Bamford and Block (1972; 1976), but an outline of the mechanism and the complicating side reactions for NCAs based on L-glutamic esters now follows.

Figure 1.3 shows the desired initiation step for primary and secondary amines where the NCA is effectively acting as an acylating agent. For L-glutamic ester based NCAs, acylation occurs at position 5 with little or no complication of reaction at position 2. The product (I) then acts as the amine in the next propagation steps. This mechanism is referred to as the primary amine or protic mechanism.

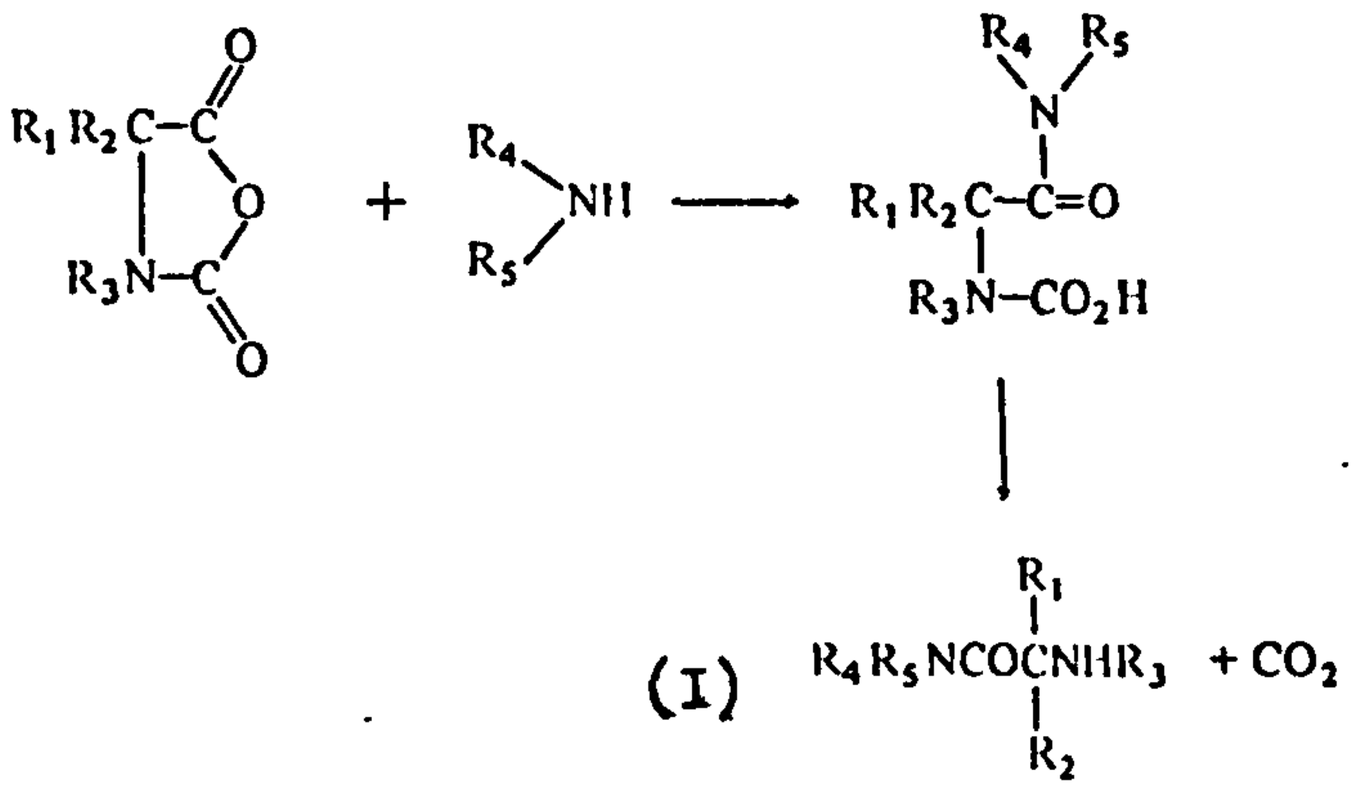

(I)

Figure 1.3 Protic Mechanism.

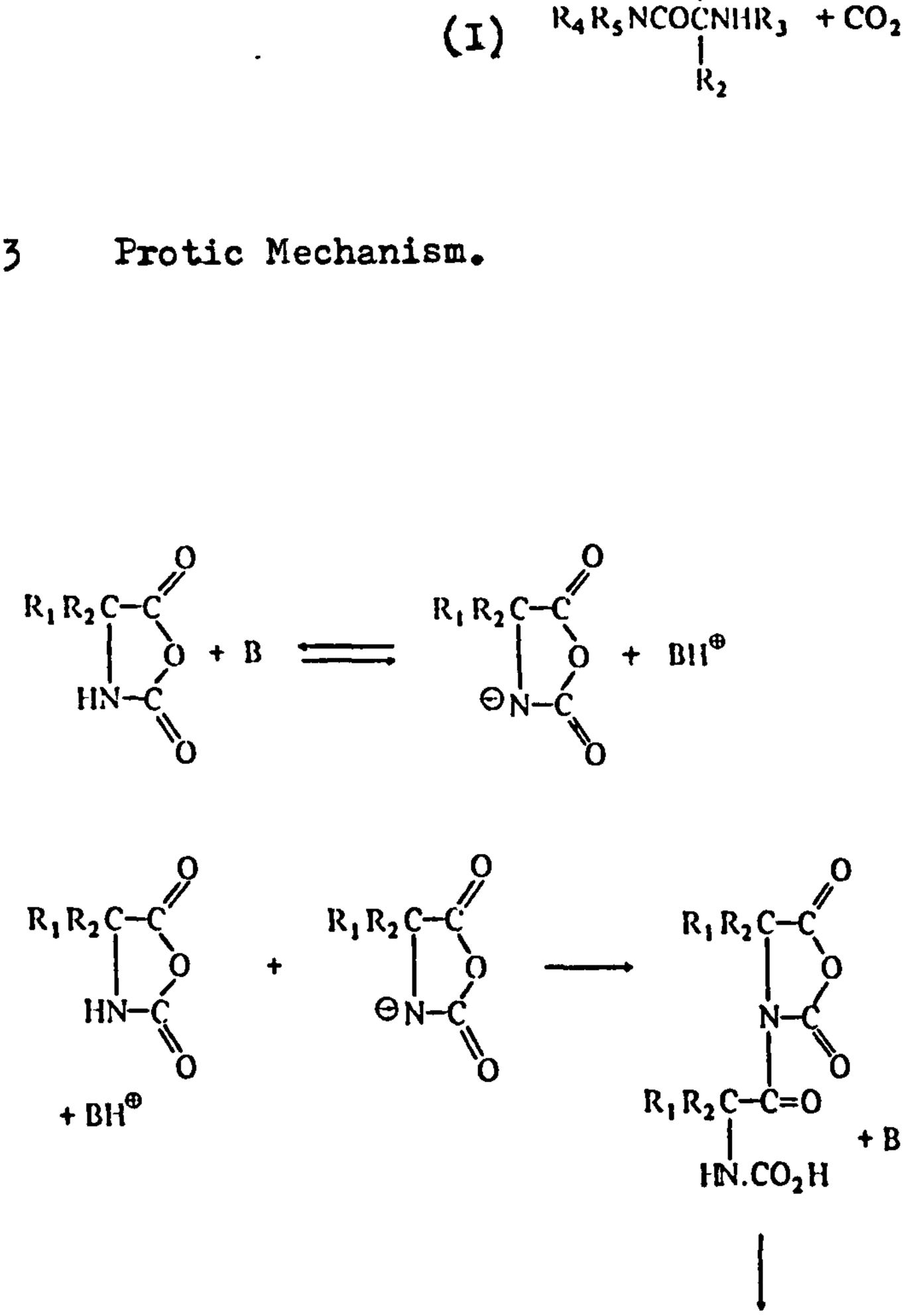

(II)

Figure 1.4 Aprotic Mechanism.

The number average degree of polymerisation <Pn> for this type of reaction can be given by:-

$$<Pn> = [M]_o / [I]_o \qquad (1.i)$$

if $[M]_o$ and $[I]_o$ are the initial NCA and initiator concentrations. This equation holds if the rate of the reaction scheme in figure 1.3 is equal to or greater than the rate of the subsequent propagation steps and there are no side reactions.

Unfortunately, amines can act as general bases, and if $R_3 = H$, an aprotic mechanism may result as well as the protic mechanism.

Figure 1.4 (Block (1983)) shows the aprotic mechanism, resulting in product (II) which is itself bifunctional (NCA ring and primary amine) and hence open to further propagation by either mechanism. When both mechanisms occur, <Pn> becomes greater than the expected $[M]_o/[I]_o$ value, and may be bimodal (two widely separated molecular weight distributions), if a primary or secondary amine is used.

Controlled low molecular weights are best achieved using primary amines with low basicity such as n-alkyl amines, to favour the protic mechanism.

High molecular weights are favoured by the use of aprotic initiators (tertiary amines), in dry conditions (water and impurities prevent polymerisation to high M.W.). In particular, ageing of the polymerisation can greatly improve the molecular weight (Peggion (1966)), as can

purification of the NCA by removal of trace acid chloride or HCl (produced by the phosgene reaction).

Kinetic investigations of the polymerisation have been studied (Williams et al. (1971), Bamford and Block (1962)), and have shown how certain solvents effect the rate of reaction. Explanation of the effects have been accounted for by either phase separation (Williams et al. (1971)), or changes of conformation in the growing polymer chain (Bamford and Block (1962)), as it reaches a certain length.

1.1.3 Alternative Synthetic Aspects

Having just described the synthetic route for PBzLG in some detail, a number of other reactions are now described which have been shown to be useful for producing either other glutamate esters (which can be used to produce other poly(glutamates)) or side chain modifications in PBzLG itself. In either case, the examples are given as they relate to reactions that were subsequently attempted in the experimental section of this work.

The synthesis of γ-BzLG given in figure 1.2, involves a direct esterification of L-glutamic acid, and as far as the benzyl derivative is concerned, leads to reasonable yields of product. Unfortunately for other γ-esters, a combination of poor yields and di-ester formation (due to the forcing conditions) make the isolation of the γ-ester difficult.

Figure 1.5 shows an alternative route to prevent di-ester formation which uses a copper(II) glutamate complex

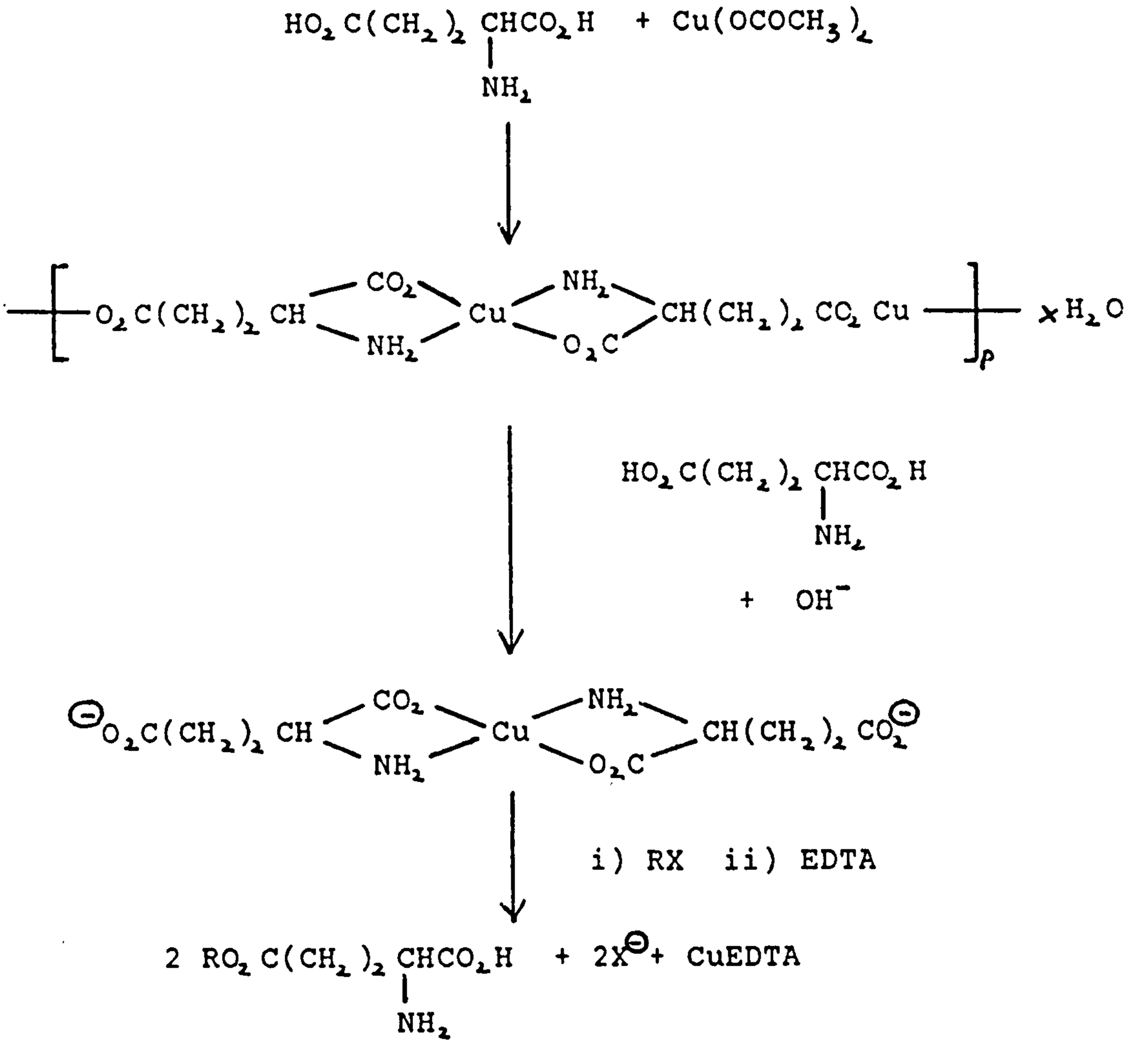

Figure 1.5 Synthesis of γ-esters via Cu(II) complex.

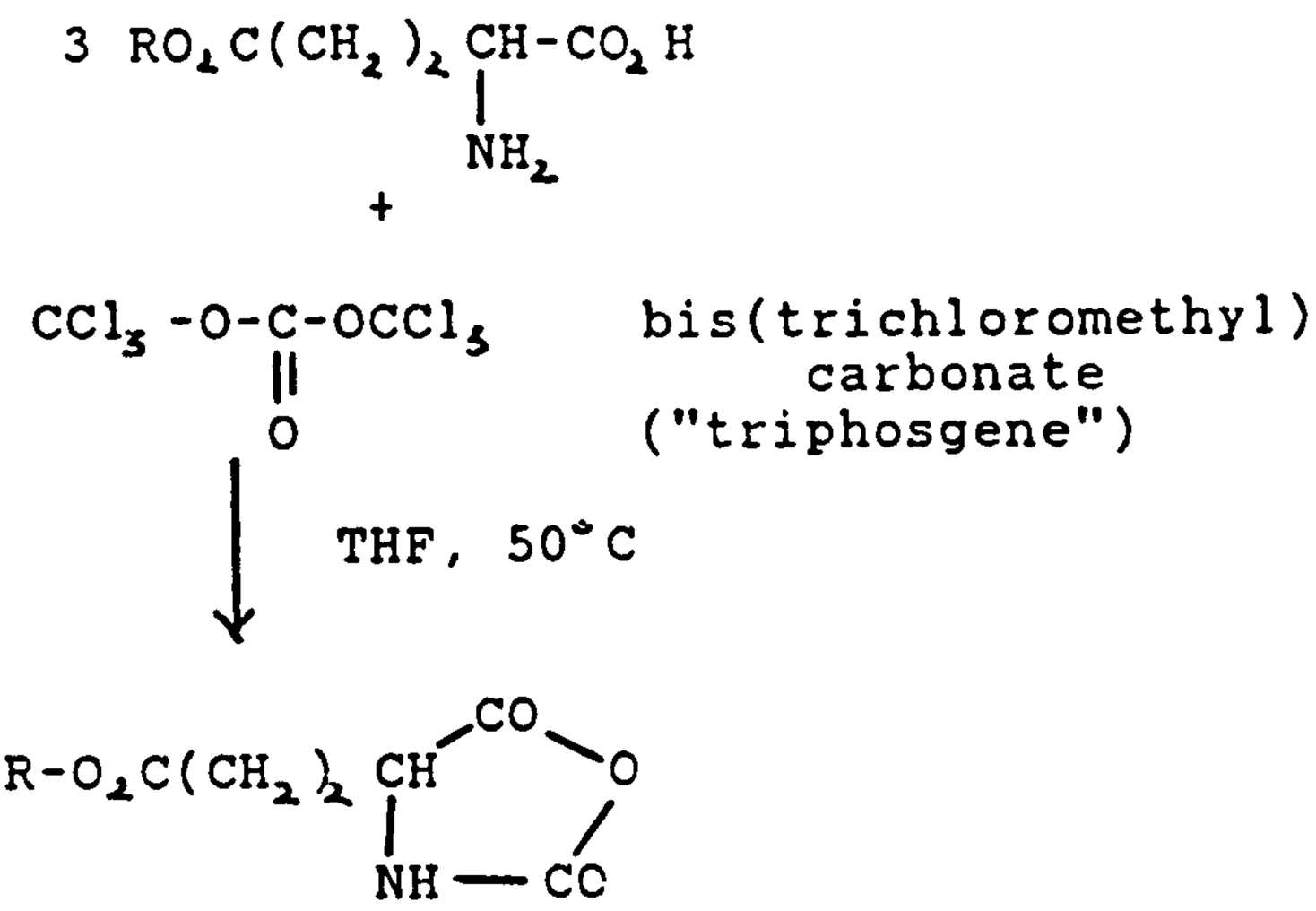

Figure 1.6 Synthesis of NCA using "triphosgene".

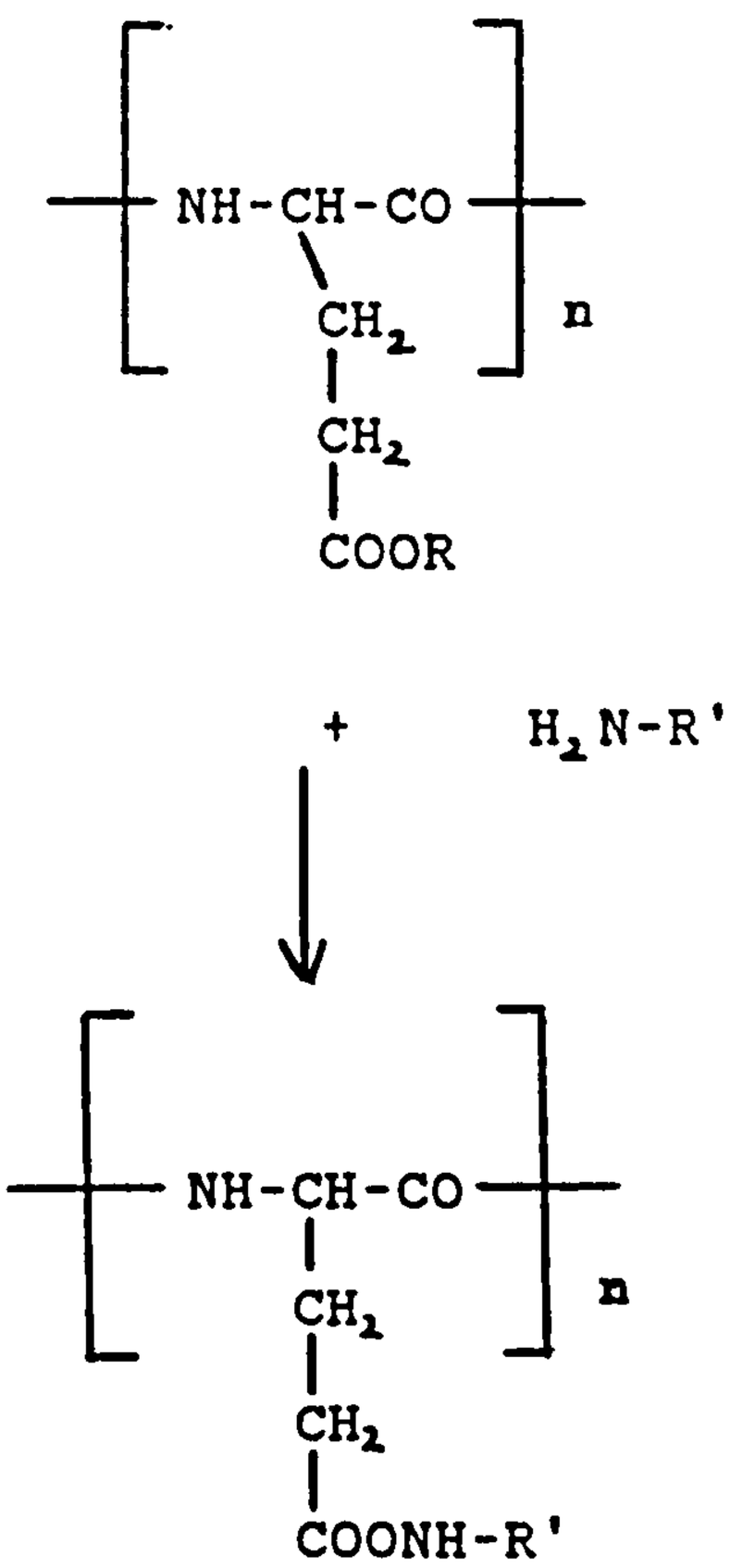

Figure 1.7 Side chain modification of polyglutamate using an amine.

intermediate. At the heart of the reaction, the complexing of the Cu atom to one end of the glutamic acid protects that end from alkylation on the addition of the alkyl halide. Hence, the subsequent addition of the strongly complexing EDTA to release the product results in γ-ester only. The paper by van Heeswijk et al. (1982) covers some synthetic aspects of this reaction.

Figure 1.6 shows a possible alternative to the use of the toxic phosgene gas in the synthesis of NCA, previously described in figure 1.2. The use of bis(trichloromethyl) carbonate ("triphosgene") as a substitute to phosgene is described in the paper by Daly and Poche (1988). As a white solid (m.p 80°C), it promises to be easier to handle than gaseous phosgene and can be added to a reaction in weighed controlled amounts which helps to reduce any side reactions from the presence of excess gas. It is also soluble in typical recrystallisation solvents for the NCAs (i.e. THF or hexane), so any residual triphosgene can be removed by recrystallisation of the product.

The paper gives a number of products that have been synthesized using triphosgene which include the benzyl and stearyl NCA derivatives.

Figure 1.7 shows one aspect of side chain modification of polyglutamates using reagents with amino functionality, with the intended end product being the γ-amide or substituted γ-amide of poly(α-glutamic acid). An idea of the types of amino reagents used in this reaction are covered in a number of papers. In the most simple cases,

poly(γ-glutamine) has been made by reaction with ammonia or the appropriate amine (Bruckner et al. (1953); Kotai (1967)). In these cases, the only possible complication has been trans-amidation with the peptide links of the polymer backbone, which may lead to some reduction in molecular weight. In the case of more exotic reagents, amino alcohols have been used (Vanwart et al. (1973), Hill et al. (19770)) to prepare water soluble polymers which provide polypeptide analogues of proteins for conformational studies in aqueous environments.

1.1.4 Conformational Forms

Figure 1.1 shows only one of the three main forms in which PBzLG may exist and is the same structure as proposed for proteins by Pauling and Corey (1951).

The helical structure is maintained by intramolecular hydrogen bonding, and may exist in both solution and the solid state. The spiral pitch is approximately 0.54 nm, with about 3.6 monomer units per turn.

The polymer chains of PBzLG have been formed from chiral monomer residues, i.e. L-enantiomers. This produces a right-handed spiral pitch to the helix, which would be destroyed if a racemic mixture of monomer enantiomers was used.

In contrast to the α-helical structure, figure 1.8 shows the second conformational structure, the β-pleated sheet form. This structure is only found in the solid state, and intermolecular H-bonding is shown to be

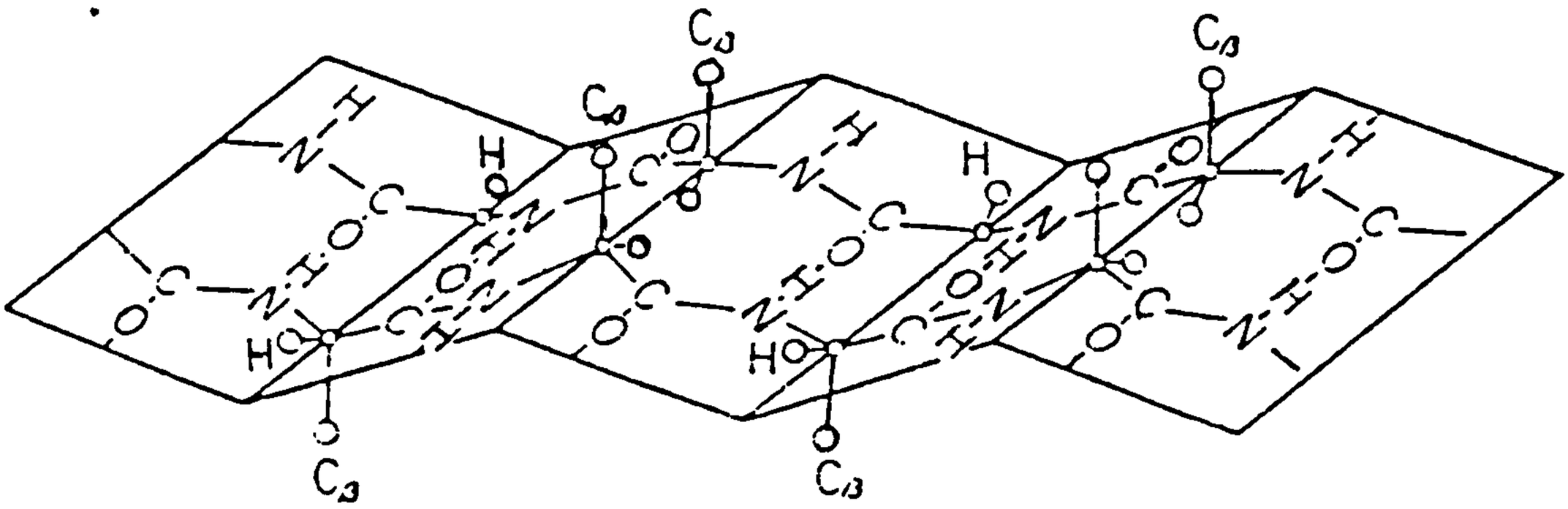

Figure 1.8 β-conformation of polyglutamates.

important. This structure is also only found with low molecular weight polymer, and often co-exists with the α-form. The extent of the β-form depends on which solvent has been used to cast the film in the first place. If needs be, the β-form structure is better observed by using poly(γ-methyl-L-glutamate) (Kujijama et al. (1973)).

Energetic studies (Scheraga et al. (1967); Nemethy and Scheraga (1965)) of PBzLG have confirmed the α-helix to be the lowest energy state, but the stability of the structure in the case of solution, is highly dependent on the solvent. Instability in the structure can cause a helix-to-random coil transition, which is the third conformational form of PBzLG and which is common to all polymers.

The solvents for PBzLG are usually categorised into two groups. Those that support the α-helical conformation are referred to as helicogenic solvents and include, chloroform, dichloroethane (DCE), dichloromethane (DCM), dioxane, THF and DMF. Those that allow a random coil structure to exist in solution are called random coil solvents and include, dichloroacetic acid (DCA) and trifluoroacetic acid (TFA).

The nature of the side groups certainly dictates the type of solvent that will dissolve the polymer. Poly (-n-dodecyl-L-glutamate) dissolves in hydrocarbons (Smith and Woody (1973)) (which are not solvents of PBzLG), as one might expect from the aliphatic nature of the side chains. For PBzLG, large dielectric constant doesn't seem to be the critical factor for a liquid to be a good α-helical

solvent. Instead, high polarisability of the solvent molecules seems to be a more important factor.

Extensive studies have been made on PBzLG in solution, often to investigate the conformational nature of the molecules and in particular to examine what factors produce the helix-to-coil transition. Owing to the rodlike nature of the molecules, this has allowed a number of different experimental techniques to be used which examine different properties of the molecule.

a) thermodynamic properties

i) light scattering (Doty et al. (1956), Fujita et al. (1966), Gerber and Elias (1968))

b) hydrodynamic properties

i) viscosity (Doty et al. (1956), Fujita et al. (1966), Vitovskaya and Tsvetkov (1976))

ii) shear modulus (Warren et al. (1973), Ookubo et al. (1976))

c) dielectric properties

i) measuring dipole moments (Block et al. (1970), Wada (1959))

ii) loss process (Block (1983))

In general, the trends observed for these properties have been related to a number of factors including, molecular weight dependence, aggregation, solvent used and persistence length of rigid helix. (Note: the references given are not exhaustive but are intended to highlight these factors).

Evidence for the α-helix was first given by Doty et al.

(1956), based upon their light scattering measurements which estimated the length of a single residue within the helix as 0.153-0.128 nm (expected value is 0.15). Certain workers (Fujita et al. (1966)) disagreed with this value for h, suggesting a much looser wound helix. However, work by Gerber and Elias (1968) also estimated a reasonable value of 0.16 nm. Discrepancies in the value of h were usually attributed to association, polydispersity or simply the inadequacies of the model used.

For many helicogenic solvents used, the presence of associated or aggregated groups of helices was common, particularly in benzene. In DMF (Gerber and Elias (1968)) and other amides, association was minor and the association in solvents such as chloroform, DCE or dioxan could be reduced by adding small quantities of DMF (Powers (1970)). In particular, decreases in viscosity, and increases in loss process frequency (Block (1983)) were clear indications of deaggregation. Not surprisingly, in helicogenic solvents other than DMF, high concentration and high molecular weight favour more extensive association.

It is thought association occurs in two forms. In the first case, intermolecular H-bonding between end residues (Rohrer and Elias (1972)) (which have not been incorporated in the α-helix) can occur, leading to a head-to-tail arrangement of molecules. Secondly, strong dipolar interactions between adjacent molecules can form an antiparallel arrangement (Powers (1970)).

Consequently, an alternative method to produce

dissociation has been to add small amounts of random coil solvents which solvate end residues, but in not so great a concentration as to cause complete random coil formation.

Molecular weight dependence and the persistence length of the rigid helix are closely linked. The presence of a persistence length was suggested after observing the loss of linearity in certain properties. Doty et al. (1956) had already suggested a degree of flexibility when their light scattering results became nonlinear for high molecular weight samples. Vitovskaya and Tsvetkov (1976) suggested that rigidity was only maintained over about 150 nm (1000 residue lengths), so longer helices were curved. The loss of linearity for dipole moment versus molecular weight observed by Block et al. (1970) concluded a persistence length of around 70 nm, again indicating a flexible nature to the longer molecules.

The study of relaxation processes using both shear modulus and dielectric loss, revealed 3 processes. For low frequencies, there was a slow end over end relaxation. At intermediate frequencies the relaxation was described as flexural (shear modulus work), or vibrational like a spring (dielectric work). While at high frequencies the relaxation was attributed to side chains. In the case of the frequency of the first two processes, a molecular weight dependence was observed as one would expect for the molecular motions involved.

One phenomenon of interest concerning PBzLG in solution, is the helix-to-coil transition. In the past this

has been most easily achieved by using mixed helicogenic and random coil solvent systems. Detection of the transition has then involved many techniques (Block (1983)) ranging from NMR and infra-red, to flow birefringence.

For fixed solution conditions, the helicogenic:random coil solvent composition, molecular weight and temperature are factors which can effect the transition.

As far as molecular weight is concerned, it is only worth noting that for very short molecular chains (< 10 residues), the ability to form helices is restricted by the lack of chain units. Modelling work by Zimm and Bragg (1959), showed a minimum restriction of about 9 units per chain, below which helix formation will not be stable. Considering the helix requires about 3-4 units to produce one turn, and there will be unbound end residues, this lower limit is not too surprising, and may be greater.

The effect of temperature is shown in figure 1.9 based on work by Cabani et al. (1976). The figure shows two transitions, (coil to helix (low temperature) and helix to coil (high temperature)), which are dependent on the solvent system used.

An important point to note from this figure is that solutions of PBzLG containing only helicogenic solvent will support the α-helix configuration at working temperatures.

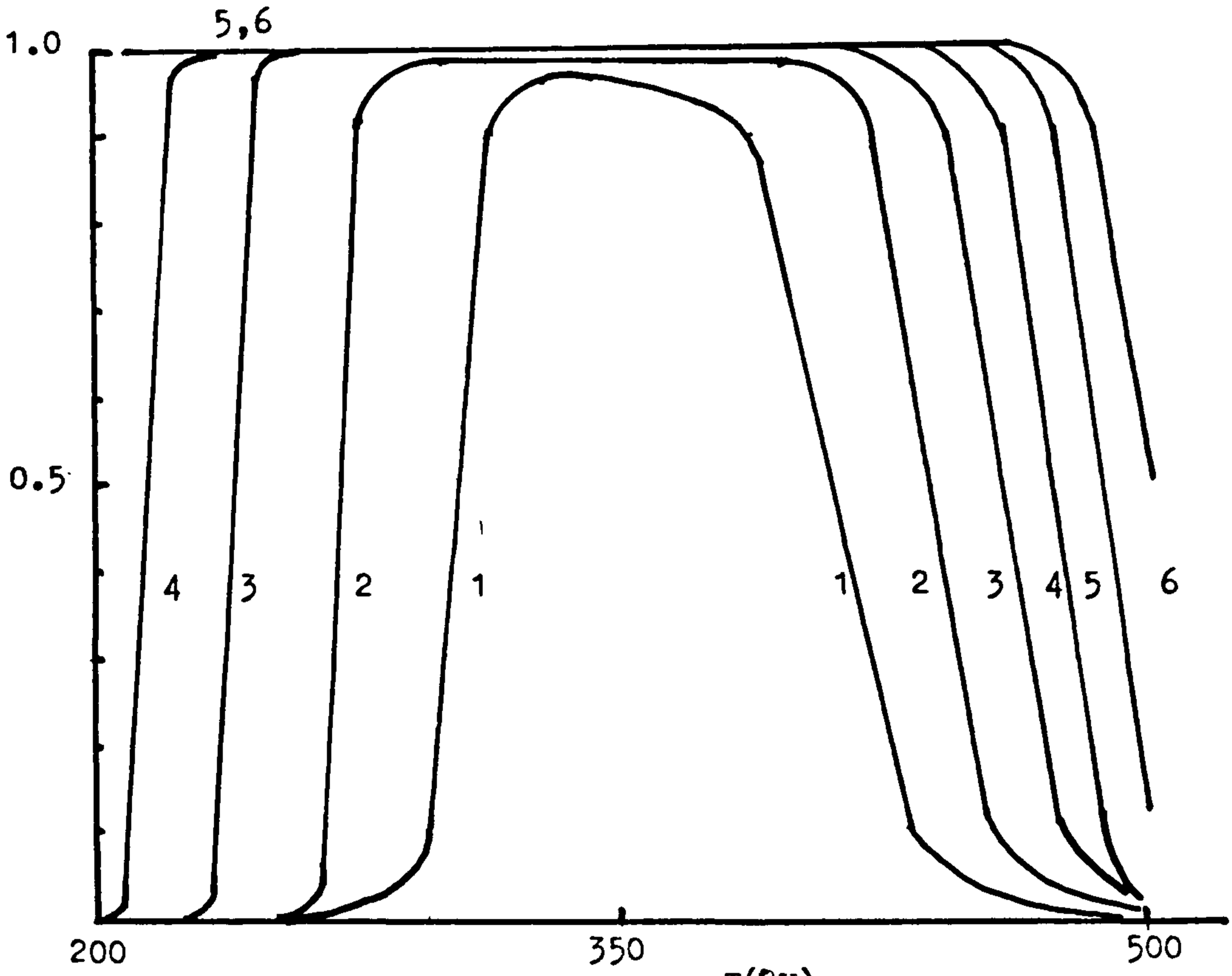

Figure 1.9 Helical content vs. temperature predictions of Cabani et al. (1976) for various solvents (1-6) of varying helix breaking activity (a_t), (1.0, 0.8, 0.6, 0.4, 0.0).

1.2 Poly(n-hexylisocyanate) (PHIC)

1.2.1 Introduction and Synthesis

The general formula for a Poly(alkylisocyanate) or l-nylon is as follows,

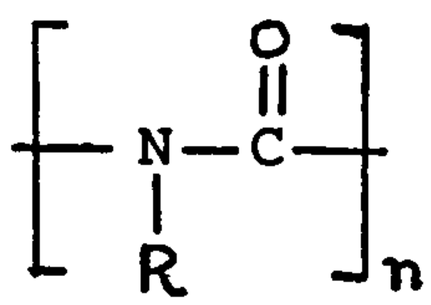

where for PHIC, R = $CH_3(CH_2)_5$-- .

Figure 1.10 shows the proposed mechanism (Shashoua et al. (1960)) for the polymerisation of monoisocyanate. (Monoisocyanates are usually prepared by the Curtius Reaction (Curtius (1930)). The mechanism shows anionic catalysis leading to propagation as far as the linear trimer. The use of low temperature, ensures high molecular weight polymer forms by preventing cyclic trimer formation. Sodium cyanide is the most common initiator used, and the mechanism given applies for this catalyst. Bur and Fetters (1976) describe the use of some other initiators which operate by other mechanisms. In one case, an organometallic species produced near mono-disperse molecular weight distributions, whereas in another case, sodium naphthalene produced irregularly structured chains which lost their long range order.

1.2.2 Conformational Structure

A paper by Bur and Fetters (1976) reviews the study made on the physical properties poly(n-alkylisocyanates). In terms of quantitative analysis, the paper only considers

Initiation Step :

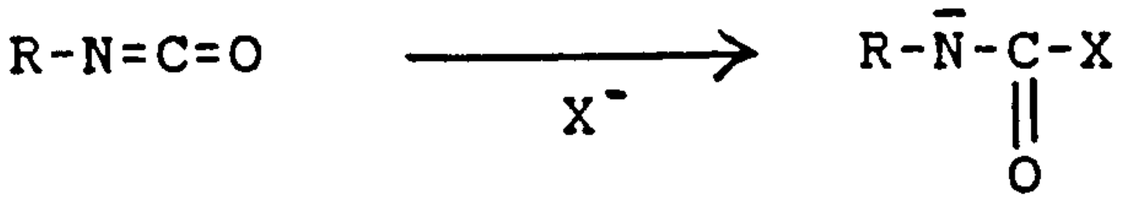

where X = CN^-

Propagation Step :

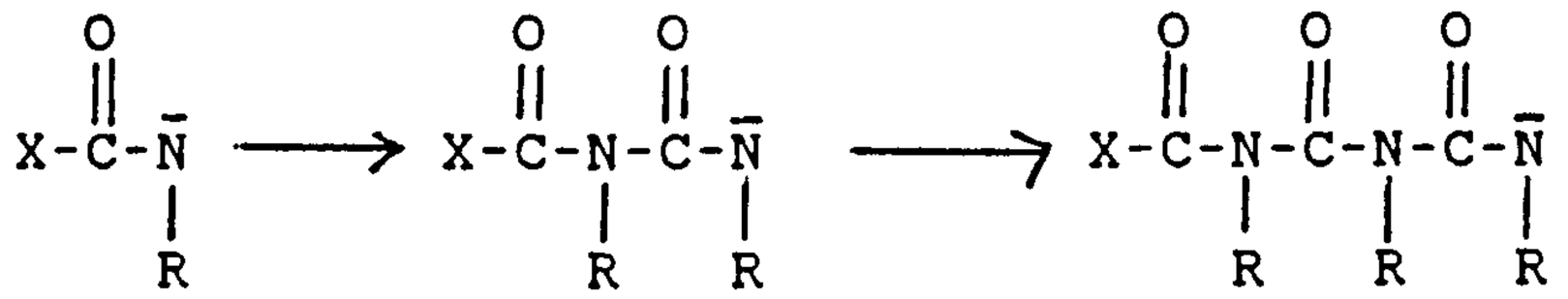

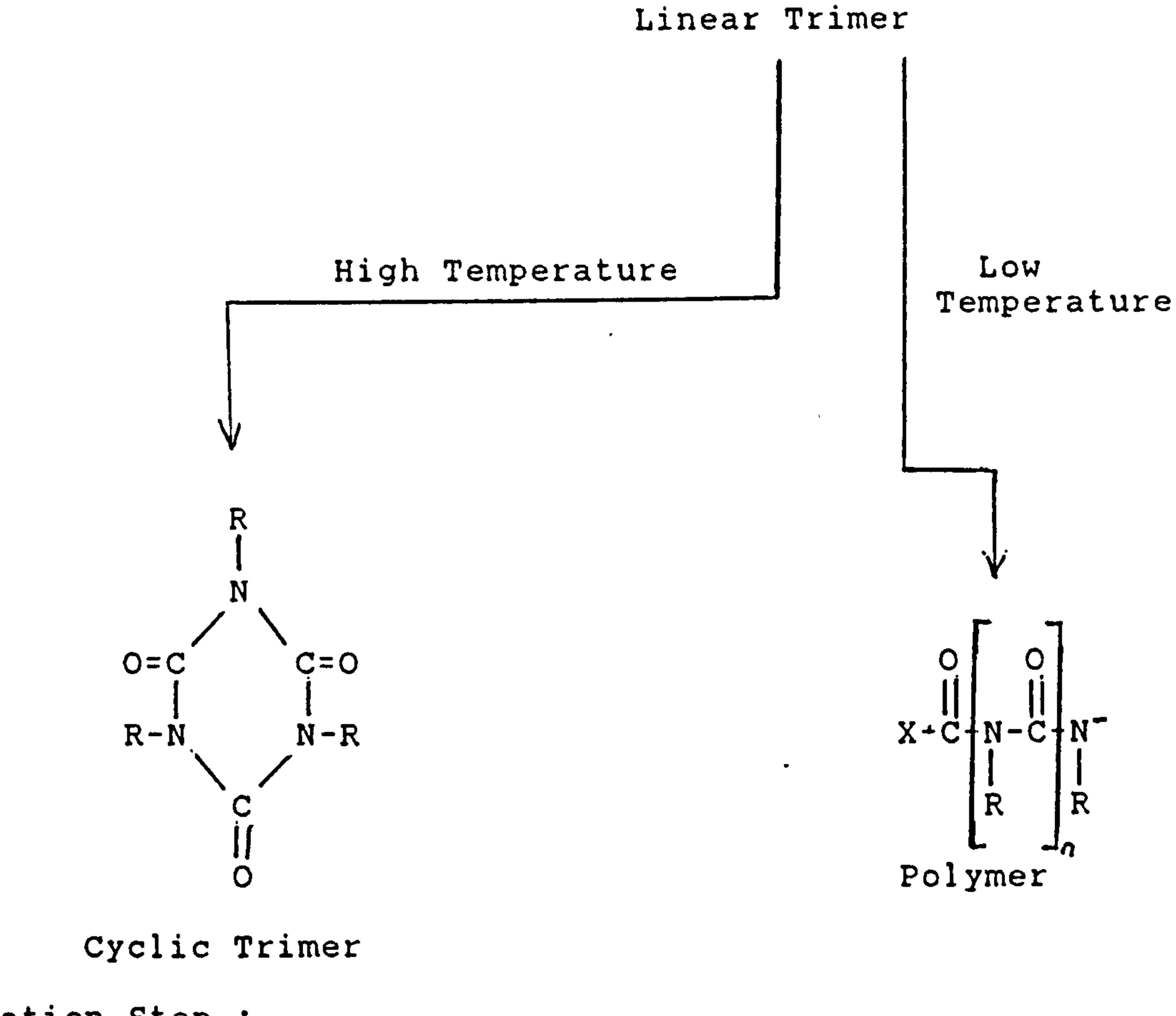

Termination Step :

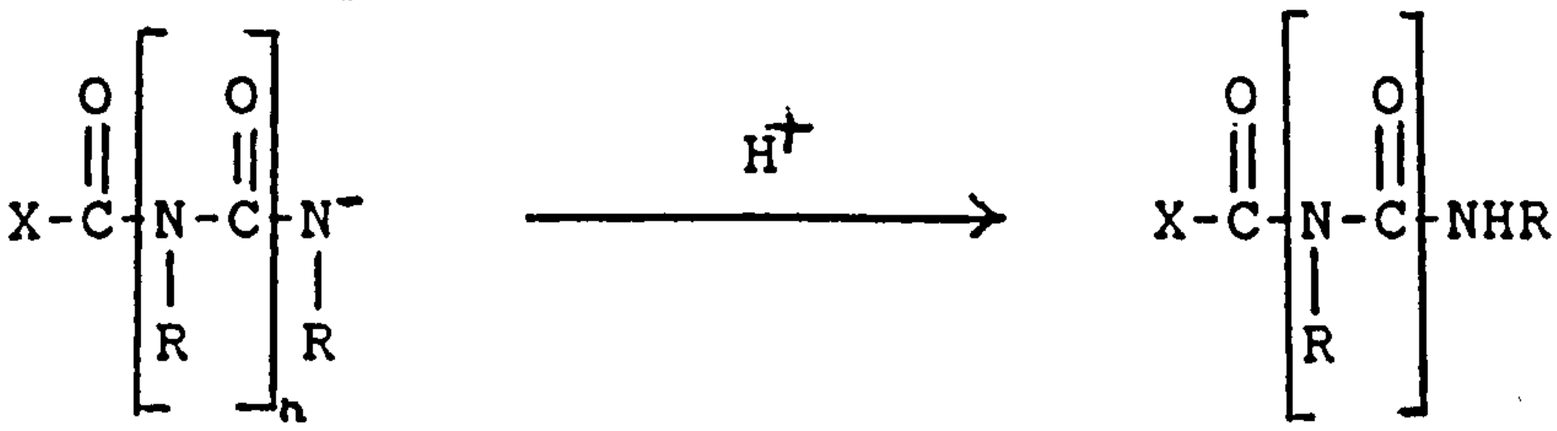

Figure 1.10 Synthetic mechanism for polyisocyanates.

results made on samples with sharp molecular weight distributions, owing to the sensitivity of the length of rigid rod molecules on such properties as dielectric relaxation, intrinsic viscosity or light scattering.

Although Buchard's measurements (1963) of the intrinsic viscosity versus molecular weight were not made on well fractionated samples, he was correct in concluding the poly(n-butylisocyanate) (PBIC) molecule to be stiff and well extended because of very poor non-Gaussian behaviour observed.

Both dielectric loss and static dielectric constant measurements (Bur et al. (1969; 1973), Lockhead and North (1972)) made on the butyl, hexyl and octyl polymers in solution, indicated a change from rigid rod, through flexible rod, to random coil conformations for weight average degrees of polymerisation in the range of 10^3-10^4 (i.e. rigid rod conformation exists at lower molecular weights, and random coil at higher values).

In general terms, the results showed that for molecular weight ranges in which rigid rod conformation existed, the ratio of average dipole moment (of the molecule) to weight average degree of polymerisation was constant. The estimated value of dipole moment per monomer unit directed along the long axis was found to be 1.13 D. As flexibility and random coil nature set-in, the proportionality of dipole moment to molecular weight (or rod length) was lost.

Good comparison of results with those predicted by a model known as the Kratky-Porod (worm-like) model were made

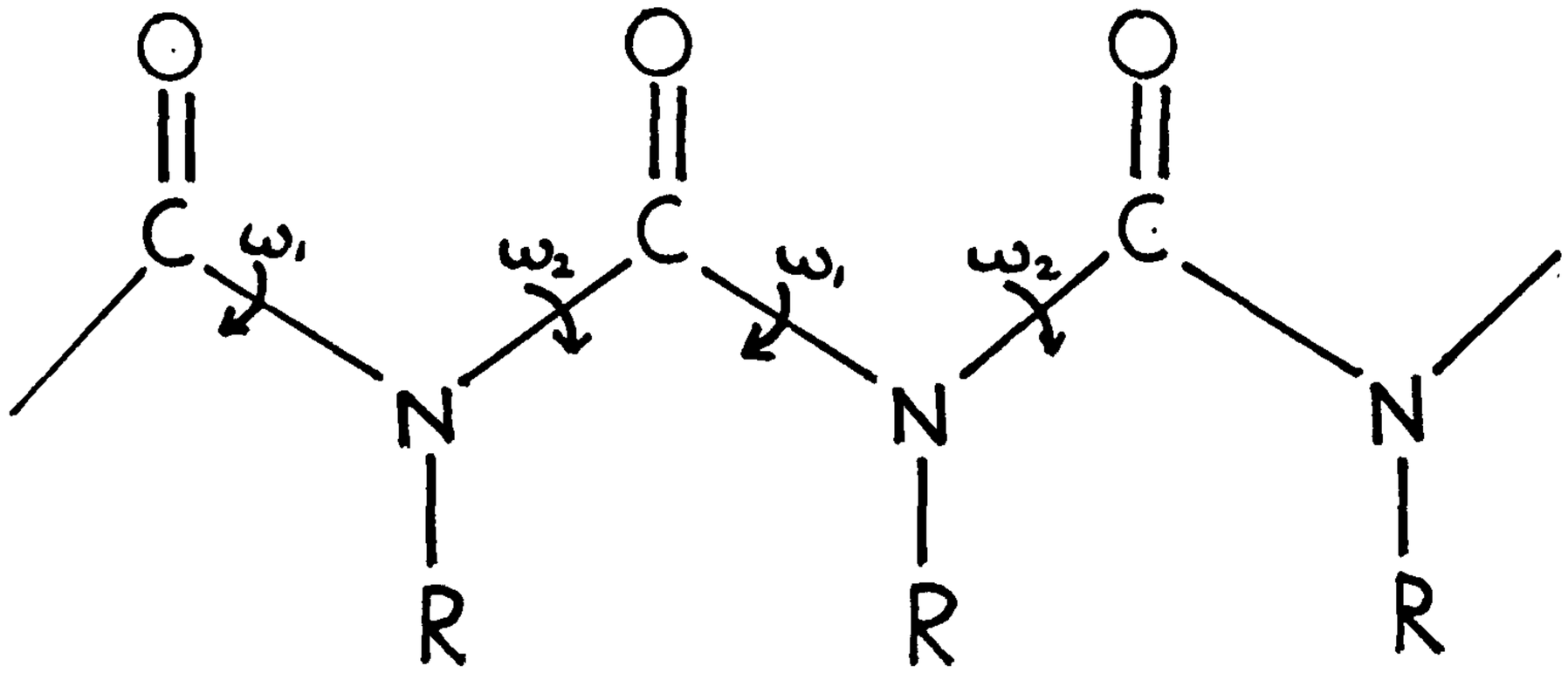

a)

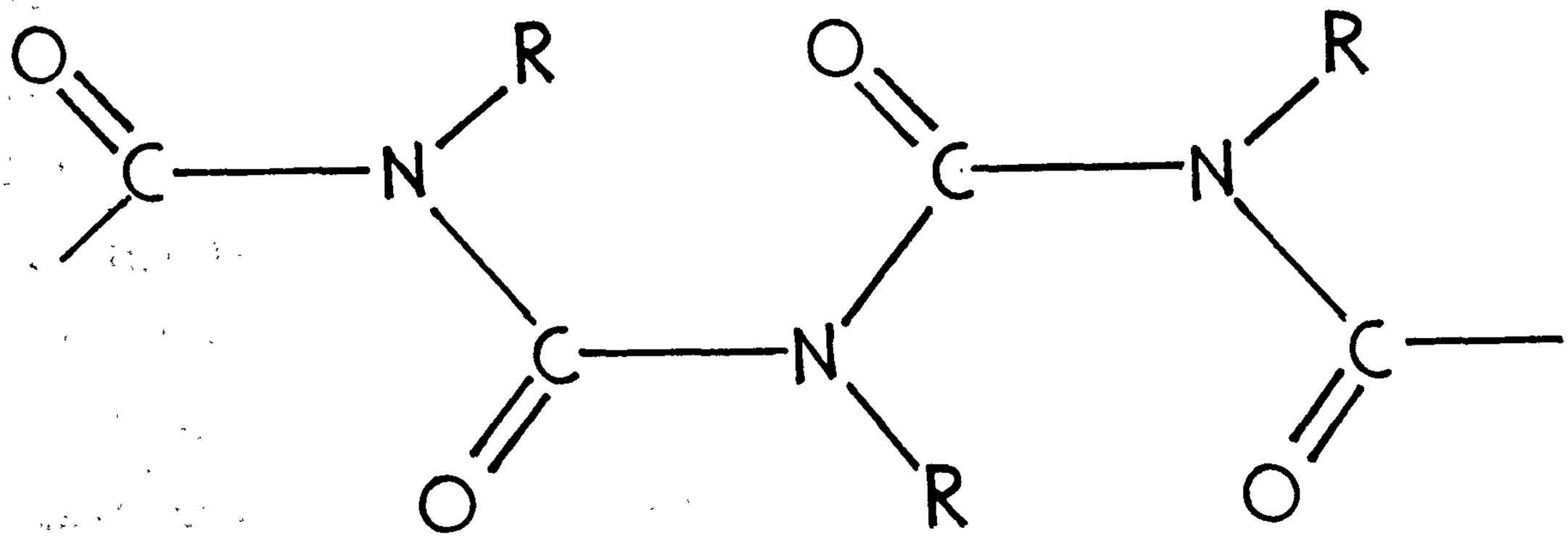

b)

Figure 1.11 a) Trans, and b) Cis-trans configuration of poly(n-alkylisocyanates).

by Bur and Roberts (1969). Discrepancies between experimental and theory were accounted for in terms of irregularities in the chain. The model predicted a persistence length of 1400 (70000 M.W).

For light scattering measurements, a value of 550 was determined (Bur and Fetters (1976)), although different solvents were used for the two cases.

Solvent effects have been studied to see if solvating processes are important in maintaining the stiff nature of the molecules. Results tend to suggest that in toluene, CCl_4 or theta solvents the rigidity of the molecule is dominated by short range forces, i.e. solvent effects are minimal.

Alteration of the conformation has shown to be the case in other solvents, if they disrupt the molecular configuration at specific sites by solvation (chloroform) or protonation (TFA).

Work by Troxell and Scheraga (1971) on PBIC, looked at electric dichroism within the solution, and concluded ideas of how and why the molecule exists in a rigid state. Figure 1.11 shows the trans and cis-trans configurations for poly(n-alkylisocyanates). Troxell and Scheraga (1971) suggested free rotation about the main chain backbone was poor owing to the severe steric hinderance between the n-alkyl side chains and the carbonyl groups. In the trans case, there is an unfavourable repulsive interaction between the negatively polarised carbonyls, and also between pairs of positively polarised nitrogens. In the

cis-trans case, steric crowding is evident between the carbonyl and the alkyl chain. To overcome both problems, slight rotation of the C-N bonds of the main chain occurs to slightly distort the cis-trans configuration, and relieve the overcrowding.

The resultant helical dimensions were then estimated by a number of workers of which a combination of ideas from Troxell and Scheraga (1971), and Schmueli et al. (1969) leads to the following values which best match experimental data:-

a (ω_1,ω_2) degrees	Monomers Per Turn	Rotation Per Monomer degrees	Translation Per monomer angs.	Dipole Moment per Monomer/ D
(-40,160) (40/200)	8/3	135	1.94	1.49(b)

a) Refers to figure 1.11; for left and right handed helix; $\omega_2=\omega_1=0$ for trans configuration .

b) Experimental value =1.13 D.

At present this is the most accurate representation of the poly(n-alkylisocyanate) rod conformation in solution.

Phase Transitions of Polyisocyanates in the Solid and Solution

This particular area of study is neatly covered by two papers by Aharoni (1980a; 1980b), which are effectively summarised by figures 1.12a-b.

Figure 1.12a was obtained using a polarising

a)

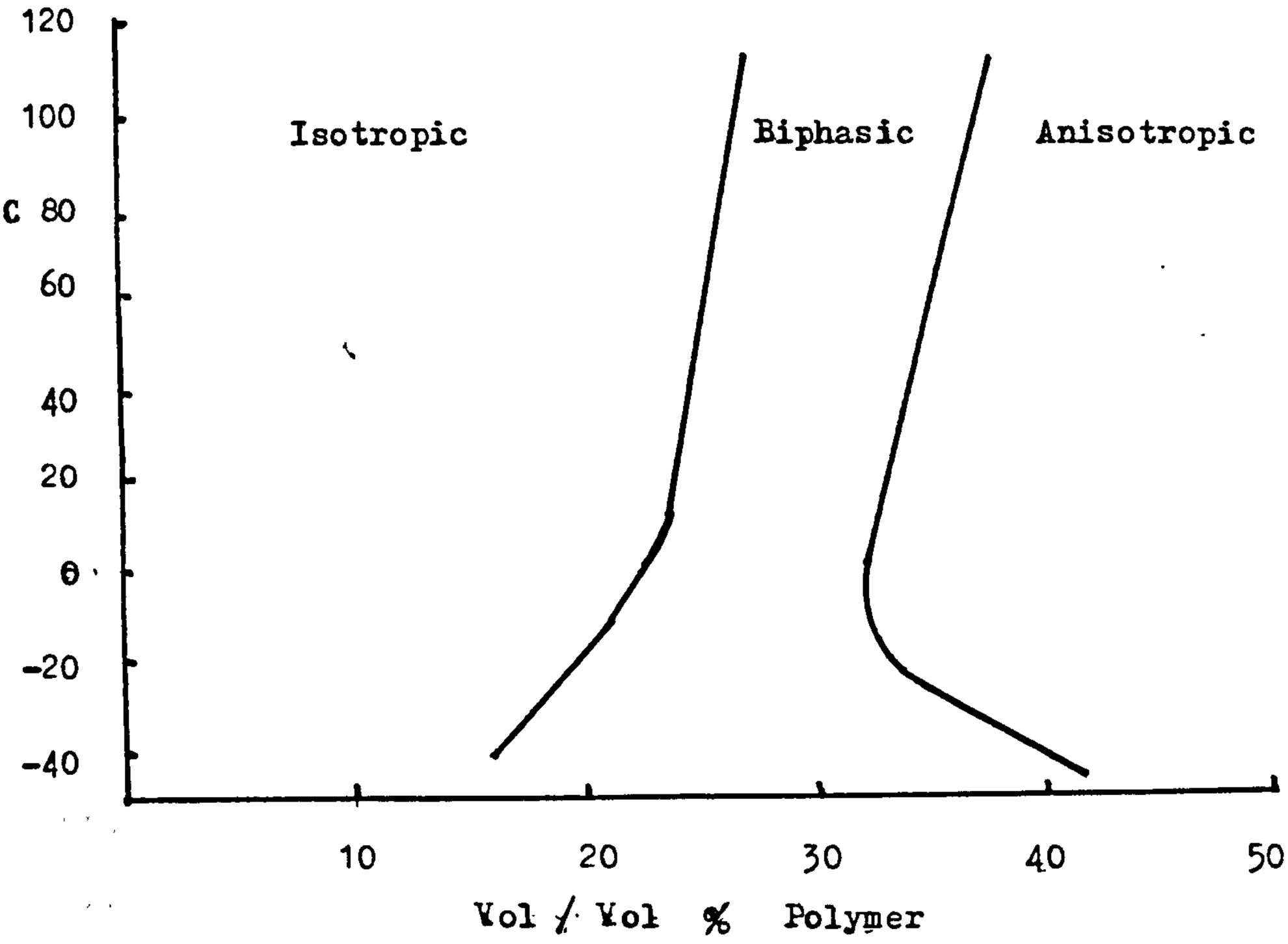

b)

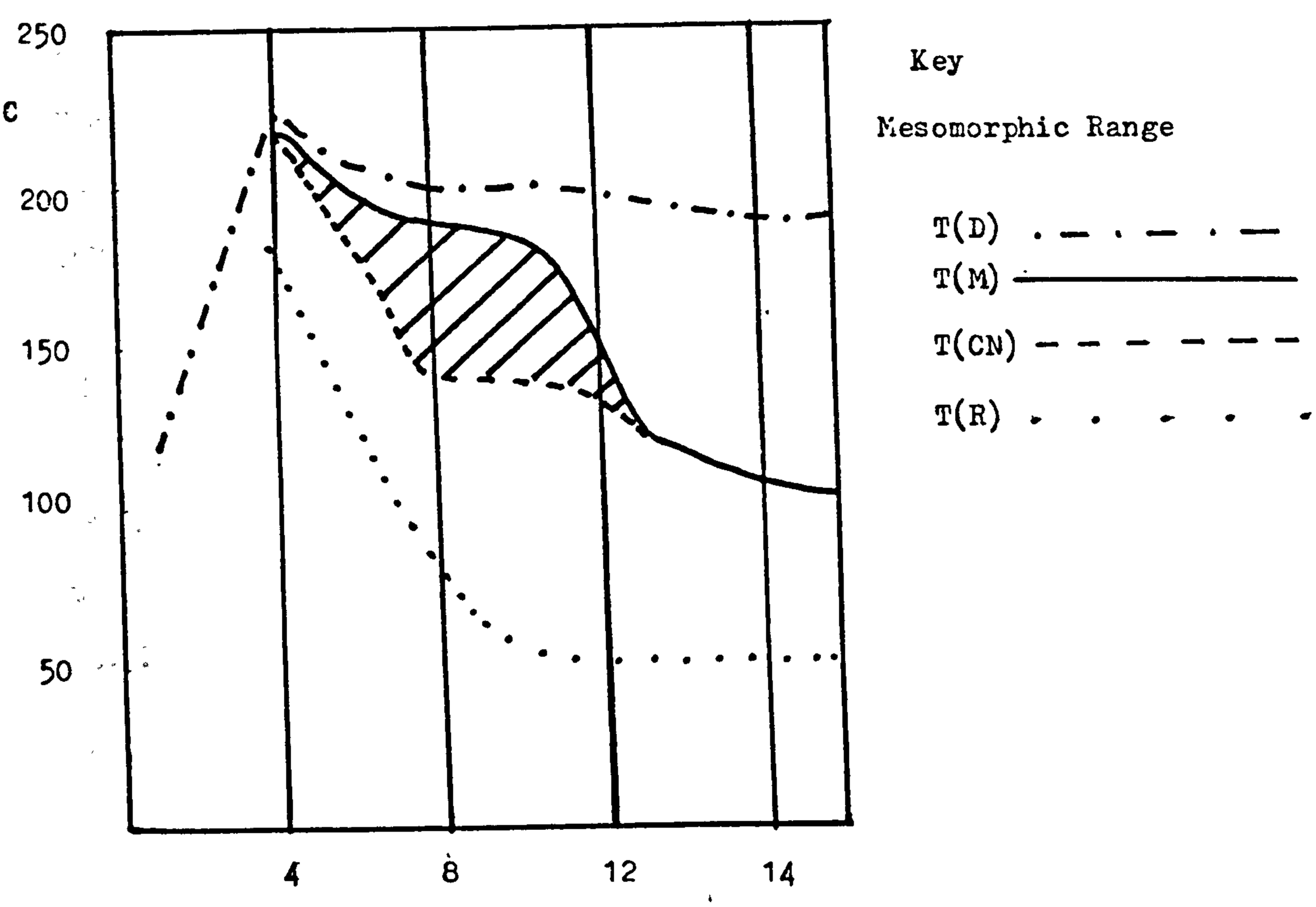

Figure 1.12 Phase diagrams for a) PHIC in toluene, b) Solid poly(n-alkylisocyanates).

microscope with a heating stage, to observe the temperatures at which phase changes took place. The anisotropic phase is thought to be nematic, typified by a bright uniform birefringent view. In contrast, the isotropic phase shows no structure at all, i.e. a fully extinguished view.

Within the biphasic regions, inclusions of isotropic phase within an anisotropic matrix, or vice-versa depending on the concentration.

Figure 1.12b shows the phase diagram obtained for the n-alkyl homologous series of polyisocyanates. Thermal decomposition is certainly a problem with polyisocyanates. Gradual decomposition usually sets in about 120°C and accelerates at 140°C. Degradation takes the form of cyclic trimer formation, where trimer units simply uncouple from the polymer chains. Hence, the data for figure 1.12b was obtained with the minimum of heating on the hot stage to prevent unnecessary degradation.

Temperature values obtained by Shashoua et al. (1960) which were referred to as "softening temperatures", and melting or decomposition temperature match closely the lower and upper curves shown on figure 1.12b. However, observations reported by Bur and Roberts (1969) could not find any liquid crystal state.

The following definitions describe the various transitions observed for figure 1.12b.

Symbol	Transition	Nature of Change/view
T(CN)	crystal/semicrystalline to nematic (l.c.)	solid polymer to flowing birefringent mass
T(M)	Melting point l.c. to isotropic liquid or solid to isotropic liquid	Completely dark view
T(D)	decomposition temperature	onset of degradation
T(R)	relaxation transition	point of increased birefringence below T(CN)

Aharoni (1979) quotes a value of the glass transition temperature for the n-butyl, n-hexyl and n-octyl polyisocyanates as near -15°C.

CHAPTER 2

2.1 General Liquid Crystal Properties of PBzLG Solution

The lyotropic liquid crystalline nature of PBzLG in helicogenic solvents was first reported by Elliot and Ambrose (1950), who observed birefringence when minimal solution concentrations had been obtained (approximately 15 % w/w quoted). Their work also involved the production of solvent cast films which were oriented by smearing concentrated solutions with the edge of a razor blade prior to evaporation of the solvent. The resultant films showed clear evidence of alignment when viewed through crossed polarizers, the grain of which appeared to be perpendicular to the draw direction and resembled the twisted fibres in a piece of rope.

Following on, Robinson (1956) showed that for the birefringent solutions of PBzLG, parallel equidistant lines were visible even using natural light, with the periodicity extending over 10 microns. This was interpreted as being due to the formation of a lyotropic, cholesteric liquid crystal phase, if a helicogenic solvent was used. The onset of the liquid crystal phase at a particular concentration was dependent upon the molecular weight and the solvent used. In all cases however, two distinct concentration points were observed, i.e.

point A:- where the isotropic solution became biphasic, and on increasing the concentration,

point B:- where the biphasic region changed to a total cholesteric phase.

X-ray studies by Robinson et al. (1958) suggested that the oriented cholesteric phase was composed of 2-D hexagonally packed α-helical rods, with an axis of torsion perpendicular to the rods, and directed along the crystallographic axis (rather than bisecting the angle between crystallographic axes).

Another aspect of the cholesteric phase, was that the optical periodicity due to the torsion of the planes, was half the pitch of the super helix (of the planes) and was proportional to the temperature. Robinson (1961) also noted that the spacing of the equidistant lines, was solvent dependent, such that in a mixed solvent system of chloromethane and dioxane, the spacing became infinite (i.e. nematic phase could be induced). Other solvent and thermal effects are reported by Samulski and Tobolsky (1974) and Uematsu and Uematsu (1978).

It is not too unexpected that PBzLG formed a liquid crystal in view of its structural nature, particularly considering the theoretical aspects studied by Flory (1961), on rigid rodlike molecular interactions, which predicted the points A and B experimentally observed.

2.2 Alignment of Molecule/Dipoles

The alignment of molecules or dipoles within samples offers one possible route to form the well ordered, non-centrosymmetric structures which are important for nonlinear optical and piezoelectric properties. In

inorganic and organic crystals this is achieved in the crystallisation process, where the resultant molecular structures are usually well documented and related to a relevant point group.

In other noncrystalline materials, certain processing techniques can be used to alter the usual amorphous state and introduce some degree of alignment. This is particularly common in polymeric materials.

A classic example of this is in the processing of poly(vinylidene fluoride) (PVDF) films for piezoelectric purposes, which incorporates two aspects of alignment (Kepler (1978a)). In the first instance, molecules are mechanically aligned in the films by hot pressing/rolling the sample, which stretches the films to around four times their original length. In this case, the chain axes of the molecules are highly oriented in the draw or rolling direction. In the second instance, a net polarisation (alignment of dipoles) is induced in the film using an electric field poling process. This process takes advantage of the typical thermal properties of polymers which possess a glass transition temperature (T_g). On heating polymers above their T_g value, enough free volume is introduced into the polymer structure to allow localised motion of chain segments and side chains.

In the PVDF case, a temperature of 100°C is used and the subsequent application of a high electric field (5×10^7 V/m), produces some degree of alignment of dipoles within the now 'free' moving segments and side chains. This

alignment is then retained by cooling the sample to room temperature below the T_g value, with the field still applied.

These two alignment processes only highlight the importance of a non-centrosymmetric structure, as far as SHG applications are concerned. Only after the poling process has been completed is such a structure induced in the film. The mechanical alignment of the polymer chains in the draw direction, still only produces a structure with a random orientation of dipoles perpendicular to the chain axes (film surface).

Alignment of Molecules within Solution

The degree of freedom of dipolar movement within polymer films above their T_g, is obviously limited in comparison to that possible for similar motion within molecules dissolved in solution.

In the solid polymer film case, a concerted motion of a number of neighbouring segments is required to achieve dipole alignment, whereas in the solution case, the reduction in neighbouring molecular interactions does not hinder dipole/molecular alignment to such an extent. In either case, the degree of alignment is then strongly dependent on the size of the field that can be applied.

In solution, ionic impurities either allow conductive processes which limit the field that can be applied, or in liquid crystal systems cause William's domains (Williams (1963)) which disrupts the alignment. In addition, thermal disruption is always a competing force with the electric

field.

A useful approximation to determine the strength of field required to produce alignment within a solution of temperature T, containing molecules with dipole moments μ is,

$$\mu E \simeq kT. \qquad (2.i)$$

Using this equation, it is possible to see the reason for the interest in using rodlike molecules such as the poly(glutamates) and the poly(isocyanates) for producing aligned samples.

The helical nature of these molecules is such that the components of the dipole moments acting along the axis of the helices for each monomer unit of the chain are additive. Hence, in high molecular weight samples of these materials, molecules can be assumed to possess a single large dipole moment which is simply related to the number of residues in the chains; e.g.

for PBzLG- weight average molecular weight-550,000
anisometry (helix length to diameter) ca. 100
dipole moment per molecule (Levine and Bethea (1976)) 8000D,
for PHIC-weight average degree of polymerisation-1000
dipole moment (Bur and Roberts (1969)) 1000 to 1200 D
(chain persistence length (Bur and Fetters (1976)) 50-60 nm).

The implication of the size of these dipole moments is that only moderate electric fields (>10000 V/m) or magnetic fields (>10T) can induce extensive alignment of the molecular axes in dilute solution or liquid crystal phases.

2.3 Alignment of Poly(glutamates) in Solution and in Solid Samples

Mention has already been made of the cholesteric liquid crystal properties of PBzLG in solution, and a lot of the alignment studies of PBzLG started from the liquid crystal state.

i) Electric Field

Iizuka (1969; 1971) studied the application of an electric field to liquid crystal solutions (> 6%w/w) of PBzLG (degree of polymerisation-650) in dibromomethane, dichloromethane and chloroform. A field of only 84 V/cm was required to produce alignment, which took about 1000s to complete. The ease of the alignment (small field) was attributed to head-to-tail packing of α-helices in the liquid crystal bundles/layers, so that the layers as a whole had a huge resultant dipole moment. The slow rate of orientation was attributed to the interactions between bundles in the concentrated conditions.

Toth and Tobolsky (1970) carried out similar studies on a 310,000 M.W. sample of PBzLG in the same solvents and observed alignment at a field of about 310 V/cm. For fields less than this, a coloured cholesteric texture was observed when the sample was viewed parallel to the field direction between crossed polarizers. On increasing the field above this value, the view turned black. This was attributed to a cholesteric to nematic transition. They also observed a gentle stirring at 310 V/cm, which became violent on increasing the field. Similar disturbances were observed

for PBzLG-dioxane systems by Minami et al. (1978).

The cholesteric to nematic change has been studied by Duke and Dupre (1974) using laser light beating spectroscopy. They suggest two reorientation processes are involved, on application of the field (i.e. a rapid structural change within 2-5 minutes, and a longer process which requires 30 minutes to stabilize). They suggest the first process is a reorientation of cholesteric microregions whose axes are not perpendicular to the suddenly imposed field direction, followed by the slow unwinding of the cholesteric planes into the nematic state.

ii) Other Alignment

Although the use of electric field alignment is most important as far as SHG is concerned, other alignment processes of polyglutamates have been studied which are worth mentioning.

The mechanical alignment of PBzLG solution (Elliot and Ambrose (1950)) by smearing with the edge of a razor blade to form a thin, well oriented, evaporated film, has already been mentioned in the earlier liquid crystal section.

The other main alignment process has involved the use of magnetic fields.

Samulski and Tobolsky (1968) produced solvent cast composite samples of PBzLG in an inert, nonvolatile component called Aroclor by evaporation from chloroform while a 10 kG magnetic field was applied. X-ray studies showed the field was sufficient to produce alignment within the samples in the same direction as the applied field, and

reflections characteristic of the α-helix were observed.

Go et al. (1969) report that PBzLG was only oriented by 9600 G magnetic field when dibromomethane or dichloromethane were the solvents. They report that no such orientation was obtained when evaporation occurred from chloroform, benzene or dioxane. However, they did use a lower molecular weight sample than Samulski and Tobolsky, which coupled with solvent effects may have meant the field used was not strong enough to align in the case of the 3 other solvents.

In further studies, Samulski and Tobolsky (1971) describe their solvent cast, magnetically aligned films as uniaxially, oriented, nematic films with the helical axes aligned parallel to the magnetic field.

A more detailed study of the morphology, of a magnetically aligned PBzLG film was carried out by Wilkes and Ban (1972a-b; 1973). Their X-ray studies also indicted the helices were preferentially aligned (on average) along the magnetic field direction, but more importantly, a well-ordered suprastructure within the film was clearly visible.

This consisted of bands (referred to as super-rods) of alternating light and dark regions (when viewed through crossed polarizers), lying almost perpendicular to the field direction (i.e. like a "zebra-crossing"). These super-rods were 30-40 microns wide, and when the sample was rotated through 45°, they could be seen to undergo a reversal in dark and light. This implied the optic axis of a super-rod was at 45° to its two neighbours, but the optic axes of

alternate super-rods were identical.

Within each super-rod was a finer structure of fibrils (1-2 microns wide), so that the super-rod resembled a strand of twisted rope. The paper suggests the α-helices are oriented perpendicular to the axis of the fibrils, so the fibril is formed by helices stacking side by side.

A more recent study of a magnetically aligned film of PBzLG has been covered by Murthy et al. (1986). Rather than describing the alignment as uniaxial orientation, which might occur in a mechanically oriented fibre, it is suggested three dimensional order arises, based on hexagonal packing of the helices throughout the whole sample. This is proposed because the alignment process orientates microregions already containing the well-ordered hexagonal structure, thus forming a much larger 3-D order of hexagonal structure.

It is important to remember, that the liquid crystal state is an aligning process in itself, and work by Tsutsui and Tanaka (1980a, b) has attempted to immobilize cholesteric textures of poly(n-butyl-L-glutamate) (PBuLG) in what can be described as a guest host polymer system. In this work, suitable vinyl monomers were used as the solvent for PBuLG to form cholesteric solutions, which were then immobilised by polymerisation of the solvent. In such a system of rigid rod/flexible polymer molecules, phase separation should not occur during curing (polymerisation), either because the entropies of mixing between flexible and rigid polymers is greater than between flexible pairs

(Aharoni (1980c), which leads to a thermodynamically stable mixture, or because high viscosity imposes a kinetic barrier and causes a metastable state which is a very long lived solid solution.

Tredgold and Ali-Adib (1988) produced a guest host, magnetically aligned composite film of PBzLG in poly(3-chloro-2-chloromethyl-1-propene) by applying a magnetic field, evaporating off most of the monomer solvent, and then polymerising. The film had been aligned parallel to its surface, and the resulting examination of the film in terms of the transmittance of polarised light revealed four points of extinction for a 360° rotation of the sample, i.e. implying biaxial nature. They reported areas of up to several square millimetres showing uniform birefringence.

CHAPTER 3

PIEZOELECTRICITY

3.1 The Piezoelectric Effect

A material is usually considered to be piezoelectric if it exhibits a change in polarisation ΔP as a result of an applied stress σ, i.e.

$$\Delta P = d\sigma \qquad (3.i)$$

where d is referred to as the piezoelectric modulus.

Equation 3.i is an insufficient description of piezoelectricity, since P is a vector and both d and σ are tensor quantities. Nye (1957) gives a comprehensive study of tensor notation, but an outline to assist in understanding the notation used in the rest of the chapter is given in appendix 1.

Equation D, in appendix 1 leads to the matrix d_{ij} with 18 coefficients which is usually represented as follows.

$$\begin{vmatrix} d_{11} & d_{12} & d_{13} & d_{14} & d_{15} & d_{16} \\ d_{21} & d_{22} & d_{23} & d_{24} & d_{25} & d_{26} \\ d_{31} & d_{32} & d_{33} & d_{34} & d_{35} & d_{36} \end{vmatrix} \qquad (3.ii)$$

The appendix mentions that these 18 coefficients may be reduced to a smaller number of independent coefficients, depending on the symmetry of the material. It is useful to know how the matrix is affected by a certain symmetry and what symmetries describe the piezoelectric polymers to date.

3.2 Piezoelectricity in Polymers

The piezoelectric effect in polymers was first discovered in wood cellulose (Fukada (1955; 1968)), with the origin of the stress-induced polarisation being accounted for by the piezoelectric properties inherent in the cellulose micelle. As with most polymers, cellulose is not obtained in a perfect crystalline state, and contains both small crystallites and disordered amorphous regions. However, delignified wood may be regarded approximately as an assembly of uniaxially oriented cellulose fibres. The long axes of the crystallites within the cellulose are also oriented with respect to the fibre direction, but are randomly oriented normal to this direction.

Shubnikov (1946) called such a system a "piezoelectric texture", and Marutake (1958) classified the texture into 3 groups according to the symmetry. The following matrices represent the 3 groups, and can be shown to apply to other piezoelectric polymer systems.

D_∞ Group

$$(d_{ij}) = \begin{vmatrix} 0 & 0 & 0 & d_{14} & 0 & 0 \\ 0 & 0 & 0 & 0 & d_{25} & 0 \\ 0 & 0 & 0 & 0 & 0 & 0 \end{vmatrix} \qquad (A)$$

$C_{\infty v}$, C_{2v} Groups

$$(d_{ij}) = \begin{vmatrix} 0 & 0 & 0 & 0 & d_{15} & 0 \\ 0 & 0 & 0 & d_{24} & 0 & 0 \\ d_{31} & d_{32} & d_{33} & 0 & 0 & 0 \end{vmatrix} \qquad (B)$$

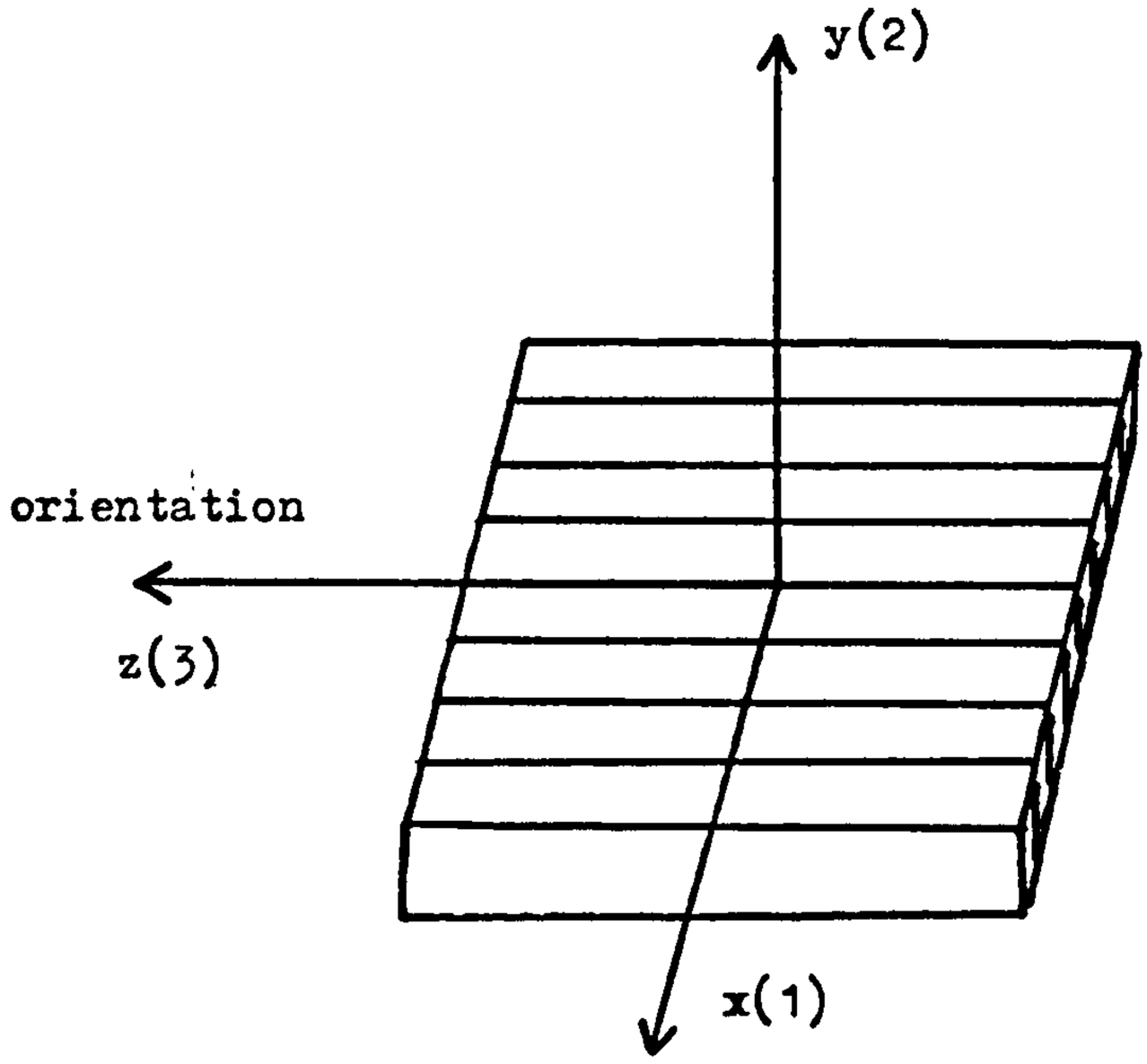

Figure 3.1 Coordinate System for D_∞ and C_∞ groups.

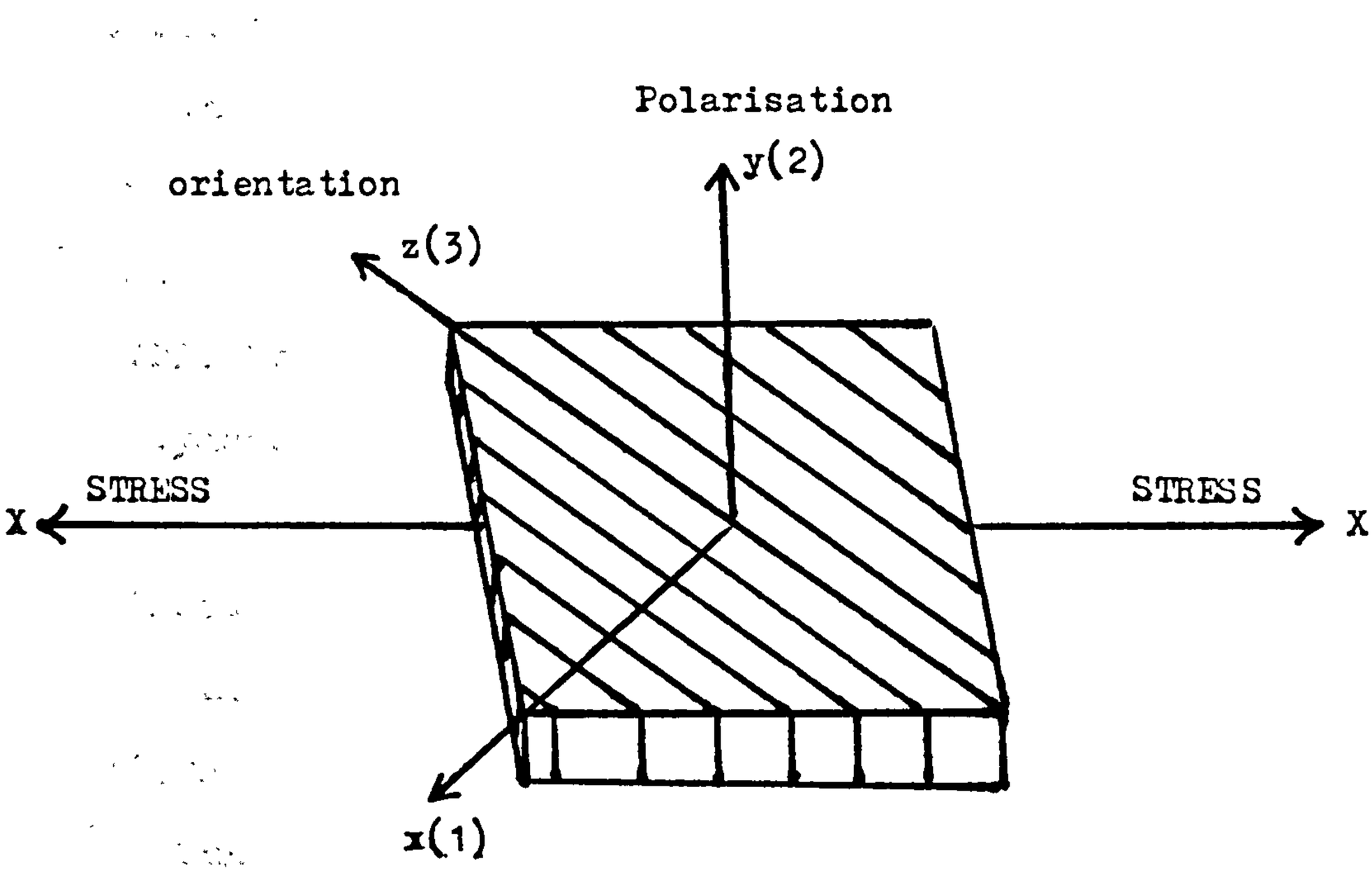

Figure 3.2 Maximum Polarisation $P_y = d_{25} X_{xz}$ for stress at 45 degrees to orientation for D_∞ and C_∞ groups.

C_∞ Group

$$(d_{ij}) = \begin{vmatrix} 0 & 0 & 0 & d_{14} & d_{15} & 0 \\ 0 & 0 & 0 & d_{24}. & d_{25} & 0 \\ d_{31} & d_{32} & d_{33} & 0 & 0 & 0 \end{vmatrix} \qquad (C)$$

Note: the symmetries of the group are represented by Schonflies' symbols (Atkins (1982)).

As most samples of polymers are tested in the form of a film, the rectangular coordinates which apply to the matrices (A) and (C) are usually assigned as in figure 3.1. In the case of unpoled oriented polymers such as wood and drawn PVDF, the z-axis is chosen as the direction of orientation.

The D_∞ group matrix is found to apply for many uniaxially drawn polymers including, polyglutamates (Fukada and Takashita (1971a)), wood (Fukada (1955)) and unpoled PVDF. No polar axis exists in the case of uniaxially drawn polymers, and piezoelectricity is achieved by applying a shear stress in the plane of the film at an angle to the direction of orientation. The polarisation is then observed in the y-direction, and is greatest for stress applied at 45° to the orientation, as in figure 3.2 .

Fukada and Takashita (1971a) explain for the specific case of poly(γ-methyl-L-glutamate) with a β-form conformation, how piezoelectricity arises from a unpolarized, oriented structure. In the β-form

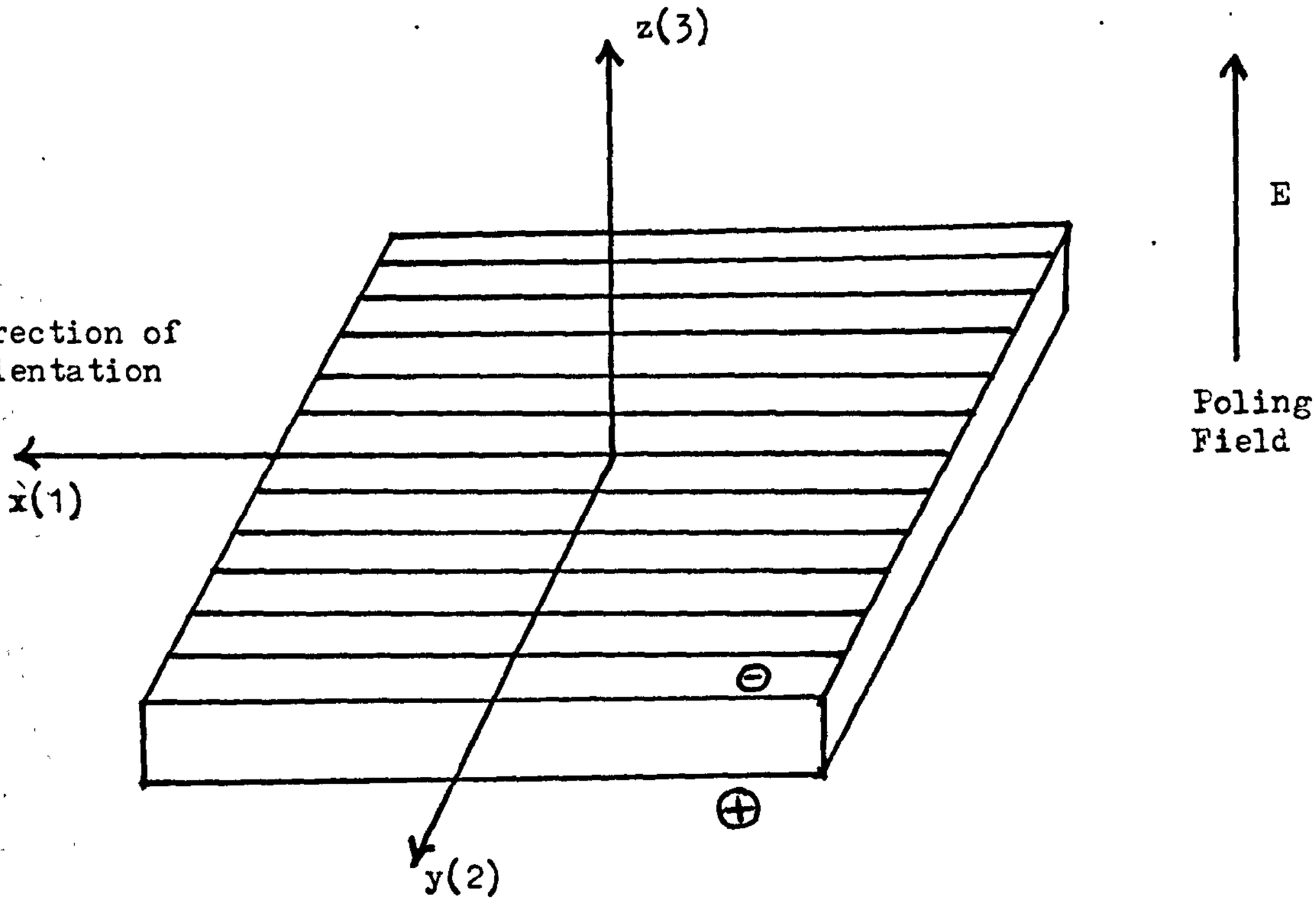

Figure 3.3 Rectangular coordinates for elongated, polarised polymer film of C_{2v} group.

conformation, the molecular structure is a pleated sheet of antiparallel chains, with hydrogen bonding of CO and NH groups of neighbouring chains taking place in the plane of the sheet. Shear within this structure results in reorientation of the CO and NH groups out of the plane of the sheet but in opposite directions to one another, resulting in polarisation.

The C_∞ group symmetry, is applicable for uniaxially oriented systems in which there is also polarisation parallel to the direction of orientation. This symmetry has been demonstrated in bone and tendon (Fukada and Yasuda (1957)).

In the case where films have been electrically poled normal to the plane of the film there seems to be the convention to make this direction the z-axis. Hence, figure 3.3 is representative of the coordinate system for such a poled case, and also covers situations where polymers are drawn and poled, e.g. PVDF (Nix (1986)). Nix descibes this symmetry of poled and drawn PVDF as C_{2v}, hence, matrix (B) may be applied. In the case where a film may have only been poled and not drawn (Broadhurst et al. (1973)), then matrix (B) still applies, but $d_{15}=d_{24}$, and the symmetry is described by the $C_{\infty v}$ group. Poled piezoelectric ceramics such as lead zirconate are described by this symmetry.

3.3 Experimental Techniques for measuring Piezoelectricity

Most polymers to date have been studied in thin film form, unlike typical inorganic piezoelectric materials, whose brittle crystalline structure prevents the

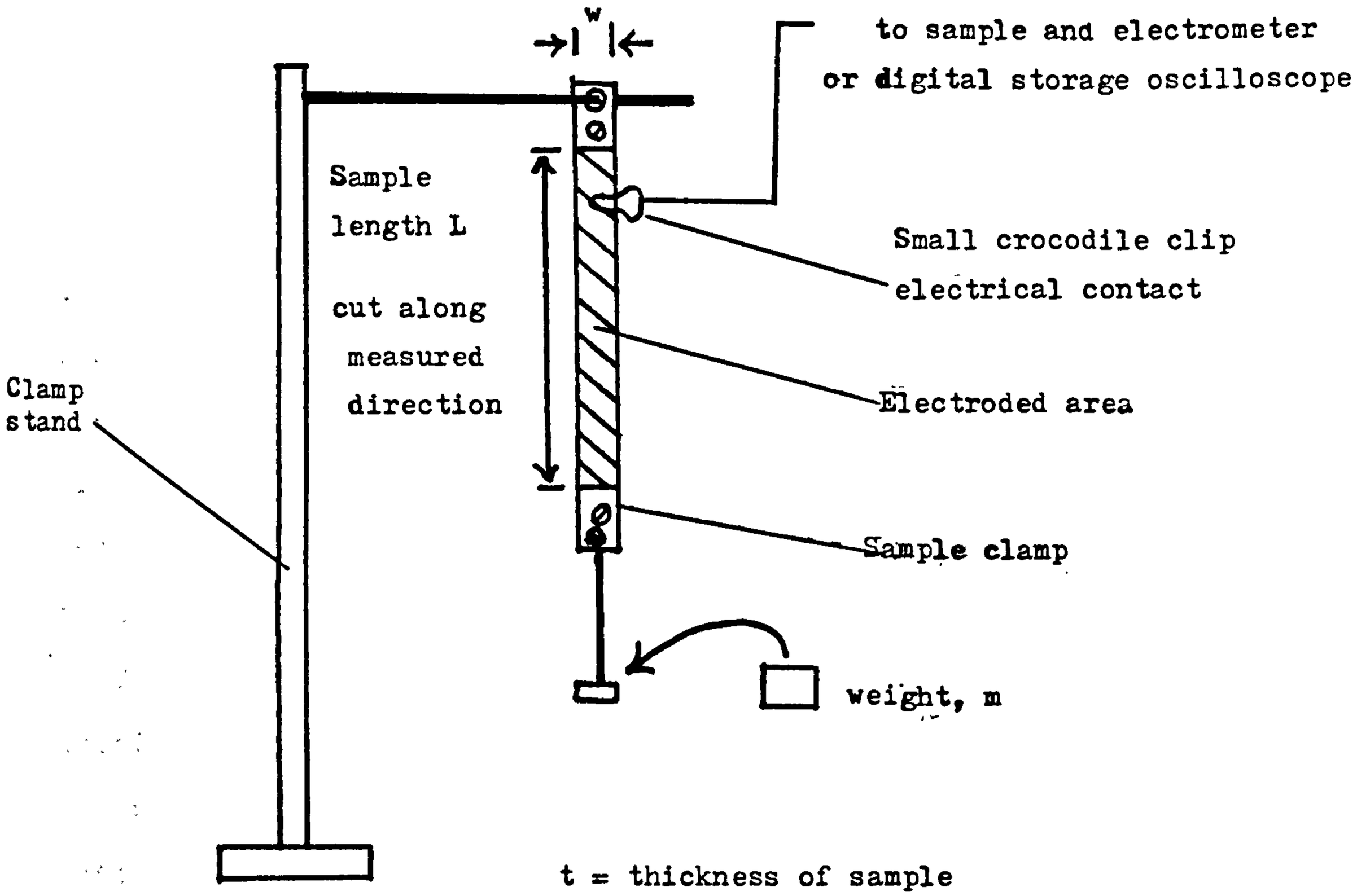

t = thickness of sample

Figure 3.4 Schematic apparatus for measuring d_{31} and d_{32}

d_{31} or d_{32} is calculated from

$$d_{31} = \frac{CVt}{mgL}$$

where $C \gg$ sample capacitance

V = voltage measured on electrometer.

$g = 9.8\ ms^{-2}$

manufacture of easy to handle large area films.

Perhaps the easiest way to measure the piezoelectric coefficients of thin polymer films is to prepare long thin samples with electrodes on opposite sides, attach one end to a rigid support, and attach a small weight to the other. Then, with an electrometer connected between the electrodes, measure the charge induced on the electrodes when a small additional weight is added to the lower end. Figure 3.4 shows a typical schematic set-up for such a technique, and d_{31} and d_{32} have been measured for PVDF (Kepler (1978b)), using such a method.

In work with thin polymer films, the electrodes are usually thin evaporated metal films. For accurate measurements, it is important that the electrodes be sufficiently thin that they do not affect the mechanical properties of the sample.

It is slightly more difficult to measure d_{33}, the piezoelectric coefficient associated with a uniaxial stress normal to the surface of the film. The difficulty arises in applying a uniaxial stress to the thin film, because the film has to be completely free to move laterally while the stress is applied.

The converse piezoelectric coefficient d^c_{33}, (i.e. the change in thickness resulting from the application of an electric field applied normal to the film) has been measured using a laser interferometer (Kepler (1978b)). Such a method offers adequate sensitivity to measure the converse piezoelectric coefficients of thin films, although

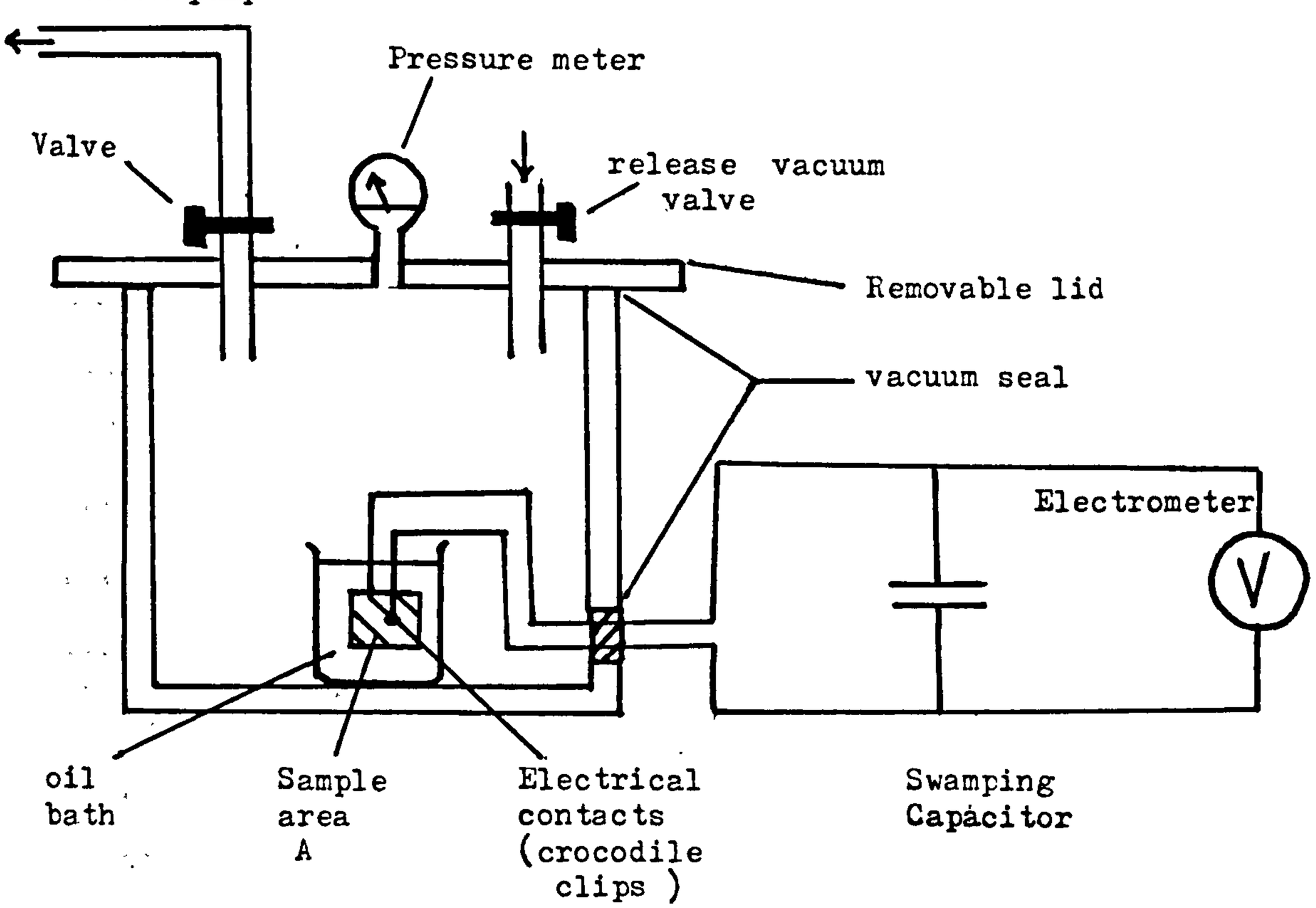

Figure 3.5 Schematic apparatus for measuring d_h

d_h is given by $d_h = \frac{CV}{PA}$

it is fairly difficult to design a sample holder which allows free lateral expansion of the sample while the thickness change is induced.

As it is relatively easy to measure d_{31} and d_{32}, d_{33} may be determined by measuring the hydrostatic piezoelectric coefficient (d_h) which is related to these other coefficients by equation,

$$d_h = d_{31} + d_{32} + d_{33} \qquad (3.iii).$$

This method has been used (Kepler and Anderson (1978b)), and it was shown that the results agreed with the value of the converse piezoelectric coefficient measured using the laser interferometry. When using such a technique, care should be taken to prevent pressurised heating of the sample, because of the inherent problem of pyroelectricity in poled piezoelectric materials.

Figure 3.5 shows a typical set-up for measuring d_h. The electrical contacts are lightly clamped to the sample electrodes, and the sample is kept at constant temperature by immersion in a nonconducting oil, e.g. silicone fluid. The cell is then pumped down to vacuum, and d_{3h} is calculated by releasing the vacuum and measuring the induced charge on an electrometer.

Work by Nix (1986) described a direct method for the measurement of d_{33} for samples of PVDF. The method was direct in that only one measurement was required, without having to resort to the measurement of d_{3h} , d_{31} and d_{32}, before using equation 3.iii. The paper also distinguished

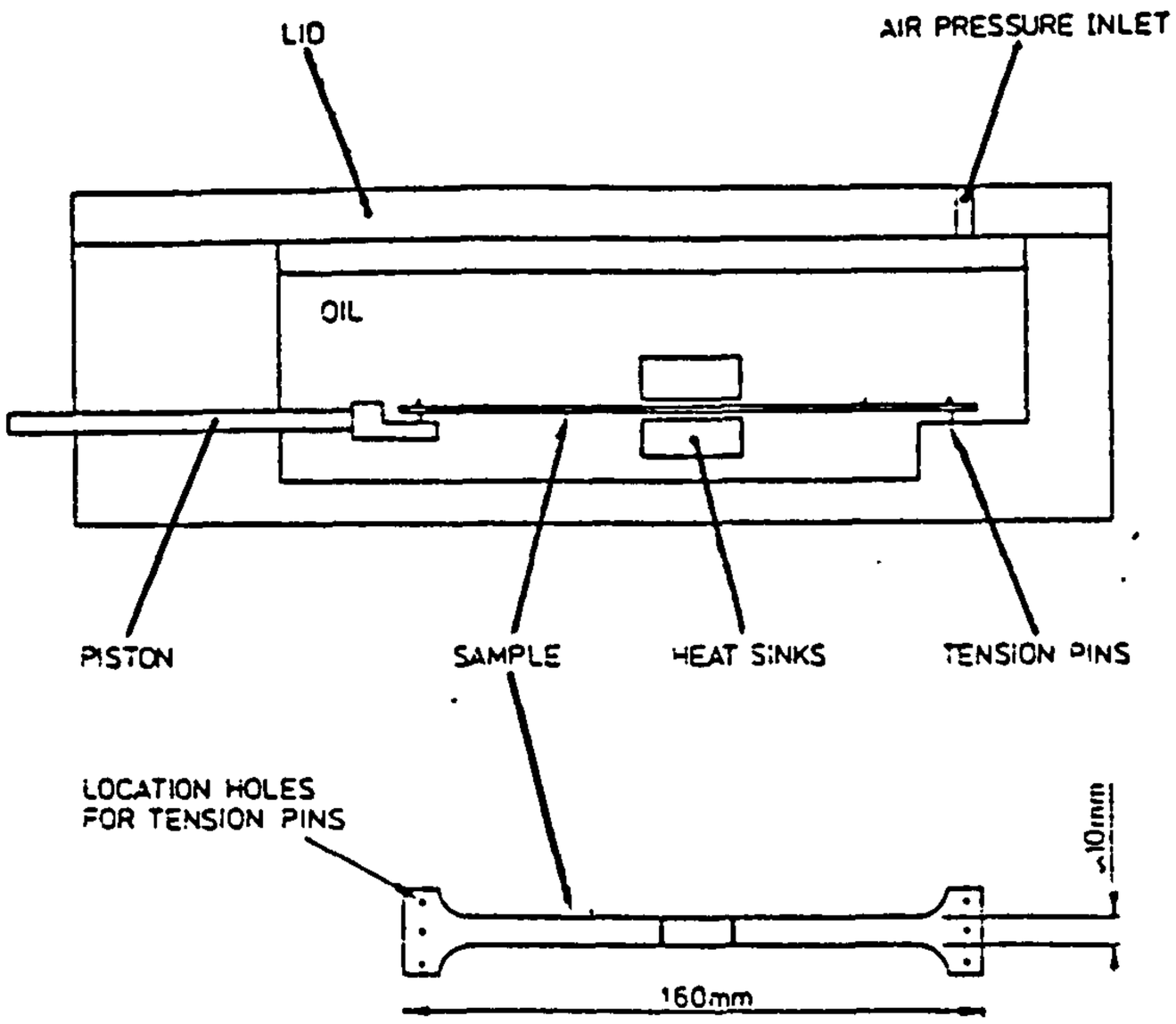

Figure 3.6 d_{33} pressure vessel and sample

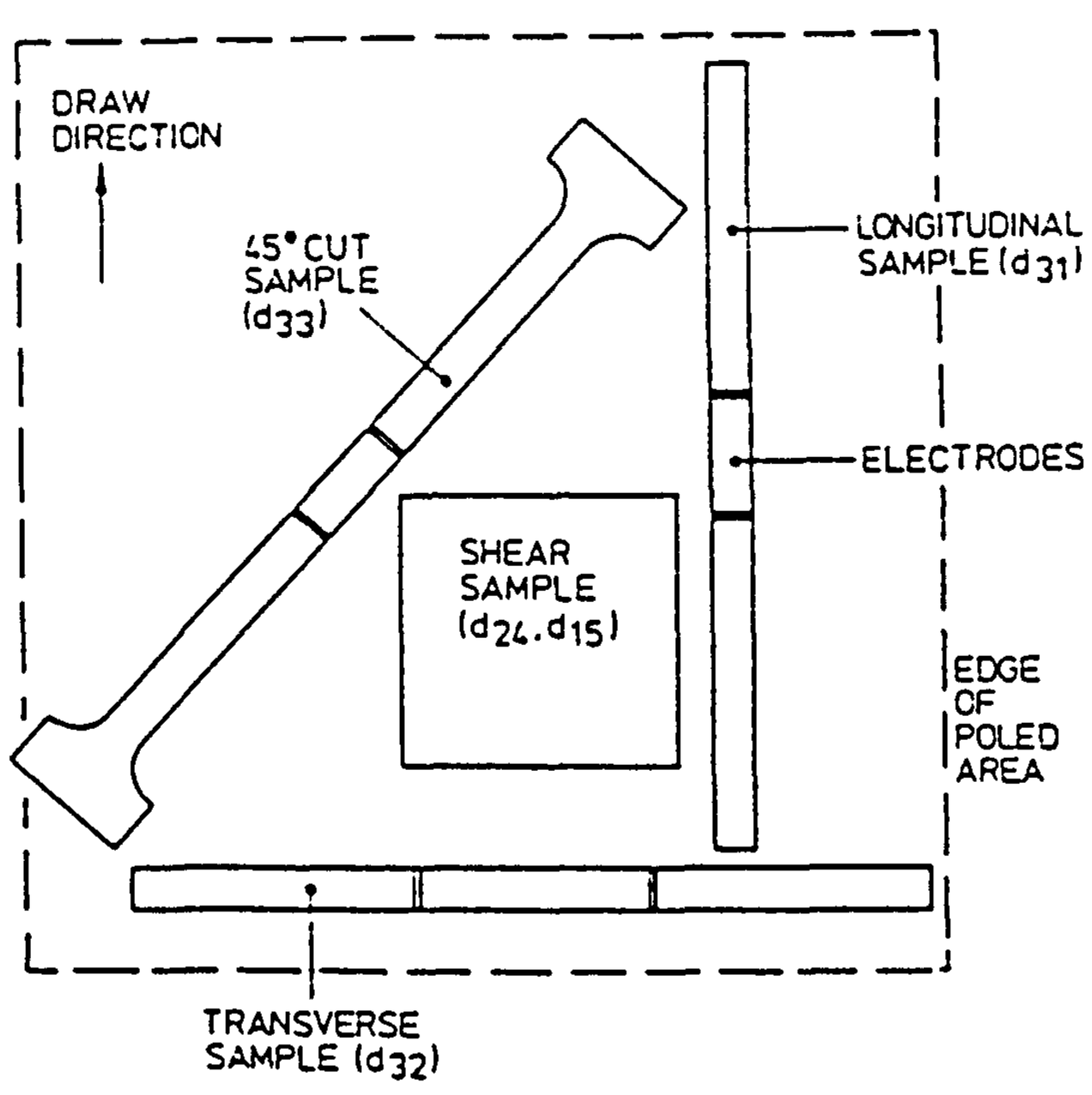

Figure 3.7 Typical arrangement of samples cut from poled area.

between the measured coefficient d^m_{33}, and the true coefficient d_{33}, which arose because the area of the deposited electrodes deformed as the film was stressed, i.e.

$$d^m_{33} = \frac{1}{A_3}\cdot\frac{d}{\partial\sigma_3}(A_3P_3) \qquad (3.iv)$$

where A_3 = area of electrode

P_3 = remnant polarisation

σ_3 = Stress.

Figure 3.6 shows the cell used in this method, and figure 3.7 shows the critical shape of sample cut out from the poled PVDF sheet at 45° to the draw direction.

By using a sample cut at 45°, and considering the new piezoelectric coefficients that would apply for a rotation of 45°, it was shown that,

$$d^m_{33} = -\frac{1}{A^1_3}\frac{\partial}{dp}(A^1_3P^1_3) \qquad (3.v)$$

if $\sigma'_1 = +p$, $\sigma'_2 = \sigma'_3 = -p$

where ^{1} refers to the new axes.

The above conditions of stress were achieved by superimposing tensile stress, $\sigma'_1 = 2p$ and hydrostatic stress $\sigma'_1 = \sigma'_2 = \sigma'_3 = -p$ in the cell. The area of the piston was twice the cross-sectional area of the sample, so that on application of hydrostatic pressure p, there was the simultaneous axial stress 2p, that was required.

Using equation 3.v, a plot of sample polarisation versus pressure gave d^m_{33} as the gradient.

Other Techniques (Dynamic Measurements)

A number of Japanese groups have used a technique originally developed by Fukada et al. (1969).

In this apparatus a thin film was held under tension, and the longitudinal stress on the sample was varied sinusoidally. The stress or strain and charge output from electrodes on opposite sides of the sample were measured simultaneously. This technique has been used to examine the frequency and temperature dependence (Fukada (1971b; 1974)) of the piezoelectric coefficients and generally it has been found, that the piezoelectric charge signal is not in phase with the stress or strain because of the viscoelastic nature of polymers.

Ultrasonic Measurements

Ohigashi (1976) and Bui et al. (1971) have used an acoustic resonance technique to measure piezoelectric properties. The technique consists basically of measuring the electrical impedance of a freely vibrating sample as a function of frequency near a resonance. From this dependence, the electro-mechanical coupling coefficients K_{31} , K_{32} and K_{33} are determined, and the piezoelectric coefficients are determined in turn from them.

Kepler reports that Dameron and Linvill (1980) have used a technique, whereby two sheets of PVDF were clamped between two high mechanical impedance metal posts and

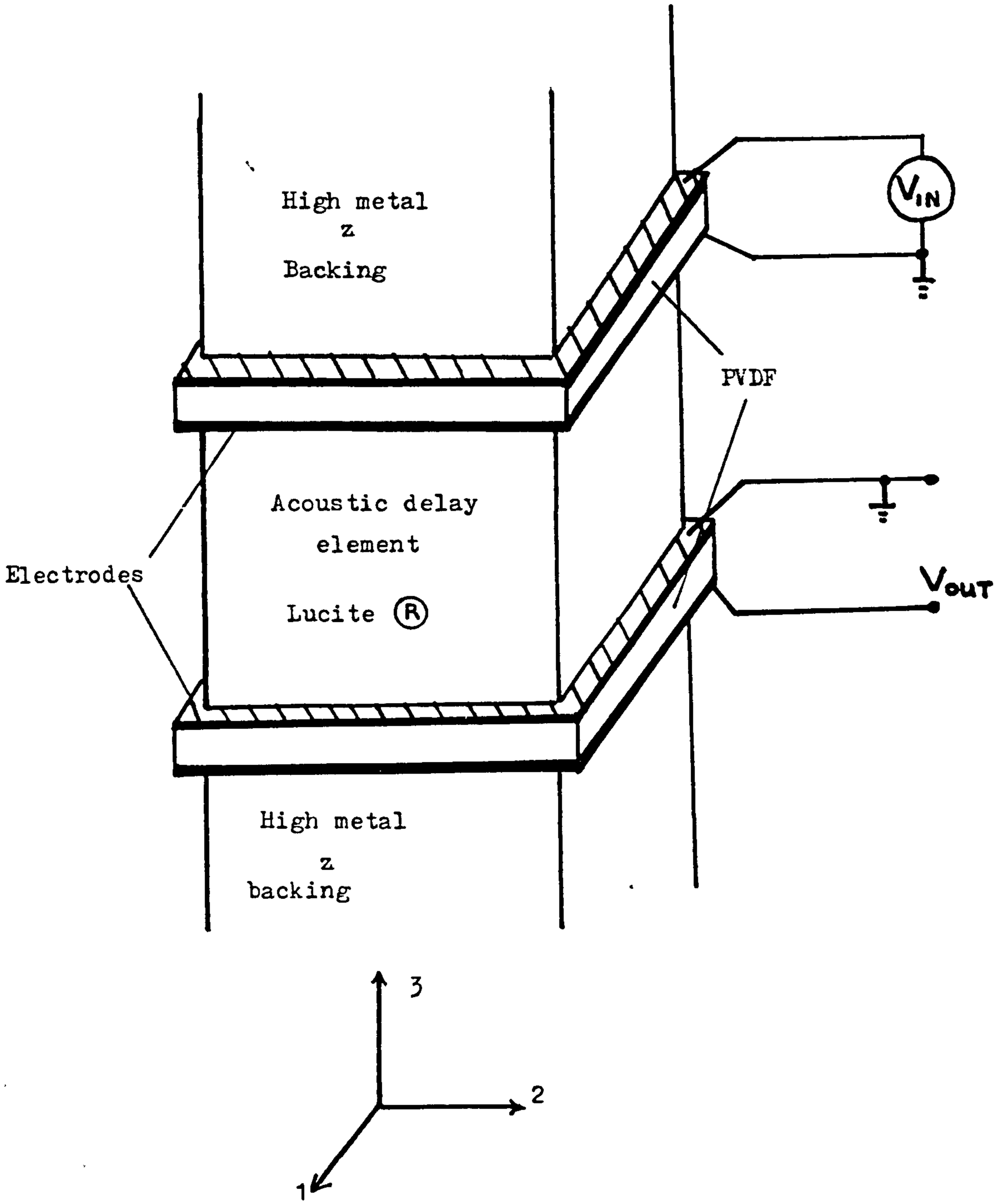

Figure 3.8 Experimental arrangement used by Dameron and Linvill (1980) for measuring K_{33} for PVDF.

separated by a sheet of Lucite ® which matched the mechanical impedance of PVDF. The spacer provided an acoustic time delay between a signal generated by one PVDF sheet and the detection of that signal by the other (see figure 3.8).

The value of K_{33} (and hence d_{33}) was then calculated from the ratio of the voltage used to generate the signal with one polymer film V_1, and the voltage detected in the other film V_2, by the equation, .

$$K_{33} = \frac{2}{1 - \frac{\alpha V_1}{V_2}} \qquad (3.vi)$$

where α is the loss of signal resulting from transmission through the spacer.

This technique was not limited to the resonance frequency of the sheet as in the case of Bui et al. (1971) and Ohigashi (1976), however, it does not allow the film to move laterally which is important. Linvill (Kepler and Anderson (1980)) has proposed that a similar technique can be used to measure K_{31} and K_{32}. .

Work by Alquie and Lewiner (1985) used a technique which examined the effect of a pressure wave propagation within a piezoelectric sample. The technique attempted to look at the uniformity of poling within samples which may be poor owing to the number of different processes that can take place during the application of high electric fields in the poling process itself. Figure 3.9 shows a schematic set-up for the technique, whereby the laser provides a

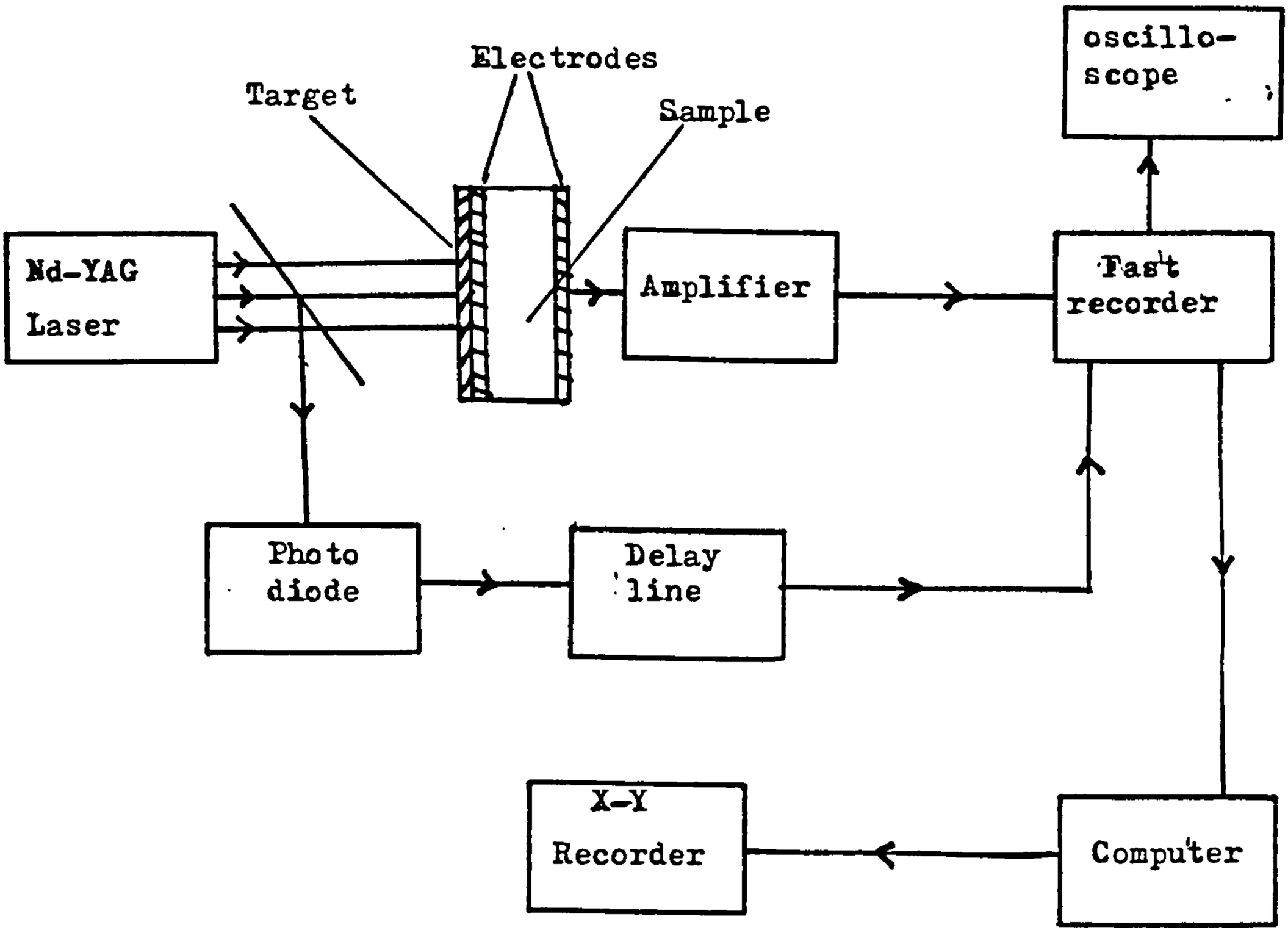

Figure 3.9 Experimental set-up used for laser-induced pressure wave propagation method, (Alquie and Lewiner (1985)).

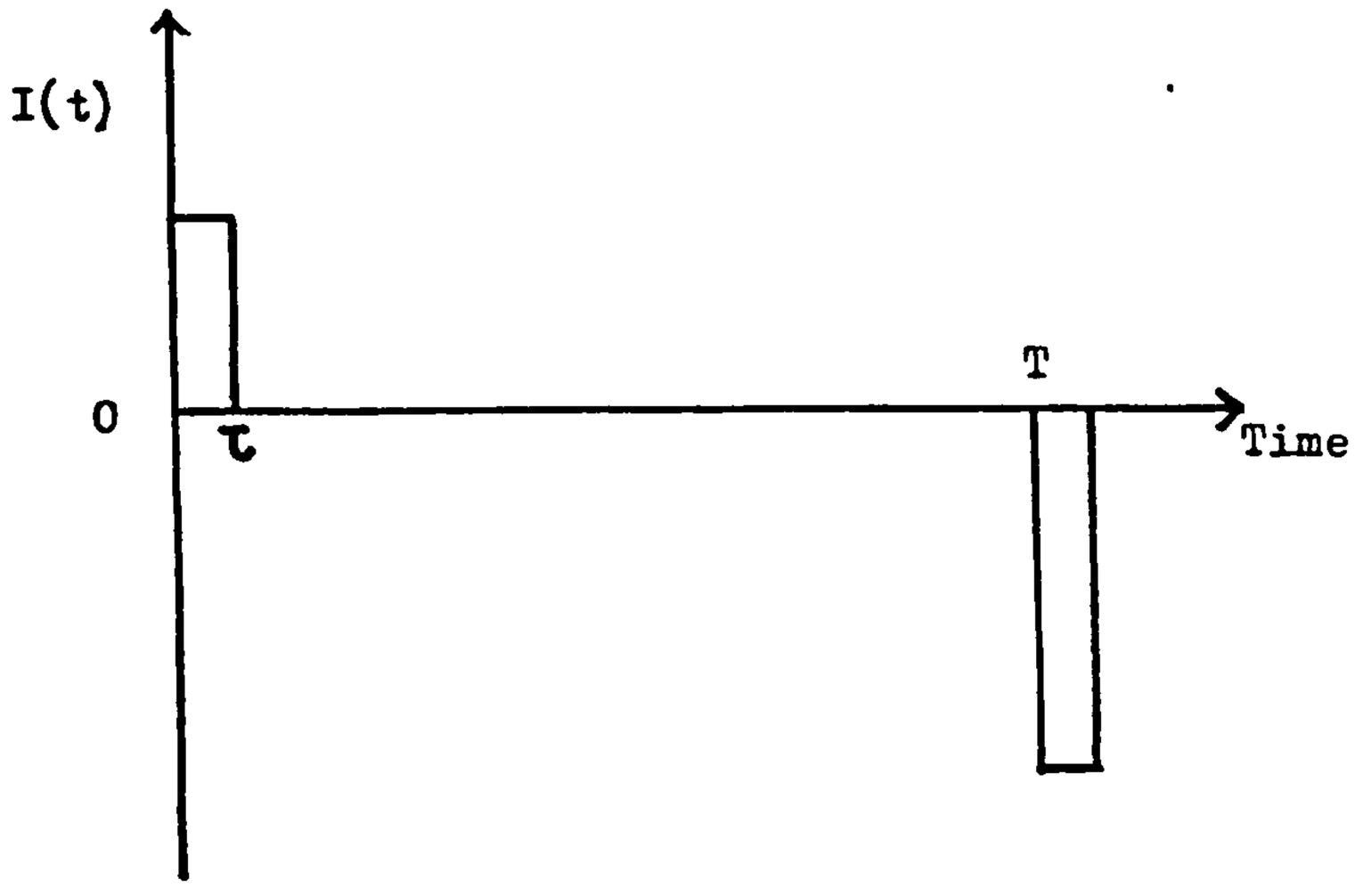

Figure 3.10 Current plot for material containing no space charge, no permanent polarisation, with uniform piezoelectric coefficient.

short (typically 30 ps to a few ns) pressure pulse on the surface of the sample. The pressure pulse then travels through the sample, interacting with the atomic structure before reflecting off the opposite side of the sample. The current produced as a result of this pressure wave is amplified and recorded against time.

Typical plots for some piezoelectric materials obtained by Alquie and Lewiner are given in figure 3.11a-c. Figure 3.10 shows the expected current-time plot for a material containing no space charge and no permanent polarisation, but with a uniform piezoelectric coefficient for the direction of pressure wave propagation. τ refers to the penetration time of the pulse within the sample, and T, the transit time through the sample. The amplitude of the second peak should be twice that of the first, and no current is observed between τ and T. Of the examples given, figures 3.11a,3.11b match closely with figure 3.10 and hence show good homogeneity of piezoelectricity over the whole sample. Only figure 3.11c seems to be a poor sample. Hence, the technique offers a useful probe for determining how well piezoelectric materials have been prepared, and therefore it may be used to optimise poling conditions.

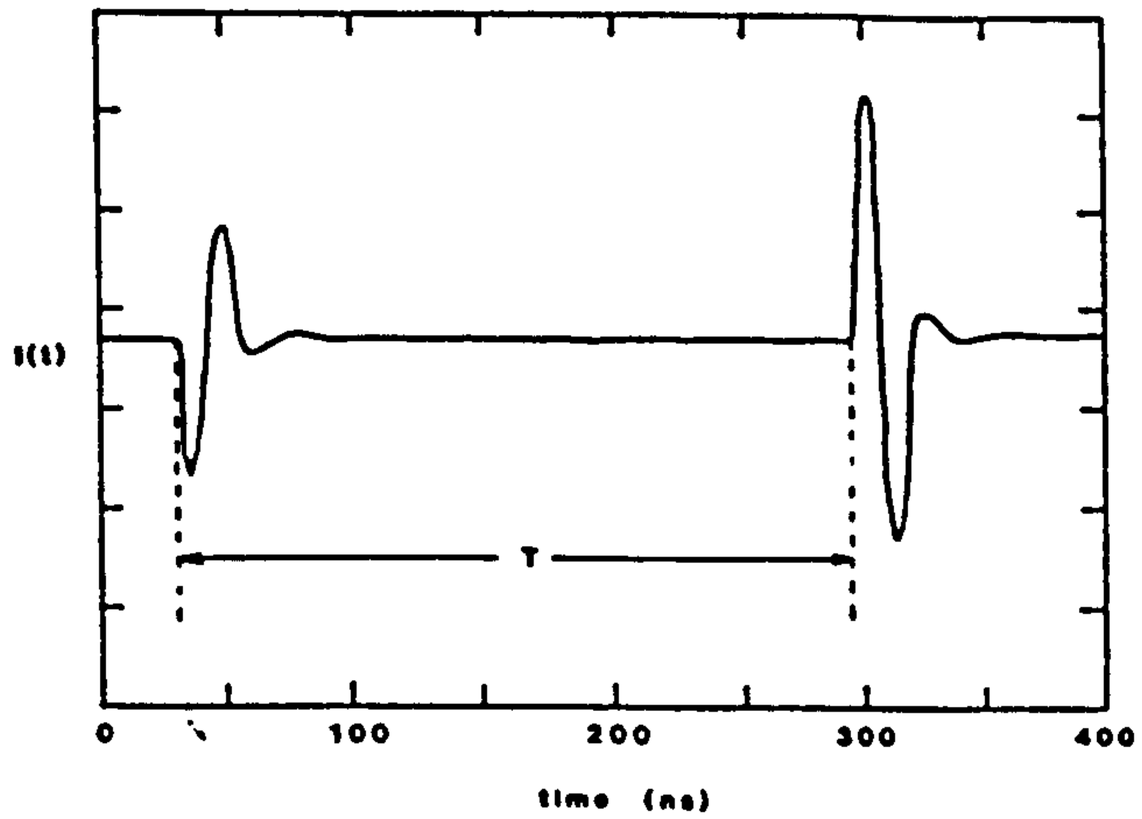

a) - Short-circuit current during the propagation of a pressure pulse in a 1.5 mm thick quartz crystal.

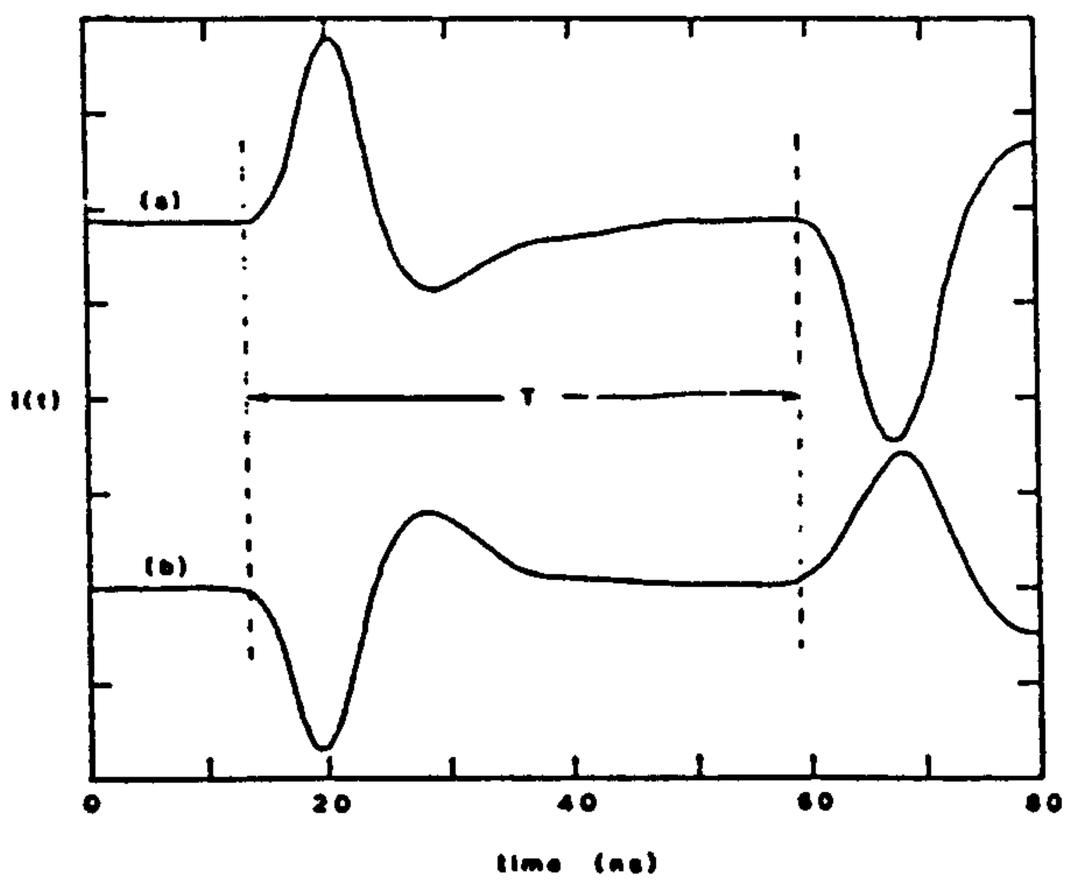

b) — Same as in figure a, for a 110 μm thick polyvinylidene fluoride film. a) For a propagation in one direction, b) For the reverse direction of propagation.

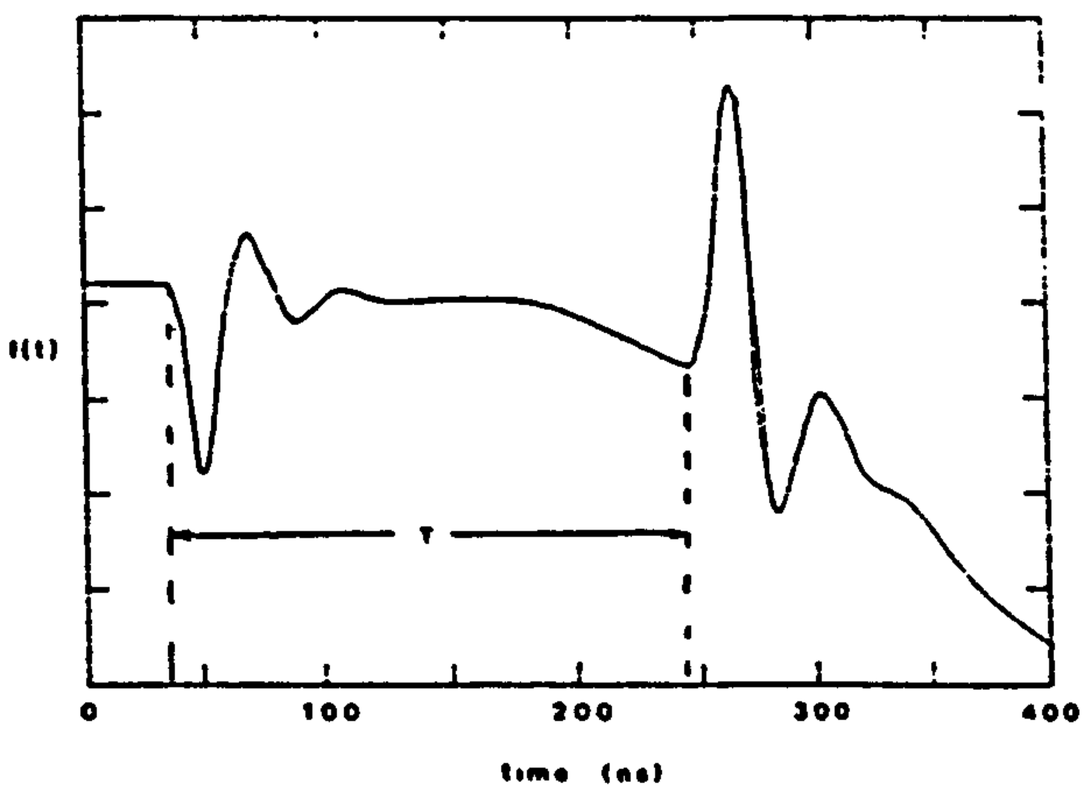

c) — Same as in figure a, for a 1 mm thick ceramic transducer.

Figure 3.11 Experimental current plots for some materials, (Alquie and Lewiner (1985)).

CHAPTER 4

NONLINEAR OPTICS

4.1 Basic Principles

Nonlinear optics examines the change in phase, frequency or amplitude of electromagnetic waves incident on various media. Classical physics shows using Maxwell's equations (Kip (1969)), that a light wave consists of an electric and magnetic field which oscillate at right angles to each other, as well as at right angles to the direction of propagation. If light passes through a medium, the velocity (c) of the wave is then represented by,

$$c = \frac{1}{(\mu \varepsilon)^{1/2}} \qquad (4.i)$$

where μ = permeability and ε = permittivity for medium in question.

The refractive index (n) of a medium is the ratio of the speed of light (c_o) in a vacuum to that in the medium, i.e.

$$n = \frac{c_o}{c} = \left(\frac{\mu\ \varepsilon}{\mu_c\ \varepsilon_o}\right)^{1/2} \qquad (4.ii)$$

where μ_o and ε_o are the respective values of permeability and permittivity for a vacuum.

Conducting materials tend to be opaque, so most transparent materials are non-magnetic, and will have μ the same as μ_o.

Hence, the refractive index of transparent materials may be related to the dielectric constant K by,

$$n = \sqrt{\frac{\varepsilon}{\varepsilon_o}} = \sqrt{K} \qquad (4.iii)$$

If we now consider a molecule within the medium which experiences a local electric field (E), which is a combination of the electric field from the traversing light beam and the "modifying effects" of the surrounding molecules, then the induced polarisation (P) of the outer electrons of the molecule may be represented as an expanded power series of E as follows:-

$$P = \alpha E + \beta E^2 + \gamma E^3 + \ldots\ldots\ldots\ldots \qquad (4.iv)$$

where, α = polarisability

β = second order hyperpolarisability

γ = third order hyperpolarisability.

For an isotropic material, the induced polarisation is always parallel to the electric field, and the first term of the equation applies, and may be written as,

$$P = \varepsilon_o \chi E \quad \ldots\ldots\ldots\ldots\ldots \qquad (4.v)$$

where χ = electric susceptibility (K-1).

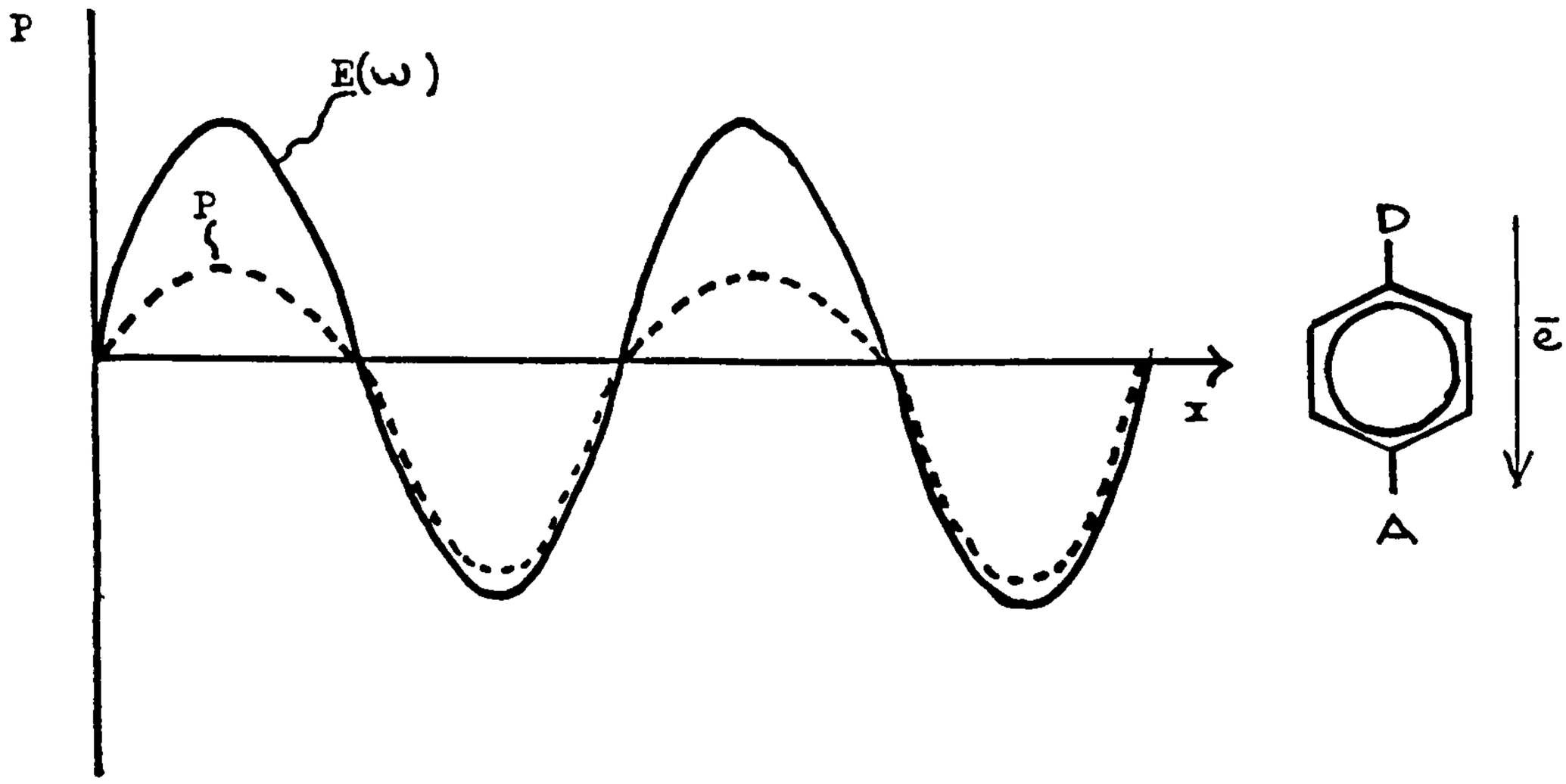

Figure 4.1 Non-centrosymmetric molecule.

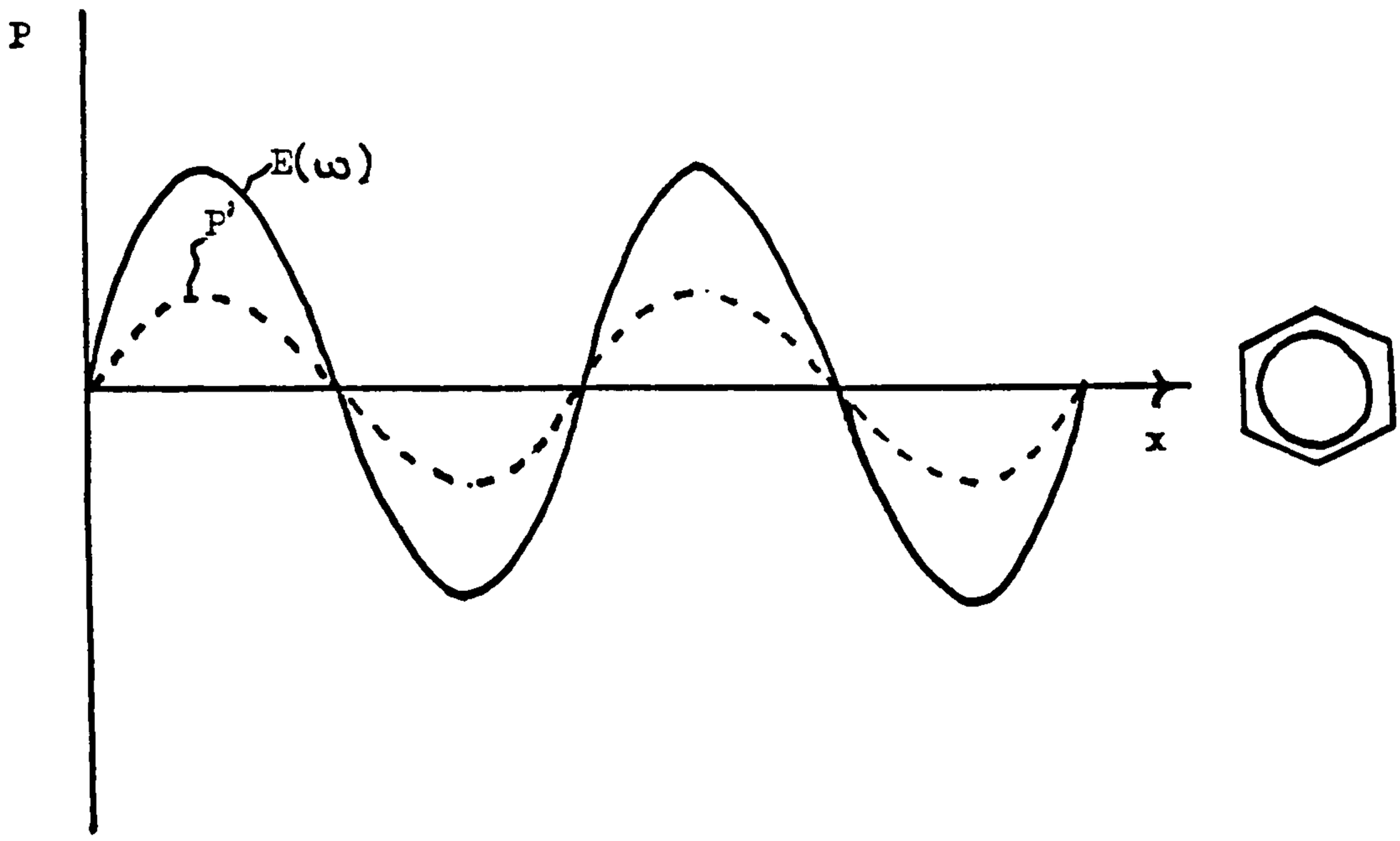

Figure 4.2 Centrosymmetric molecule.

Figures 4.1-2 Plots of nonlinear polarisation response, P, to an incident electromagnetic wave of field strength $E(\omega)$ at frequency (ω).

In the case of an anisotropic material, the induced polarisation changes with direction of the applied field, so that χ needs to be represented as a tensor. In other words, an anisotropic material shows a change in refractive index with angle, a phenomenon known as birefringence.

So far, only linear effects (i.e. proportional to the applied field) have been described, utilising only the first term of equation (4.iv).

The nonlinear effects can readily be explained in a molecule which is more easily polarised in one direction e.g. para-nitroanaline (p-NA).

Figure 4.1 shows how the donor/acceptor qualities of substituents favour polarisation of the molecule in one particular direction (i.e. amine to nitro in the case of p-NA as indicated by the asymmetric curve P). The equivalent curve P' as shown in figure 4.2, for the polarisation of a benzene molecule, indicates no such preference for polarisation in either direction, i.e. a symmetric response.

The Fourier Theorem (Dence (1975)), when applied to the two polarisation curves gives P and P' as a sum of sinusoidal functions. In the asymmetric case we find only even harmonics (0, 2ω, 4ω etc.), while in the symmetric case only the odd harmonics (ω, 3ω, 5ω etc.) can describe the polarisation. The general outcome of this is that the second harmonic coefficient (β) of a centrosymmetric molecule is zero, so no SHG occurs. The coefficients of the harmonic terms decrease with increasing

harmonicity, and hence, intense (laser) incident fields are required to detect the larger harmonic terms, (e.g. third harmonic generation).

The example not only highlights how the phenomenon of second harmonic generation (SHG) (frequency doubling) occurs for the p-NA molecule, but how SHG occurs in non-centrosymmetric structures in general, and hence is one of the important criteria required in designing molecules to show the effect.

Macroscopic Nonlinearities

When it comes to measuring nonlinear optical properties, the sample being tested is composed of many molecules. The "modifying effects" of neighbouring molecules have already been mentioned, and if β is to be calculated from a macroscopic measurement made on the sample, then these effects have to be taken into consideration.

For the case of a large volume of material, equation 4.iv may be rewritten such that,

$$P = \chi^{(1)}E + \chi^{(2)}E.E + \chi^{(3)}E.E.E \quad ..... \quad (4.vi)$$

where $\chi^{(n)}$ is the nth order susceptibility and corresponds to the macroscopic equivalents of α, β, γ etc..

4.2 Properties of Ideal Crystals to Show SHG

The need for a high β value and a non-centrosymmetric structure have already been shown to be the elementary requirements of a material for showing the SHG effect. However, for high average power SHG to be produced efficiently within a material, other criteria are also required.

a) The material must possess a high damage threshold allowing high intensity lasers to be used.

b) Closely related to the problem of threshold damage, is the optical absorption of the material at ω (the laser frequency) and 2ω (second harmonic). Not only will absorption reduce the intensity of the second harmonic, but also, the associated heating of the sample can lead to damage. This has certainly been a problem in designing organic molecules with conjugated π-electron systems, e.g. stilbenes which are coloured. Hence, one of the major challenges has been to make organic molecules with high nonlinearity, but with no absorption over the 350 to 850 nm range.

c) High thermal conductivity of materials would assist in reducing damage, by heat dissipation.

d) Most importantly, phase-matching of ω and 2ω must be achieved. Phase-matching is assisted by optical uniformity within the material (i.e. long range molecular order), but temperature variation within a sample can alter molecular positions leading to modification of phase-matched conditions.

Phase-Matching (Maker et al. (1962); Giordmaine (1962))

The SHG power $P(2\omega)$ generated by a monochromatic plane wave of angular frequency ω, and of power $P(\omega)$ in a parallel slab of thickness L can be expressed as:-

$$P(2\omega) = \frac{8(\mu_0)^{3/2}(\varepsilon_0)^{1/2}\omega^2 d_{ij}^2 P^2(\omega) L^2}{\pi h^2 n(2\omega)[n(\omega)]^2} \cdot \left[\frac{\sin(L\Delta k/2)}{L\Delta k/2}\right]^2 \quad (4.vii)$$

where, $n(\omega), n(2\omega)$ = refractive index of crystal at the fundamental and the second harmonic frequencies respectively.

d_{ij} = relevant SHG coefficient of the crystal,

h = spot diameter of the laser,

Δk = magnitude of the wave vector mismatch between the fundamental and the second harmonic wave such that

$$\Delta k = k_1(\omega) + k_2(\omega) - k_3(2\omega)$$

where, $k_1(\omega)$, $k_2(\omega)$ are the wave vectors of the fundamental, and $k_3(2\omega)$ is the wave vector of the second harmonic wave.

The origin of phase-matching is related to the relative speeds at which the fundamental and the second harmonic waves travel through the material. If the two waves start in phase, and travel at the same speed, the fundamental will induce further SHG within the material, which will add constructively to the second harmonic wave. Conversely, any mismatch in the speeds of the two waves will lead to induced SHG, out of phase with other second harmonic

components which will reduce the intensity of the wave.

To achieve velocity matching, $n(2\omega)$ must be equal to $n(\omega)$. However, refractive index is frequency dependent, so normal phase matching would not be expected for two differing frequencies. For a birefringent material, it is possible to find an angle of propagation through the material so that the two refractive indices are equal.

One implication of a material possessing a non-centrosymmetric structure, is that it then has one or more optic axes. If the crystal structure possesses only one optic axes, the crystal is said to be uniaxial, i.e. the refractive index is the same in the x and y plane but different in the z-direction. (the optic axis). For a biaxial crystal, there are two optic axes, and the refractive indices are different for all 3 cartesian directions.

Uniaxial Crystal

The uniaxial nature of a crystal can be shown schematically as a stacked pancake arrangement of molecular layers, as in figures 4.3(a) and 4.3(b) with the z-direction as the optic axes.

For figure 4.3(a), an electromagnetic wave moving along the optic axes has two components of polarisation in the xy plane, which may be in the x-direction and y-direction respectively. Owing to the uniformity of the refractive index (n_o) within that plane, the polarisation of the two components is the same and the electric field components E_x and E_y oscillating in the x and y directions can be

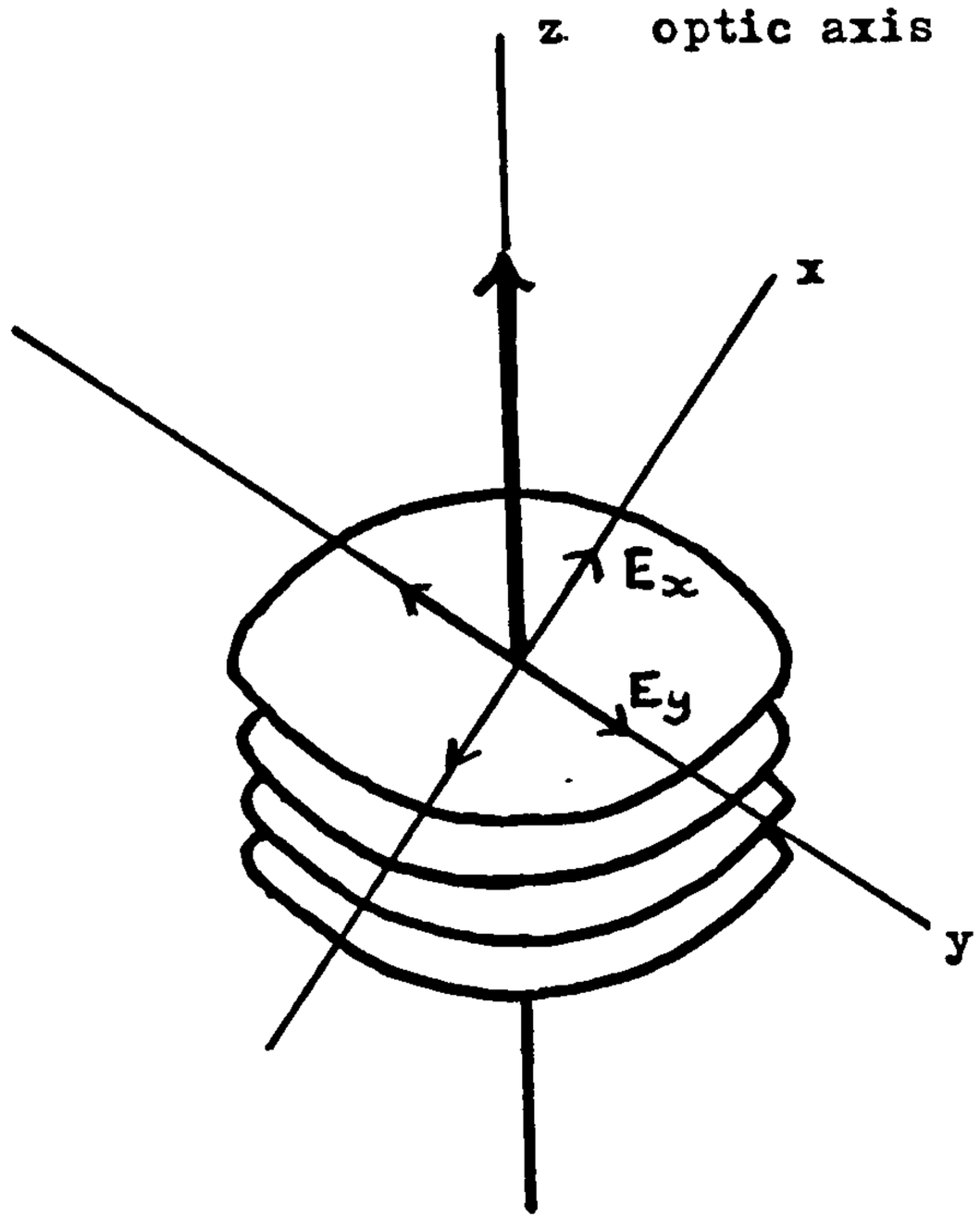

a) Propagation along the optic axis.

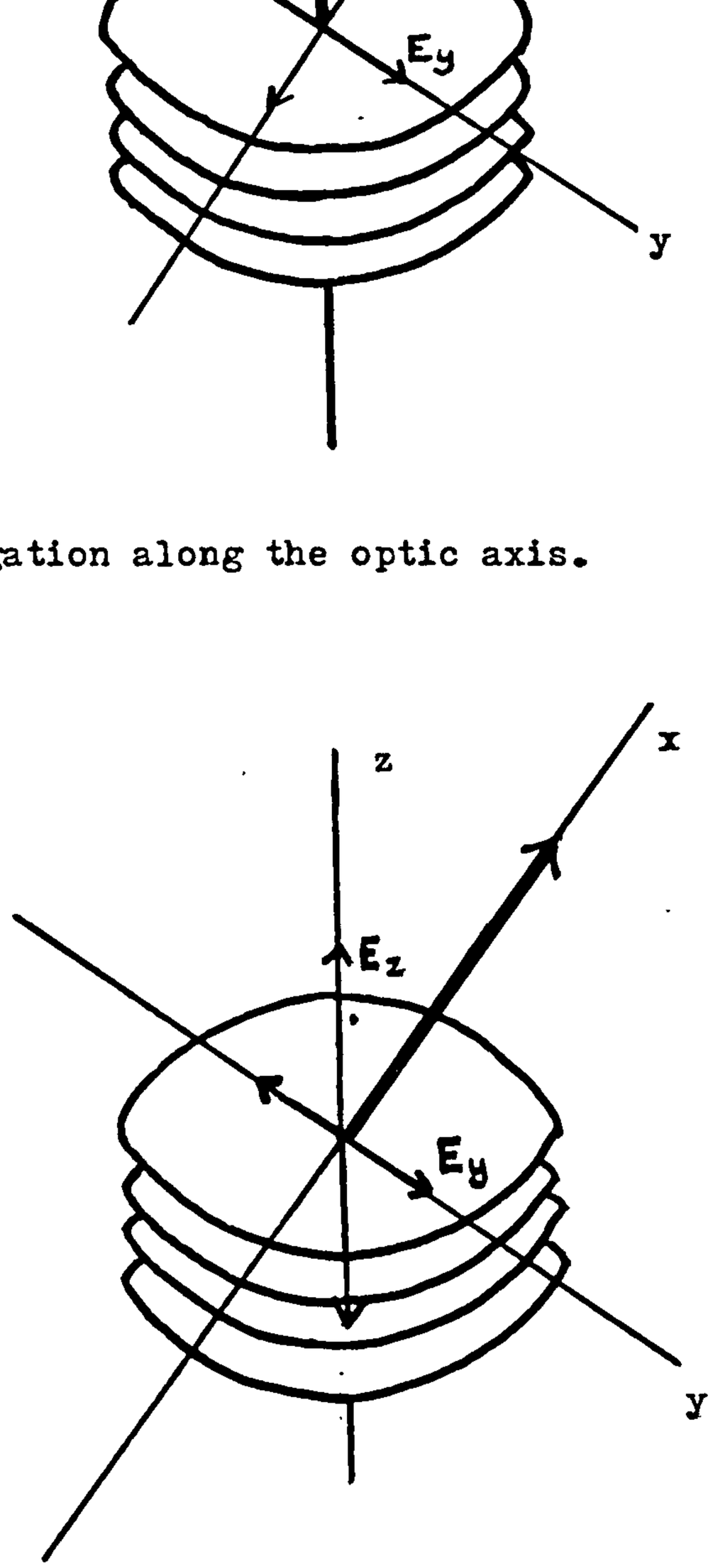

b) Propagation perpendicular to the optic axix.

Figure 4.3 Pancake arrangement of molecular layers in a uniaxial crystal.

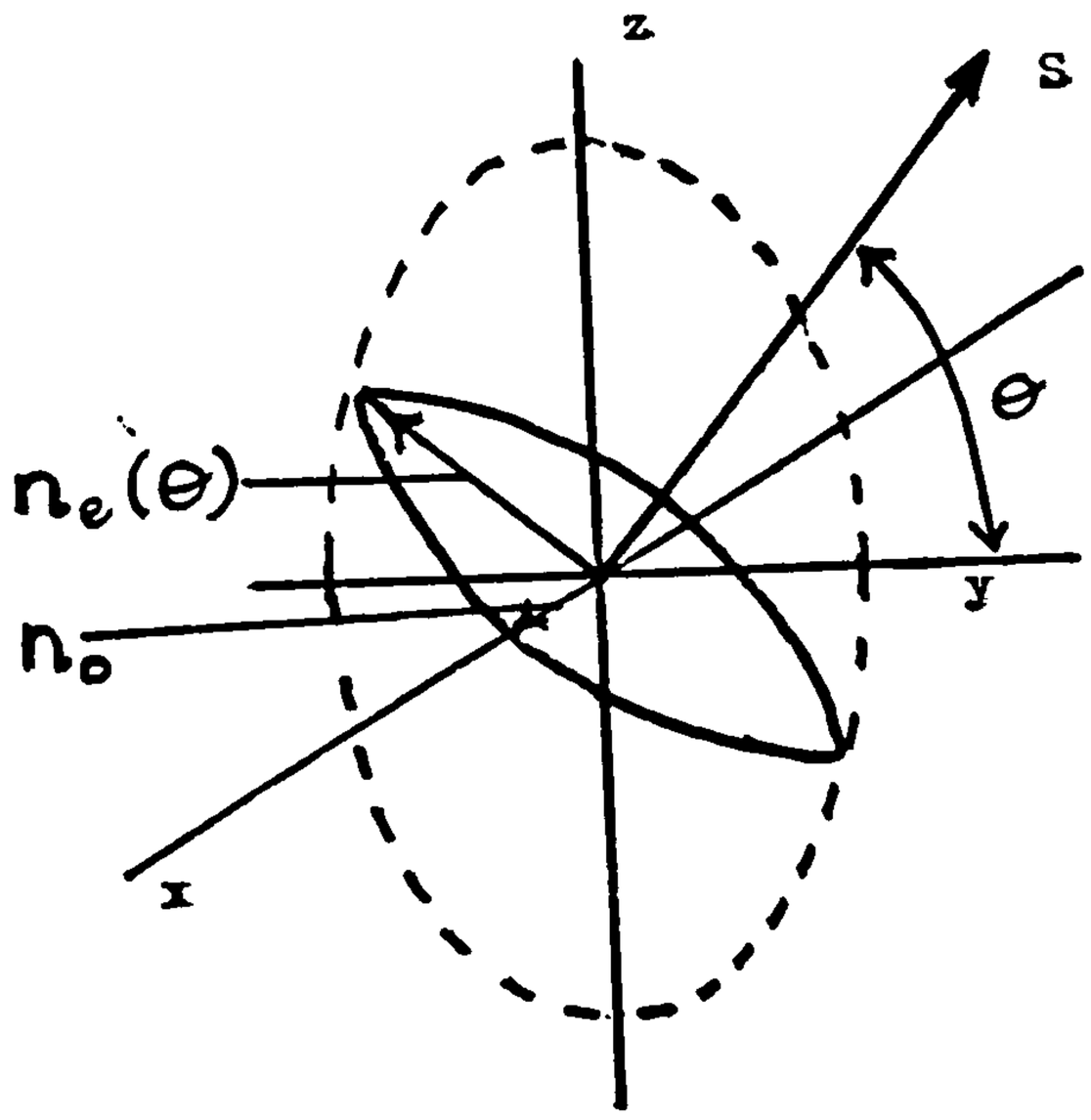

a)

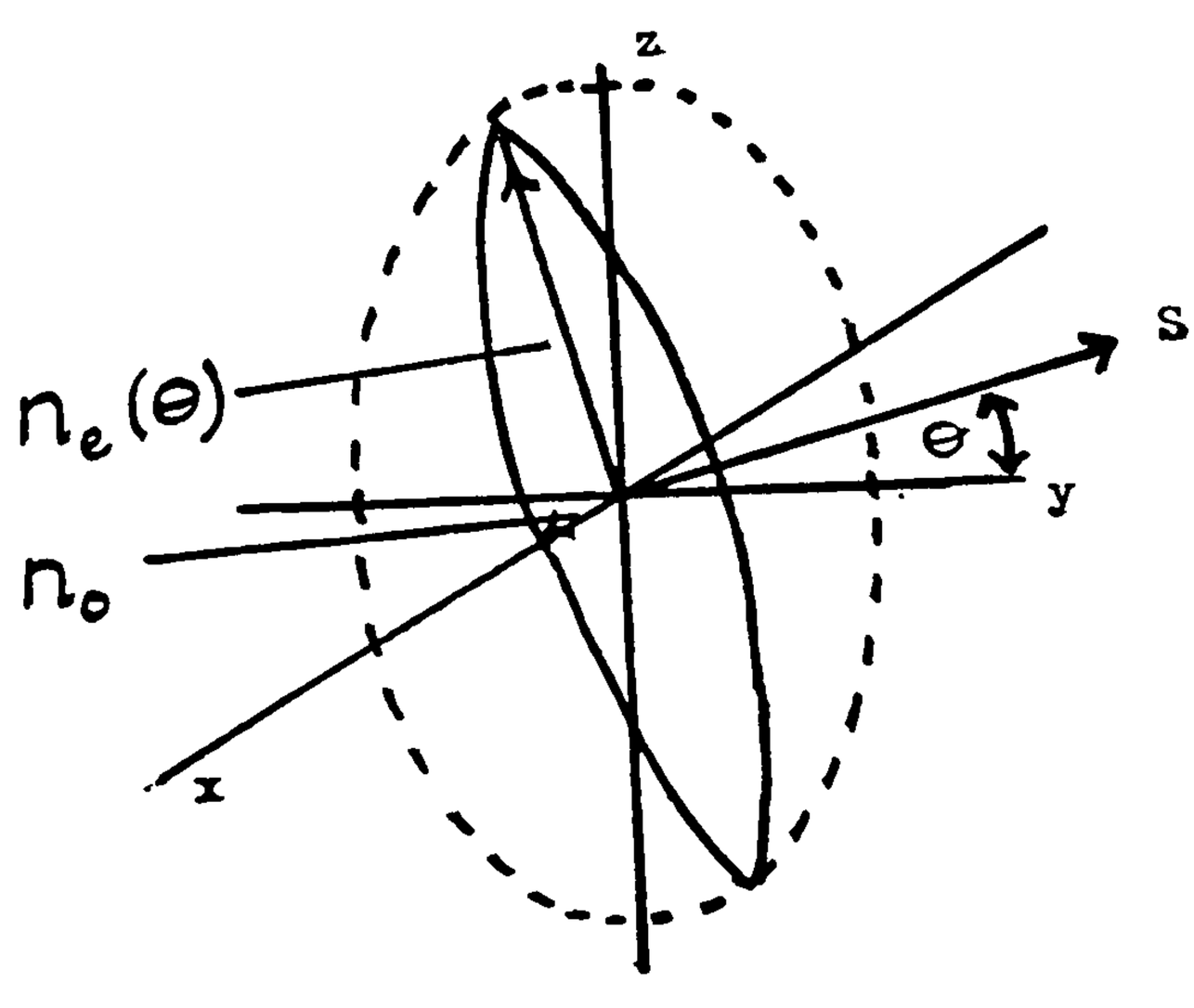

b)

Figure 4.4a-b The refractive index ellipse for a positive uniaxial crystal showing propagation in two directions.

described by:-

$$E_x = A_x e^{i(k_z z - \omega t)} \quad , \quad E_y = A_y e^{i(k_z z - \omega t)} \qquad (4.viii)$$

where, A_x and A_y are the amplitudes of the waves and, k ($= n_o 2\pi / \lambda_o$) is the wave vector.

For figure (4.3b), an electromagnetic wave moving in the x (or Y) direction has electric field components E_y and E_z where,

$$E_y = A_y e^{i(k_x x - \omega t)} \qquad E_z = A_z e^{i(\tilde{k}_x x - \omega t)} \qquad (4.ix)$$

where, $k_x = n_o \cdot \frac{2\pi}{\lambda_o}$ $\qquad$ $\tilde{k}_x = n_e \cdot \frac{2\pi}{\lambda_o}$

Note:- the value of refractive index used (n_o or n_e) for a wave vector is related to the direction of oscillation of the wave and not the propagating direction of the wave.

n_o and n_e are also referred to as the ordinary and extraordinary indices of refraction. As a consequence of these two differing refractive indices, the variation of refractive index in x, y and z space, can been shown to take the form of an ellipse. Depending on the relative magnitudes of n_o and n_e, the uniaxial crystal is referred to as negative ($n_o > n_e$) or positive ($n_e > n_o$).

Figures 4.4(a),4.4(b) show two situations for waves travelling through a positive uniaxial crystal, at two different angles. The wave propagation directions are indicated by the directions of the wave normals S. The

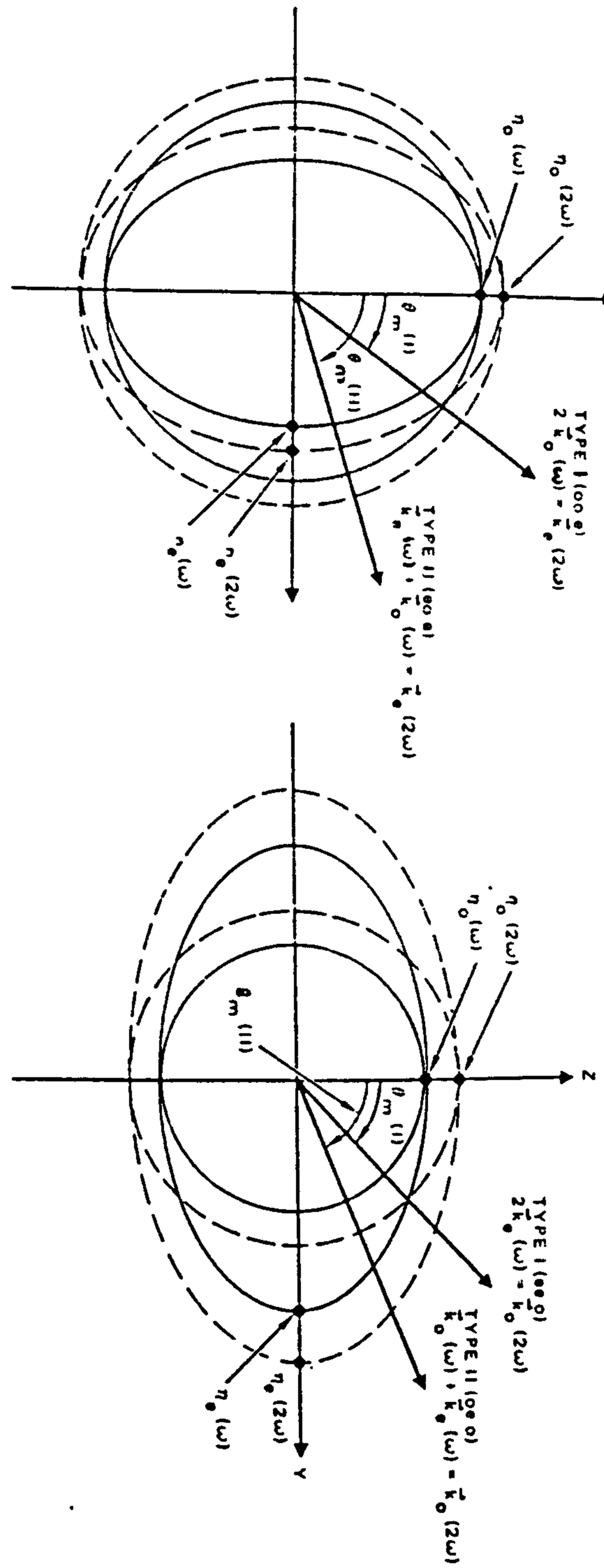

(a) Type I and II phase matching for SHG in a negative uniaxial crystal. The ordinary ray normal-surface of the fundamental (ω) wave intersects the extraordinary ray normal-surface of the second harmonic (2ω) wave, defining a cone (and its mirror image) of phase-matching wave normals [$k(\omega)$] shown here in a y-z plane projection. θ_m (I) and (II) are the phase-match angles. When either θ_m(I) or θ_m(II) equals 90°, noncritical phase-matching is obtained. (b) The corresponding diagram for a positive uniaxial crystal.

Figure 4.5 Phase-matching conditions for uniaxial crystals.

plane which is normal to S, (which contains the origin), intersects the ellipsoidal index, forming an ellipsoidal locus, whose semiaxes define n_o and $n_e(\theta)$.

For the two cases, n_o is independent of θ (which is universally true for uniaxial crystals) whereas, $n_e(\theta)$ varies between the values of n_e and n_o.

If it is assumed the example shown applies for a wave of frequency ω, then a similar ellipse exists with slightly different proportions which applies for twice this frequency, i.e. the second harmonic. By overlapping these ellipses, a possible phase-matching may exist, which has to take into account the problem that waves of differing frequency show different refractive indices in the same material.

Figure 4.5 summarises how it is possible for different components of $n(\omega)$ and $n(2\omega)$ to be equal at 2ω and ω, in the two possible cases of positive and negative uniaxial crystals.

(The subscripts o an e refer to the ordinary and extraordinary components, and $k(\omega$ or $2\omega)$ refer to the wave vector of the relevant wave frequency).

In summary:- type I phase-matching involves an ordinary component from one frequency matching an extraordinary component of the other;

type II phase-matching occurs if the fundamental wave can be coherently split between an ordinary and an extraordinary wave, (i.e. $(n_e(\omega, \theta) + n_o(\omega))$.

For each type, phase matching occurs for a particular

angle, the locus of which describes two cones (one being the mirror image of the other).

Biaxial Crystals

Phase-matching in biaxial crystals is a lot more complicated than in the uniaxial case owing to the three different components of refractive index. The relative size of these three components, dictates the shape of the loci of the phase-matching directions, for the two types of phase-matching. These are summarised in the paper by Hobden (1967).

4.3 Organic Materials For Second Harmonic Generation

4.3.1 Introduction

The requirement of SHG active materials to have no centre of symmetry either at the molecular, or in the bulk material state, has led to most device materials having to be based on single crystals associated with a non-centrosymmetric point group. It has also been recognised that in certain respects, organic materials could prove to be more suitable than inorganic ceramics, particularly in terms of the varied synthetic design routes available to the organic chemist.

As a result, great steps have been taken to try to understand how the design of organic molecules can enhance the observed SHG effect. Figure 4.6 gives an idea of the present state of play between inorganic and organic materials as far as nonlinear optics is concerned. Although

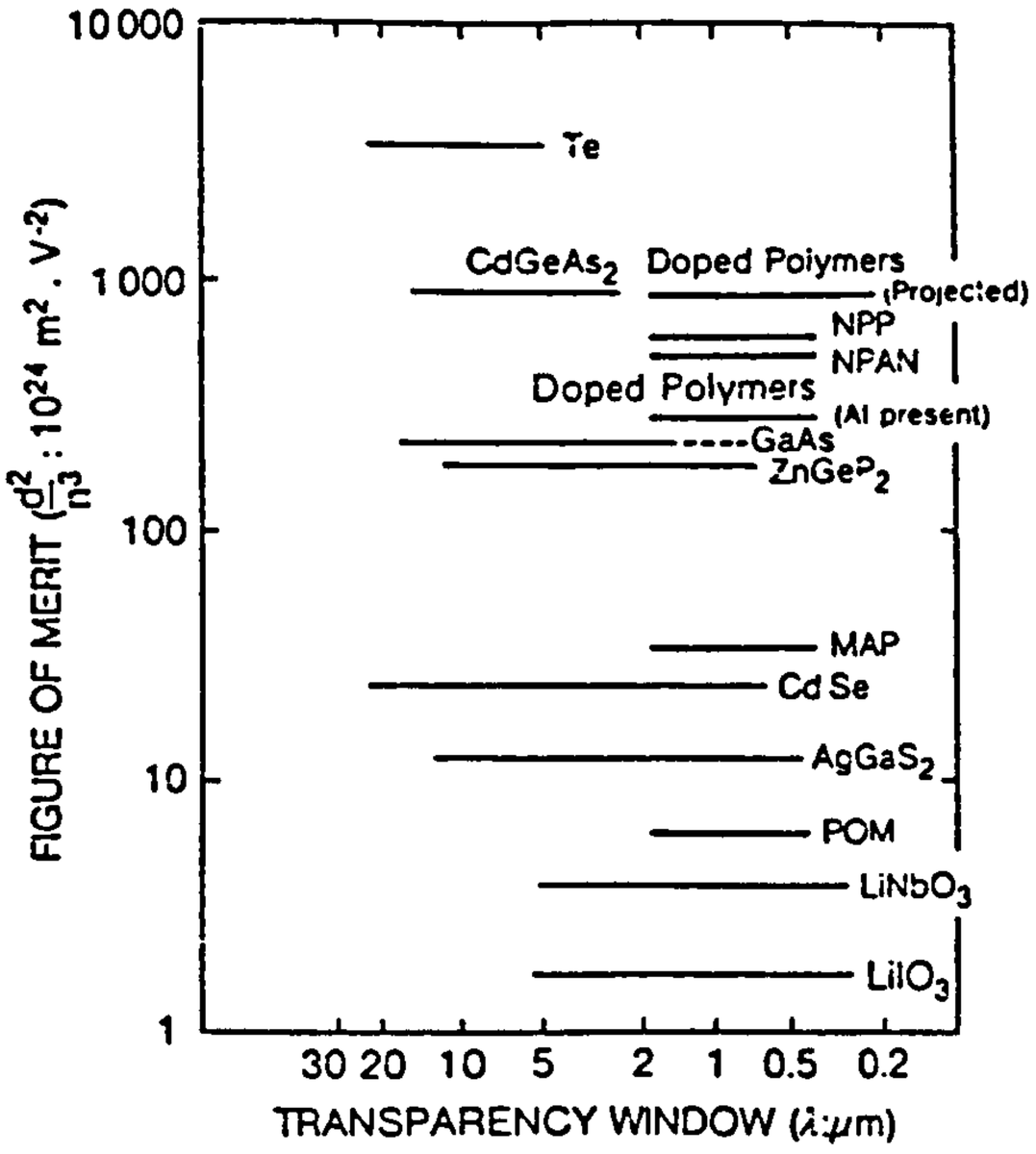

Figure 4.6 Comparison of SHG activity for inorganic and organic materials, (Broussoux et al. (1989)).

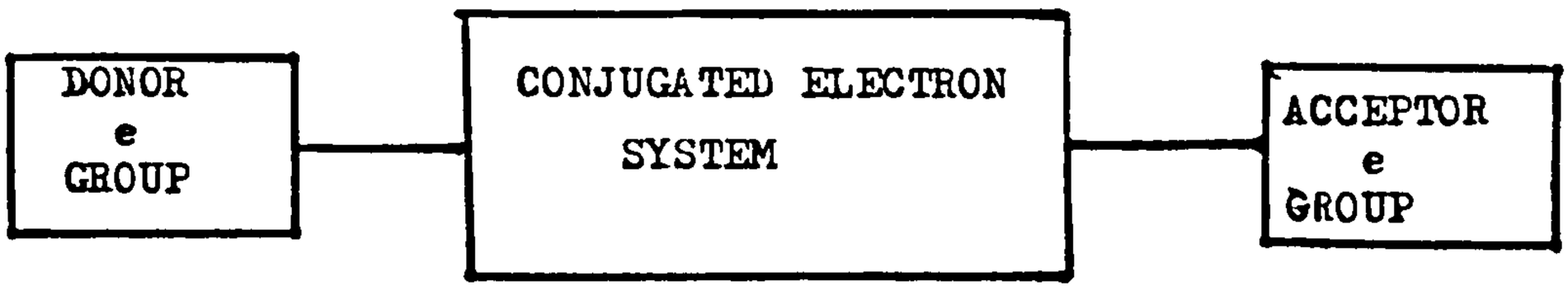

Figure 4.7 Basic molecular structure known to show good SHG.

the figure of merit offers some kind of comparison, it has already been mentioned (in the section on ideal crystal properties) how such factors as processability, optical damage, transparency and ageing must also be accounted for. Hence, the known ability of organic materials to resist high power laser beams (> GW.cm^{-2}), is particularly important in integrated optical applications.

Of the other factors mentioned, ageing and processability seem to be main areas for concern. As far as processability in organic materials is concerned, two main areas exist.

In the case of crystals, then similar problems to that of inorganic materials exist (i.e. single crystal growth). In the second case, doped polymer film manufacture (using spin coating techniques) occupies the main avenue of research. The efficiency of these films is clearly seen in figure 4.5, and they offer a route to the fabrication of nonlinear optical wave guides, overcoming the problem of the need for large area, single crystal substrates. However, the relaxation of aligned dipoles/molecules within poled polymer systems raises its head as an ageing problem in this area.

4.3.2 Molecular Structure

Since the early observations of SHG from organic molecules by Rentzepis and Pao (1964) and Heilmer et al. (1964), investigation into the effects of molecular structure on SHG efficiency has been considerable.

On a theoretical level, two semi-empirical methods have

been employed to assist the synthetic chemist, i.e. "finite-field" perturbation approach (Zyss and Chemla (1987)) and the sum over state approach (Pugh and Morley (1987)).

The general outcome that figure 4.7 represents a general molecular structure suitable for SHG activity, originates from the ease of electron mobility of the π-bond (c.f. the σ-bond) under an external electric field, and the contributing effects of the donor and acceptor groups, to remove the centre of symmetry of the π-electron cloud.

Hence, research using substituted benzene molecules (Levine and Bethea (1975)) and stilbene derivatives (Oudar (1977)) has been undertaken. In summary, a number of general points have arisen from this work.

In the case where the substituents interacted weakly with each other, theoretical polarisabilities were in reasonable agreement with observed experimental values. However, when an electron donor group and an electron attracting group were positioned at two electronically interacting sites of the conjugated electron system (i.e. allowing a strong charge transfer interaction between the D and the A groups), a large enhancement in β was observed. The value of for these molecules was subsequently separated into two parts:-

$$\beta = \beta_{add} + \beta_{CT} \qquad (4.x)$$

where β_{add} was an additive part associated with the substituent induced asymmetry in the charge distribution, and β_{CT} was the charge transfer effect.

The following expression, (derived from the perturbation approach) then became useful for predicting ideal molecular structures.

$$\beta_{CT} = \frac{3\, e^2 \hbar^2 W f \Delta\mu}{2m[W^2-(2\hbar\omega)^2][W^2-(\hbar\omega)^2]} \quad (4.xi)$$

where W = energy of optical transition (charge transfer band),

$\hbar\omega$ = fundamental photon energy,

f = the oscillation strength of the optical transition, and

$\Delta\mu = \mu_g - \mu_e$ = difference between ground and excited state dipole moment.

In general, the expression predicts that a large β should be obtained from molecules with a structure like figure 4.6, which possess a high transition probability (increasing f) and a large $\Delta\mu$. However, it is important to note other points.

1) Although dipole moments of ground state may be known for organic molecules, the excited state values are not necessarily available.

2) The absorption frequency of the charge transfer band should be close to twice the fundamental beam frequency. However, a compromise must be found here between SHG and transparency of the second harmonic frequency.

β values (10^{-40} m^4/V) for a series of p-disubstituted benzene derivatives obtained by the EFISH technique at λ = 1.89 μm in DMSO

D — C₆H₄ — A **3**

A \ D	CH_3	OCH_3	NH_2	$N(CH_3)_2$
CN	12	20	56	60
CHO		35		96
$COCH_3$			100	
NO_2	30 to 38	59 to 73	192 to 199	215

a)

β values (10^{-40} m^4/V) for a series of p-substituted nitrobenzene derivatives obtained by the EFISH technique at λ = 1.35 μm in DMSO.

$(CH_3)_2N$ — C₆H₄ — A **4**

A	NO_2	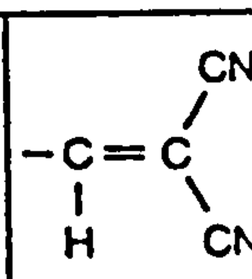	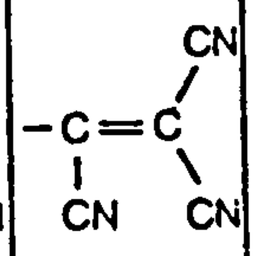
β (10^{-40} m^4/V)	88	130	326

b)

Figure 4.a-b Tables showing the effect of substituents on SHG activity.

β values (10^{-40} m^4/V) for a series of p-disubstituted polyphenyl derivatives c

H_2N–(C$_6$H$_4$)$_n$–NO_2 5	
n	β (10^{-40} m^4/V)
1	24
2	84
3	210

Figure 4.c Table showing the effect of length of conjugated π-electron system on SHG activity.

Influence of the planarity of the molecules on β values (10^{-40} m^4/V)

MOLECULES	β ($10^{-40}m^4V^{-1}$)
$(CH_3)_2N$–C$_6$H$_4$–C(CN)=C(CN)$_2$ 7	90
1,2-dihydroquinoline–C(CN)=C(CN)$_2$ 8	174
$(CH_3)_2N$–C$_6$H$_4$–CH=N–C$_6$H$_4$–NO_2 9	98
$(CH_3)_2N$–C$_6$H$_3$(OH)–CH=N–C$_6$H$_4$–NO_2 10	258

d)

Figure 4.d Table showing the effect of molecular planarity on SHG activity.

i) Nature of Substituents

Tables 4.a (Nicoud and Twieg (1987)) and 4.b (Katz et al. (1988), Leslie et al. (1987)) demonstrate the effect of different substituents on the SHG efficiency of the general molecules shown in each table. The trends in these values can readily be related to the relative strength of the electron-withdrawing or electron-donating ability of the substituents.

ii) Length of Conjugated π-System

Table 4.c (Leslie et al. (1987)) shows the positive effect of increasing the length of the conjugated π-system from one benzene to three. However, it was found (Allen et al. (1986)) that this was an optimum value for the length of the molecule, with further addition of benzene rings diluting the observed SHG efficiency of the bulk material.

iii) Planarity of Molecules

Table 4.d (Leslie et al. (1987)) shows two examples of how the change in planarity of the conjugated system with different substituents improves the SHG efficiency. In the first case, the covalent bond to the benzene ring (molecule 8), forces coplanarity. In the second case, the ortho hydroxy group produces an intramolecular hydrogen bond which holds the molecule in a planar structure.

4.3.3 Measurement of SHG Efficiency(β)

A number of techniques exist for the measurement of SHG efficiency of prepared samples.

i) Kurtz Powder Technique (Kurtz and Perry (1968))

This is a quick, convenient method which allows rapid analysis of powdered polycrystalline samples, and which removes the need for the growth of large single crystals.

In the technique, the use of a powdered sample allows statistical averaging to occur in that the laser beam used to test the samples strikes a large number of randomly oriented molecules. Control of the powdered sample particle size is particularly important in the technique, as particle sizes close to the coherence length of the sample, improve the observed SHG signal.

The technique can only be used on samples which are non-centrosymmetric polycrystalline materials, and hence it is a useful tool for the screening of prospective compounds for subsequent large single crystal studies.

ii) Electric Field Induced Second Harmonic (EFISH) Generation (Bethea (1975))

Unlike the Kurtz powder technique, samples for EFISH do not necessarily need a non-centrosymmetric crystalline structure, because the samples are tested in solution, and the application of a D.C. electric field removes the orientational averaging.

4.3.4 Polymeric Materials for Nonlinear Optics

Polymeric materials for nonlinear optics can be categorised into a number of general areas, which basically involve the incorporation of active molecules/moieties within polymer matrix systems.

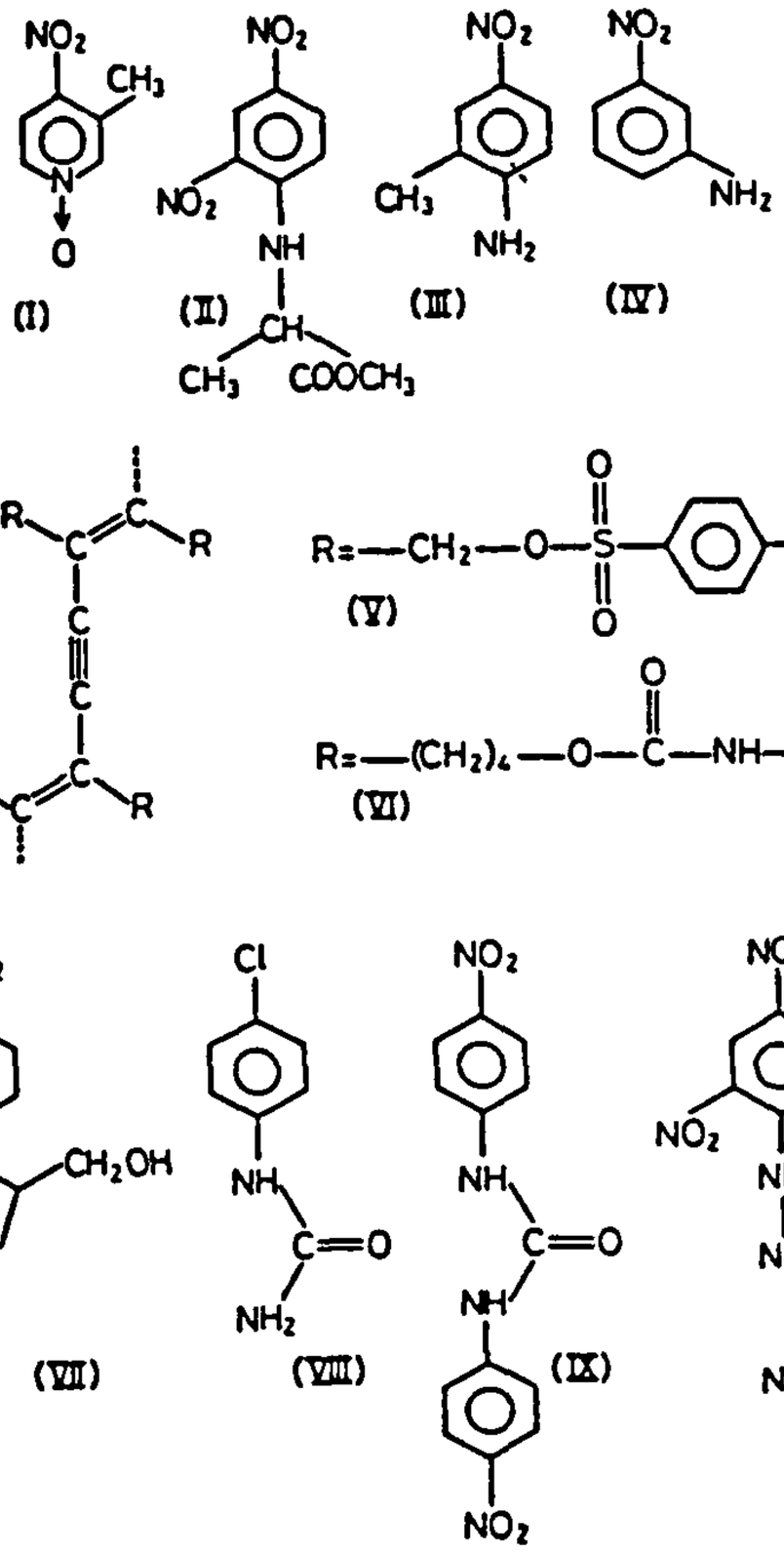

I 3-methyl-4-nitropyridine-1-oxide (POM)
II methyl-(2,4-dinitrophenyl)-aminopropanoate (MAP)
III 2-methyl-4-nitroaniline (MNA)
IV *meta*-nitroaniline (mNA)
V polydiacetylene with diacetylene monomer: bis (*p*-toluene sulphonate) 2,4-hexadiyne-1,6-diol (PTS)
VI idem with monomer: bis-(phenylurethane) of 5,7-dodecadiyne-1,2-diol (TCDU)
VII *N*-(4-nitrophenyl)-(L)-prolinol (NPP)
VIII *para*-chlorophenylurea (PCPU)
IX di-(*p*-nitrophenyl)-urea (DNPU)
X 1-(2,4-dinitrophenyl)-semicarbazide (DNP-SC)
XI 12-(4'-nitro-4-dimethylaminoazobenzene-3'-carboxyloxy)stearic acid
XII 12-(4'-nitro-4-dimethylaminostilbene-3'-carboxyloxy)stearic acid

Figure 4.8 Selection of typical SHG active moieties.

i) Guest host system:- by mixing free molecules in a matrix. (Poly(methylmethacrylate) has been one system used as the polymer matrix).

ii) Grafted system:- by grafting active molecules on to chains.

iii) Copolymer system:- copolymerizing monomers containing active molecules and nonactive monomers.

iv) Excluded zone system:- crystallising active molecules in a matrix, (Azoz et al. (1990)).

The matrix can be amorphous (Esselin et al. (1988)), liquid crystalline (Meredith et al. (1982)) or semicrystalline and ferroelectric or not, which are summarised in the paper by Broussoux et al. (1989).

In general, the active moieties resemble the conjugated π-electron systems previously described, although in the grafted and copolymer systems, certain chemical groups are required (e.g. reactive groups, monomeric qualities) to allow the desired side chain and copolymerisations to take place. Figure 4.8 shows a typical selection of active moieties.

In the liquid crystal matrix, side chain liquid crystal polymers are used in the hope that the inherent alignment in the liquid crystal regions will assist the alignment of the active additive (Williams (1984)).

Common to all these systems is the need to pole these materials using a thermal cycle, to produce the non-centrosymmetric structure. Broussoux et al. (1989) compares a guest host system and a copolymer system where the active

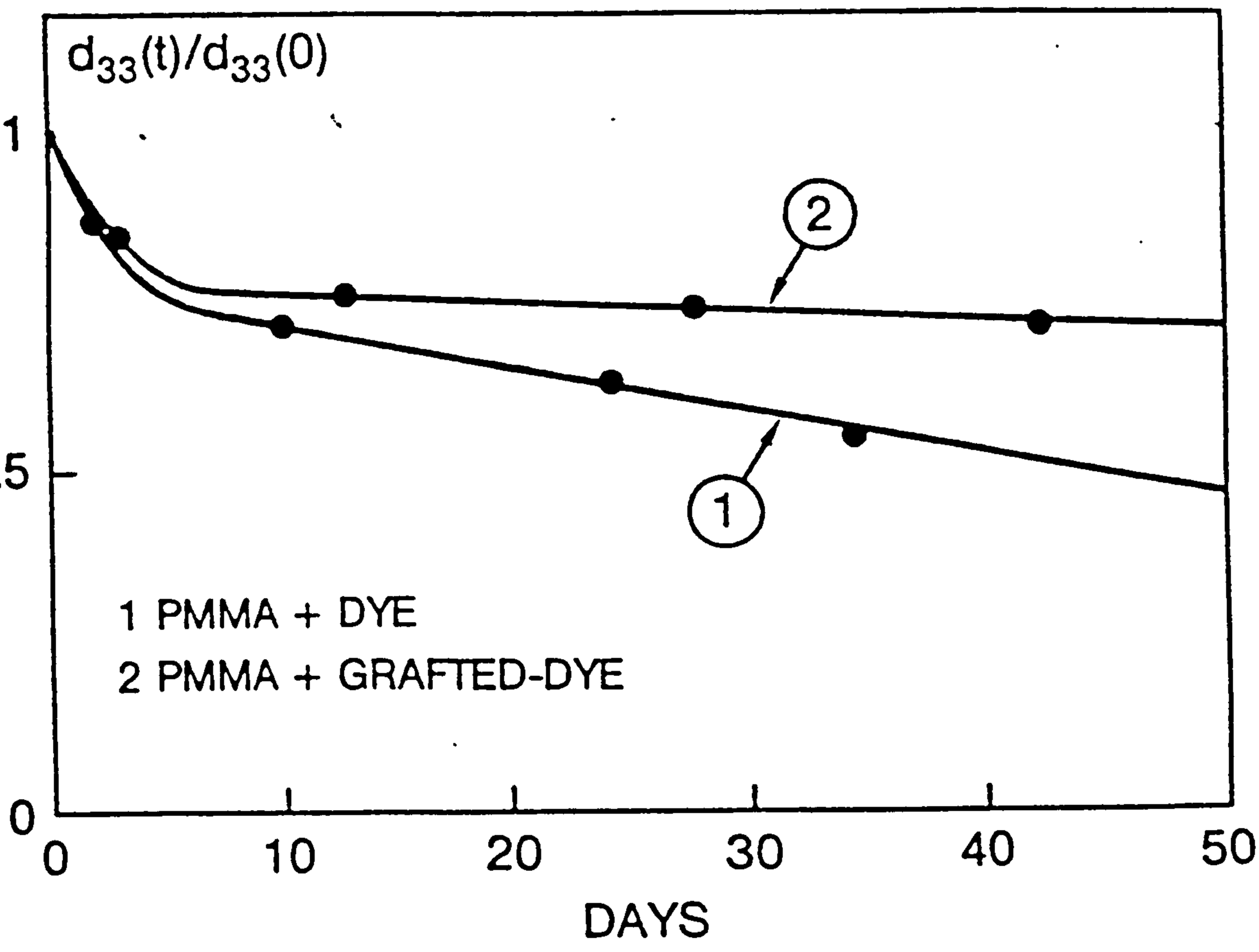

Figure 4.9 Ageing of SHG signal in poled polymer systems.

moiety in each case is essentially the same. Similar trends of SHG signal versus electric field (square law with intensity), poling temperature (maximum around T_g) and concentration of active component (linear dependence with d_{33}) were observed for the two cases. More interestingly, the retention with time of the SHG activity was greater in the copolymer case because of its grafting to the main chain (figure 4.9). Reference is also made to certain ferroelectric copolymer derivatives of PVDF which seem to show better retention of SHG signal with time although they are not so active as the doped systems.

Similar decay of SHG signal as that depicted in figure 4.9 is also observed in a paper by Dai (1990), for polyphenylene ether based poled thin films.

4.5 Applications of Nonlinear Optical Materials

In some cases, the measurement of SHG is of secondary importance as other applications utilising the $\chi^{(2)}$ coefficient can be more interesting. In addition, the measurement of $\chi^{(3)}$ is far more important for nonlinear optical materials with centrosymmetric structures. Hence, the following table highlights applications associated with $\chi^{(n)}$ coefficients in general.

Coefficient	Effect	Application
$\chi^{(1)}$	refraction	optical fibres/waveguides Zyss (1985)
$\chi^{(2)}$	SHG	frequency doublers in Lasers (e.g. C.D. Player Broussoux et al. (1989))
$\chi^{(2)}$	Pockels or Electro-optic Effect	Electro-optical Modulators Broussoux et al. (1989)
$\chi^{(3)}$	Third Harmonic Generation	Frequency triplers Zyss (1985)

CHAPTER 5

LANGMUIR BLODGETTRY

5.1 Historically

The first scientific mention of floating organic monolayers is Benjamin Franklin's (1774) communication to the Royal Society in 1774 which described how one teaspoon of oil spread out to over one half an acre on a lake on Clapham common. It was Lord Rayleigh (1890) however, whose simple quantitative measurement estimated this layer of oil to be only one nanometre thick. Research then moved into the kitchen, where Pockels (1891) used her sink as what we now call a Langmuir trough. It was in an early paper (Langmuir (1917)), that Langmuir described such a trough, and how it could be used to measure the size and shape of molecules dispersed on an air-liquid interface. He also reported the transfer of such molecules onto a solid substrate, but it was Blodgett (1935) who gave the first detailed account of such transference. Hence these transferred monolayers became known as Langmuir-Blodgett films.

Technique and Materials

The Langmuir-Blodgett (L.B.) technique offers a controlled method of producing well ordered assemblies of molecules, which can be as thin as a single monolayer.

In general, the molecules used in this technique are long chain, amphiphilic (both hydrophilic and hydrophobic) organic molecules, which are able to disperse on an air-liquid (usually aqueous) interface. Figure 5.1 shows some

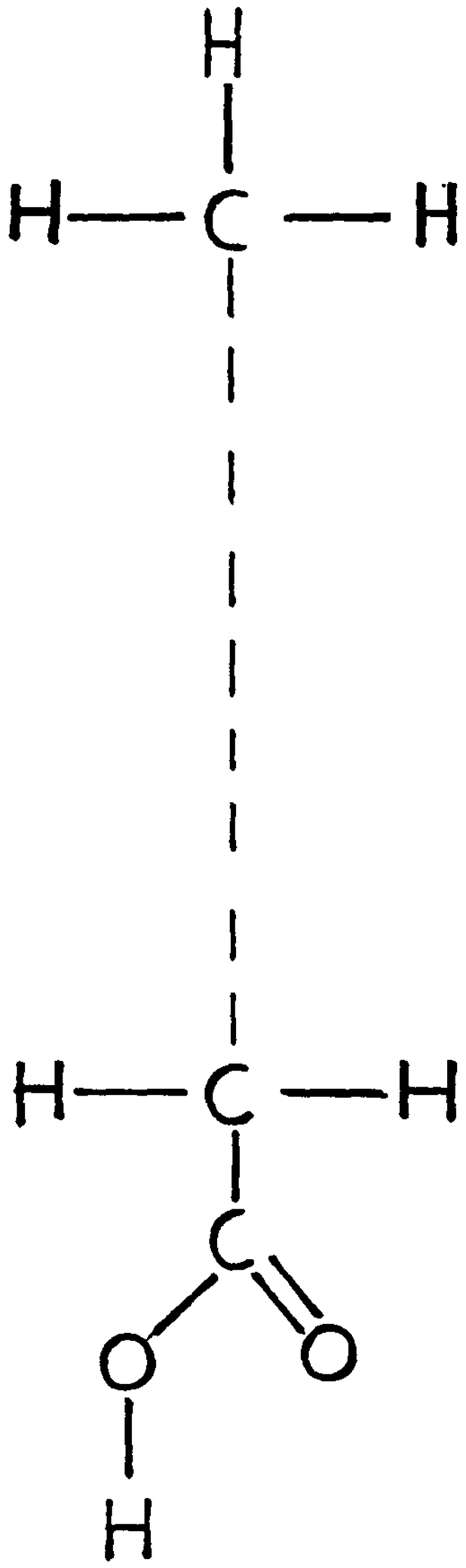

$C_{17}H_{35}COOH$

Stearic Acid

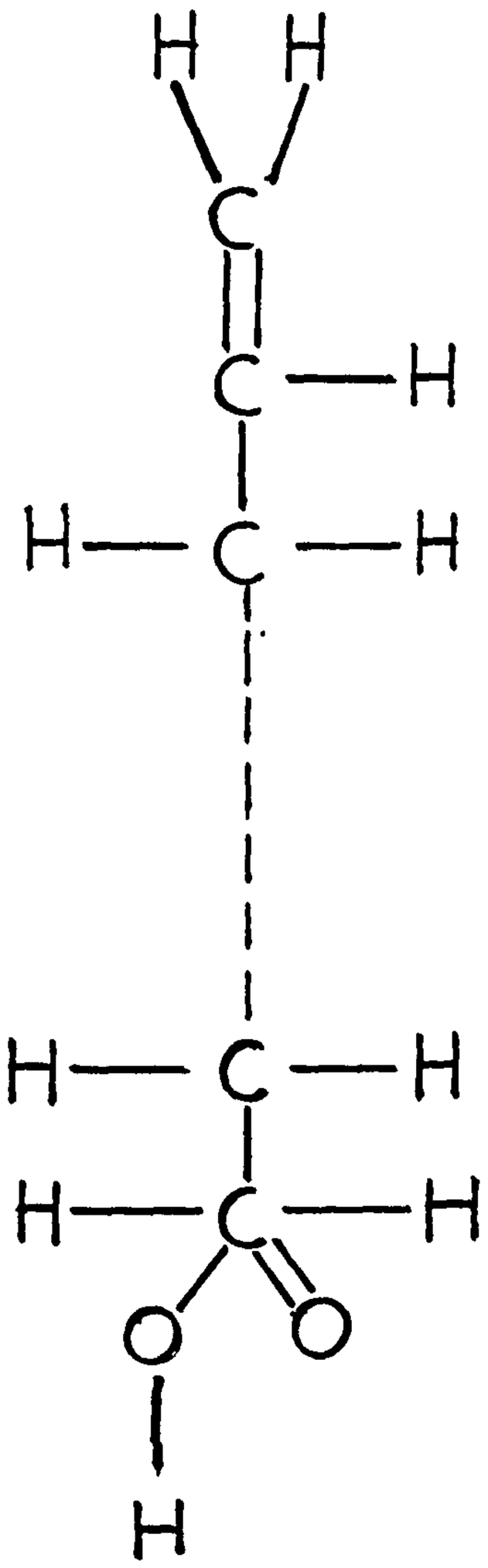

$CH_2=CH(CH_2)_{20}COOH$

ω -Tricosenoic Acid

Figure 5.1 Typical L.B. molecules.

typical examples of these molecules, with their hydrophobic alkyl chains, and hydrophilic heads. It is the polar heads which attach themselves to the interface while the hydrophobic chains extend above it.

Other types of polar heads which have been fitted to the alkyl chains are as follows:- $-CH_2OH$, $-CN$, $-CONH_2$, $-CH=NOH$, $-C_6H_4OH$, $-NHCONH_2$, $-NHCOCH_3$. However, such groups as $-SO_3^-$, or $-NR_3^+$, have gone too far by rendering the molecules soluble, in a similar manner to detergents.

Although, earlier research into the L.B. technique used long alkyl chains and short polar heads as in figure 5.1, the subsequent use of aromatic groups and unsaturated chains has tended to reduce the length of chain necessary for deposition.

5.2 Langmuir Films and Langmuir Blodgett Films

Molecules are deposited on the surface by first dissolving in a volatile solvent (preferably immiscible with water), which is then applied to the surface and allowed to evaporate. At this stage, the molecules do not dissolve because of their hydrophobic tail, and do not evaporate because their polar heads strongly attach to the surface.

The molecules can now be compressed on the surface by moving barriers, so that a complete monolayer will eventually form once the enclosed area (between the barriers) is sufficiently small. The complete floating monolayer is now specifically known as a Langmuir film.

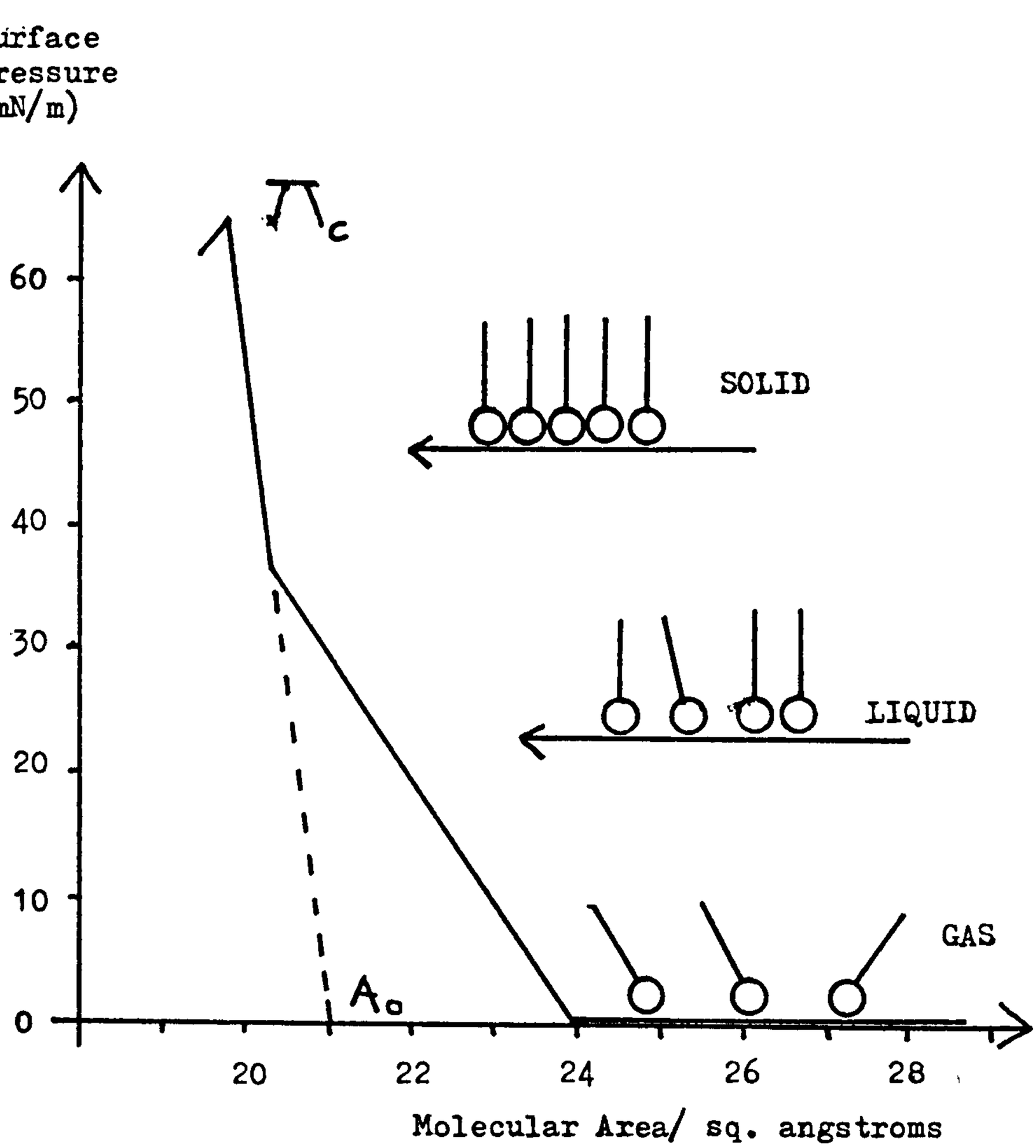

Figure 5.2 Schematic pressure-area isotherm.

It was Blodgett and Langmuir who developed the transference of the Langmuir films onto solid substrates which is referred to specifically as the L.B. technique.

The solid substrate is suitably treated to make it hydrophobic or hydrophilic, and then is passed through the Langmuir film. Depending on the substrate's surface treatment, one monolayer is deposited on either the upstroke, the downstroke, or both on passing through the monolayer.

A hydrophobic coating picks up on the down stroke, with the tails of the monolayer attached to the substrate. A hydrophilic surface picks up on the upstroke. Subsequent dipping results in the formation of multilayers on the substrate.

The state of the floating monolayer under compression is followed by measuring the surface pressure (change in surface tension). The presence of the monolayer molecules at the surface tends to lower the surface tension relative to that value normally expected for water. The variation of pressure is usually measured using Whilhelmy plates (Appendix 2) attached to a microbalance, whose output may be used to produce a plot known as a "pressure-area isotherm". The area in question is usually determined in terms of area per molecule which is readily calculated if the number of molecules deposited on the surface is known.

Figure 5.2 shows a schematic plot of a pressure-area isotherm showing all the important characteristics and parameters that are of interest. As might be expected from

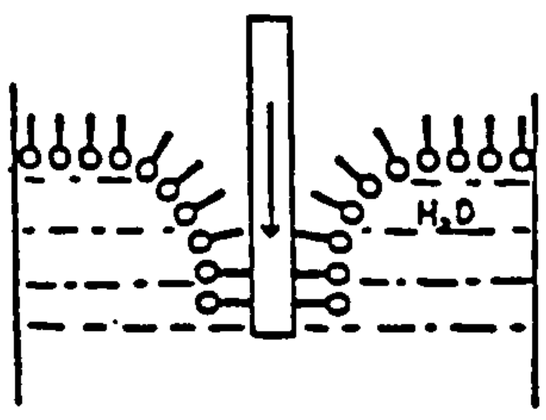

A. X-type

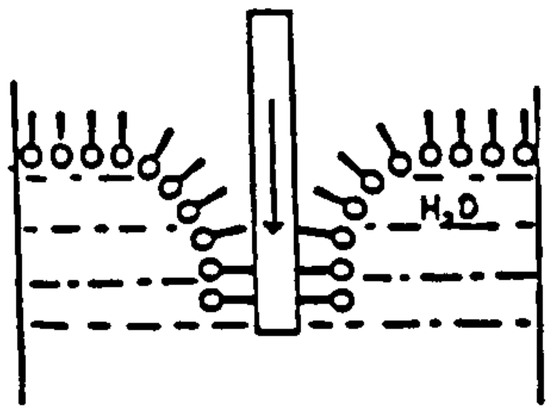

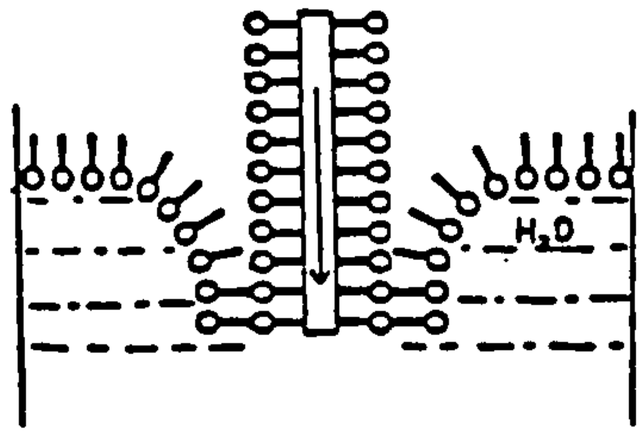

B. Y-type

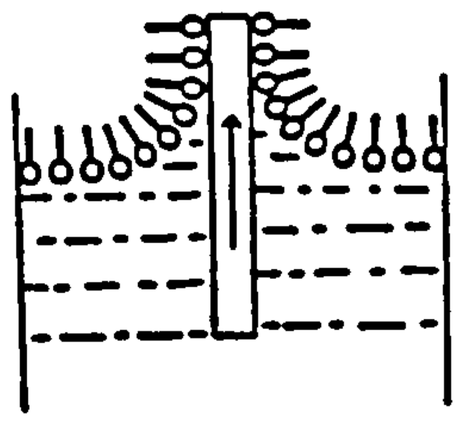

C. Z-type

Figure 5.3 Types of L.B. deposition.

kinetic theory (Atkins (1982)), all three phases are observed during compression, depending on the proximity of neighbouring molecules. Of particular interest are the two parameters π_c and A_o.

A_o is the hypothetical area occupied by one molecule in the solid monolayer at zero pressure, and is obtained by extrapolation of the steep rise in the isotherm. Usually, the measured value is related to a theoretical value for the molecule in question, and orientational deductions are made about the molecule within the monolayer. For the stearic acid shown in figure 5.1, the value of A_o is typically 22-25 $Å^2$. This corresponds to the cross sectional area of a hydrocarbon chain, suggesting that the molecules are vertically oriented.

π_c is the collapse pressure, above which the film is no longer a monolayer. Often, once π_c is reached the film will not expand reversibly. The value of π_c depends on the experimental procedure used, and so is not a reliable figure. In most dipping experiments it is often important to dip at as great a pressure as possible, in a reversible region of the isotherm, but below π_c.

5.3 Types of Deposition

Figure 5.3 shows the 3 types of multilayer deposition that can occur. Using either a hydrophilic or hydrophobic substrate, Y-type deposition tends to be the most common result with its "head-to-head" and "tail-to-tail" configuration. However, the non-centrosymmetric structures

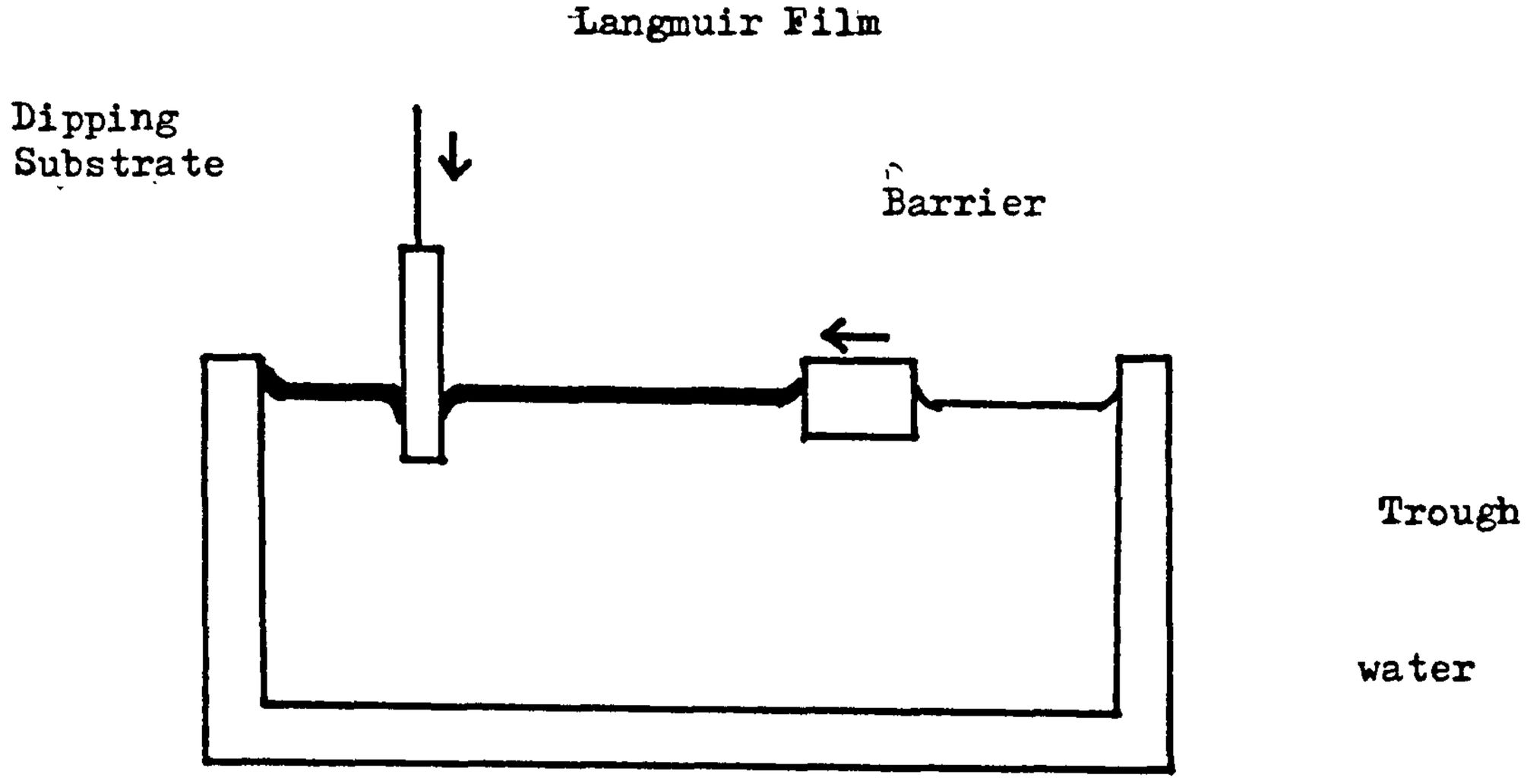

Figure 5.4 Schematic single compartment trough.

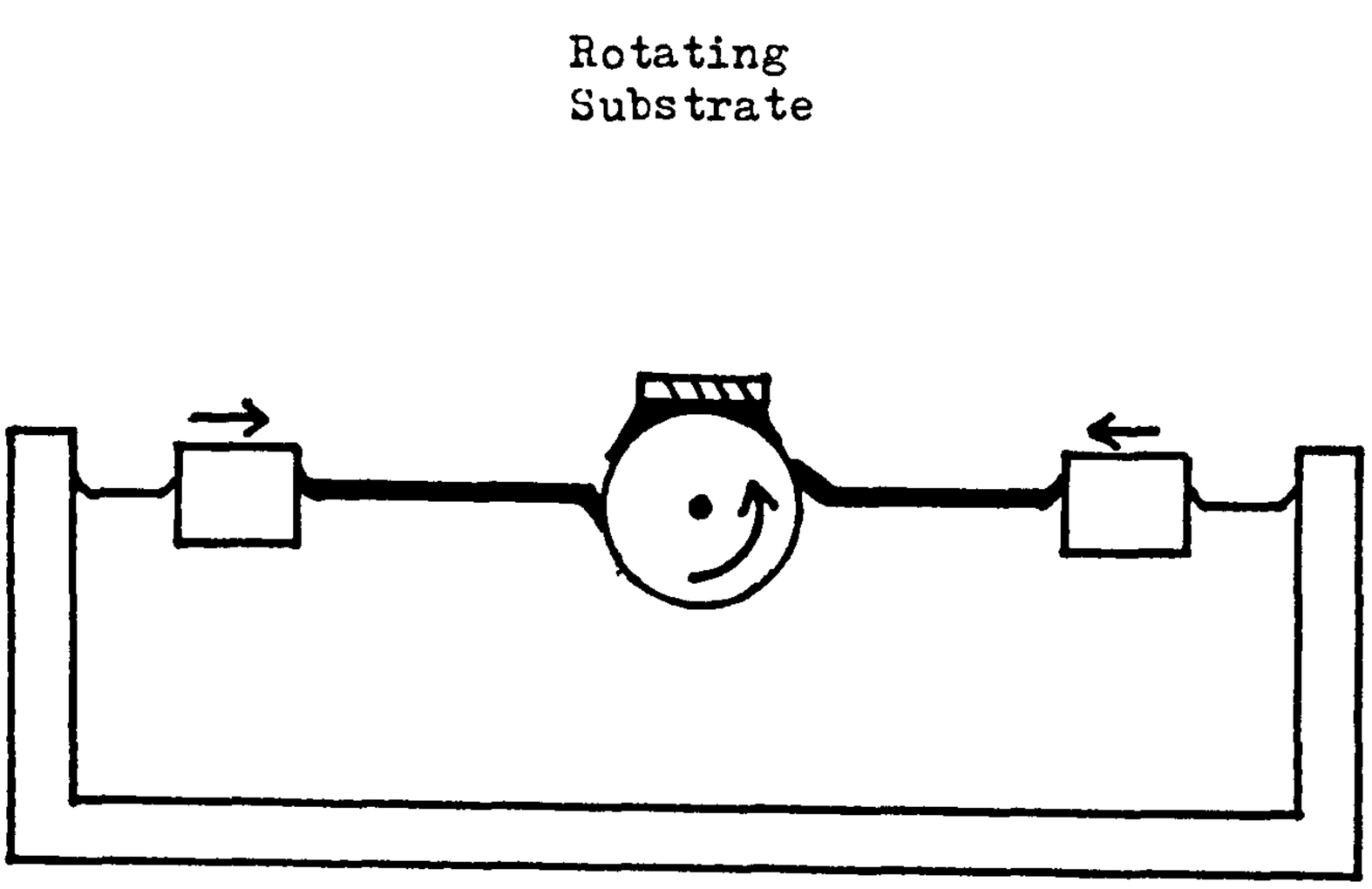

Figure 5.5 Schematic double compartment trough.

of the Z- and X-types are clearly more interesting for second harmonic purposes, (i.e. "head-to-tail configuration").

At this point it is probably wise to describe the two main types of L.B. trough available, to show how they relate to the above deposition configurations. Schematic representations of the two types are shown in figures 5.4 and 5.5.

Y-type deposition tends to occur in the "single compartment" trough as like-ends of the molecule preferentially align for each passage through the interface. Y-type deposition is also found for the "double compartment" trough if the same material is compressed in both compartments. The important attribute of this second trough is the ability to dip with alternate layers of different materials, allowing non-centrosymmetric structures to be formed (as in figure 5.6) in a film which has deposited Y-type. Figure 5.6 shows for the case of a fatty-acid and a fatty-amine, where their respective polar heads have dipole moments in opposite directions with respect to the hydrophobic chain. Hence, a resultant dipole moment exists in the multilayer for Y-type deposition.

Also, a nonactive material is sometimes dipped alternately with an active material, to produce a multilayered structure with a resultant dipole. This usually overcomes the problem of a centrosymmetric structure that probably occurs if just active material is deposited in a multilayer. However, there will be some kind

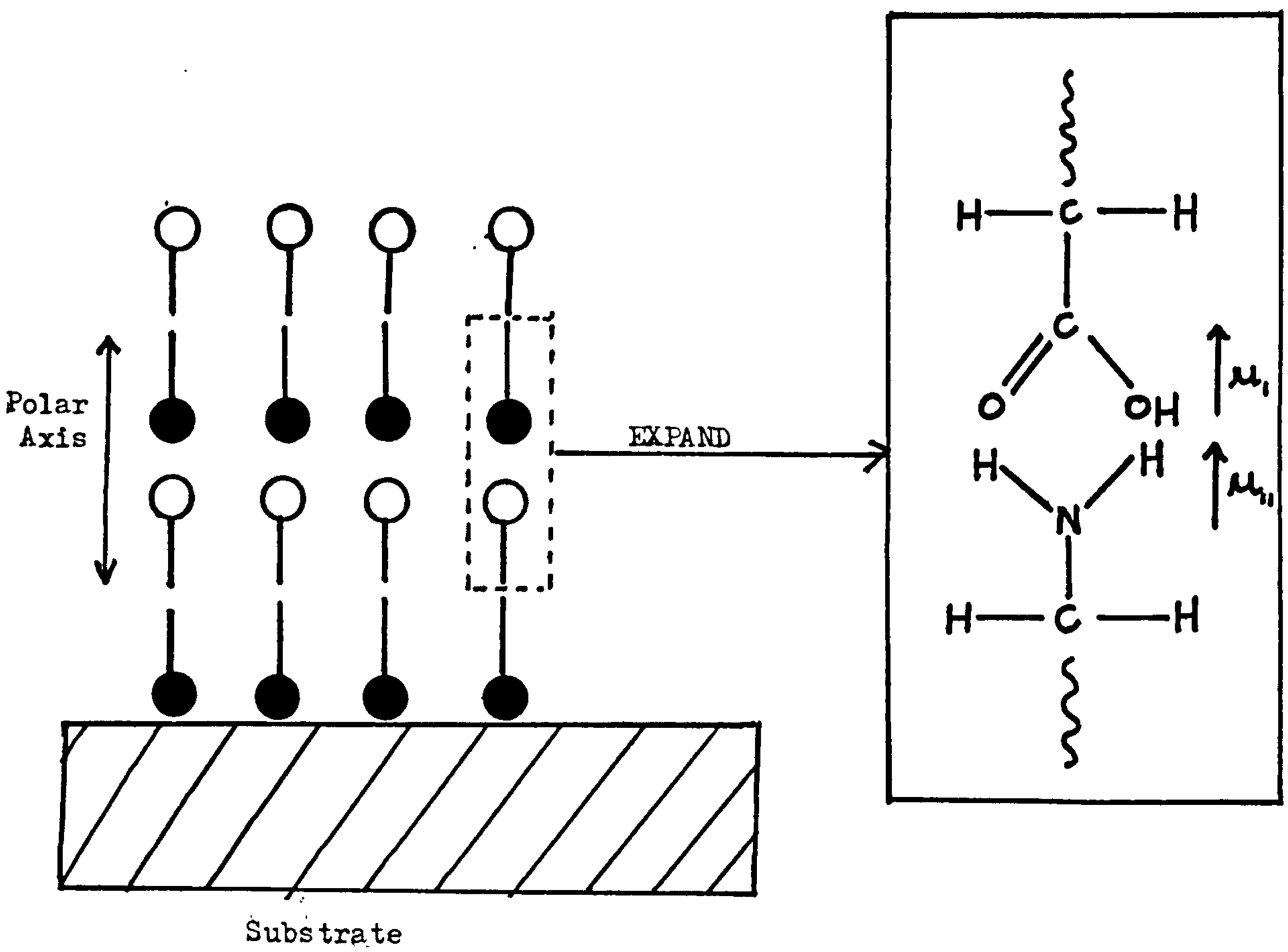

Figure 5.6 Example of using two different molecules (fatty acid/fatty amine) to produce a unique polar axis in a Y-type film.

of dilution of the effect because of the nonactive layers.

5.4 L.B. Studies of PBzLG and Other Poly(aminoacids)

Pressure-area isotherm studies of PBzLG on an air-water interface have been examined by a number of workers, and figure 5.7 is typical of the general form seen for the isotherm. The limiting areas per residue for the two pressure steps shown, have been found to be in the ranges 18-23 $Å^2$ (step A) and 12-15 $Å^2$ (step B), while the pressure of the plateau region was typically in the range 7-12 mN/m.

Molecular weight effects on the shape of the isotherm have been studied by Suzuki and Isemura (1967). His results showed that the molecular weight did not effect the limiting areas of the rise A and rise B, but there did tend to be a decrease in plateau pressure for increased molecular weight (in the range 26000 to 150000). For a number of the samples, bifunctional amine initiators had been used which introduced flexible ethylene and trimethylene alkyl chains within the polymer chains. The unusual kink observed in rise A for these particular samples was attributed to the disruption of the rigid rod nature by the alkyl linkage, suggesting α-helix was present in the monolayer.

Further evidence for the structure of the monolayer and whether α-helices are present, can be found from a number of sources. Suzuki and Isemura (1967) believe an array of two dimensional raft-like aggregates (of α-helices) form on spreading, which on compression interact so the plateau

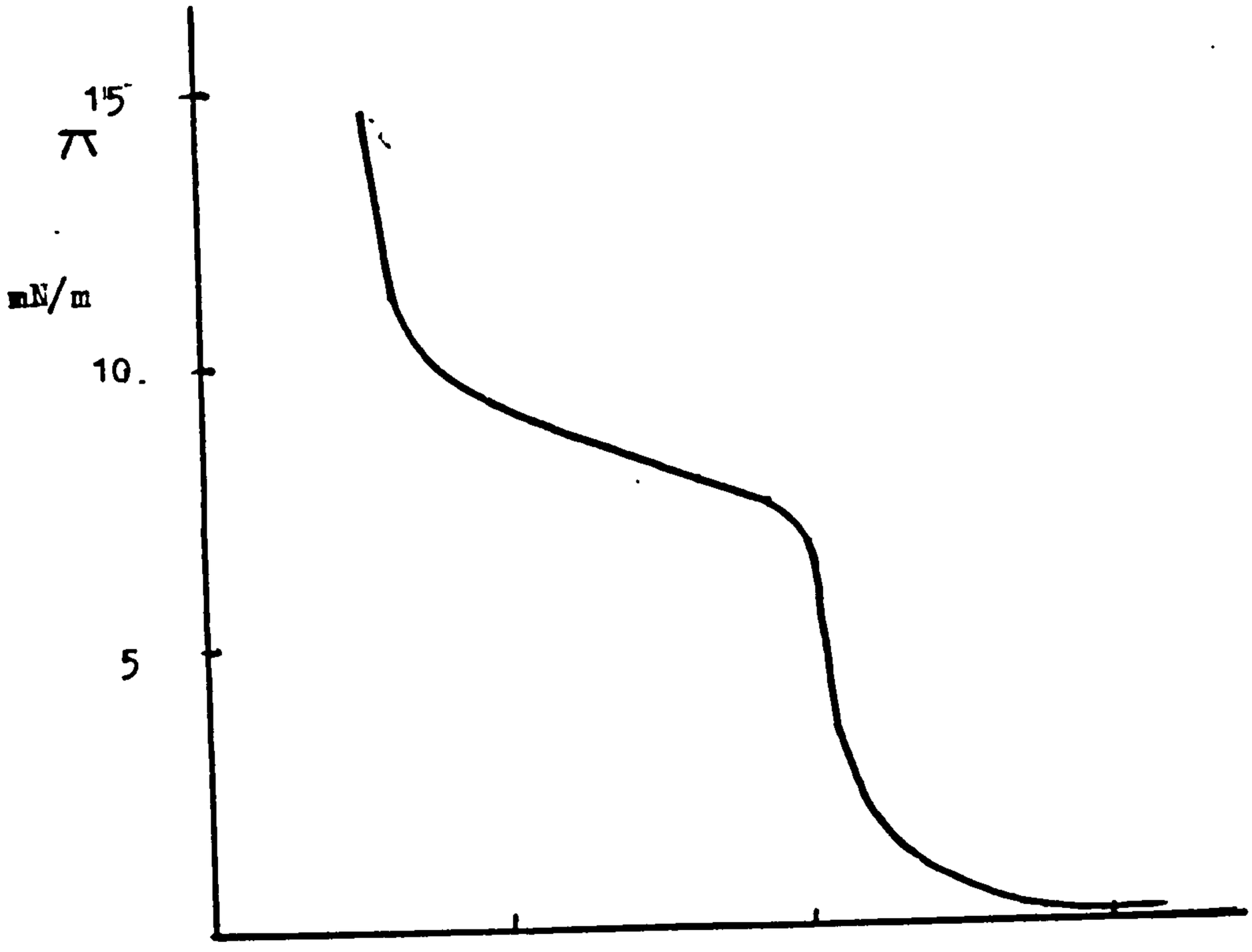

Figure 5.7 Typical isotherm for PBzLG (M.W. 90,000) given by Suzuki and Isemura (1967).

region is associated with a piling up of the rafts. Similarly, Malcolm (1968) suggests that in the plateau region, the monolayer of the α-helices folds into a bilayer.

Shuler and Zisman (1972) also associated the plateau region with the displacement of α-helices from the monolayer, but did not observe the second rise which Malcolm used to conclude bilayer formation. Shuler and Zisman suggested equilibrium had not been obtained during the later stages of compression, which resulted in the second rise. Compression-expansion processes carried out by them showed hysteresis in the isotherms, although after a given time, recompression of the monolayer did reproduce the isotherm, i.e. indicative of a short-lived state.

Electron diffraction (Malcolm (1968)) and infrared spectroscopy (Loeb and Baier (1968a,b)) have been used to confirm the presence of α-helices in collapsed layers (Malcolm (1968)) and monolayers (Loeb and Baier (1968a,b)). Multiple internal reflection infrared spectroscopy of PBzLG was used for different points on the isotherm, (the technique involved transference of monolayer onto a germanium prism) and spectra showed the presence of absorptions characteristic of α- or random coil polyglutamate, but not β-form. Similar studies (Loeb and Baier (1968b)) on PMLG, were carried out using pyridine and chloroform as the spreading solvent. These yielded limiting areas of 10 $Å^2$ (β-form), 16-17 $Å^2$ (α-form) respectively. Associated differences in the amide I and amide II

absorptions, confirmed the presence of the respective conformer in each case.

Birdi and Fasman (1972) suggested that the transition observed from monolayer to bilayer, would be sharper for the α-form than in the β-form case, because there are no intermolecular forces present to prevent molecules being dislodged from the monolayer. They also suggested there was a stronger interaction with the subphase in the β-form (i.e. the α-form has no dipole component perpendicular to the helix axis), which also inhibited bilayer formation.

Yamashita and Yamashita (1970) observed linear relationships for the plateau pressure versus temperature for various samples, and then observed a linear relationship between the associated gradients ($d\pi/dT$) and the percentage of regular helix within each sample. (Note: the percentage of regular helix had been controlled by forming DL-copolymers of PBzLG with varying amounts of L-monomer (L/(D+L) = 0.5-1.0).

The effect of different side groups on the shape of isotherms has been studied by a number of workers. Isemura and Hamaguchi (1954) noted that for side chains with less than 6 carbon atoms, a limiting area per monomer unit of 14.7 $Å^2$, characteristic of a β-conformation was found. For longer side chains, the limiting areas increased with length of chain and the α-helix was believed to be present.

Ikeda and Isemura (1961) compared the monolayer properties of PBzLG and poly(benzyl-L-aspartate) (PBzLA).

Their work used a combination of surface viscosity and surface dipole moment measurements to propose different side chain orientations in each case. For PBzLA, the carbonyl groups on the side chains extending above the surface were thought to be close enough to the surface (because of the one less methylene group in the side chain), to form an interaction. No such interaction was expected in the PBzLG case with the unsubmerged side chains free. Interestingly, both polymers were quoted as being in the β-form which may have been due to the dichloroacetic acid/benzene mixture used as the spreading solvent.

Malcolm (1975) describes the different shape of the pressure-area isotherms for different polypeptides in terms of side chain flexibility and dipolar interactions. By studying monolayers containing enantiomorphic and racemic mixtures of polymers, the difference between the energies of interaction of parallel and antiparallel helical molecules was thought to influence the shape.

Further studies by Malcolm (1971) pointed out that water-backbone interactions dominated the surface potential, for α-helical polypeptides with alkyl side chains, but for side chains containing ester groups, an additional side chain/water interaction was evident. Polarised infrared studies of collapsed layers which had been dried, and then exposed to water, methanol or ethanol, showed dichroic OH absorptions which provided evidence for the interactions in question.

Effects of the subphase on the conformation of the

polypeptide monolayer have been noted. Gabrielli and Puggelli (1975) observed α-helices on a HCl support and random coil on DCA, for PBzLG. Caspers et al. (1974) noticed a change in conformation by altering the pH of the subphase for a copolymer of methyl-L-glutamate and glutamic acid.

Hecq et al. (1976) observed a coil to helix transition for PMLG molecules on an air-water interface at approximately the heptapeptide level. A decrease in the rate of tritium exchange was evidence of the change of conformation.

L.B. studies of copolymer films of methyl-L-glutamate and various n-alkyl glutamates were studied by Duda et al. (1988). Transfer of 200 layers in Y-type deposition was achieved producing a linear plot of infrared absorption versus number of layers. The orientation of the helices was found to be parallel to the direction of deposition, with the side chains randomly oriented about the α-helical cylinder. The limiting areas of the isotherm indicated that interdigitation of the side chains occurred, because areas per monomer unit were smaller than expected.

CHAPTER 6

EXPERIMENTAL SECTION

6.1.1 Synthetic Investigation

At the outset of this project PBzLG was chosen as a suitable polyglutamate for study based upon its ideal solution properties, as well as its relative cheapness and ease of synthesis. The synthetic route for PBzLG has been described earlier in chapter 1, and the recipe and apparatus used to prepare a high molecular weight (HMW) sample for this project is given later in section 6.7.1.

The direct relationship between net dipole moment and molecular weight for α-helical molecules, and the magnitude of the electric field necessary to provide significant alignment for certain magnitudes of dipole moment, has already been discussed in the introductory sections of this thesis. Therefore, as far as primary aims were concerned for preparing poled guest host polymer systems, a HMW sample was important to assist electric field alignment of the PBzLG molecules.

For a guest host polymer system, suitable vinyl monomer solvents needed to be found to dissolve PBzLG. Ideally, these monomers would sustain the helical conformation of the PBzLG molecule, allowing electric field alignment of the helical chains within solution. Subsequent polymerisation of the vinyl monomer component with the solution still under field, should then result in a matrix of oriented guest helical polymer chains within the host polyvinyl film. This should be a structure which possesses

the necessary properties to show both piezoelectricity and SHG.

Although vinyl chloride and 1,1-divinylchloride were known to be solvents of PBzLG, and would certainly produce good polymer films, pressurised systems were not available to liquify these gaseous monomers, and their high toxicity posed too great a hazard.

Styrene, 1,4-divinylbenzene (DVB), and N-vinylpyrrolidone were found to be solvents for PBzLG and the various attempts to use these monomers and PBzLG are discussed fully, later in this section.

In general, the results obtained from this work were poor, and a number of synthetic approaches were investigated in an attempt to produce different guest host polymer systems.

The vinyl monomer, triethylene glycol dimethacrylate (TGDM), had been shown not to be a solvent for PBzLG, although it was subsequently used in small quantities with the monomers mentioned above, as a cross-linking agent to improve the film forming qualities of the guest host polymer systems. TGDM itself however was known to produce good polymer films with good optical clarity, and was also known (Tsutsui and Tanaka (1980c)) to be a solvent for poly(n-butyl-L-glutamate) (PBuLG), i.e. TGDM seeming to favour the less polar nature of the alkyl side chain.

Subsequently, the new synthetic routes in question were intended to produce either PBuLG or other poly(alkyl-L-glutamates) which might be soluble in TGDM. These routes

can be divided into two general categories:-

i) chemical modification of polyglutamate (polymer side chain reactions);

ii) preparation and use of different γ-esters to prepare different NCAs and hence different polyglutamates.

i) Chemical Modification of Polyglutamates

PBuLG had been synthesised in the past using transesterification (Selina (1986), Tanaka et al. (1973)) of either PBzLG or PMLG, with paratoluene sulphonic acid and n-butanol. This route was not attempted in this work for a number of reasons. To begin with, no sample of PMLG was available, and only a small sample of PBzLG had been prepared and could not be risked on the reaction. In addition, the reaction itself often reduces the molecular weight of the polymer sample because of the harsh acidic conditions, so the route was not necessarily ideal for producing HMW samples.

Subsequently, using ideas from a paper by Kotai (1967), side chain modification of PBzLG was attempted using an alkyl amine. The reaction scheme for this route has been shown in section 1.1.3, along with the synthetic details for the reactions carried out using n-hexylamine, given in section 6.7.3. The intended product of the reaction was not a poly(alkyl-L-glutamate), because an amide functionality would be introduced into the side chain instead of the γ-ester. However, the prime aim of replacing side chain benzyl groups with alkyl nature is still apparent.

ii) Preparation of γ-Alkyl Esters

The main criterium for choosing suitable alkyl-glutamates to prepare, was based on melting point data of the corresponding alkyl NCAs. The need for the purification of the NCA prior to polymerisation has already been mentioned, so alkyl NCAs with reasonably high melting points (> 40°C) were preferred, (i.e. it is easier to recrystallise a solid than purify an oil). Hence, the following list summarises the melting points (Block (1983)) of the corresponding alkyl NCAs, for the various alkyl glutamates that were attempted.

Alkyl NCA	m.p./°C
n-butyl	oil
i-butyl (2-methyl-1-propyl)	60-61
dodecyl	53-54.5
hexadecyl	64.5-70.5
octadecyl	77-78

Reference to the preparation of γ-benzyl-L-glutamate has already been made in describing the synthesis of PBzLG for this project. In this route, the γ-benzyl ester was prepared via the direct esterification of L-glutamic acid using the appropriate alcohol and acid catalyst. Although this route works well for the benzyl derivative, this is certainly not the case as far as other esters are concerned.

Owing to the bifunctional nature of L-glutamic acid, there is a tendency to form di-ester under the forcing

conditions used, which often hinders the isolation of γ-ester.

a) Via Cu(II) Complex

Hence, early attempts to prepare γ-alkyl-L-glutamates tried to use a more selective synthetic route, involving alkylation of a copper (II) complex N,N,N',N'-tetramethyl guanadinium salt with an alkyl halide. The reaction scheme for this route is given in section 1.1.3, whilst the recipe used which was based upon a paper by van Heeswijk et al. (1982), is given in section 6.7.4.

b) Acid-catalysed Esterification

Having already mentioned di-ester formation to be a problem associated with this kind of reaction route, Sugai et al. (1966) reported that reasonably high yields of various γ-alkyl-L-glutamates could be achieved using small amounts of alcohol with aqueous concentrated HCl or 60-80% sulphuric acid. Subsequently, in view of the poor results coming from the Cu(II) complex route, various attempts to synthesise γ-alkyl-L-glutamates by this new route were made using the recipes given in the paper by Sugai et al. (1966), (section 6.7.4).

Synthesis of Poly(alkyl-L-glutamates)

Owing to the limited success and the poor yields obtained in synthesising various γ-alkyl-L-glutamates by the routes just described, only the n-butyl and i-butyl esters had been made in sufficient quantities to allow the next synthetic stages of the work to continue.

A synthesis of NCAs and the subsequent polymerisation of these two alkyl esters was described in the paper (Sugai et al. (1966)), which had been used to prepare the esters themselves. However, a different synthetic route was used to prepare the NCAs using triphosgene, based on a paper by Daly and Poche (1988). Triphosgene promised to be much safer to handle than gaseous phosgene, because it was a white solid which could be used in controlled, weighed amounts, to deliver three molecules of phosgene in situ. This paper certainly showed the use of triphosgene to be successful on the stearyl ester, so it was hoped other alkyl derivatives would also be suitable.

The subsequent polymerisation step of any NCA prepared using this triphosgene route was based on the Sugai et al. (1966) paper.

The details of the NCA synthesis and the subsequent polymerisations are given in section 6.7.5.

Poly(isocyanates)

As in the case of polyglutamate esters, the solution properties of poly(isocyanates) discussed in section 1.2.2, made them useful materials for investigation.

A sample of poly(n-hexylisocyanate) (PHIC) was already available, which had been prepared previously at Liverpool University (Moore (1985)), using the method of Shashoua et al. (1960), which has already been covered in section 1.2.1.

The molecular weight of this PHIC sample was measured

at Liverpool using gel permeation chromatography (GPC), and was given as:-

number average molecular weight (M_n)= 42,278

number average degree of polymerisation = 333

weight average molecular weight (M_w)= 108,409

weight average degree of polymerisation = 854

Although a sample of poly(n-butylisocyanate) (PBIC) (origin unknown) was also available, it was very small and was only used in solubility experiments for guest-host polymer systems. A summary of these experiments is now given for the two polyisocyanates.

	Solubility?	
	Yes	No
PHIC	DVB	TGDM,TGDA
	Styrene	MMA,HEMA
PBIC	----	TGDM,TGDA,HEMA

In view of this poor choice of monomer solvents, coupled with the unsatisfactory results which had been obtained from the polyglutamate systems, only limited guest host polymer studies using PHIC/DVB/styrene systems were investigated. These are discussed in section 6.2.1.

Although extensive synthetic work was carried out to produce ideal guest host polymer systems (as described in the earlier part of this section), it is evident that the results from the use of these materials were generally very poor.

In general, the major problems with the guest host polymer systems can be summarised as follows:-

a) small choice of suitable vinyl monomers capable of dissolving PBzLG or PHIC, coupled with an inability to synthesis other polyglutamates that would have suitable vinyl monomers;

b) inability of suitable vinyl monomers to withstand high fields, resulting in poor films (i.e. conductivity problems);

c) phase separation in all guest host polymer film samples prepared.

However, the fact that samples of potentially useful material had been made, allowed further research to go ahead into trying to produce aligned polymer films.

6.1.2 Electric Field Poling of Solvent Cast Polymeric Films

General Approach

The general ideas used in this approach were very similar to those used to produce the poled guest host polymer systems already described.

To begin with, suitable helicogenic solvents of PBzLG and PHIC needed to be found to allow polymer solutions to be made. As in the guest host polymer case, the first requirement of the solvent was to provide an environment with enough freedom to allow alignment of the α-helical molecules by the applied electric field. In contrast however, the role of the solvent after this was not so important as it only had to be removed by evaporation, and

did not require the vinyl monomer properties needed to freeze in the alignment. Consequently, the range of solvents available for the casting method was a lot greater.

In the casting method, the freezing of the alignment within the film occurs because of the concentrated, viscous nature of the polymer film in the later stages of the evaporation, which should prevent the relaxation of the aligned helices.

One immediate benefit of the casting method is that the final film consists of neat, active (in terms of SHG effect) polymer, so it is not diluted by any of the nonactive polyvinyl polymer, as in the guest host polymer case. Two expected benefits of this were that firstly, detection of a SHG signal would be improved if the SHG efficiency of the sample was poor, and secondly, the chances of phase separation in a single polymer component material (c.f. composite polymer case of the guest host polymer system) should be significantly reduced.

One possible draw back of the casting method was that solvent might become trapped within the polymer film acting as a plasticiser and allowing relaxation of the alignment to occur once the field had been removed. However, it was hoped that owing to the molecular weight and size of the helical polymers used, and the fact that the whole molecule itself would have to relax (rather than just a side chain), there would not be enough free volume to allow this.

With such a wider choice of solvents now available for

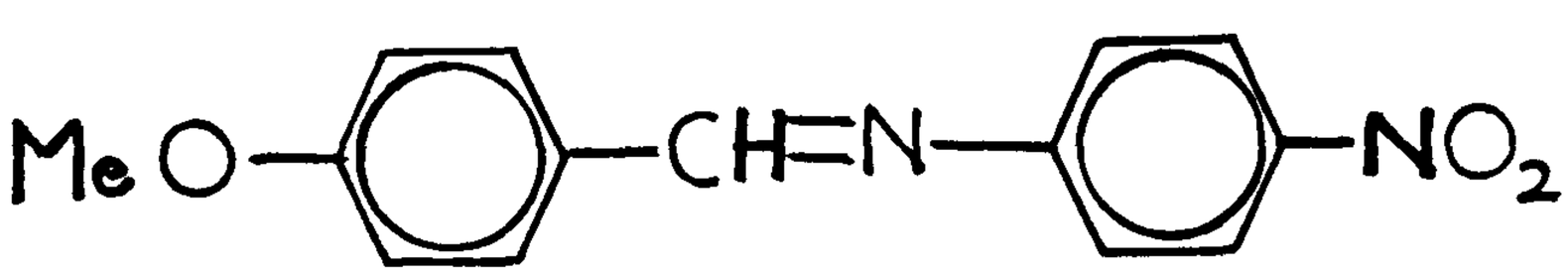

4-methoxy-4'-nitro-N-benzylideneaniline

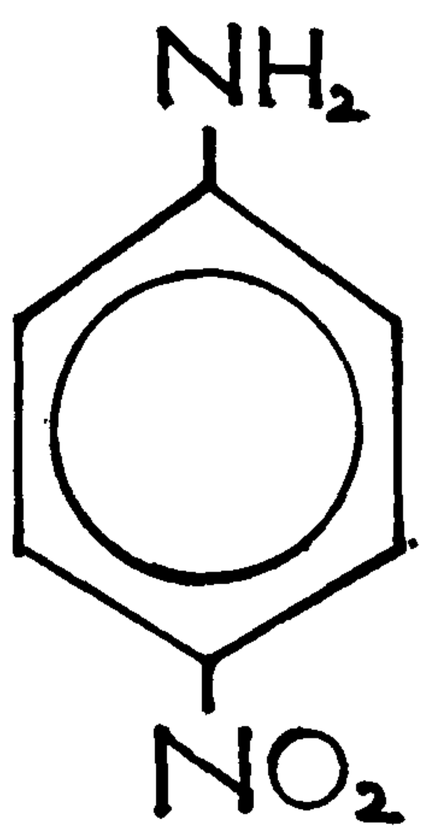

4-nitroaniline

Figure 6.1.1 High β molecules used as additives.

the casting method, the chance to introduce a third component into the polymer solution (particularly materials with a known high β) was greatly improved. Both 4-nitroanaline and 4-methoxy-4-N'-nitrobenzylideneaniline (see figures 6.1.1) were known to have high β values, and were handily available. However, only limited time was available to carry out work in this area, which explains why only sketchy results are given.

All practical details covering the work carried out using the casting method are described in section 6.4.

6.2 Poled Samples of Guest Host Polymer Systems for Piezoelectricity

6.2.1 Poling/Polymerisation Cell and General Sample Preparation

Figure 6.2.1 shows the combined poling and polymerisation apparatus used to produce poled samples of the guest host polymer systems, with figure 6.2.2 showing the photopolymerisation cell in more detail.

The stainless steel disc (lower electrode) was polished to a mirror finish (using diamond grit polishing wheels), to assist in the removal of films after polymerisation. The glass disc (upper electrode) was coated on its underside with a conducting layer of tin oxide.

The removable steel disc electrode made electrical contact with the outside casing through the central column. The height of this column (and hence the steel disc) could be controlled by turning the micrometer. In principle, the

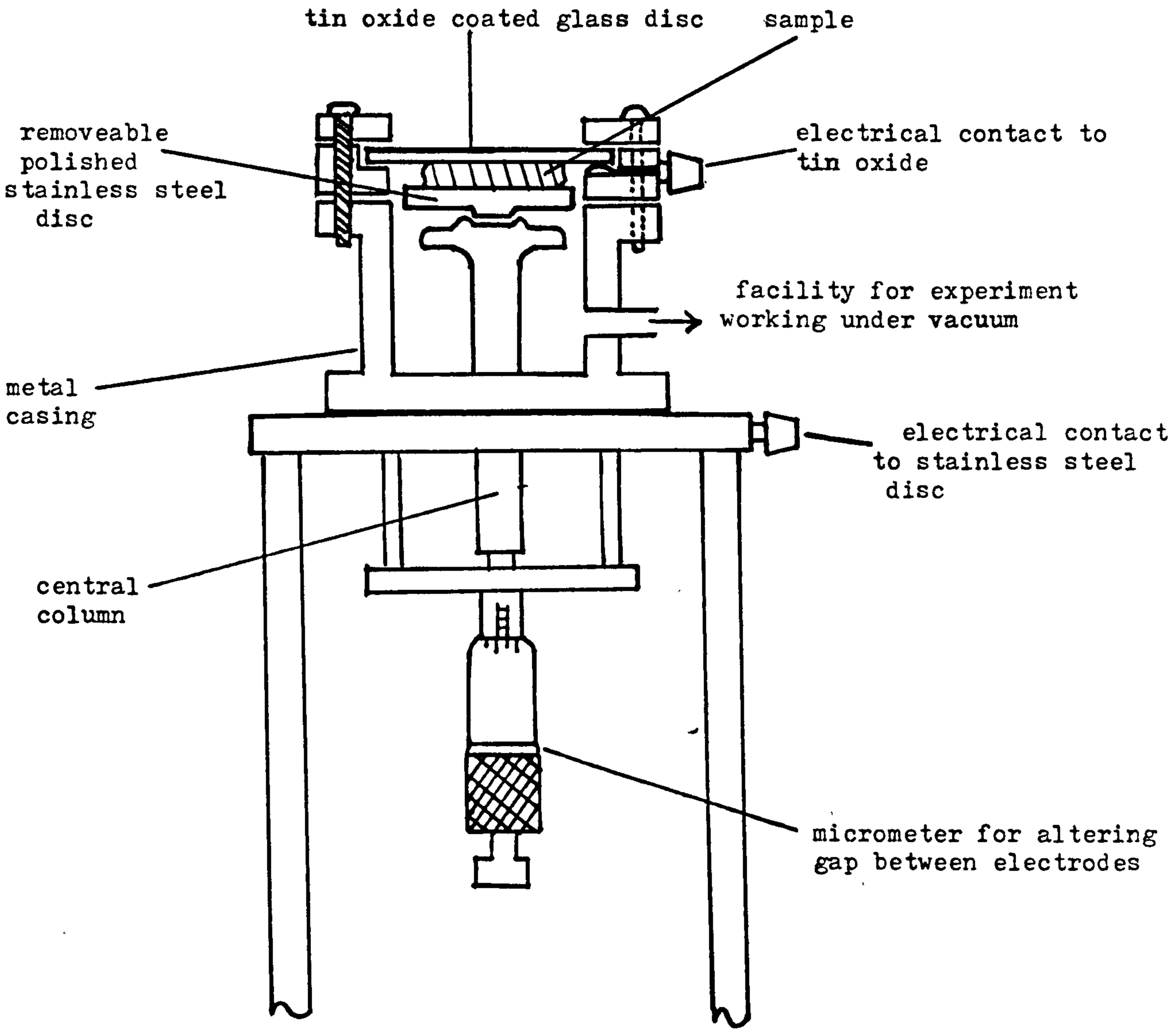

Figure 6.2.1 Cell for joint thermal polymerisation and poling.

micrometer could be used to set a specific gap between the two electrodes, i.e. calibration of the micrometer for a zero gap would be taken at the reading at which electrical contact was made between the two electrodes, and thicknesses (gaps) then calculated by subtracting the reading.

In practice however, the steel disc was not found to be parallel to the glass surface, so to prevent a wedged gap (and hence non-uniform field), small pieces of glass were placed as spacers between the electrodes and the micrometer just tightened to the constant thickness of the spacer.

Electrical contact to the tin oxide coating was made by the glass disc lying on a brass contact. This was clamped tightly together when the cell was fully assembled, as in figure 6.2.1.

Heating for the polymerisation step was supplied from a heat lamp, which explains the need for an upper glass electrode to allow light energy into the sample to heat it. This lamp was positioned directly above the photopolymerisation cell, and the temperature of the reaction was followed indirectly, in terms of the temperature on the top of the glass surface using a thermometer as shown. Temperature control was achieved by simply raising or lowering the lamp.

Electric field was supplied from a Kiethly high voltage power supply (up to 2.5 kV) and any current demand was measured on a milliammeter.

Note: when clamped tight together, a seal arrangement (not

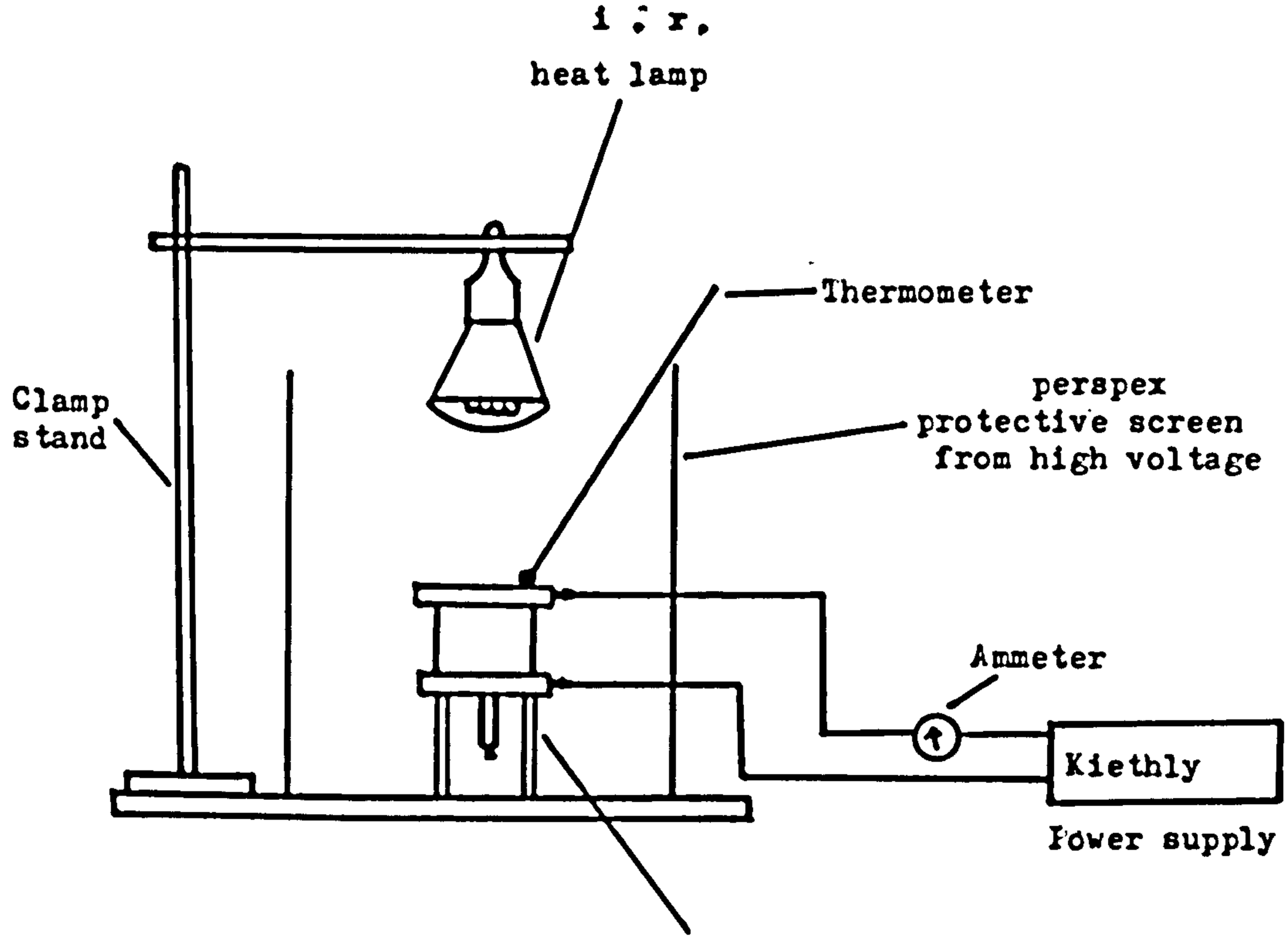

Thermal polymerisation Cell (figure 6.2.1)

Figure 6.2.2 Experimental set-up for poling/curing process.

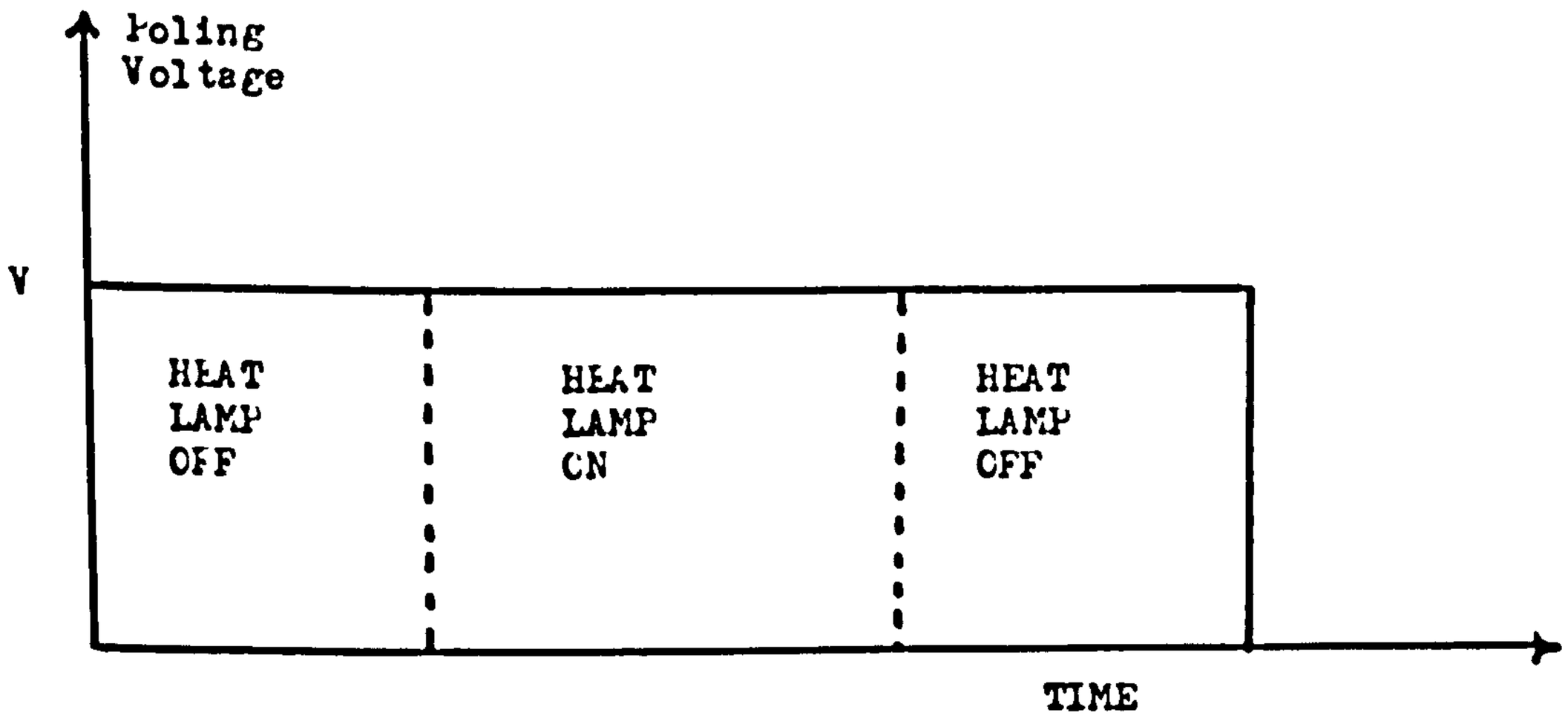

Figure 6.2.3 Typical experimental procedure for poling/curing process

shown) allows the cell to be under vacuum, if any air sensitive materials are being used. However, this facility was not used in this work.

Hence, for a general poling/photopolymerisation of a sample, the glass disc was first removed by dismantling the cell. Three small glass spacers were then placed equidistant around the rim of the steel disc and a pool of polymer/monomer was poured onto the middle of the disc. The glass disc was then replaced and the cell was reassembled. The steel electrode could then be raised slowly (to prevent air bubbles trapping in the solution), until the micrometer was tight and the solution had been sandwiched between the two surfaces of the discs (as in figure 6.2.1). (Note: the viscosity of the solutions was usually such, that they flowed quite slowly, and gave plenty of time to carry out the reassembly of the cell).

The photopolymerisation/poling process could then take place using the heat lamp and the power supply circuit as shown in figure 6.2.2.

Figure 6.2.3 shows the ideal poling/cure procedure that is required for producing guest host polymer systems and which was employed for the early samples in this work (c.f. precure samples later).

The electric field was usually applied for about two minutes before switching on the heat lamp, and cure times of 2 hours at 90°C, represent the most extreme conditions ever used or required to cure the films. After curing,

samples were allowed to cool for 30 minutes before removing the field.

The cell was then dismantled, and the sample could then be removed, usually still attached to both discs. Removal of the samples from between the discs was often a difficult process, even with polished surfaces. Usually, they were broken off in a number of pieces.

In some cases, silicone fluids were used as release agents, i.e. the silicone fluid was smeared over the two electrode surfaces using a tissue, before applying the monomer solution. The silicone fluid needed to be applied as thinly as possible, to prevent contamination, and to ensure most of the field was applied across the sample solution and not the release agent.

Polymer/Monomer Systems for Guest Host Polymer Materials

The following combinations summarise the polymer/monomer systems used to try to synthesize guest host polymer samples.

1) PBzLG-TGDM

2) NVP-TGDM-PBzLG

3) NVP-Styrene-PBzLG

4) DVB-Styrene-PHIC

Monomers used

Figure 6.2.4 shows the general formulae for the four monomers used, and a table showing the respective initiator required to polymerise them. All the monomers could be made to cure thermally at temperatures between 60-90°C, in less than 3 hours using the respective initiator.

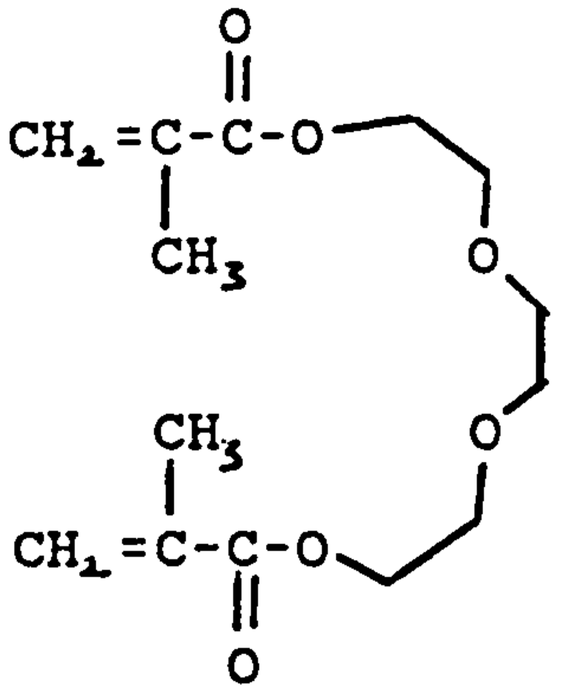

TGDM
Triethylene glycol dimethacrylate

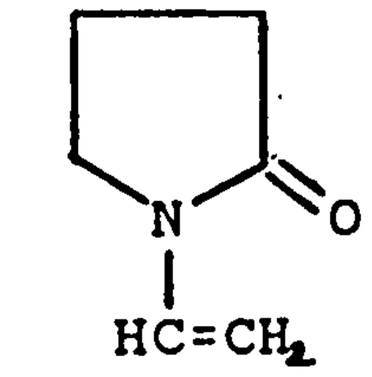

NVP
N- vinyl pyrrolidinone

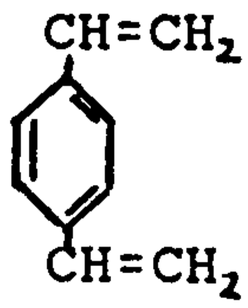

DVB
Divinyl benzene

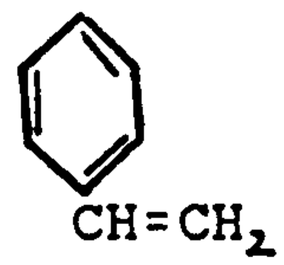

Styrene

Monomer	Initiator
Styrene	Dibenzoyl peroxide
NVP	Azo-isobutyronitrile (AZBN)
TGDM	Dibenzoylperoxide
DVB	Dibenzoylperoxide

Figure 6.2.4 Monomers and initiators.

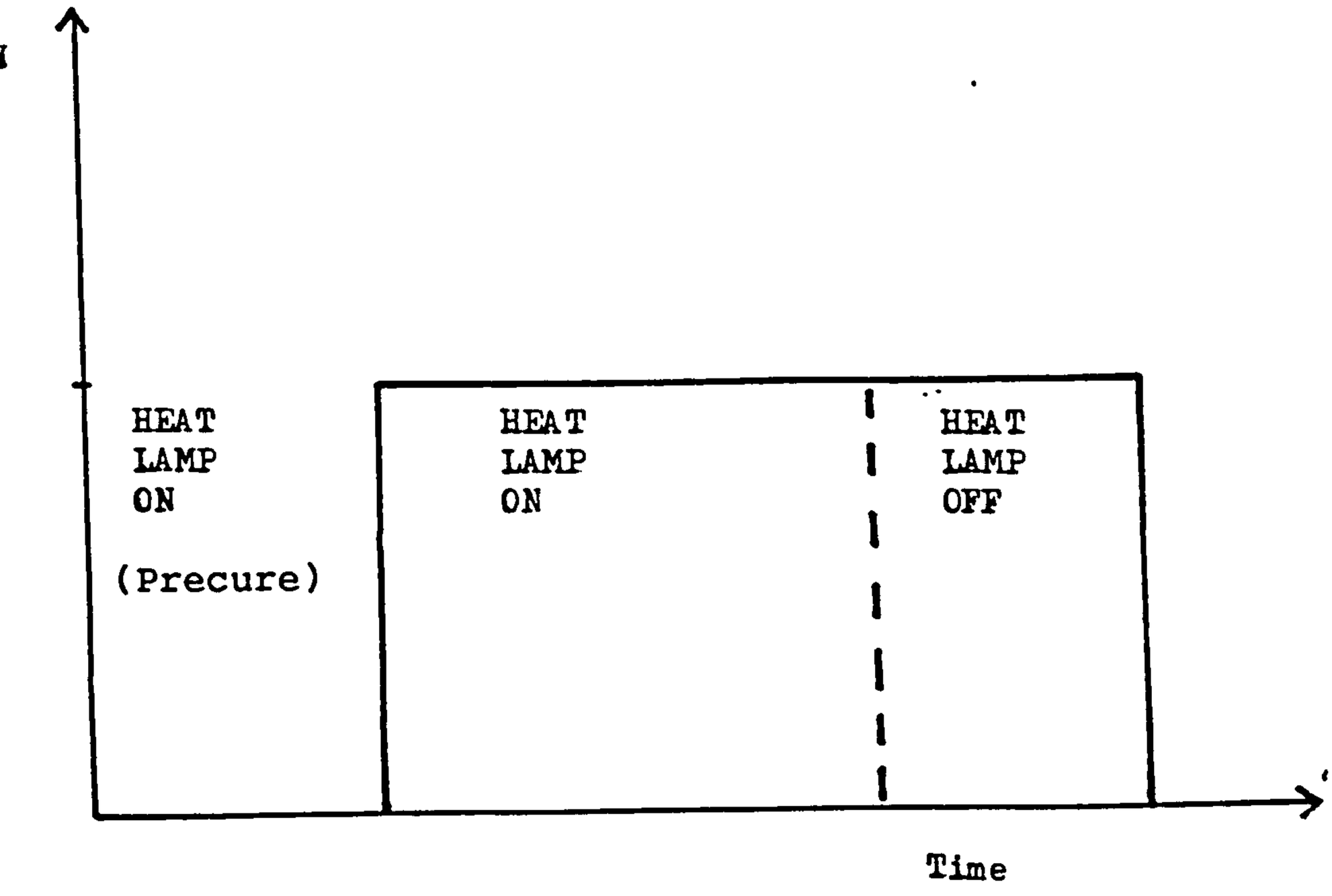

Figure 6.2.5 Typical poling/curing process with precure.

Both styrene and DVB had to have inhibitors removed before they could be used. This was achieved by washing with sodium hydroxide solution followed by drying with anhydrous magnesium sulphate.

All the monomers were stored in cool, dark conditions, and over molecular sieve to exclude water prior to their use. This second point was particularly important for NVP because it was a hygroscopic material.

Although TGDM and DVB could readily produce polymer films by themselves, their primary role when added in a mixed solvent case (i.e. NVP and styrene respectively), was to utilise their bifunctional nature by acting as cross-linking agents.

PBzLG-TGDM System

Work with this particular system represents the first area of guest host polymer work studied.

To overcome the problem of the insolubility of PBzLG in TGDM, PBzLG was first dissolved in dichloromethane or dichloroethane. TGDM was miscible in both these solvents and could then be added to the polymer solution in varying amounts so that phase separation did not visibly occur. A film of concentrated PBzLG-TGDM was then formed by evaporation of the chloro-solvent. It was then hoped phase separation would not occur, before the film could be poled and cured. Evaporation of the solvent was carried out in a fume cupboard, on the removable, lower stainless steel disc of the photopolymerisation cell so that the resultant

concentrated film was already attached to one of the electrodes. The film could be then readily moved to the cell on the electrode, and trapped between the pair of electrodes in a similar manner to that already described.

Initial observations were made using a 10% w/w solution of PBzLG:TGDM in excess dichloroethane (over 5 times by weight). As evaporation of the dichloroethane took place, a skin formed on the surface of the solution film which drastically slowed down this process. The use of a vacuum to accelerate the evaporation, only tended to produce films full of bubbles.

The concentration of the solution was dropped to 5% w/w and films were allowed to evaporate for over 24 hours at room temperature. Already, the resultant rubbery films showed some degree of polymerisation, as well as clear signs of milky phase separation. On attempting to pole and completely cure the films, bubbles were seen to form between 75-80°C which was due to traces of dichloroethane boiling.

A change to dichloromethane (being a lower boiling point solvent) was then tried to improve the rate of evaporation. Films were then prepared by evaporation in an oven at low temperatures of about 40°C, for varying amounts of time. These partly cured films could then be poled and fully cured. Clearly, the length of time of the evaporation/precure stage was important to ensure all dichloromethane had escaped prior to the poling, but too long a precure may also have prevented alignment of the

helical PBzLG to occur.

PBzLG-NVP-TGDM System

In principle, the solubility of PBzLG in NVP offered the ideal guest host polymer system. However, being miscible with TGDM, meant NVP could be used to replace the dichloro-solvent previously required. Hence, the resultant system did not need to be evaporated prior to poling and curing, and the mixture of NVP and TGDM offered the possible versatility associated with a copolymer system. The cross-linking nature of TGDM tends to produce very brittle poly(TGDM) films, whereas poly(NVP) tends to be too soft. Hence, ideal mechanical properties which are important for piezoelectric films, could possibly be tailored by altering the copolymer monomer:monomer ratio.

On preparing solutions of PBzLG in NVP/TGDM the PBzLG was first dissolved in the NVP overnight. TGDM was then carefully added and rapidly stirred into the solution. This always resulted in initial phase separation of gel particles, owing to the problem of trying to uniformly mix the non-monomer solvent component within the viscous polymer solution. Even for 5% w/w solutions of PBzLG:monomer, the viscosity of the solution was difficult to handle. Stirring the solution, always tended to trap air bubbles within the viscous mixture. These were most easily removed by placing the solution within a vacuum before use.

Once an air-free solution (containing initiator) had been achieved, poled films could be prepared as described

using figure 6.2.1. To facilitate the transfer of the viscous solution onto the polished, stainless steel electrode, the solutions were gently warmed, remembering to avoid initiation.

Figure 6.2.3 has already been mentioned as being the typical poling/cure procedure followed and this was the case for the early samples of this particular system.

However, some samples were also prepared using a precure period before applying the field, as in the case of the PBzLG-TGDM system. This was mainly employed to allow bigger fields to be applied. Figure 6.2.5 shows the typical poling/cure procedure followed when a precure was involved.

NVP-Styrene-PBzLG

Unpoled, cured films of 20% and 30% v/v styrene:NVP could not be made to polymerise using 1% dibenzoyl peroxide or AZBN, even after 5 hours at 85°C. As a result, further work to introduce PBzLG into this monomer mixture was not continued.

DVB-Styrene-PHIC

Although PHIC was found to be soluble in both monomers, little polymerisation was found for 10% v/v styrene:DVB solutions using dibenzoyl peroxide. Subsequent work in this area was not continued.

Control Samples

The function of the host polymer was only intended as an encapsulating medium, with a nonactive role as far as piezoelectricity was concerned. However, having been formed in a poling environment, it too may have contributed to the said effect which was being observed for the aligned, helical polymer component.

Similarly, an effect may have been observed without the need to pole the samples, possibly because of liquid crystal alignment.

In either case, whenever a poled sample was prepared for one of the polymer/monomer systems mentioned, it was always important to prepare the necessary control samples to rule out the above possibilities.

6.2.2 Results

PBzLG/TGDM

All fully cured films containing PBzLG showed phase separation and were opaque. The poled and unpoled control samples of the fully cured neat TGDM samples were transparent, confirming the good optical clarity that had been expected for this material.

The following table shows the conditions and parameters that were determined to produce reasonable films of PBzLG/poly(TGDM). The control sample conditions are also given.

Sample PBzLG:TGDM w/w %	Precure Time (40°C oven) Days	Applied Field V/mm	Cure Time hr	Temperature °C	Current μA
(a) 5:95	15	150	3	80	< 20
(a) 5:95	15	0	2	80	< 20
(b) 0:100	15	150	2	80	< 20
(b) 0:100	-	0	2	80	< 20

(a) No initiator needed. (b) 2 % w/w dibenzoyl peroxide initiator.

For precure times less than 15 days, there still seemed evidence of trace dichloromethane within the film which was seen as bubble formation on heating above 40°C, and resulted in poorly cracked samples. Only for samples with precure times less than a day, was there a measurable current (never greater than 0.1 mA), but these would not polymerise.

PBzLG/NVP/TGDM

Solution Properties

In practice, on addition of TGDM to PBzLG/NVP solutions, it was found that the percentage w/w fraction values of PBzLG determined how much TGDM could then be added without permanent visible phase separation occurring within the solution. The following values are the approximate percentages determined from observations made on a number of solutions during the preparation of

different samples.

% w/w PBzLG:monomer	% w/w TGDM:(PBzLG+NVP)
5	up to 25
10	up to 15
>10	0

(Note: if 10% w/w fraction of PBzLG was used, then the weight fraction of TGDM could not exceed 15% without phase separation occurring within the mixing solution).

Lyotropic Liquid Crystal

Typical liquid crystal properties were observed using a Leitz polarising microscope. PBzLG was found to form a lyotropic liquid crystal state at a concentration > 14.5% w/w in NVP. The bulk solution at this concentration was yellow with signs of slight turbidity.

Cured Films

All cured samples containing PBzLG showed phase separation and were optically poor, whereas blank co-polymer films of TGDM and NVP tended to show good optical clarity. Table 6.2.2a shows the compiled experimental conditions used to produce the various cured films of the PBzLG/TGDM/NVP system.

6.2.3 Discussion

Although the NVP-PBzLG system appeared to be an ideal guest host polymer system in terms of solubility, in retrospect this was its only attribute. The main reasons why no active samples were prepared can be summarised as

Table 6.2.2a

Sample PBzLG:NVP:TGDM %w/w		Precure Time min.	Approx. Field KV/mm	Cure Time min.	Temp. °C	Film Quality
0:50:50		0	0.8	75	85	G
0:40:60		0	0.6	70	80	G
0:30:70		0	0.5	130	70	G
0:20:80		0	0.4	100	80	G
5:95:0		0	0	60	70	P(S)
5:85:10		0	0	120	70	G
19:63:18		0	0.2	75	70	P(S)
19:63:18		0	0	60	70	P(S)
0:100:0	(A6)	0	0	84	80	P(S)
0:80:20		0	0	120	120	P(B)
0:70:30		0	0.4	50	70	G
0:60:40		0	0.3	40	83	G
7:85:8		0	0	40	73	P(S)
8:80:12	(A3)	0	0	105	70	P(B)
5:75:25		32	0.8	30	70	G
5:77:18		45	1.2	25	70	G
5:80:15	(A5)	38	1.0	30	75	G
5:80:15		40	1.4	50	78	P(B)
5:80:15		45	1.6	60	72	G
5:80:15	(A2)	35	1.6	60	78	G
0:82:18		40	1.6	60	70	G
5:80:15		40	1.6	70	79	G
10:85:5		0	0.03	50	72	G
10:90:0	(A1)	0	0.1	80	72	P(S)
0:0:100	(A4)	0	0.4	88	80	G

Note:- film quality refers to the mechanical properties of the film. G : Good. P : Poor. (S) Too Soft. (B) Too Brittle.

Initiator concentration for above - < 1%.
Current Demand - < 4 mA.
Sample Thickness - approx. 0.4-0.8 mm.

follows.

i) The high conductivity was certainly the major problem, as this prevented a large enough field being applied to align the system because electrolysis appeared to be occurring.

ii) Owing to the experimental set-up, it was evident that a heat gradient was causing uneven polymerisation of the samples. This was due to the top surface of the cell being hotter than the metal disc, so that an uneven rate of polymerisation occurred forming an electrical insulating layer which prevented even poling of the cooler areas.

iii) The precure employed, may have been too long to allow subsequent alignment of the whole molecule (helix).

iv) 10% w/w systems may have been too dilute, to produce detectable signals. Although the problem of phase separation would not have prevented the measuring of piezoelectricity, it was the problem of trying to handle incredibly viscous solutions of PBzLG that prevented more concentrated PBzLG/Poly(NVP) films being made.

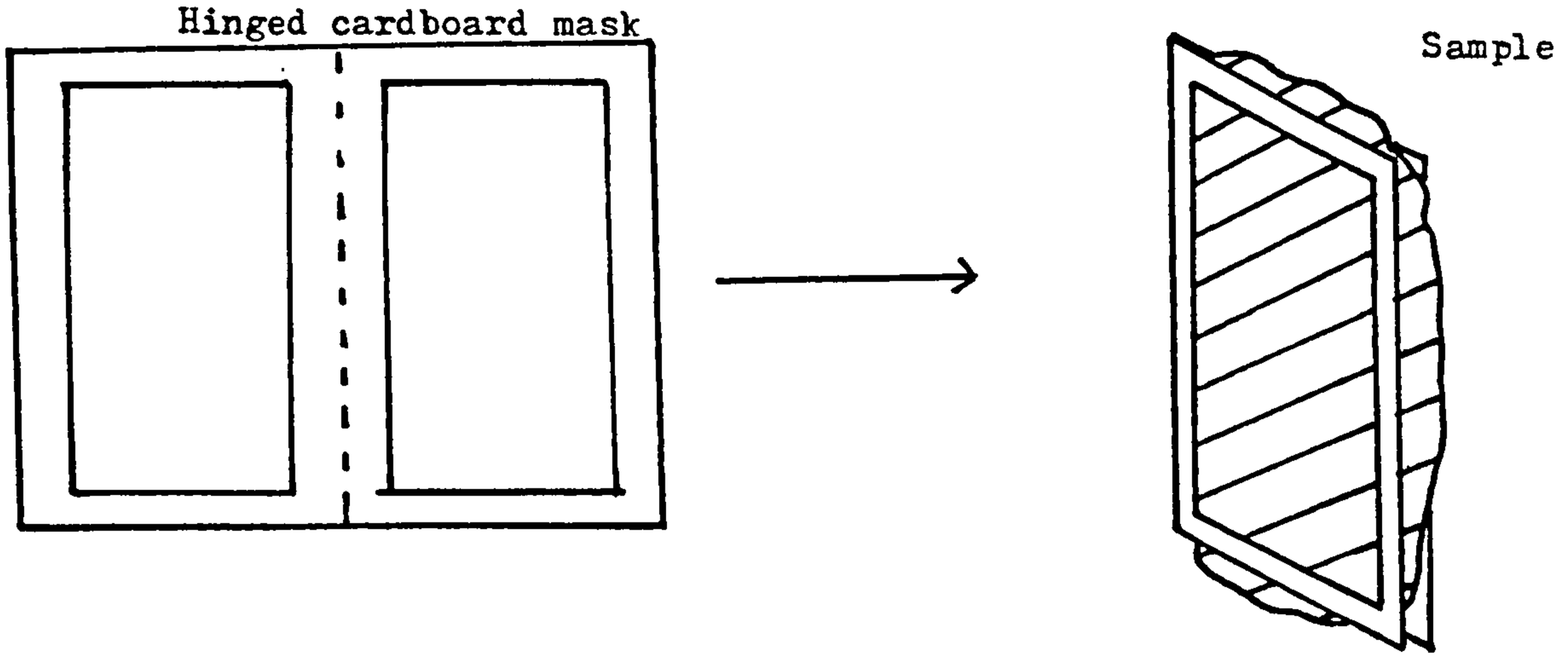

Figure 6.3.1 Hinged cardboard mask used to produce equal areas of evaporated electrode on each side of sample.

6.3 Piezoelectric Testing

6.3.1 Experimental Details

Electrodes

All the guest host polymer samples tested for piezoelectricity were coated with aluminium electrodes deposited by a vacuum evaporation technique. The area of the electrodes deposited was defined by placing a cardboard mask around the sample. The mask was a hinged, template design as in figure 6.3.1, which ensured the electrodes deposited on either side of the film were of equal area and also aligned.

An Edwards Coater was used with the sample placed at a distance of about 12 cm from the aluminium evaporation source. The source was a tungsten, coiled filament which could be fitted with aluminium ingots. In general, evaporation deposition was carried out at about 10 mbar, with a current of between 30-40 A supplied to the filament. Deposition was carried out on both sides of the film until an acceptable conductivity could be measured using an AVO meter, (i.e. FSD on most sensitive resistance setting).

Hydrostatic Measurement

The use of the hydrostatic measurement technique, offered a quick, simple method of determining the levels of piezoelectricity in the samples.

Figure 3.5 shows the cell designed to apply a hydrostatic pressure pulse to the samples. A low viscosity, silicone fluid was used to prevent unwanted heating effects, and to ensure a uniform pressure was applied.

Figure 3.5 shows the effective electrical circuit connecting the sample to the electrometer, which was used to measure the voltage developed across the deposited electrodes of the sample.

The swamping capacitance C, connected in parallel with the sample, amplifies the signal and swamps out noise. The value of the swamping capacitance was chosen such that C >> sample capacitance, and the total parallel capacitance C_T is effectively given by,

$$C_T \simeq C$$

The formula for d_{3h} can then simply be derived as follows. The charge Q, generated between the electrodes of area A, for a pressure pulse ΔP is given by:-

$$Q = d_{3h} \times \Delta P \times A$$

but $$Q = C_T \times V$$

therefore, $$d_{3h} = \frac{C_T \cdot V}{\Delta P \cdot A}$$

Calibration of the cell

Cell calibration was made using a thick, poled sample of PVDF, supplied and tested by the Allen Clark Research Centre, Plessey Caswell. They had obtained a value of 7.86 pCN^{-1} for the sample in question, measured in their own equipment of similar design to that shown in figure 3.5.

Sample Testing

On testing for piezoelectricity, the lid of the cell was first removed, allowing the sample to be clamped between the electrical contacts. These were the two jaws of

a spring loaded clamp, with each jaw insulated from one another allowing the two contacts to the electrometer to be connected to the two jaws. The sample was then submerged into the silicone fluid, and the lid of the pressure vessel replaced.

The cell was then pumped down using a diaphragm pump, by closing the inlet valve and opening the outlet valve to the pump. When a pressure reading of 30 in/hg (101,592 Pa) was achieved, the outlet valve was closed.

Before taking a hydrostatic piezoelectric reading, the electrometer had to be zeroed on a suitably sensitive voltage scale, (usually determined after a number of runs). Having zeroed the electrometer, the pressure was then rapidly released by throwing open the inlet valve.

A typical response of the electrometer, was a steady climb in voltage to a maximum value, followed by a slow decay (> 5s). This slow decay gave plenty of time to read the maximum value. A number of such readings were averaged for each sample before trying to determine a value for d_{3h}. (Note: in between each reading, the electrometer was set to zero).

In general, piezoelectric measurements were made as soon as possible after making the samples (preferably within a day) because of the worry of the relaxation with time of the aligned dipoles within the poled sample.

6.3.2 Piezoelectric Results

Cell Calibration

The calibration testing of the piezoelectric cell proved to give an acceptable value for the hydrostatic piezoelectric constant, compared with a value determined by Plessey Caswell.

d_{3h} values/pCN^{-1}

Cell Calibration	Plessey Caswell
6.68 ± 0.2	7.86

Lower Limit

When a sample (such as a glass slide), was tested in the cell, a very small voltage was obtained, even though no signal was expected. This value was taken as the lower limit below which piezoelectricity could not be detected.

Lower Limit Signal (for C = 90.47 nF and P = 101.6Pa)

= 0.0013 V

Guest Host Polymer Samples

No piezoelectric signal above the lower limit value was detected for any of the samples given in table 6.2.2a.

6.4 Electric Field Poling of Solvent Cast Polymeric Films

6.4.1 Experimental Set-up

The poling set-up used for the poled guest host polymer system could not be used for this method because as figure 6.2.1 shows, the evaporating solvent could only escape sideways, in the gap between the two disc electrodes. Inevitably, this would have led to poor films, because:-

a) uneven evaporation would occur, giving uneven films;

b) solvent would easily become trapped;

c) the evaporation process would take too long, and would lead to uncertainty about whether it was complete or not;

d) the evaporated films would have been thinner than the original electrode separation, so the field across the sample would have been lost at some point during the evaporation.

Figure 6.4.1 shows the simple electrode set-up that was designed and used for this work to try and overcome some of the above problems.

By poling the evaporating film on the surface of a glass slide, a much larger area of the film was open to the atmosphere, allowing fast evaporation, and reducing the amount of solvent likely to be trapped within it.

It was hoped the field would be maintained across the sample using this cell design, because the evaporating solution was now being supported in what can be described as a small trough with the electrodes acting as the walls. Hence, as the solution/film evaporated and settled into the

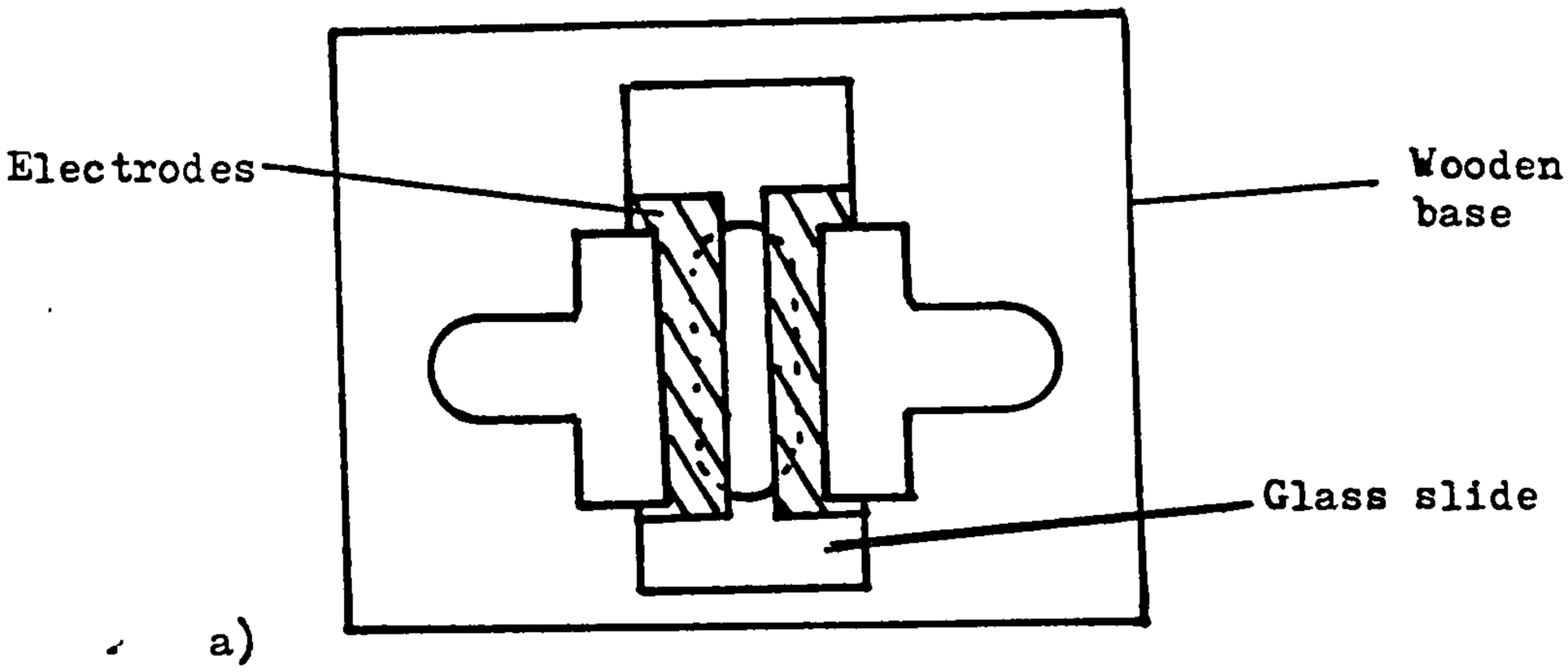

a)

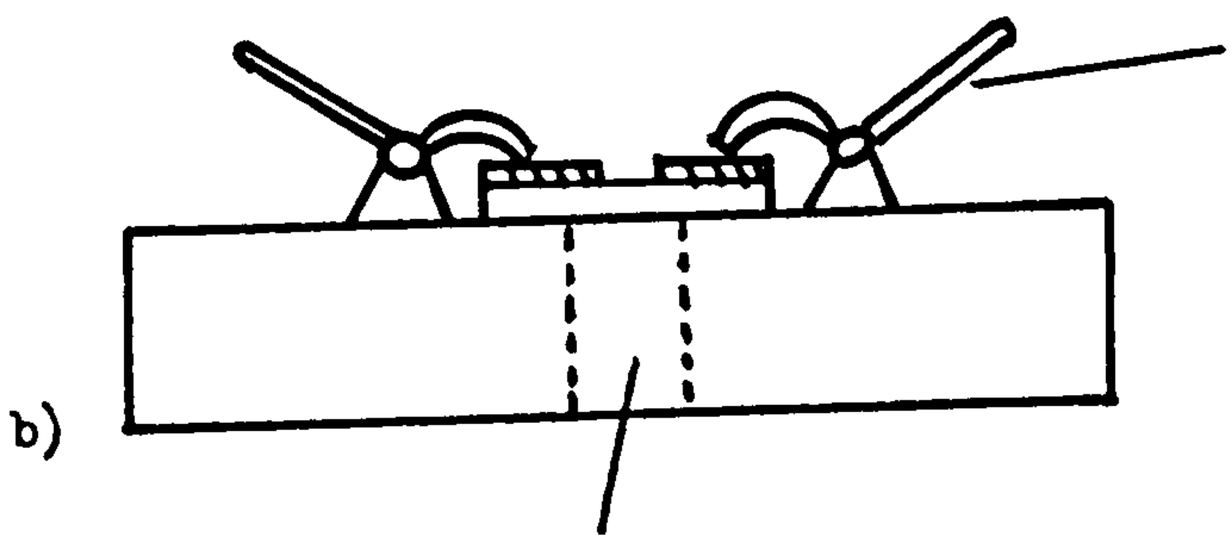

b)

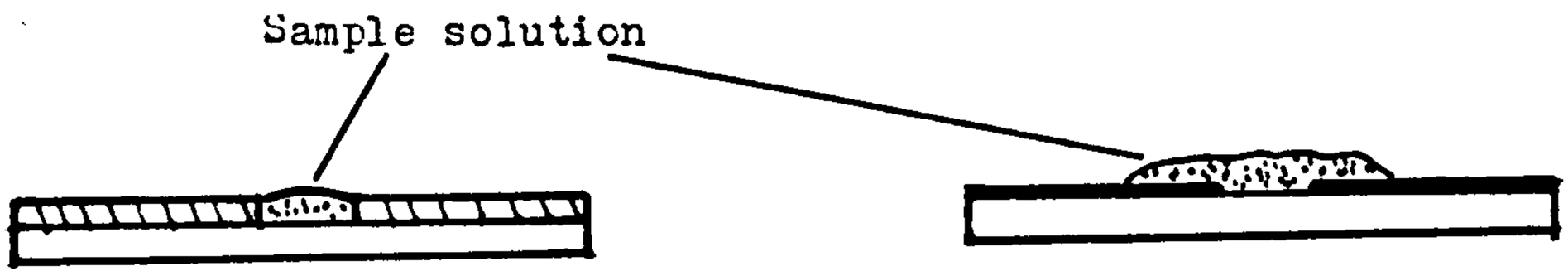

c) Stainless steel electrodes (0.25 mm)

d) Evaporated aluminium electrodes (< 1 μm)

Figure 6.4.1 Apparatus and electrode configuration for poling/casting.

trough, it should have still remained in contact with the electrodes.

The cell was designed with spring loaded contacts to allow easy removal of samples (on the glass slide), and to allow cleaning and polishing of the electrodes if needed.

The drilled hole in the wooden base of the cell was intended to allow microscopic observations to be made through the film during the evaporation/poling process.

With this kind of cell and poling/casting approach in mind, a number of questions had to be answered, which included:-

a) what type of electrodes should be used?

b) what solvent to use?

c) what initial concentration to use?

In practice, two different types of electrodes were tried with the cell set-up as shown in figure 6.4.1c-d.

In the first case, two aluminium electrodes (< 1 μm thick) were evaporated onto the slide surface using an Edwards Vacuum Coater, by simply lying a narrow strip of tape across the slide to act as a mask during the coating process, and which could be easily removed after. Conductivity of these electrodes was deemed suitable, when a full scale deflection was obtained for the most sensitive resistance setting of an AVO meter.

Alternately, two stainless steel strips which were 0.25mm thick, with flat, polished edges (polished on diamond grit wheels), were rested on the glass slide with a

fixed gap between them. In this second case, the spring loaded nature of the electrical contacts helped to hold the steel strips in place, (i.e. clamped against the slide surface).

By experiment, the stainless steel electrodes were found to be the most suitable system, because they tended to give more even poling, and allowed a controlled amount of solution to be applied each time.

By applying a blob of solution in the gap at one end of the parallel stainless steel electrode set-up, an even thickness (0.25mm) of solution could be applied for the evaporation, by drawing a flat edge (which was wider than the gap) down the length of the electrodes, and smoothing the solution into the gap.

Hence, for a typical, single evaporation/poling process, having applied the solution between the electrodes as described above, the field was then immediately applied (from a Kiethly high voltage supply) and the evaporation was carried out in a fume cupboard for a minimum of one hour, before removing the field. Any current demand during the evaporation was observed using the microammeter (100 μA FSD) connected in series.

The electrodes were then usually removed from the film by cutting with a razor blade close to each electrode face, which conveniently left the sample still attached to the glass slide, ready to be tested.

6.4.2 Polymeric Materials and Solvents

Both HMW PBzLG and PHIC poled/cast films were prepared by this method. Dichloroethane and dioxane were found to be suitable helicogenic solvents for PBzLG whereas toluene was used for PHIC. In either case, all the solvents were dried over molecular sieve (24 hours) and distilled before use.

All polymer solutions were allowed to stand for at least 24 hours before use, not only to allow complete solution, but also to allow the escape of any trapped air bubbles introduced into the viscous solutions by stirring.

Concentrations were chosen such that the resultant solutions were manageable liquids, (i.e. were viscous enough to be ladled into the electrode gap using a flat spatula). In some cases, the solutions were gently warmed by standing in a water bath (approx. 50°C) for about 10 minutes prior to use, to assist in spreading between the electrodes.

6.4.3 Experiments

Having effectively described the general method followed to produce one poled, cast polymer film above, the complete work carried out using the poling/casting cell can be summarised in terms of a number of experiments employing this method.

<u>Sample Preparation</u>

1) Variation of Poling Field at Fixed Concentration

<u>PBzLG</u>

10 films of PBzLG were prepared from a 15% w/w solution

in dioxane, for electric fields of:-

0, 33, 66, 100, 133, 166, 200, 233, 266 and 300 V/mm.

Note: the electrode gap was 3.0mm.

PHIC

7 films of PHIC were prepared from a 3.76% w/w solution in toluene, for electric fields of:-

0, 57, 114, 171, 200, 228 and 286 V/mm.

Note: the electrode gap was 3.5mm.

2) Variation of Film Thickness at a Fixed Field

PBzLG

6 films were prepared at a fixed field of 133 V/mm (3mm gap). The magnitude of the field was chosen to ensure significant alignment had taken place, so that a detectable signal could be measured.

Variation of film thickness was achieved by evaporating different concentrations of PBzLG/dichloroethane solutions.

An initial 20% w/w solution of PBzLG (0.2035g) in dichloroethane (0.800g) was used to make the first film. This solution was diluted with more dichloroethane five times, with a new film being made after each dilution. The amount of dichloroethane added was, 0.196, 0.117, 0.102, 0.100 and 0.100. Note: after each dilution, the new solution was always stirred and then allowed to stand in warm water (approx. 50°C) for at least 2 hours before use.

3) High β Additives

Both 4-nitroanaline and 4-methoxy-4-N-nitrobenzylidene analine were found to be soluble in dioxane. Hence, solutions containing PBzLG and one of these additives were

prepared in dioxane, (using similar preparation precautions as for the neat polymer solutions) and then used to produce evaporated, two component films. The conditions used to produce the films are neatly summarised in the results section.

4) Unpoled, Evaporated Films (Control Samples)

As in the case of the guest host polymer systems, unpoled, control samples were made for all the evaporated, poled samples, by allowing polymer or polymer/additive solutions to evaporate in the electrode set-up, without a field being applied.

Note: in addition, some very thin, unpoled, evaporated films were also prepared by either spin coating a very dilute solution (< 1% w/w), or by smearing a solution on a glass slide using the edge of a sharp razor blade. In the latter case, it was intended that mechanical ordering would be obtained, and by smearing as thin as possible, "instant evaporation" would lock the alignment within the film.

Other Experiments

1) Observations were made using a Leitz microscope with crossed polarizers, during the poling/evaporation process for PBzLG and PHIC film formation. This was easily achieved by placing the casting cell, on the microscope stand and utilising the drilled hole, design feature of the cell. The observations reported in the results section, were compiled from a number of evaporations.

2) Thermal effects on the poled nature of PHIC films were studied by:-

a) trying to pole a precast film by a typical heat (150°C) / poling (633 V/mm) process (as is usually performed when poling polymers with glass transition temperatures);

or b) preparing a poled sample by the evaporation technique, heating half of it at 150°C for 20 minutes without a field, and then comparing the two halves.

3) The thickness of samples was measured using an instrument called a Rank Taylor Hobson Talysurf. The instrument was capable of producing a profile plot of the film surface, to an accuracy of +/- 0.5 microns, by drawing a diamond stylus over it. In practise, the stylus was first drawn along the surface of the glass slide until a flat trace was obtained which could act as the reference height. The stylus was then run up over the edge of the film from the glass surface to give the required profile of this step and the first few centimetres of the film surface. Thickness profiles of the samples were usually measured in the centre of the films, running the stylus perpendicular to the applied field (i.e. parallel to where the electrodes had been), since it was these regions of the films which were subsequently tested for SHG. The step in question, was always made quite clear by cutting the film with a razor blade, parallel to the poling direction.

A sample of some of these profiles are given in the result section (figures 6.6.10 and 6.6.3) of this work.

6.4.4 Results

1)View of Poling/Evaporation Process Using Polarising Microscope

PBzLG

Typically disordered cholesteric (focal conic) liquid crystal properties were only observed during the evaporation process, once the solution had become concentrated enough, (probably around 14% w/w in dioxane). At this stage, without a field present, there was a general flow of l.c. texture. On application of a field as low as 40 V/mm, strong swirls of texture were seen emanating from points on the positive electrode, but not from the negative one.

In the later stages of the evaporation, this swirling motion gradually slowed under the more viscous properties of the concentrated solution. The disruptive nature of the swirling motion was evident in many of the final films which still resembled a focal conic texture.

In a lot of the poled PBzLG films, this focal conic texture tended to obscure other areas or layers which resembled a well ordered structure. Where this ordered structure was observed, the grain of the alignment appeared to run parallel to the electrode surface, (i.e. perpendicular to the field).

PHIC

A dark view was seen throughout most of the evaporation process. However, in the later stages, coloured bands parallel to the electrodes were seen to emerge and

remained, for a particular orientation of the sample. On rotation of the sample through 90 degrees, the coloured bands were lost revealing a textured grain (figure 6.6.21).

2) Thermal Effects on PHIC

Treatment	Cross-polar Description	SHG Signal Rel. to quartz
Film 1		
i) Poled/Evaporated (as described)	Coloured Bands	0.07-0.10
Film 2		
i) Heat Film 1 at 150°C (20 min.)	Coloured Bands (No change)	0
Film 3		
i) Evaporate film between electrodes ii) Heat 150°C iii) Apply 633 V/mm iv) Allow to cool with field on.	No Coloured Bands (Same as unpoled evaporated film)	0

6.5 Magnetic Alignment of PBzLG/Poly(NVP) Guest Host System

The following very simple experiment was carried out to produce a magnetically aligned sample of the above guest host polymer system.

A 10% w/w solution of PBzLG in NVP was made and smeared on a glass slide. PTFE spacers were used to separate the

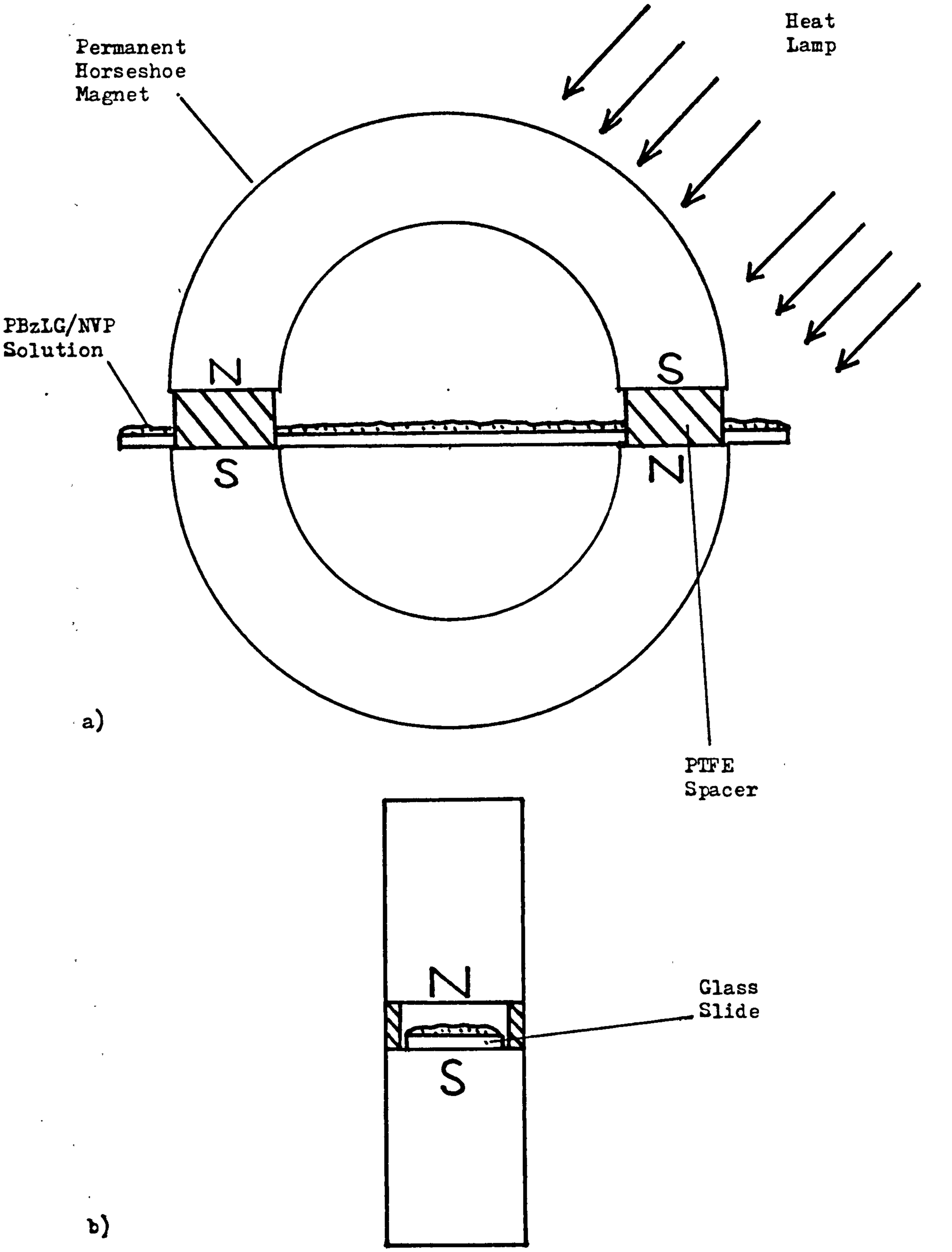

Figure 6.5.1 Side (a) and end (b) view of apparatus used for magnetically aligned film.

poles of two permanent horseshoe magnets, which were arranged so that the two pairs of facing poles attracted. The glass slide was slid into the gap between the poles as illustrated by figure 6.5.1. The film was cured at about 70°C for about one and half hours by shining the heat lamp in at an angle. Finally, the set-up was allowed to cool for 30 minutes before separating the magnets.

The sample was examined and tested using both a Leitz polarising microscope and the laser set-up for SHG detection.

Observations

The polarising microscope indicated that the magnitude of the magnetic field had been sufficient to align the PBzLG molecules in the film. Two contrasting regions of the film could be distinguished.

A) In the regions of the film where the poles of the magnet had covered the film, a completely dark view was seen which did not change on rotation of the sample through 360 degrees.

B) In other regions of the film (outside the polar regions), a texture pattern of dark and light patches was seen which changed through dark and light on rotation of the sample.

To the naked eye, these regions also looked different, with signs of phase separation (milky separation) in the regions away from the poles, and fine optical clarity in the polar regions.

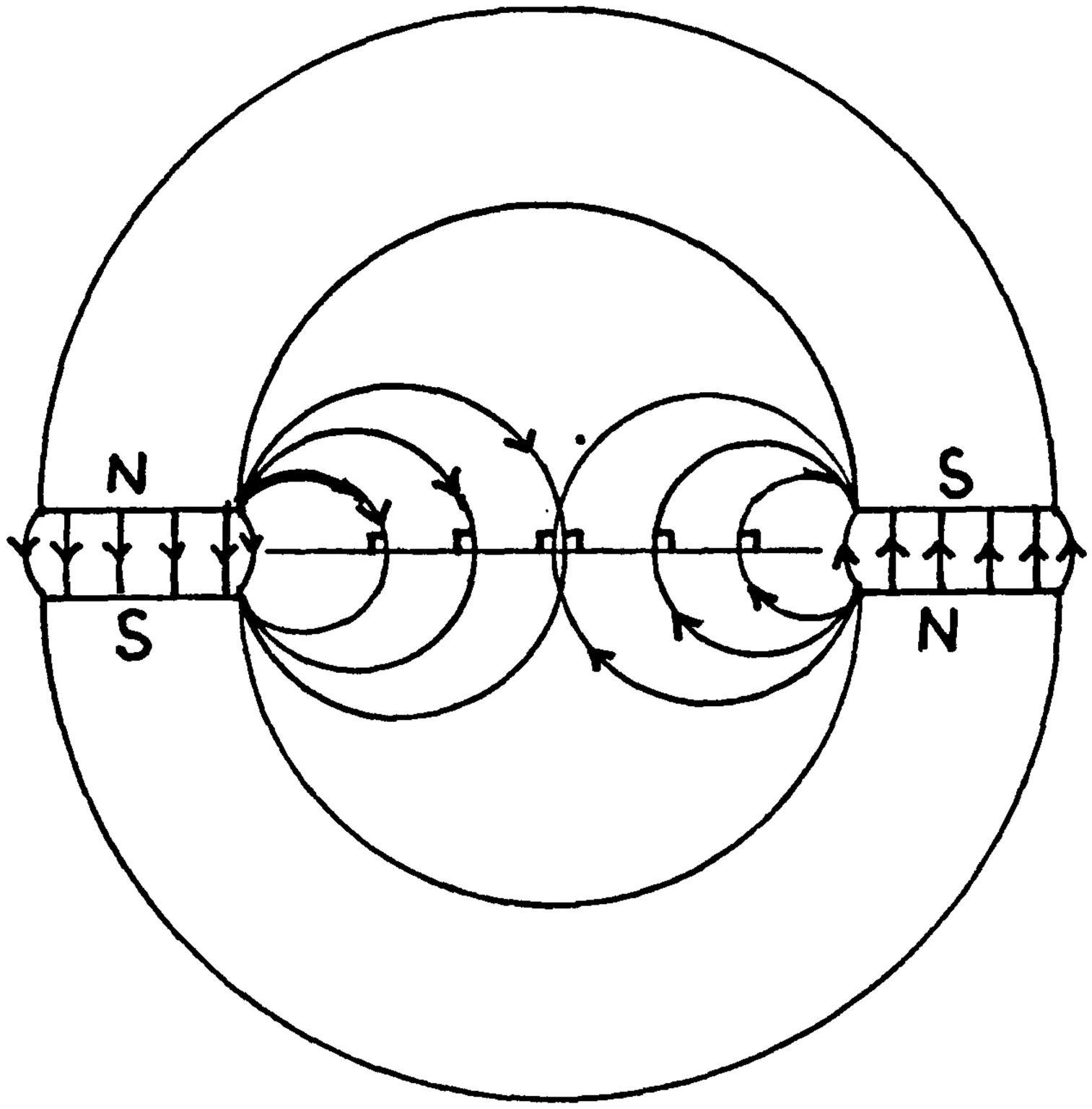

Figure 6.5.2 Magnetic flux lines for horseshoe magnet arrangement.

Comments

The distinct contrast in the two regions of the film can simply be put down to the reduction in the size of the film on moving away from the polar regions. Figure 6.5.2 shows the expected flux pattern for the arrangements of the magnets, which indicates that the field was perpendicular to the film surface at all points on the film. It also emphasises how the density of flux lines decreases rapidly, on moving away from the polar region. Hence, the completely dark view observed in the polar regions is caused by the helices aligning with their axes parallel to the field, and with random order of side chains perpendicular to the axes, so no birefringence can be observed.

On moving away from the poles, as soon as the field is no longer strong enough to orientate the helices, the sample shows its biphasic texture which has been locked within the cured host polymer system.

The subsequent lack of SHG signal (section 6.6.3) can be attributed to two possible factors.

i) Although the α-helix is a non-centrosymmetric structure, it can be incorporated in an antiparallel arrangement with other helices so that the bulk structure is centrosymmetric. In the case of a magnetic field (in contrast to the electric field case) although helices align, there is no driving force for their electric dipole moments to align parallel, and statistical randomisation tends to produce the antiparallel (centrosymmetric) situation.

ii) In view of the small SHG signal observed for a poled, neat PBzLG sample, the SHG signal from a 10%w/w PBzLG/Poly(NVP) magnetically aligned sample may have been too small to detect.

6.6 Testing For Second Harmonic Generation

6.6.1 Laser Set-up

Figure 6.6.1 shows the laser set-up used for the testing of the polymeric materials for SHG.

The elements of the apparatus were set-up on an optical bench. The Nd:YAG laser was used with its own frequency doubler (lithium niobate crystal) removed, and its output was horizontally polarised, infrared light at a wavelength of 1064 nm. The laser was only ever operated in a pulsed mode, in the frequency range of 0.5 - 3 Hz.

The optical alignment of the whole system was achieved using a low power, visible (red) helium-neon (HENE) laser which was attached to the back of the Nd:YAG laser (i.e. the placing of burn paper at varying points in the optical path revealed if burn marks made by the infrared radiation coincide with the red HENE spot).

The intensity control (in figure 6.6.1), was needed for two main reasons:-

1) to improve the signal for samples with weak SHG efficiency;

2) to prevent laser damage for samples with a low threshold level.

The filters F_1, before the sample and reference quartz,

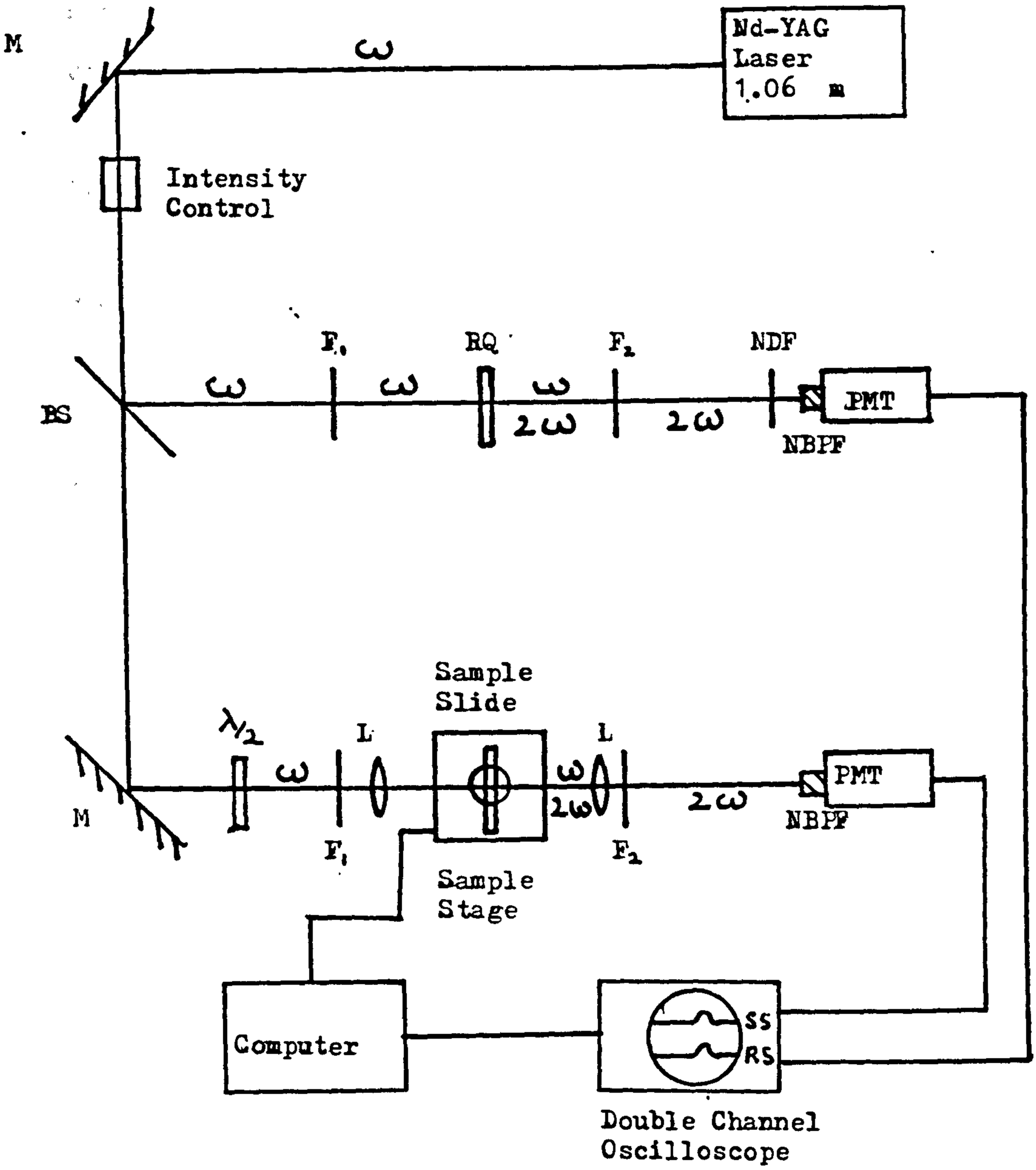

Key

Intensity control = variable neutral density filter.
F = filter
NDF = neutral density filter
NBPF = narrow band pass filter
$\lambda/2$ = half-wave plate
L = lens
RQ = reference quartz (Y-cut)
PMT = Photomultiplier tube
M = mirror
BS = beam splitter

Figure 6.6.1 Plan view of laser set-up for SHG measurement.

removed any stray green light, whereas F_2 removed unconverted infrared light, leaving the second harmonic (532 nm, green light) produced by the sample and reference to pass through.

Each PMT was fitted with a 1 nm narrow band pass filter for 532 nm, ensuring monochromated light was detected. Output from the PMTs, was recorded on a Hewlett Packard double channel oscilloscope allowing sample and reference signals to be displayed and measured (usually as an average of a number of pulses). The 'scope was always triggered using the reference signal.

Samples had usually been prepared on glass slides which readily fitted onto the sample stage. The stage was electronically controlled, allowing:-

1) the slide to be rotated horizontally, in the same plane as the optical table;

2) the slide to be scanned horizontally and vertically in the plane perpendicular to the optical table.

The stage and the oscilloscope could both be controlled from a computer program, which greatly improved the collection of data for samples which had to be scanned or rotated.

The half-wave plate shown in the sample line was used to rotate the polarisation of the laser light. The half-wave plate was rotated manually during experiments, and the important point to note was that a change in angle (A) of the half-wave plate, resulted in a change in angle (2A) for the polarisation of the laser light.

The reference line contained a 2 mm thick, Y cut quartz slab, which was fixed rigidly during testing for two reasons.

1) The quartz would only give a signal if it was correctly oriented for the horizontally polarised laser light.

2) The SHG signal varied depending on the angle of the quartz slab to the incident laser light.

Neutral density filters were needed in the reference line for samples with low SHG efficiency. Owing to the limitations of the PMTs, a signal > 1V could not be accurately measured because of saturation effects within the PMT. The use of a NDF allowed greater laser intensity to be incident on the sample without saturating the reference line. The actual value of the reference line signal (RS_c) was then given by:-

$$RS_c = RS_m \times 10^{NDF}$$

where RS_m = measured reference signal for the particular NDF value.

Sample Testing

Before deciding that a sample was not SHG active, it was important to ensure that a thorough scan of the sample had been made using reasonable intensity of infrared laser light (> 1V signal on reference line), for all orientations of the laser polarisation. This was performed for the laser beam at 45° and 90° to the sample plane.

This general approach to sample testing ensured an active sample was not mistakenly assumed inactive because it had only been tested for a set of non-phase matching

conditions.

Having found an active sample, the following summarises the characteristics and trends that were investigated:-

1) variation of signal with change in laser light polarisation;

2) variation of signal with film thickness;

3) aging effects on the signal.

Films Tested:-

1) certain guest host polymer samples originally made for piezoelectric testing, were tested in regions of the films which did not have aluminium electrodes evaporated on;

2) all L.B. Films;

3) all films cast from solvent;

4) a magnetically aligned guest host polymer sample.

6.6.2 Referencing

It was important to ensure that any measurements made using the set-up could be compared quantitatively with each other.

To begin with, a reference line was needed because the laser did not produce pulses of equal power. However, the beam splitter divided the power each time such that the ratio of power in one line to that in the other was constant for any pulse. Hence the ratio of SHG signals for the sample to quartz line should also be constant for any pulse.

At this point having used a piece of quartz in the reference line, it would be wrong to say that the value of

the ratio showed how the sample compared to quartz because:-

1) the beam splitter did not divide the power of the infrared beam 50/50;

2) half-wave plates, lenses and mirrors absorb some power on the sample line;

3) the PMTs are not identical.

In principle, to make a comparison of the sample with quartz, a second piece of quartz was used to replace the sample so that it was tested in exactly the same environment as the sample. The ratio then obtained for the second piece of quartz could be compared with the ratio for that of the sample, to allow the true quantitative comparison to be made.

In practice, whenever a sample was tested, a referencing sample (i.e. quartz or PVDF) whose SHG response was known not to vary over long periods of time, was also tested in the sample line.

Hence the ratio, $\left[\frac{\frac{S}{QR}}{\frac{RS}{QR'}}\right]$

where S = sample signal

RS = referencing sample signal

QR, QR' = quartz reference line signal

was the quantitative value used for comparing samples.

The following describes how the referencing sample was measured:-

Referencing Sample	Orientation of Measurement
Quartz, y cut 2 mm thick slab.	Slab rotated about 10° from normal incidence of laser beam coinciding with the first Maker fringe maximum.
PVDF-Poled 25μm film biaxially drawn	Film plane at 45° to laser beam (value rel. to quartz = 0.27)

Note:- in either case, the maximum SHG signal was obtained by rotation of the polarisation angle of the laser beam using the half-wave plate.

6.6.3 Results

The SHG values given in the following list are an attempt to give a quantitative comparison between the various samples produced. The values represent the best signal detected for all samples, from regions of films which showed a reasonable uniformity of thickness (i.e. flat parallel sides). For the case of poled PBzLG and PHIC, each value represents testing carried out on 20-30 samples.

The values are given relative to the 2 mm thick Y-cut quartz plate, as described in the experimental section. If needs be, a comparison relative to the PVDF reference sample can also be determined, using the scaling factor given in the "Referencing Section".

a) PBzLG/NVP/TGDM Guest Host Polymer Samples

Sample	PBzLG:NVP:TGDM % w/w	Precure Before Poling	Field KV/mm	SHG Signal Rel. to Quartz
(A1)	10:90:0	NO	0.1	< 0.001
(A2)	5:80:15	YES	1.6	0
(A3)	8:80:12	NO	0	
(A4)	0:0:100	NO	0.4	
(A5)	5:80:15	YES	1.0	
(A6)	0:100:0	NO	0	

b) Magnetically Aligned 10% w/w PBzLG/Poly(NVP)

Region of Film Tested	SHG Signal
Polar Area	0
Outside Poles	0

c) L.B. Films

All L.B. films tested gave no detectable SHG signal.

d) Films Cast from Evaporating Solvent

Sample	Thickness μm	SHG Signal Rel. to Quartz
Poled PBzLG(133.3V/mm)	20 ± 2	0.07
Poled PHIC (286 V/mm)	22 ± 2	0.35
Unpoled PBzLG	20	0
Unpoled PHIC	20	
Unpoled PBzLG- smeared	1	

e) PBzLG Films Containing Additives

i) 4-Nitroanaline (p-NA)

The following table summarises the results and observations made on PBzLG films containing p-NA, soon after preparation (within 1 hour).

Preparation Method	Concentration p-NA:PBzLG/% w/w	Film Description (2)	(1) SHG Signal Rel. to Quartz
Poled-133V/mm	13	A	0.07-0.5
Steel Electrodes	50	A	Patchy Signal
Unpoled- Steel	13	A	0.07-0.5
Electrodes	50	A	Patchy Signal
Unpoled- Thin	13	B	0.07-0.5
Smear	50	C	0
Unpoled- Spin	13	B	0.07-0.35
Coated 2500 rpm.			
Evaporated	100	D	0.07-0.5 Very Patchy Signal

(1) The SHG signal was only found for phase separated regions of the films.

(2) Film Descriptions

(A) Conglomerate of phase separated yellow crystalline structure.

(B) There was temporary solid solution for up to 2 hours before phase separation occurred to give yellow speckled regions, visible to the naked eye. In certain regions of the well ordered film, selective blue reflection of light was observed. Under the microscope, a large grain size

(relative to description C) of phase separated crystallites was observed, with an aligned background of PBzLG.

(C) Under the microscope, a small grain size (relative to description B) of phase separated crystallites was observed, with no alignment in the background of PBzLG.

(D) Films of randomly oriented large needlelike p-NA crystals.

Aging Experiments

For all these films containing p-NA the SHG signal observed was lost within 24 hours of making the films.

ii) 4-methoxy-4-nitrobenzylidene analine (MNBA)

Preparation Method	Concentration MNBA:PBzLG/%w/w	Film Description	SHG Signal Rel. to Quartz
Poled-200V/mm Steel Electrodes	10	E	0.01
Unpoled- Steel	10	E	0

(E) A yellow transparent solid solution.

Aging Observations

The signal of 0.01 was still present after 9 months.

PBzLG and PHIC Films

For figures 6.6.4-9 and 6.6.11-15, the particular samples were tested as indicated by figure 6.6.2, with the samples oriented with their poling direction parallel to the plane of the optical table.

For figures 6.6.4-9 and 6.6.11-14, the samples were fixed normal to the laser beam. The abscissa, "Polar

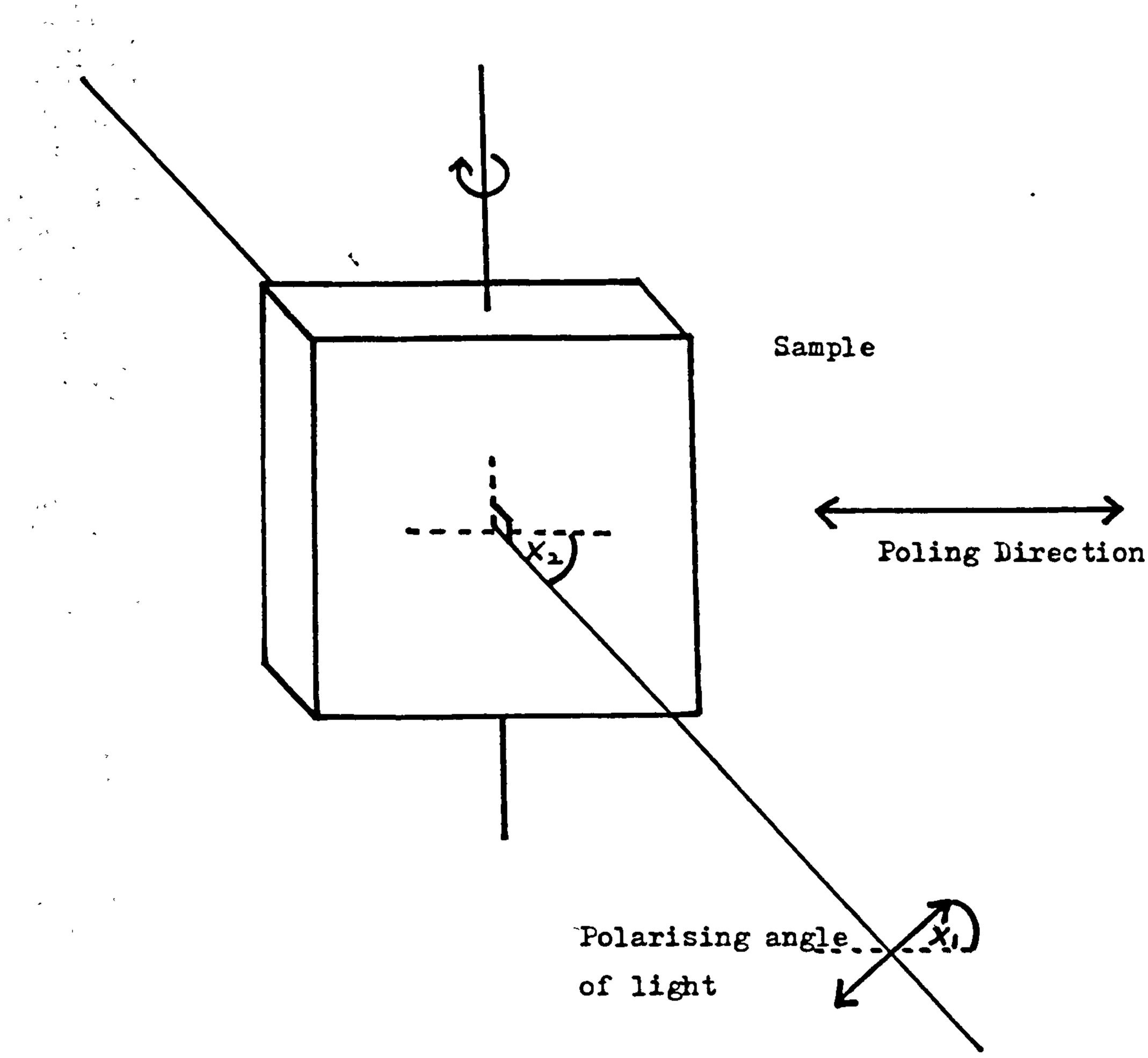

(without half-wave plate, $x_1 = 0$
i.e horizontally polarised)

Figure 6.6.2 Geometry of experimental set-up for measuring SHG, defining orientation of sample and polarising angle of light.

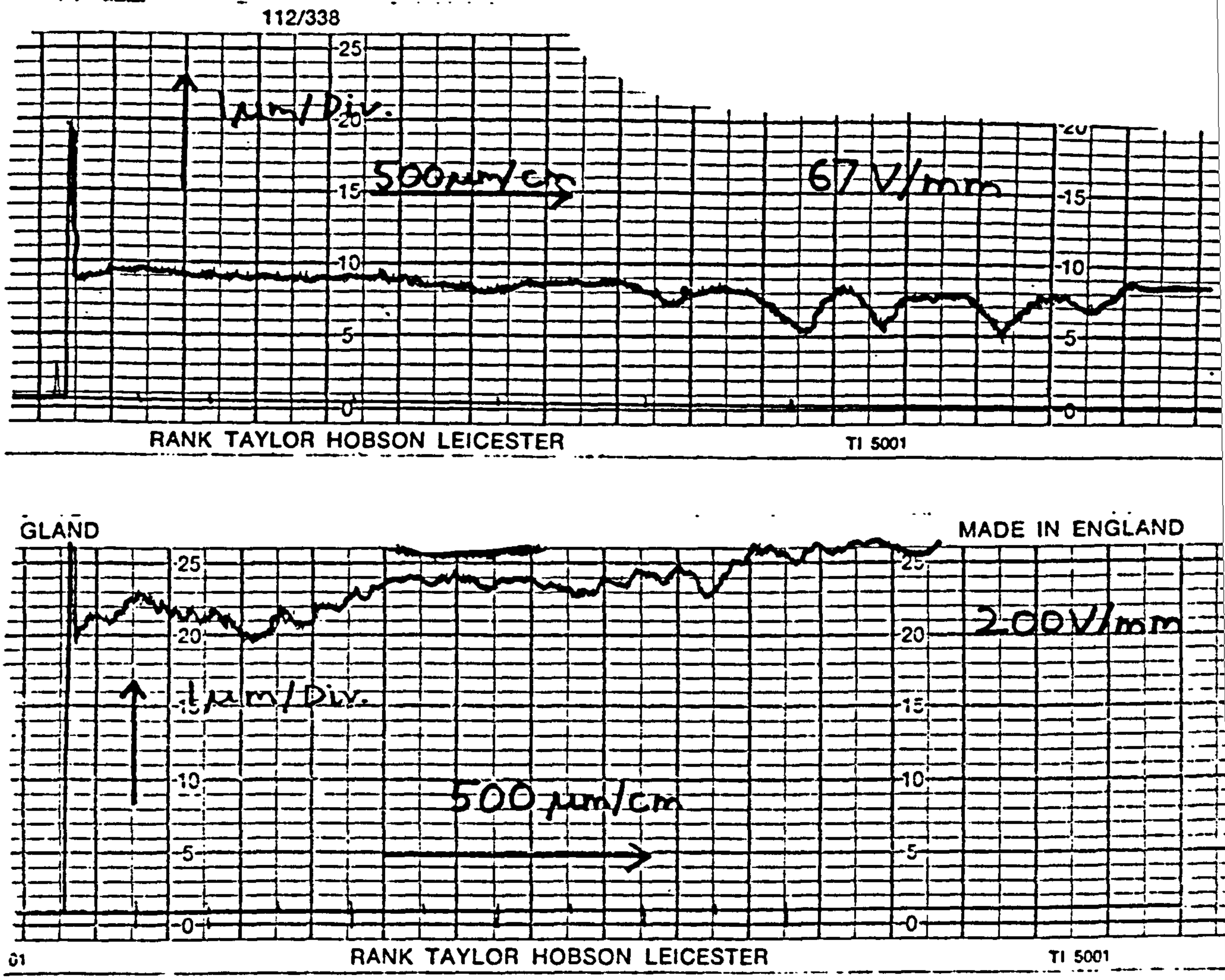

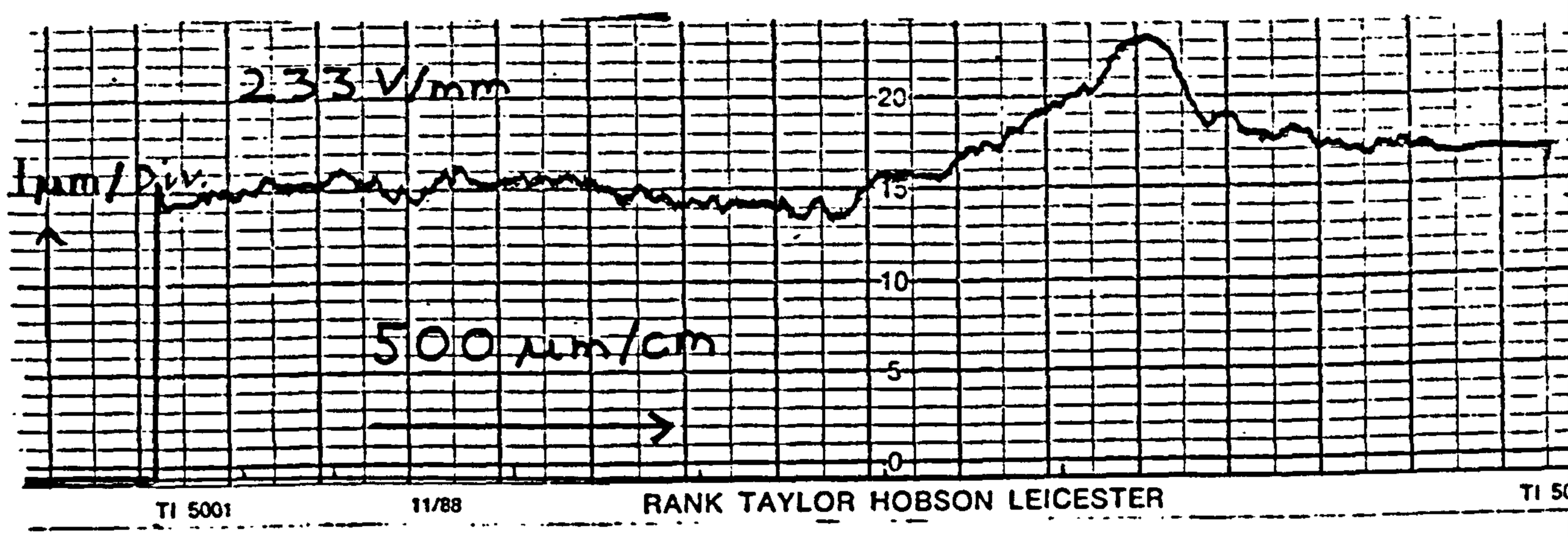

Figure 6.6.3 Talysurf plots of PBzLG films.

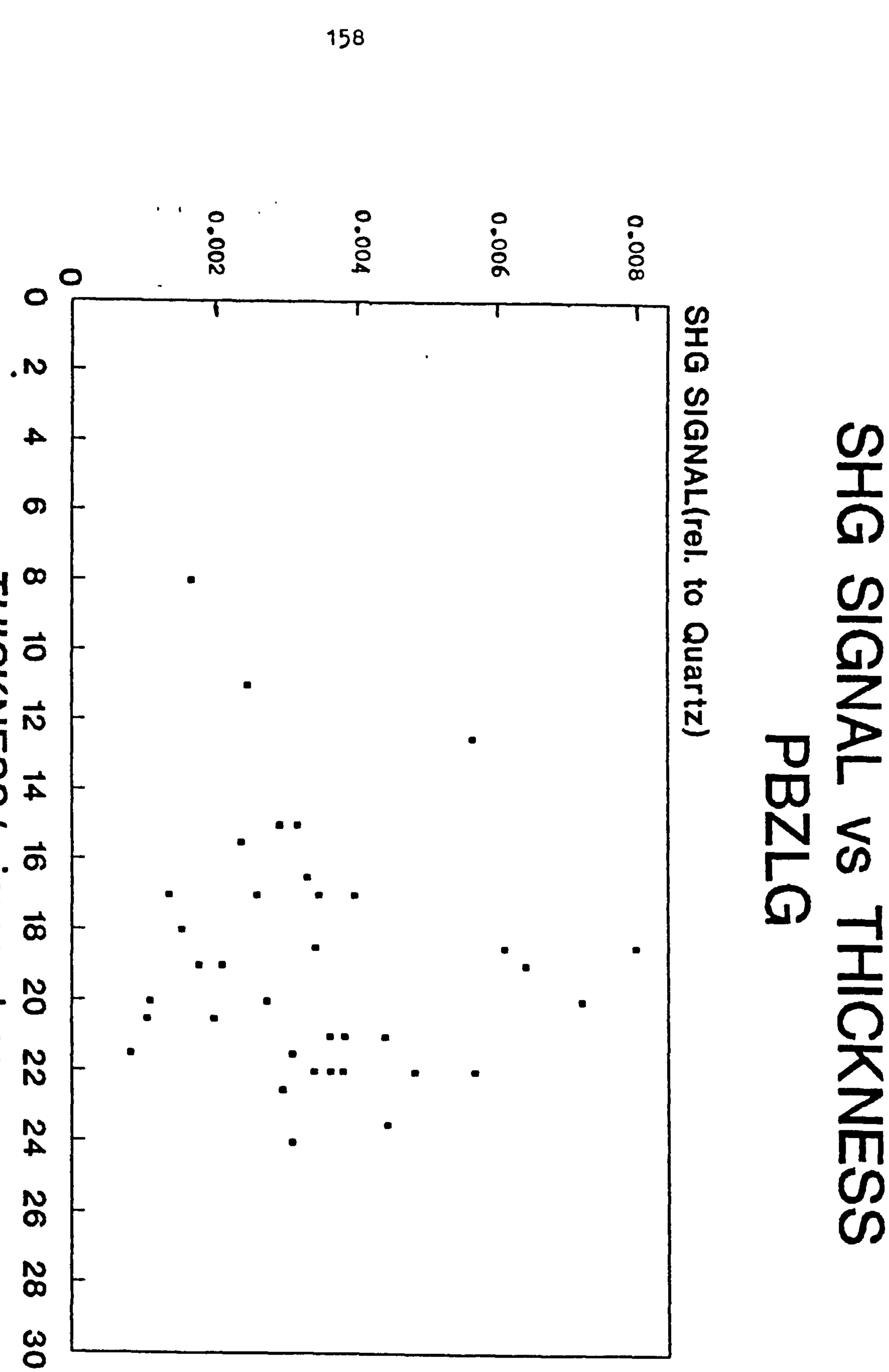

Figure 6.6.4 SHG vs. thickness for PBzLG (poled at 133 V/mm).

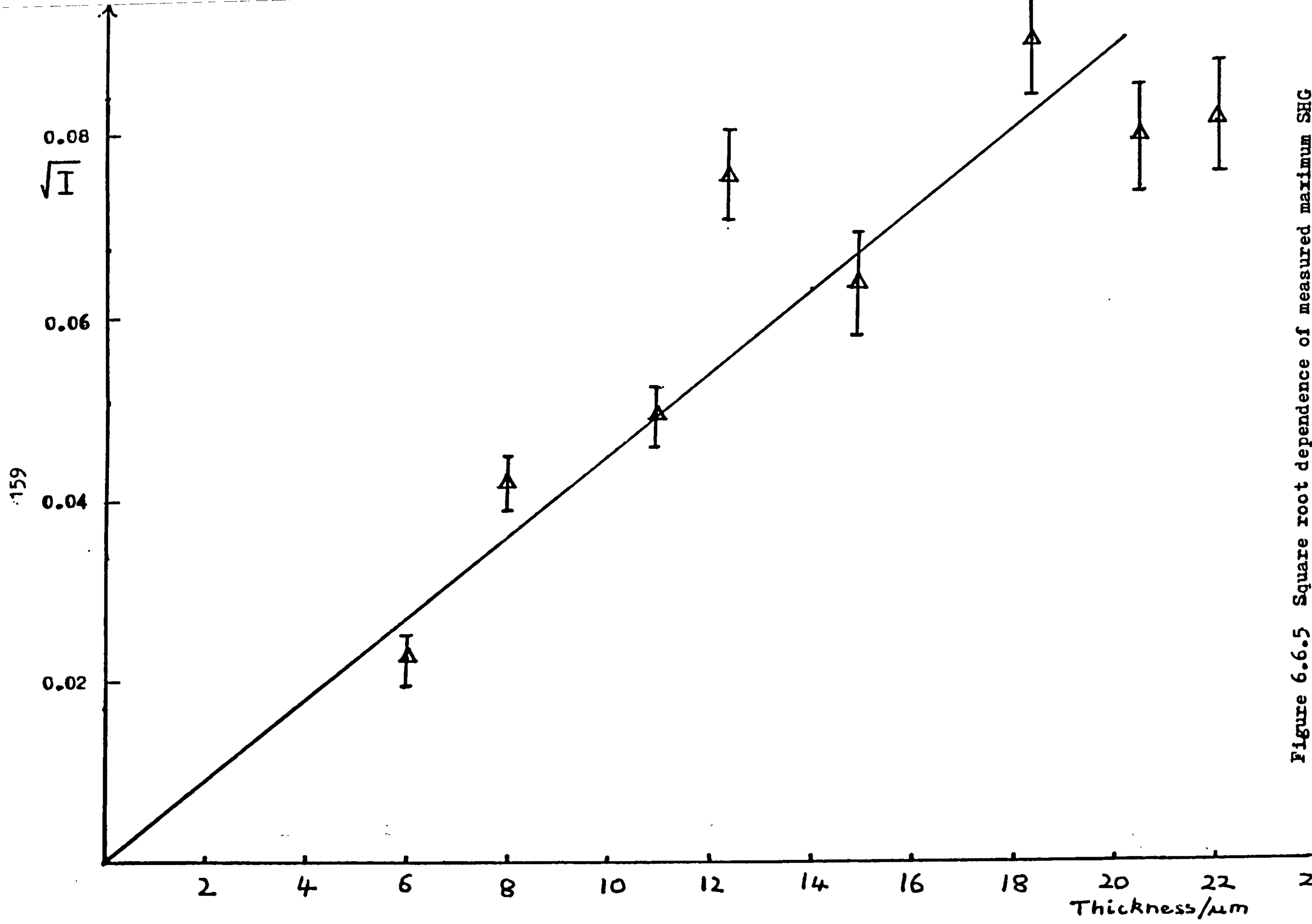

Figure 6.6.5 Square root dependence of measured maximum SHG signal vs. thickness for PBzLG.

SHG SIGNAL VS POLAR ANGLE PBZLG 300V/mm

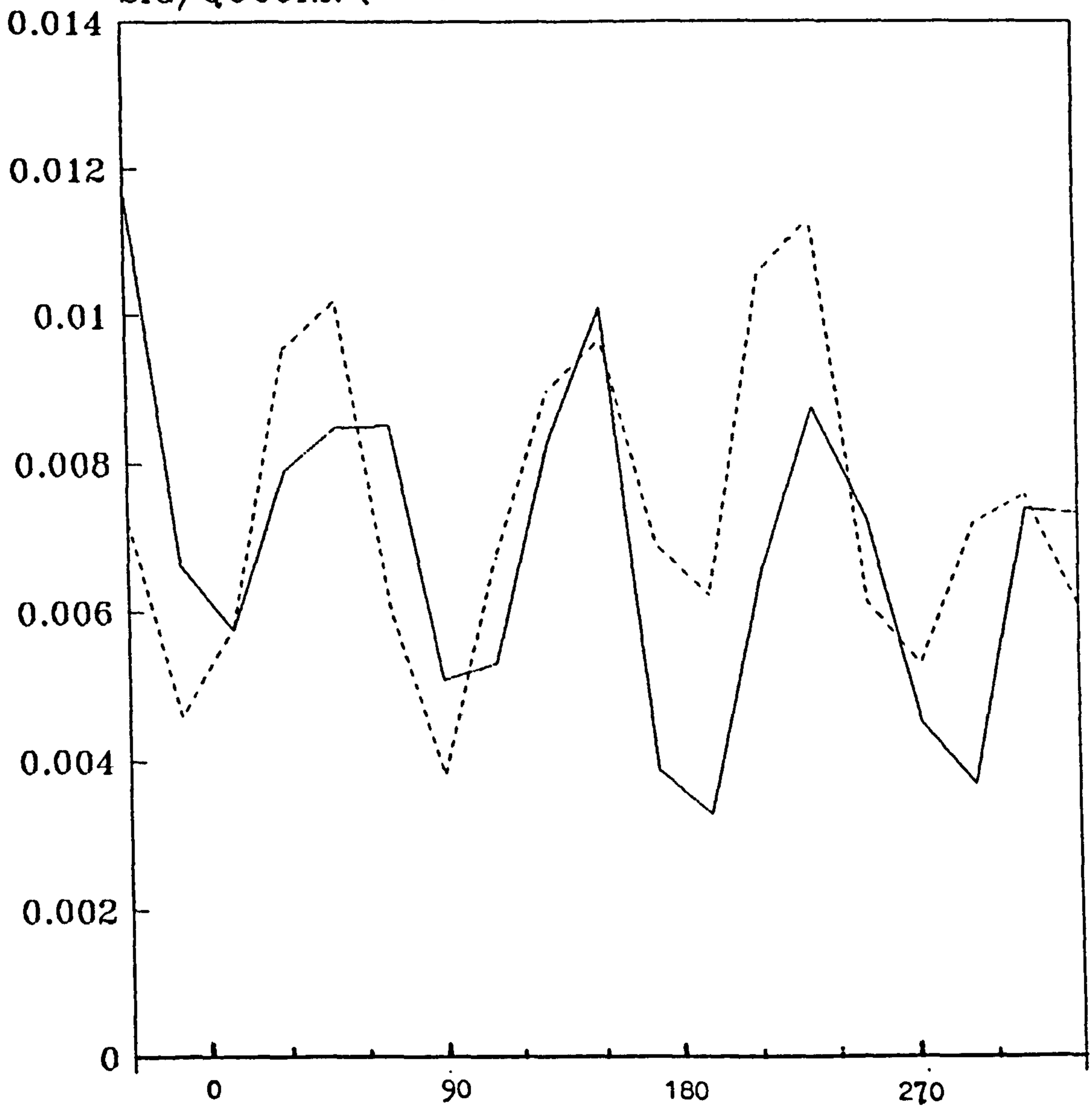

Figure 6.6.6 SHG vs. polarisation angle of light

SHG SIGNAL VS POLAR ANGLE PBZLG 233V/mm

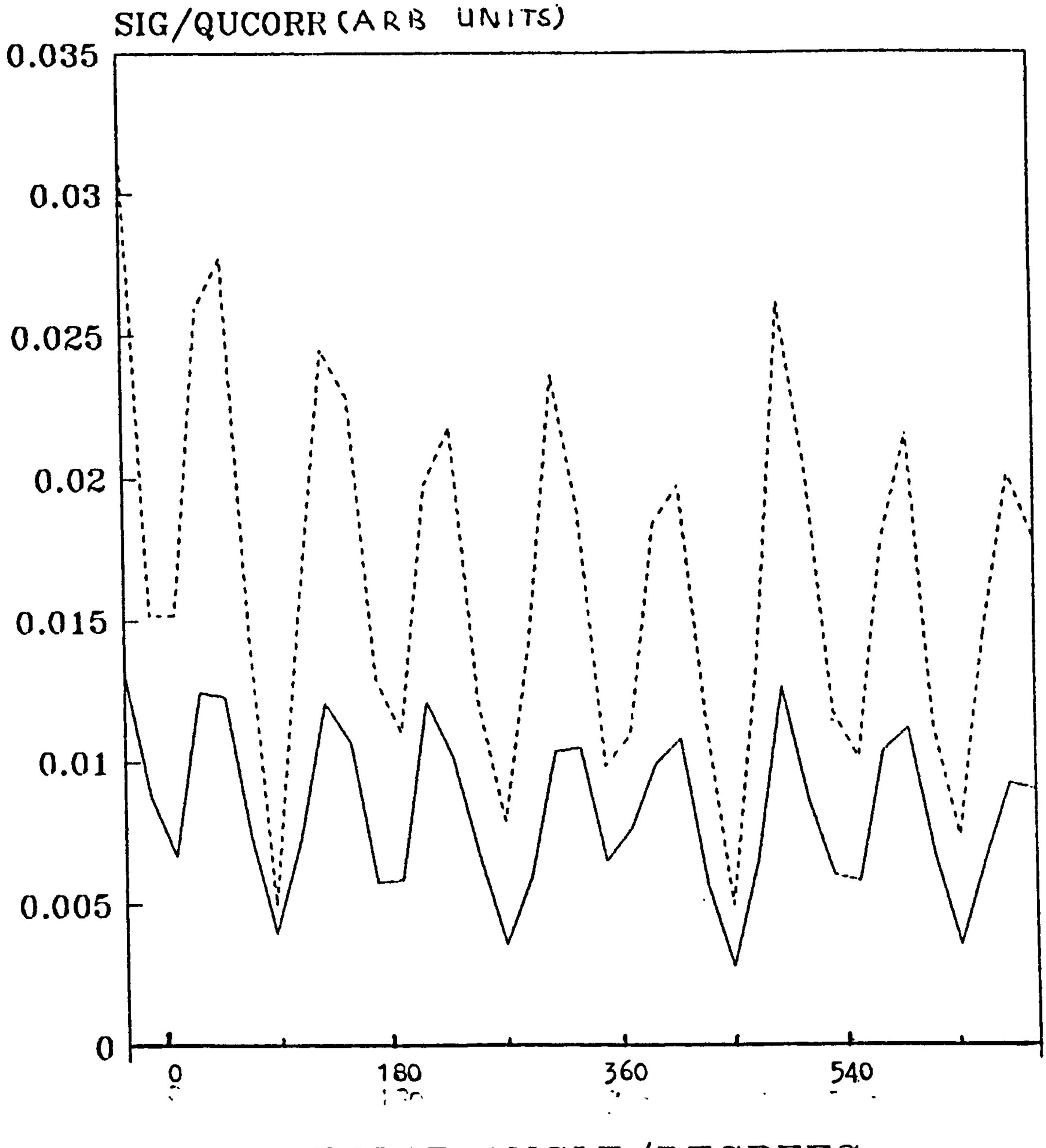

Figure 6.6.7 SHG vs. polarisation angle of light.

SHG SIGNAL VS POLAR ANGLE PBZLG 266V/mm

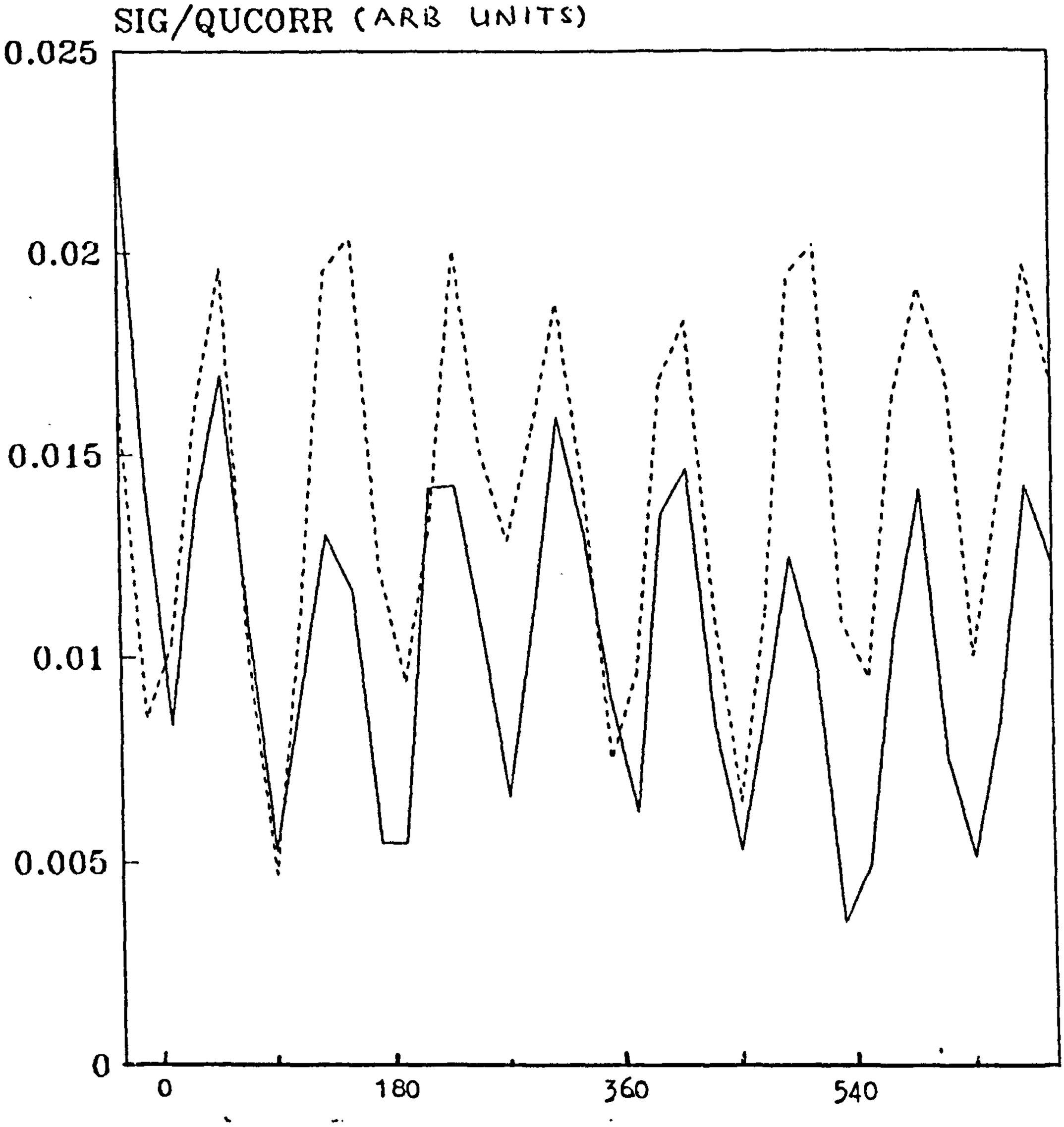

Figure 6.6.8 SHG vs. polarisation of light.

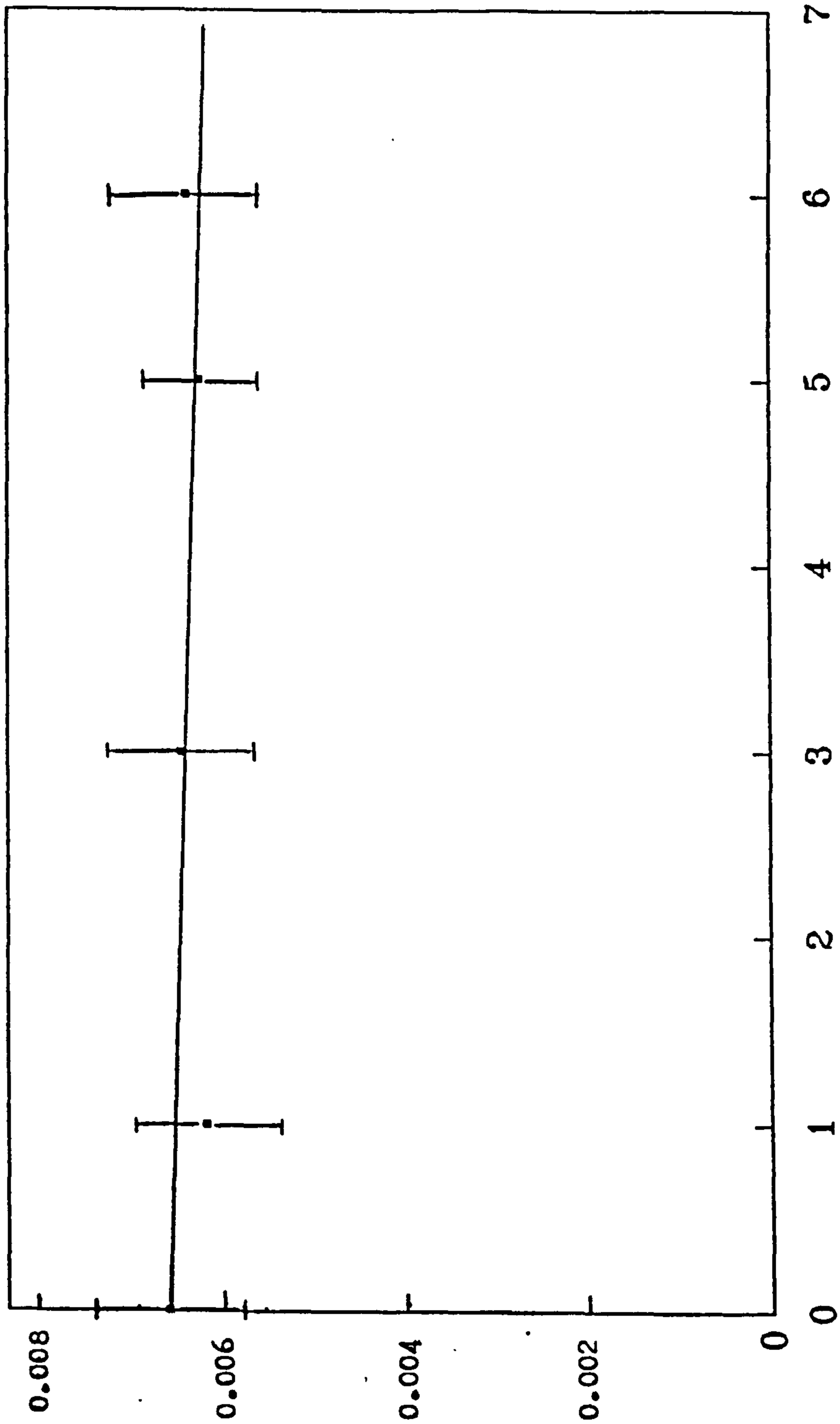

Figure 6.6.9 Ageing of SHG signal in PBzLG film.

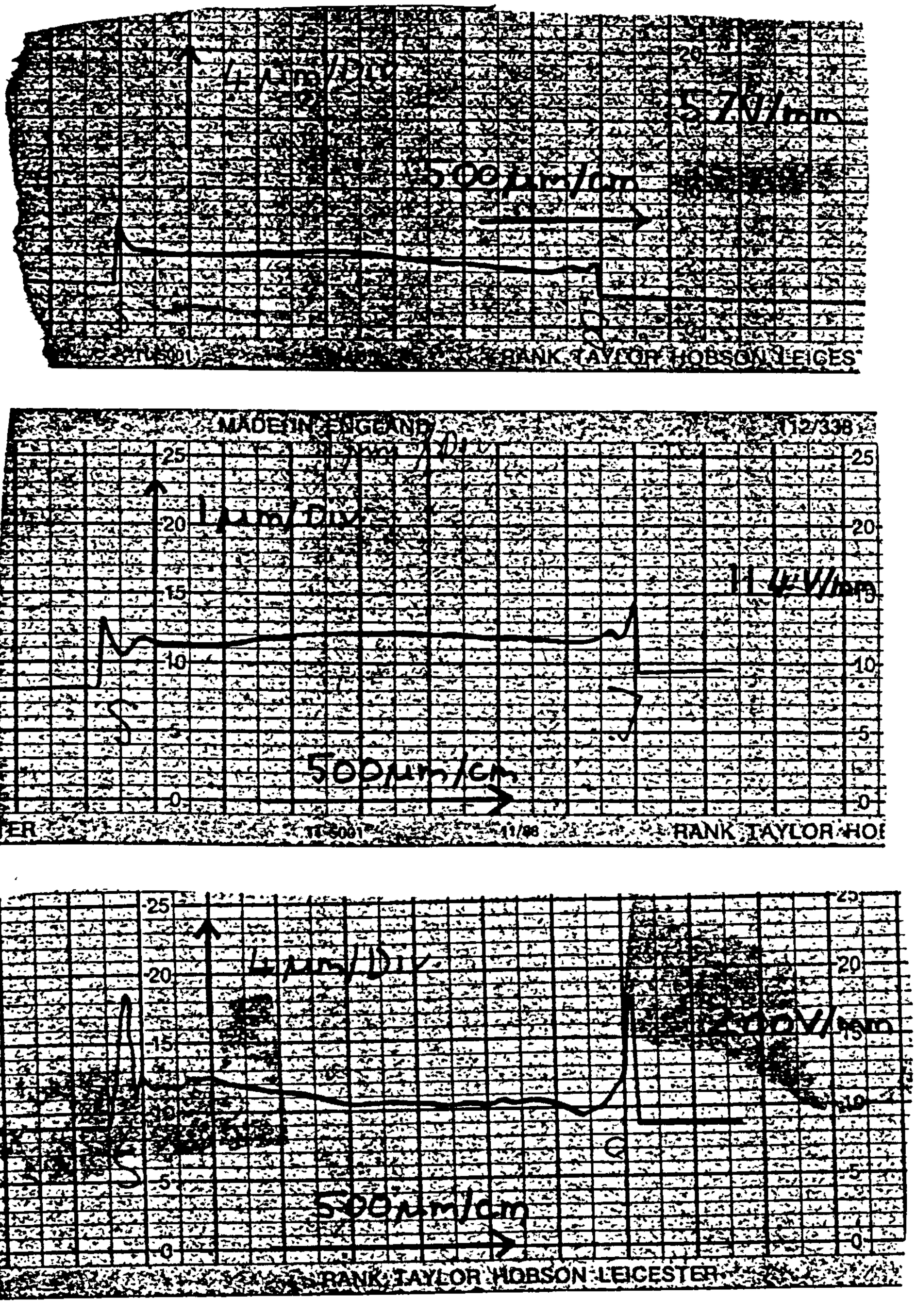

Figure 6.6.10 Talysurf plots for PHIC samples.

SHG SIGNAL vs ELECTRIC FIELD
PHIC/5(±3) micrometres

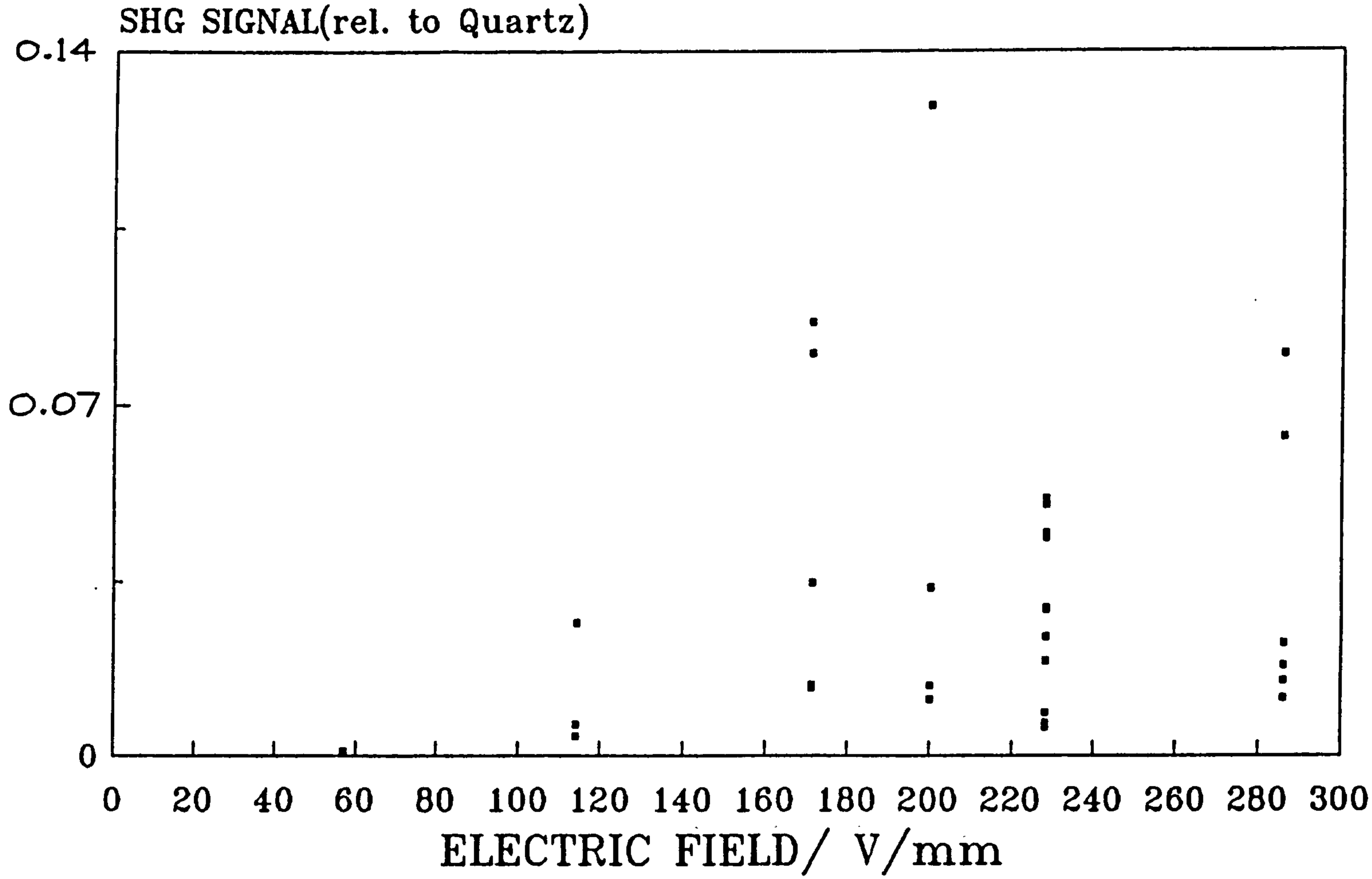

Figure 6.6.11 SHG vs. electric field for a fixed thickness.

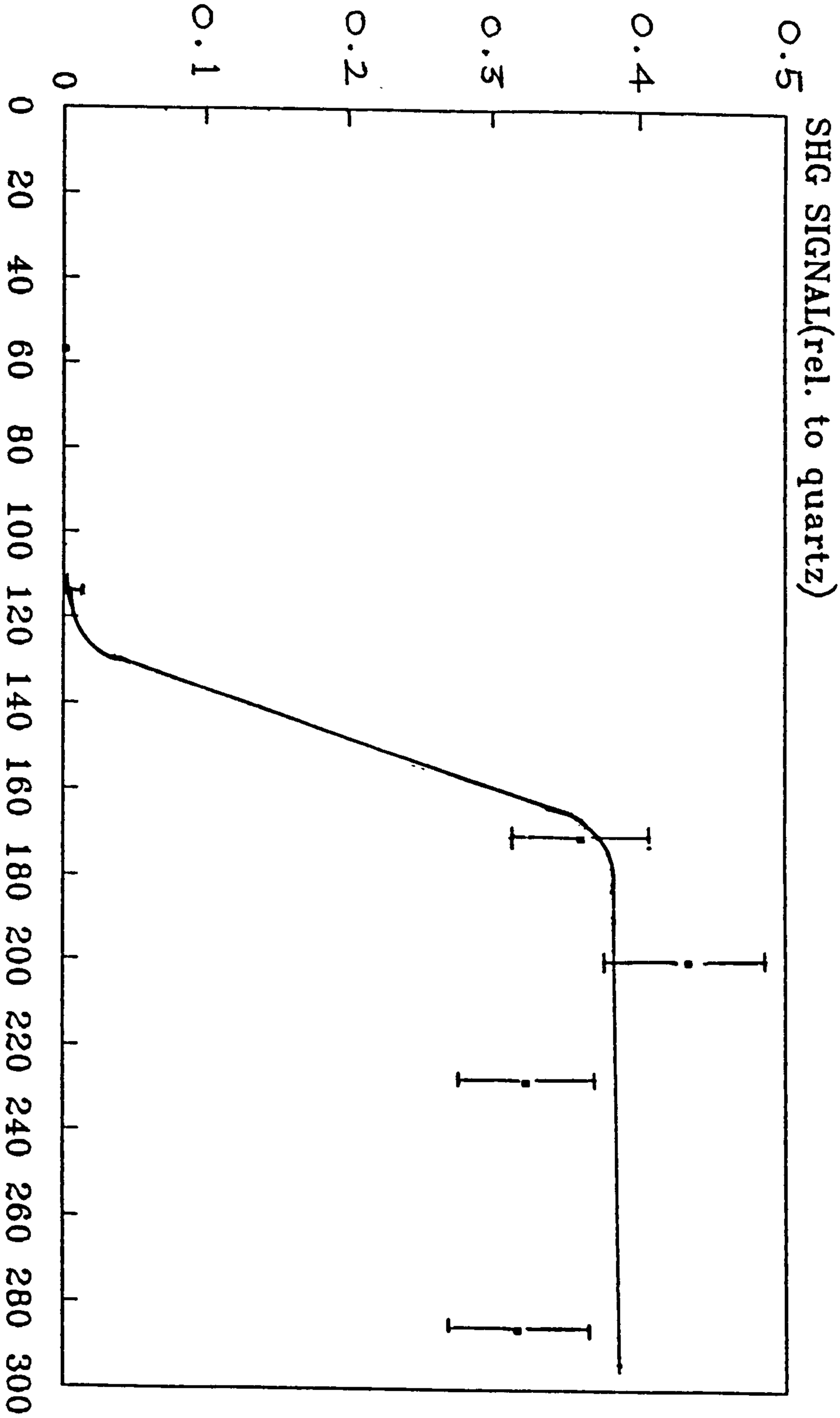

Figure 6.6.12 SHG vs. electric field for a fixed thickness.

SHG SIGNAL VS POLAR ANGLE
PHIC 266V/mm

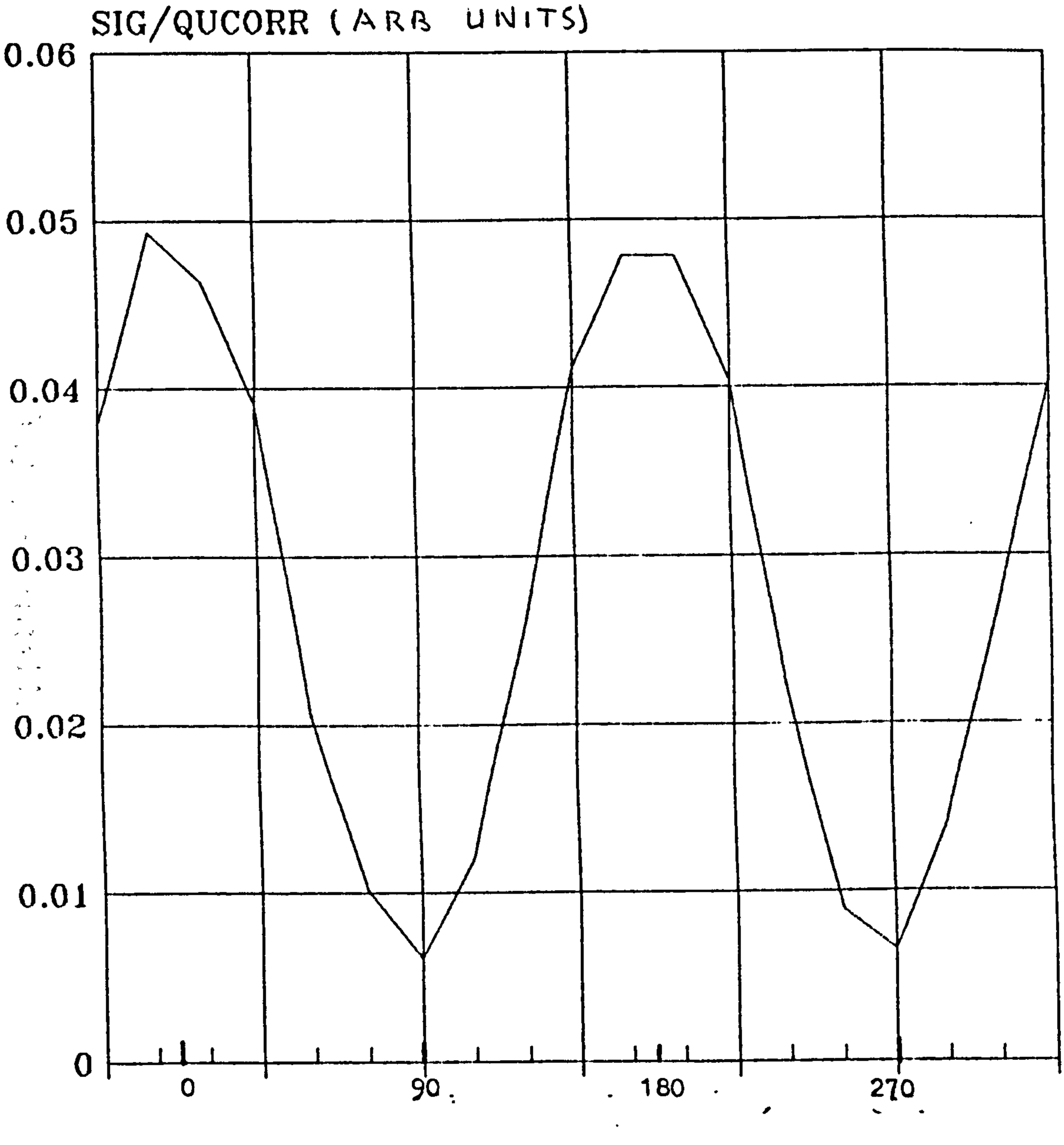

Figure 6.6.13 SHG vs polarisation angle of light.

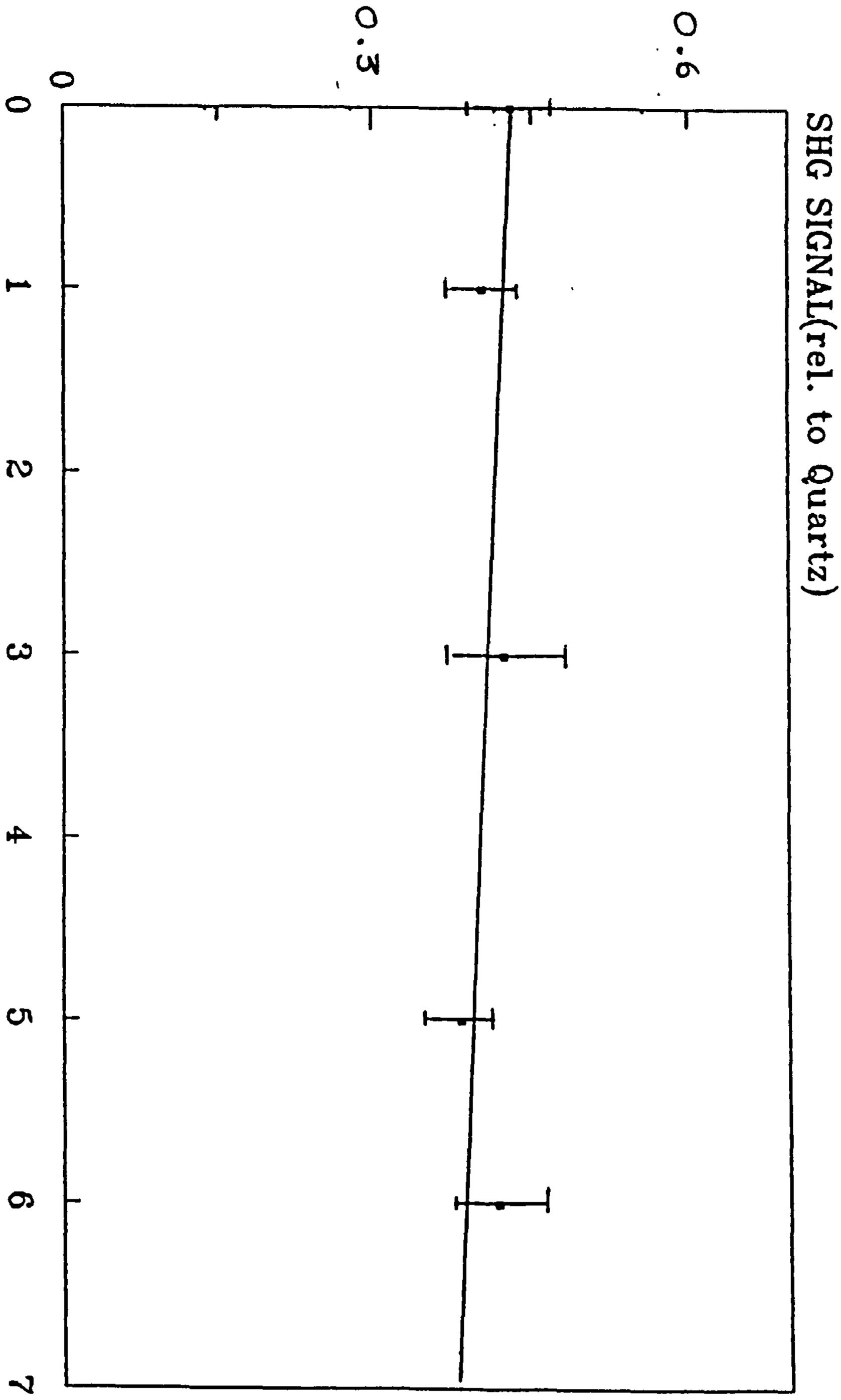

Figure 6.6.14 Ageing of SHG signal for a PHIC sample.

SHG vs ANGLE OF SAMPLE for PHIC sample

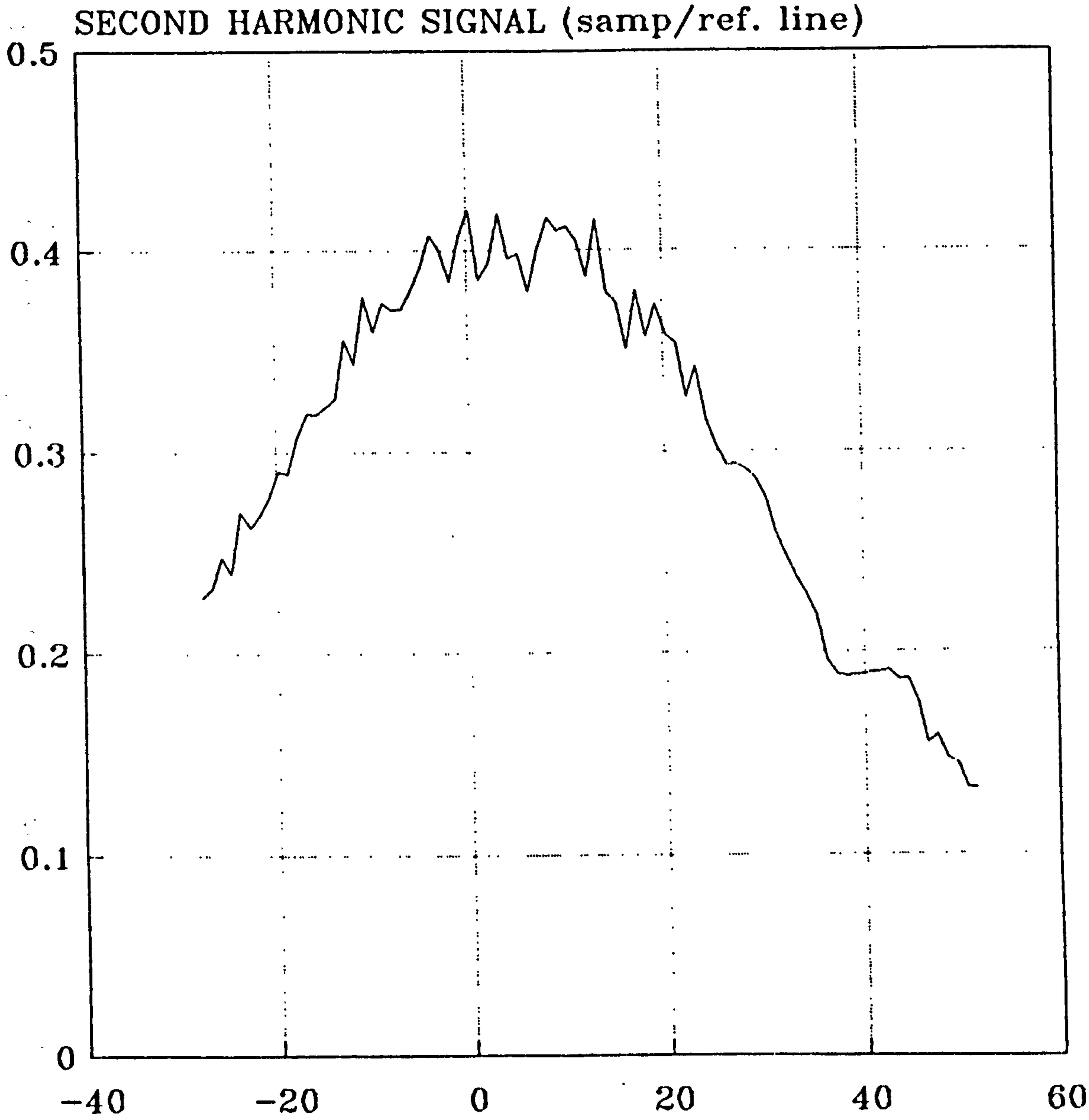

Figure 6.6.15 SHG vs. angle of sample for a fixed polarisation of light. (Maker fringe experiment).

SHG SIGNAL VS POLAR ANGLE Y CUT QUARTZ

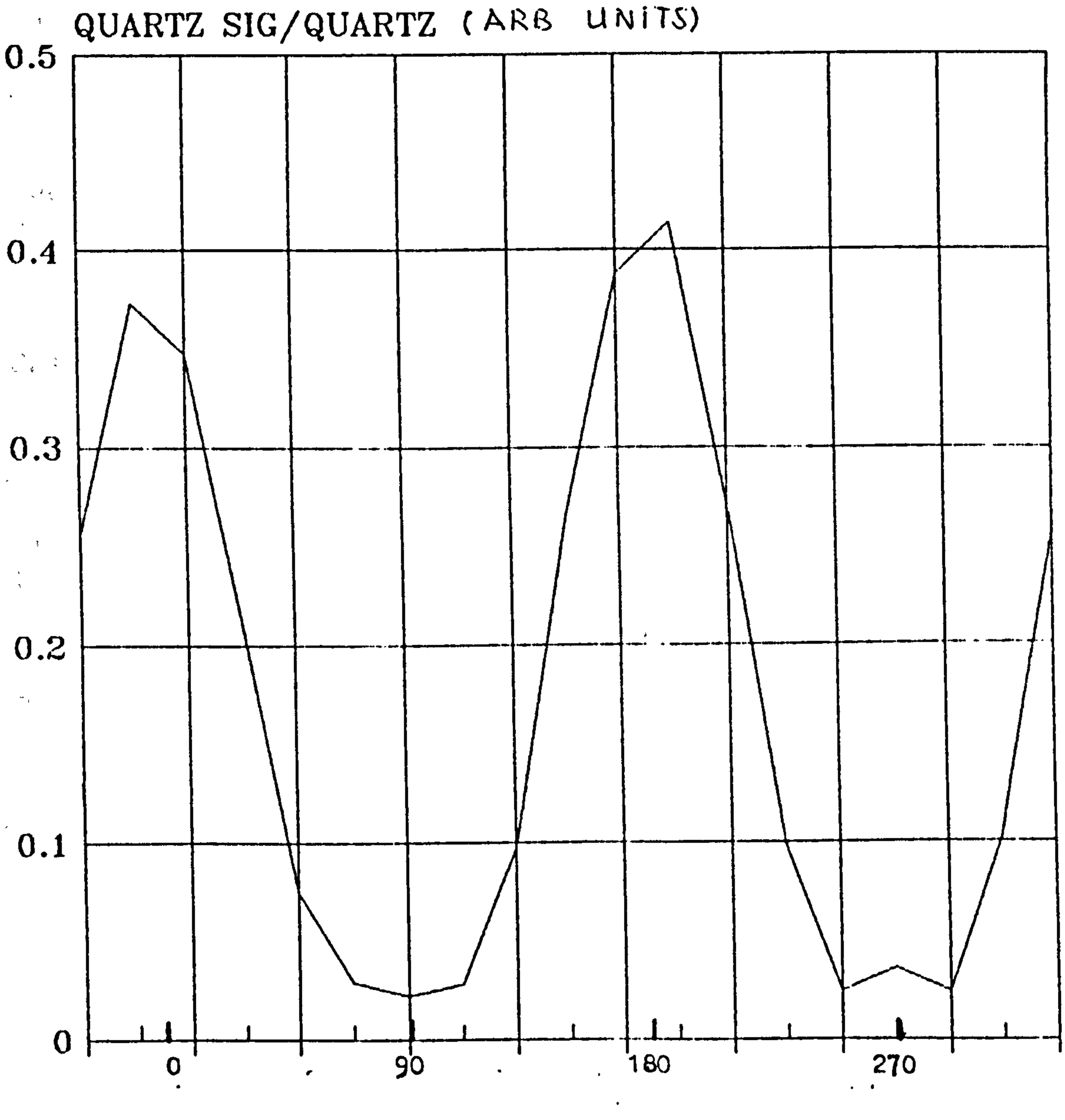

Figure 6.6.16 SHG vs. polarisation of light for the reference quartz.

SHG SIGNAL VS POLAR ANGLE PBZLG and PHIC (266V/mm)

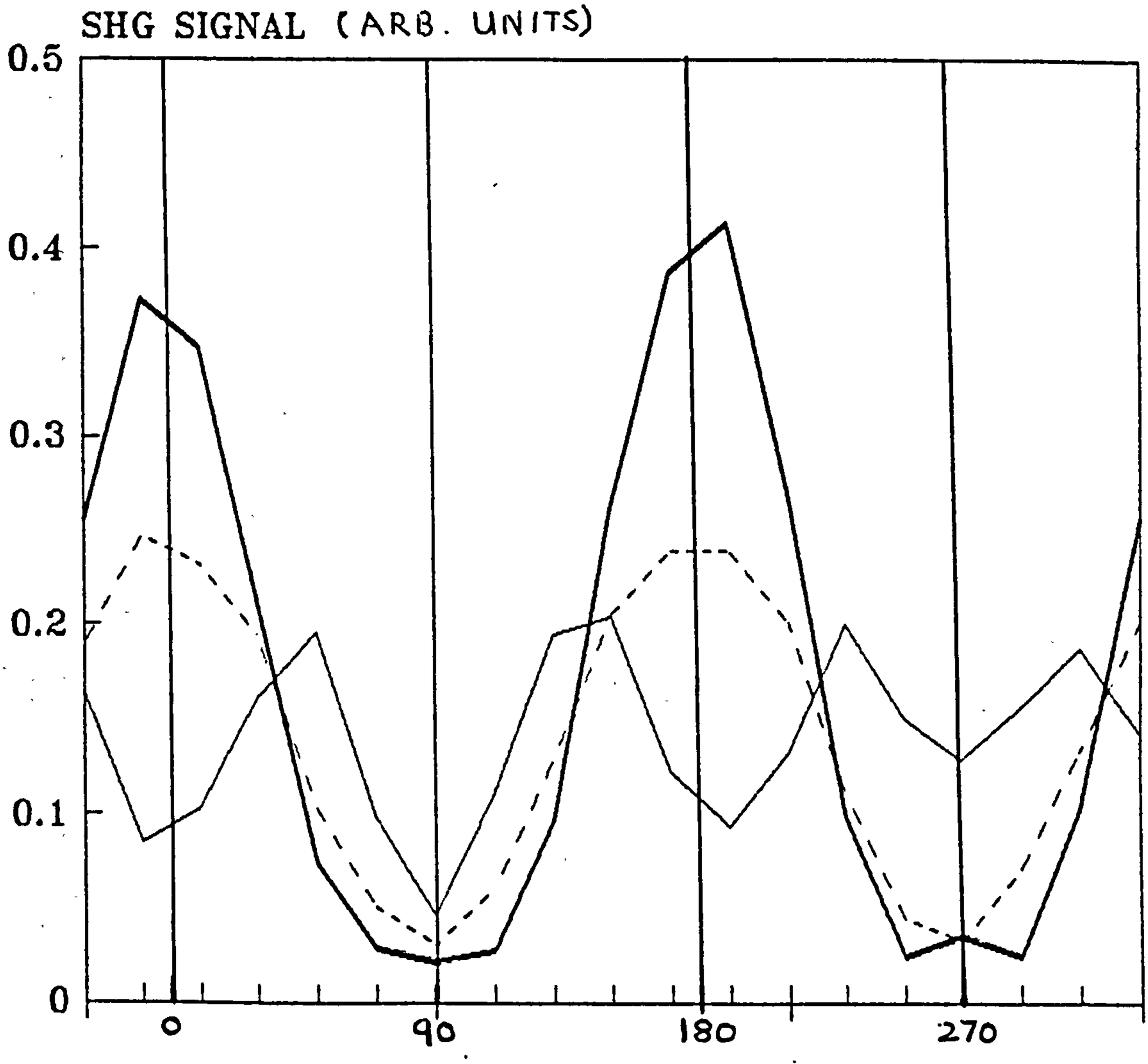

—— PBZLG (X10) —— QUARTZ Y CUT ····· PHIC (X5)

Figure 6.6.17 Comparison of SHG vs. polarisation angle of light for PBzLG, PHIC and quartz.

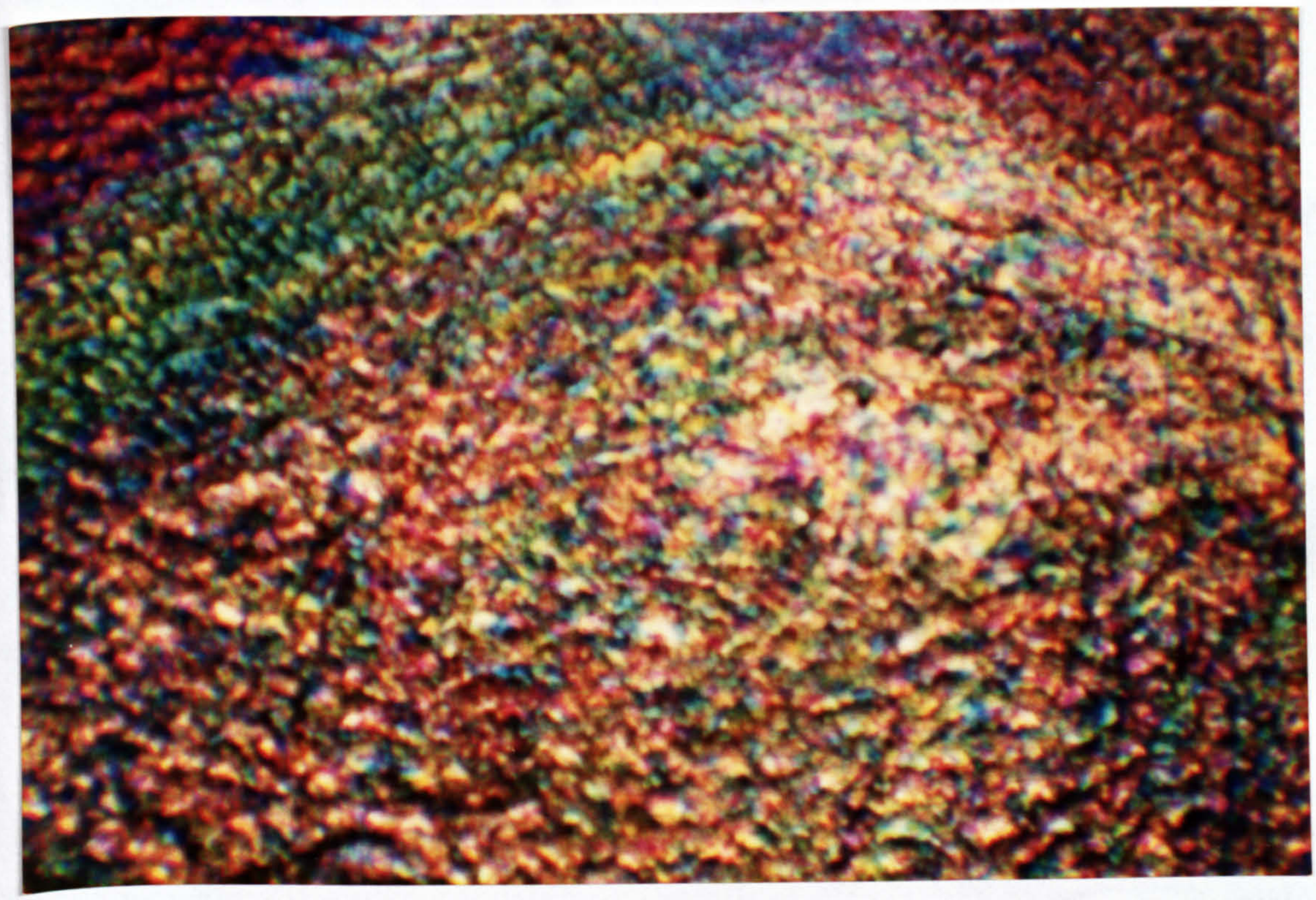

Figure 6.6.18 View of unpoled PBzLG film through crossed-polars

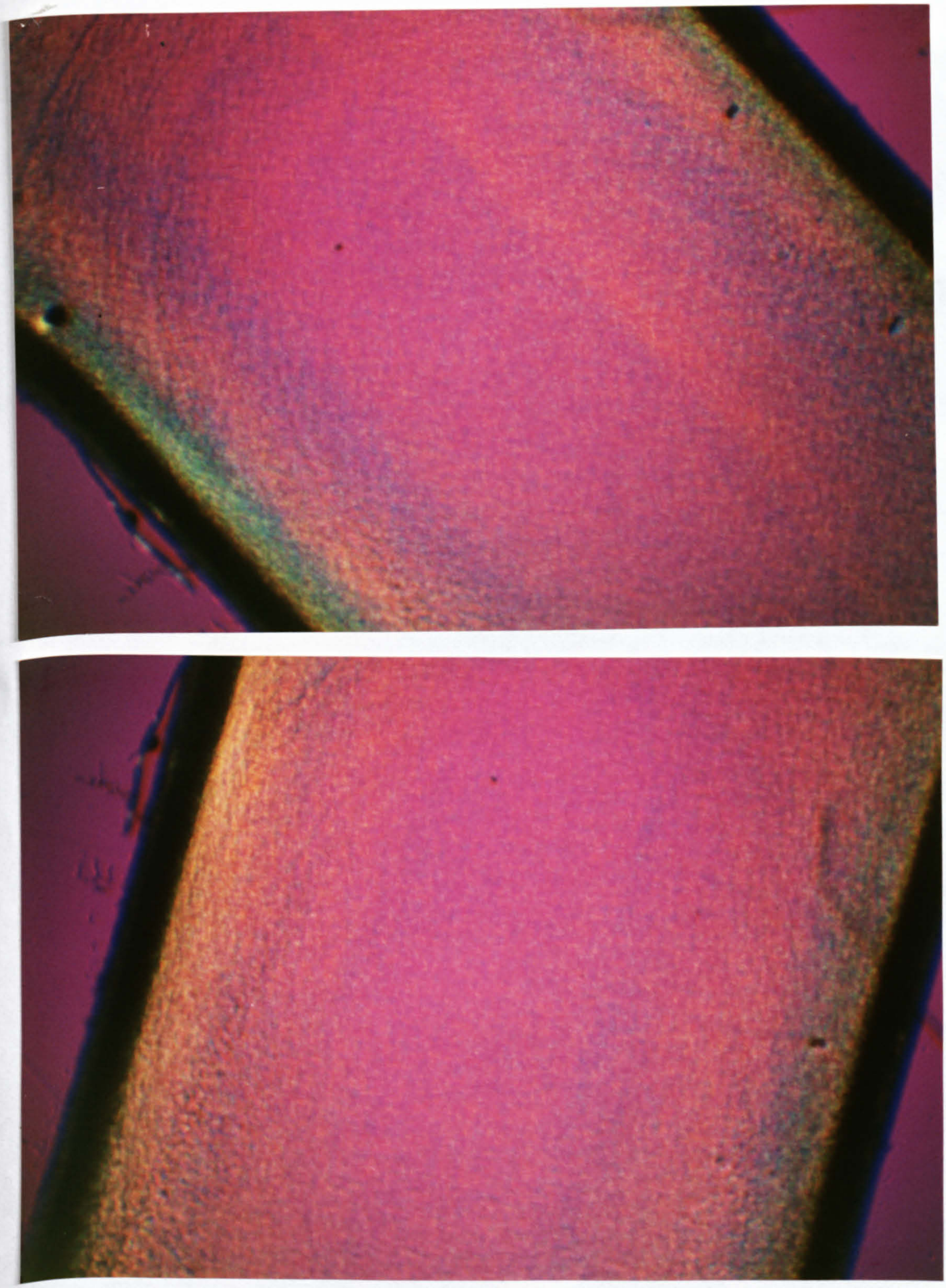

Figure 6.6.19 Two views (at right angles to each other) of an unpoled PHIC film through crossed polars.

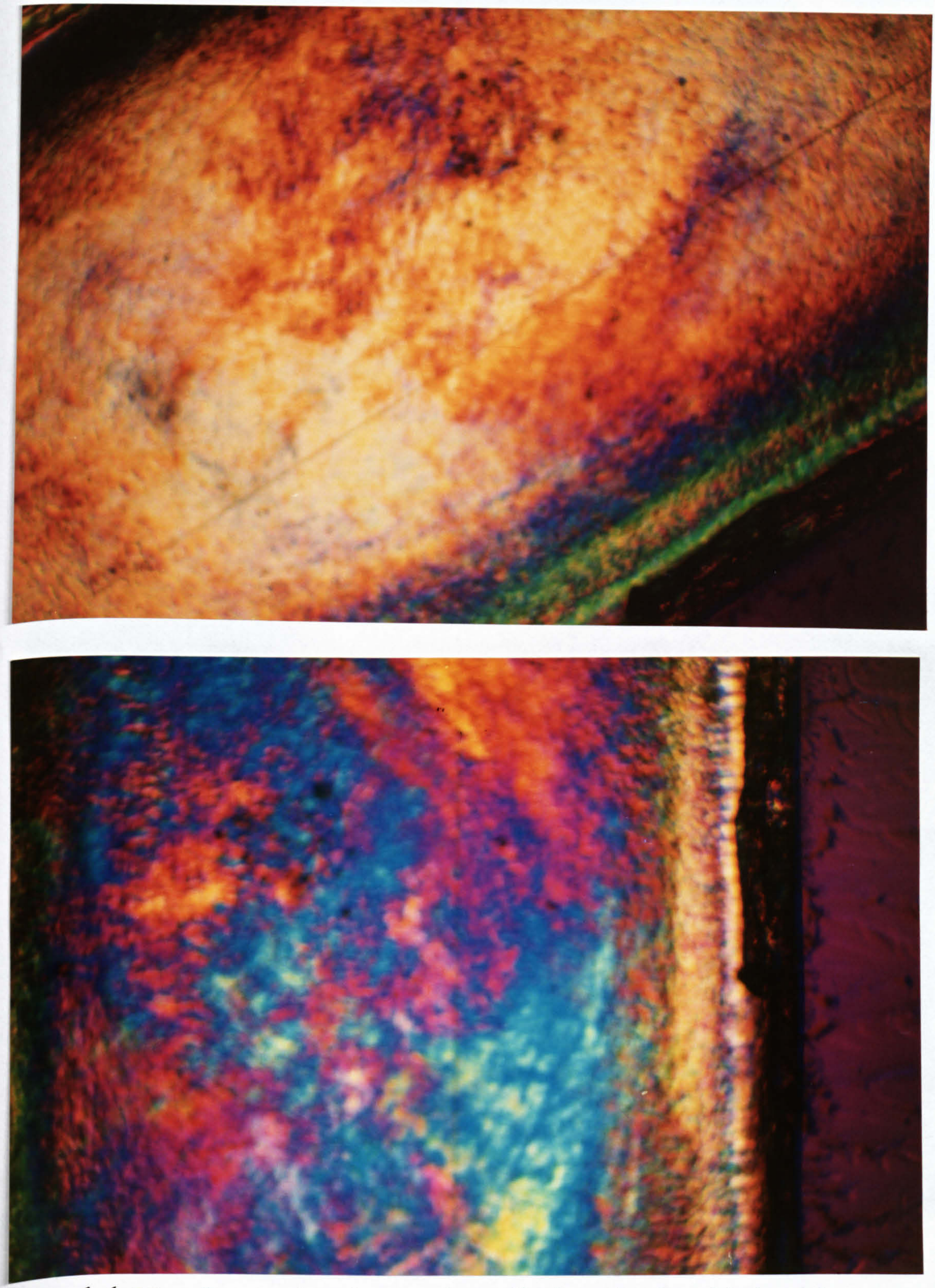

Figure 6.6.20 Two most extreme views that could be obtained by rotation of a poled PBzLG sample between crossed -polars.

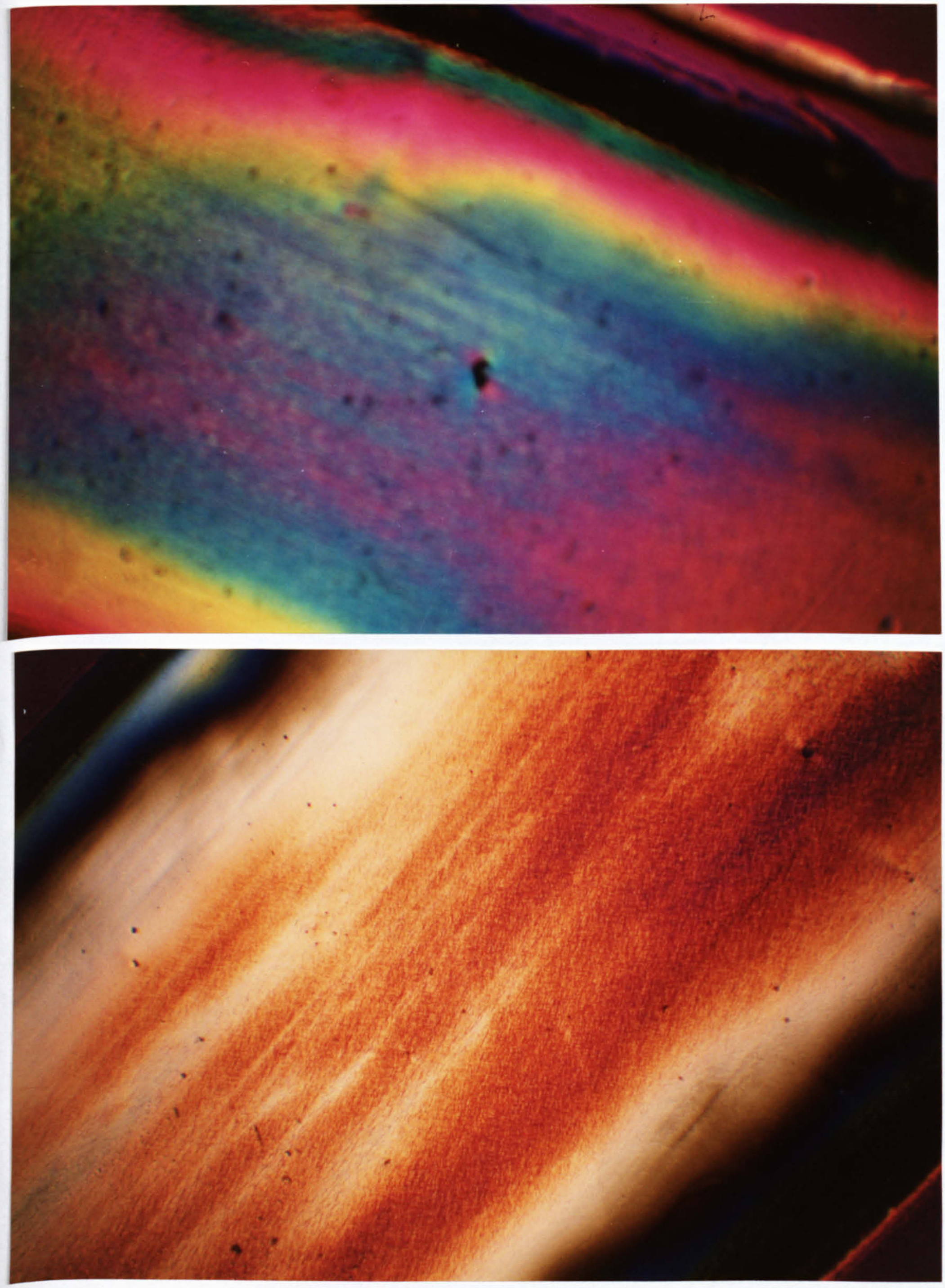

Figure 6.6.21 Two most extreme views that could be obtained by rotation of a poled PHIC sample between crossed -polars.

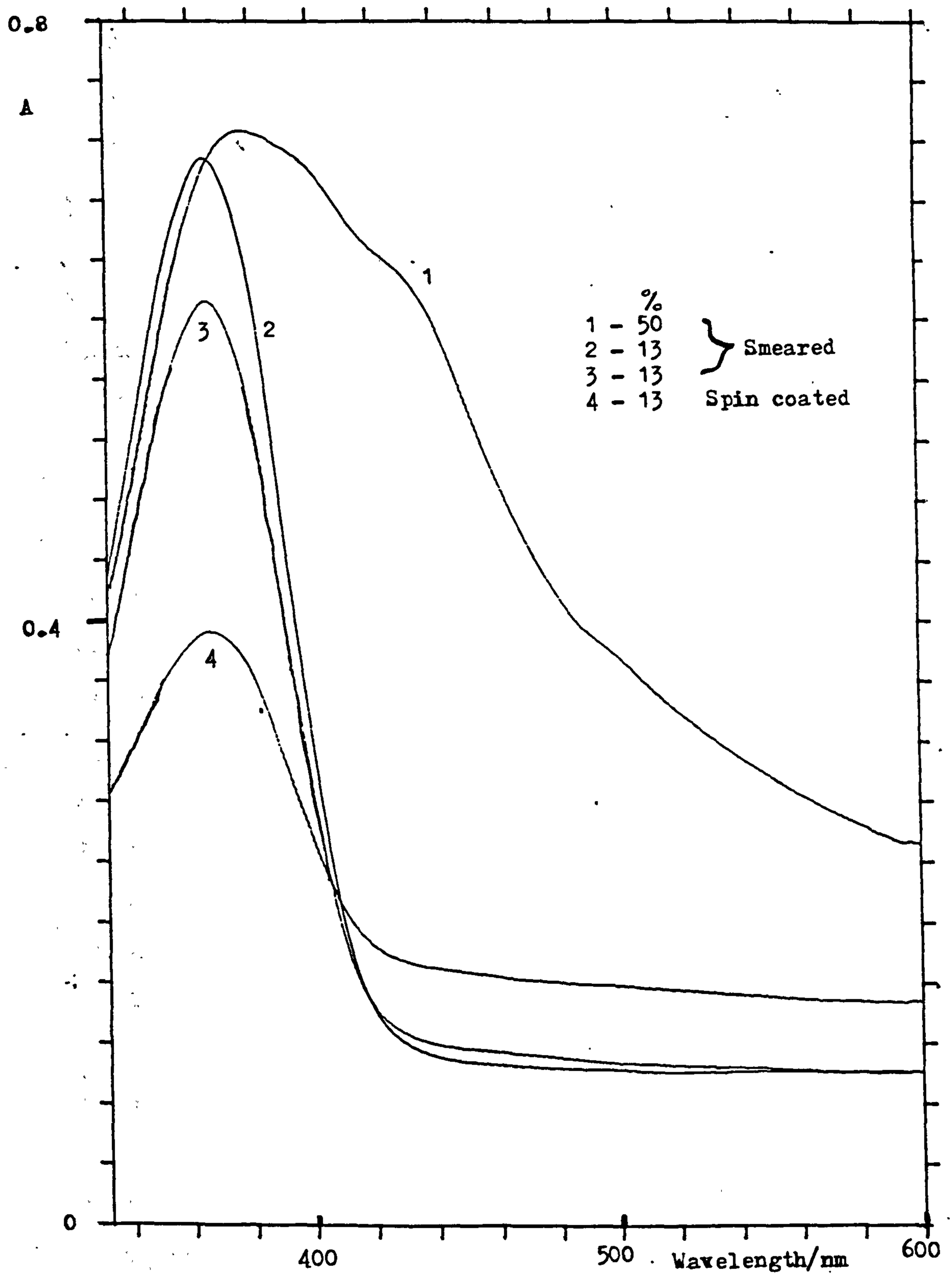

Figure 6.6.22 UV spectra of unpoled PBzLG films containing p-NA.

Angle", refers to the polarisation angle of the plane polarised laser light, changed by the rotation of the half-wave plate.

For figure 6.6.15, the sample was rotated for a fixed polarisation angle of the laser light.

For figures 6.6.6-8, the two lines simply represent testing at two different positions on the film.

6.6.4 Discussion of Solvent Cast Films and SHG Results

Uniformity of Alignment

This is best observed from the photographic evidence given in figures 6.6.18-21, which were obtained using a Leitz microscope with crossed polarisers, and fitted with a camera. Each pair of photographs for the two poled cases, represent the two most extreme views that could be obtained by just rotation of the sample between the crossed polarisers.

The effect of the field on the film is only seen if the poled and unpoled cases, and the rotation effects are taken together.

In either material, the alignment is certainly not as impressive as that expected for a uniaxially oriented system, (e.g. as observed in liquid crystal watch displays). Complete extinction on rotation of the samples between crossed polarisers, could not be found because light or dark texture could always be observed. (Note:- by way of comparison with another poled polymer system, a biaxially oriented and poled sample of PVDF showed much

sharper points of extinction on rotation).

In the PBzLG case, although coloured cholesteric texture is present in both the poled and the unpoled films, the areas of the individual micro-regions of focal conic texture (i.e. coloured patches) are much larger in the poled case (e.g. the extensive blue region for instance), which implies some kind of organisation of the smaller micro-regions has taken place, under the field, (c.f. Murthy et al. (1986)).

The fact that cholesteric colour is still present in the poled PBzLG film, implies a complete nematic order has not been attained under the action of the field. Possible reasons for this are:-

1) relaxation of the nematic order back to the cholesteric order, occurs because of uneven evaporation of the solvent, resulting in loss of field, across wetter parts of the film;

2) the swirling motion observed (Williams's domains (Williams (1963)) above 40 V/mm disrupts the nematic order;

3) the evaporation process may have been too quick to allow unwinding of the cholesteric phase. As mentioned in section 2.3, Duke and Dupre (1974) described the cholesteric to nematic change as a two step process involving reorientation of the cholesteric micro-regions (2-5 minutes) followed by the unwinding of the cholesteric planes (30 minutes). In general, using dioxane or chloroform as the solvent, evaporation was usually complete in under 10 minutes (i.e. no visible damp patches remained

on the film).

The best uniformity of alignment seen in a solvent cast PBzLG film was obtained by smearing the solution on a glass slide with the edge of a razor blade. As the solvent in the very thin layer evaporated very quickly, there was no time for any relaxation of the induced alignment, and no coloured, cholesteric texture was observed. (Note:- the resultant structure of this alignment was the same as that reported by Elliot and Ambrose (1950)).

In the case of the unpoled PHIC, no mesomorphic texture was observed, as predicted by the solid phase diagram (figure 1.12b). However, it seems strange that none is observed as the evaporation process must take the solution concentration into the biphasic and anisotropic regions as predicted in figure 1.12a, before the film is fully dry. Possibly, the rate of evaporation prevents this.

The stark contrast in the two photographs for the poled PHIC sample only highlights the effect of the field, particularly on comparison with the unpoled case. The presence of the coloured bands as being caused by cholesteric liquid crystal effects has not been reported in the literature, and would not be expected from a nematic order. Hence, their origin is still open to question, but must be related to selective reflection of light rather than absorption effects.

SHG Results

PBzLG

Detectable levels of SHG were observed in films of PBzLG which had been poled with fields as little as 40 V/mm. This field coincides with the first sign of stirring which was observed in microscopic studies described in section 6.4.4. The size of this field is consistent with observations made in previous work (section 2.3) concerning the alignment of liquid crystal solution of PBzLG using an electric field.

Equation 2.i, estimates a value 30,800 D for the dipole moment being aligned by the field of 40,000 V/m (at 298°K). Assuming a dipole moment per residue of about 4 D (Wada (1962)), suggests a degree of polymerisation of about 7700. However, this refers to the size of the liquid crystal bundle of head-to-tail arranged helices which are being aligned rather than an individual α-helix.

Figures 6.6.3 and 6.6.10 are representative of the variation of thickness of sample produced by the film casting method, as measured by the Talysurf. The scans help to show the accuracy of a thickness measurement for a specific translation point along the film from its defined edge.

(Note:- the diameter of the laser beam striking a sample was about 300 microns, so the variation of thickness over this sort of distance had to be taken into account).

Figure 6.6.4 gives the variation of SHG signal observed versus the thickness of the sample, (i.e. coupling the

laser and Talysurf data). Evidence showed that for a single thickness, great variation in SHG signal was observed, not only from sample to sample but also from point to point on the same sample. The most likely reason for this is due to uneven evaporation which introduces regions of differing chain mobility and field, due to spatial permittivity and conductivity variation. In other words, uneven poling of the sample occurs. Visual proof of this is in the photographic evidence (figures 6.6.18-21) already mentioned, which suggests that the morphology of the poled PBzLG films is nonuniform, particularly down to the dimensions of the laser spot.

One possible way to use the data in figure 6.6.4 is to assume the maximum SHG signals observed for each thickness are representative of a fully aligned state. In principle, there are grounds for such an argument since if enough data are collected, all points should fall on or within the maximum achievable SHG envelope, depending on the level of alignment achieved. Hence, figure 6.6.5 shows the expected (based on equation 4.vii) square root dependence of the maximum measured SHG signal on measured thickness and implies the optical coherence length is > 22 microns.

The angular dependence of the SHG signal from poled PBzLG films is shown in figures 6.6.6-8, all of which show four minima and four maxima over 360°. Although, the maximum value of the signal varied from point to point on the films, the positions of the maxima for any point on the film were always at the same polarisation angles (i.e. 45°

dipole moment being aligned by the field of 150,000 V/m. This relates to a degree of polymerisation of around 6750, which is far greater than the molecular weight measured for this particular sample. However, in a similar manner to PBzLG, alignment of nematic liquid crystal bundles or swarms probably accounts for this discrepancy.

Figure 6.6.13 shows the angular variation of SHG signal that was generally observed for poled PHIC samples above the threshold field. As distinct from the PBzLG case, a more conventional uniaxial symmetry is observed with maxima at 0° and 180°, and minima at 90° and 270°. This symmetry is usually expected for the alignment of dipoles using a poling process, where there is no order perpendicular to aligning direction. It is also the symmetry associated with a nematic order.

Figure 6.6.16 shows the angular variation of SHG signal that was obtained for a piece of Y-cut quartz, and figure 6.6.16 compares the angular variation for the quartz and the two polymer systems. Quite clearly, the PHIC sample shows the same angular dependence as the quartz, with the maximum SHG signal occurring, when the polarisation of the laser beam was parallel to the poling direction of the field. Conversely, the maxima for the PBzLG occur at 45° to the field direction. This implies that the most polarisable direction of the molecules are in the PHIC case, also aligned in the field direction but in the PBzLG case, aligned at 45° to the field direction. In either case however, this direction may not coincide with the long axis

of the respective helix.

Figure 6.6.13 represents the experiment carried out on PHIC to try and observe Maker fringes by rotation of the sample for a fixed polarisation angle of the light (i.e. 0°, maximum value). No characteristic maxima or minima could be observed which might have then been used to determine the coherence length in the sample. Once again, this is probably due to the variation of the alignment over a sufficiently large area of the film.

Activity and Ageing of SHG Signal

In comparison to some other polymeric systems which have been tailored to have high β values (particularly doped polymer systems), both PHIC and PBzLG show low SHG activity. Of the two, PHIC was significantly more active but this is not too surprising as it is a polymeric urea (i.e. urea itself is fairly active). The electron delocalisation in the urea group of PHIC (which is absent in the polypeptide bond of PBzLG) is the origin of the non-centrosymmetric polarisation which leads to the "large" SHG signal. However, it would appear that the intramolecular H-bonding in the α-helix does not provide the large nonlinearity that was hoped for. Although a significant β value for a PBzLG molecule has been measured (Levine and Bethea (1976)), the value per monomer residue (which is not large) must be used as far as effective bulk properties are concerned.

Figures 6.6.9 and 6.6.14 show the retention with time

of the SHG signal for both the PBzLG and the PHIC systems. The following table summarises the decay of SHG signal observed for the 6 months in question.

Age of Film days	Relative SHG Intensity(a) PHIC (228 V/mm)	PBzLG (133 V/mm)
30	0.935	0.937
90	0.984	0.979
150	0.887	0.947
180	0.968	0.968
Rms values	0.955 + 0.045	0.966 + 0.025
Decay/month(b)	< 0.003	<0.003

(a) Measured at same position for a fixed polarisation angle (0° and 45° for PHIC and PBzLG respectively) and quoted relative to the value shortly after formation, (poling field given).

(b) Obtained by linear regression.

Undoubtedly, the reason for the retention of the signal is related to the fact that for the alignment of dipoles to relax, the whole molecule must move because of the rigid-rod nature, rather than just localised chain segments.

High β Additives

p-NA

Although relatively large SHG signals were observed for poled PBzLG films containing p-NA at a concentration of 13% w/w, similarly sized signals were observed in unpoled 13% w/w films, and also in the case when a solution of p-NA was

allowed to evaporate to form a layer of p-NA crystals (even though p-NA forms a centrosymmetric crystal). However, no (or very little) signal was observed in films containing 50% w/w p-NA (either poled or unpoled).

It was evident that in the 50% w/w cases, the liquid crystal background of PBzLG was not seen, probably because of the interaction of the high concentration of p-NA, whereas it was still visible in the 13% w/w case.

The reason for the signal in the case of the neat, solvent evaporated p-NA layer is possibly due to retention of solvent which introduces some temporary non-centrosymmetric symmetry which is lost once the solvent has evaporated. This might also be the case in the 13% w/w samples. However, it is difficult to explain why it is not observed for the higher 50% w/w concentration. The only available evidence of difference between the two systems is the two relative sizes of phase separated crystallites mentioned in the results, and the UV spectra given in figure 6.6.18.

No signal was observed in regions of poled films where solid solution was present, which might suggest the poling field was not sufficient to align the additive.

Further investigation of this system would need to be studied to fully understand all these points, although phase separation makes the system poor for applications.

MNBA

This system looked quite promising as the resultant films which contained 10% w/w MNBA, remained as solid solutions, and gave SHG signals which did not age over 6 months. However, the size of the signal relative to neat PBzLG was not much greater. This may be due to either too low a concentration or too small an electric field.

Conclusions

The most impressive aspects of this work has been the retention with time of the SHG activity of both the polymer systems which might overcome the problem of relaxation of aligned dipoles in thermally poled systems. The stability of the aligned system may also be beneficial to the alignment of high β additives which may or may not be attached to the polymer chains, and which may improve the level of SHG activity and other nonlinear effects.

Of the two polymer systems studied in this work, PHIC appeared to be the best system for producing the most even alignment, mainly because of the stirring effects which plagued solutions of PBzLG under field. There is probably also a problem of light scattering effects from the suprastructure in the PBzLG case.

Uneven evaporation/poling was certainly a problem in producing nonuniform alignment, and employing spin coating/poling techniques may prove to be one way forward. However, this will certainly require the use of the more active materials mentioned above, to ensure detectable signals are produced.

6.7 Synthetic Procedures and Analytical Results

The detailed recipes used and the analytical data obtained, are now given for the intermediates and polymeric materials prepared during this project. Unless otherwise described, starting reagents were used in the form supplied by Aldrich Chemical Co. or B.D.H Ltd..

6.7.1 High Molecular Weight Sample of PBzLG (see figure 1.2 for reaction equation)

1) L-Glutamic Acid to γ-Benzyl-L-Glutamate

A mixture of 70g L-glutamic acid, 250 cm^3 benzyl alcohol and 70 cm^3, concentrated hydrochloric acid was heated until a solution formed. After standing for 2 hours at room temperature, the γ-benzyl-L-glutamate hydrochloride was precipitated into acetone (approx. 4 dm^3), and then filtered. The creamy white precipitate was then dissolved in 500 cm^3 of cold water and the resultant acidic solution was neutralised using powdered sodium hydrogen carbonate. The neutralisation was followed using pH paper, and a white precipitate steadily formed between pH 7 to 8. The white product was purified by crystallisation from hot water, and dried in a vacuum oven at 60°C, (yield ca. 12g (10%)).

In terms of sample analysis, elemental analysis and m.p. were carried out on the γ-BzLG ester. The measured and theoretical values are given as follows:-

	%			
	H	N	C	m.p./°C
Sample	6.36	5.88	60.48	161-162
Theoretical	6.37	5.90	60.74	181-182 (a)
($C_{12}H_{15}NO_4$)				

(a) According to Aldrich Chem. Co.

Comparison of m.p. and infrared spectrum made with a sample of the ester from Aldrich, confirmed a melting point of approximately 161°C (by mixed melting) and an identical spectrum.

Solvents

Prior to the remaining stages of the synthesis, solvents had to be dried or distilled, to prevent inhibiting effects preventing HMW sample forming.

i) Ethyl acetate:- this was dried (24 hours over anhydrous potassium carbonate) and distilled for the crystallisation and polymerisation of the NCA. Only distilled ethyl acetate was required for the preparation of the NCA.

ii) Dichloromethane:- this was dried over molecular sieve for 24 hours, and then distilled with the middle fraction being collected.

2) γ-Benzyl-L-Glutamate to NCA (Fuchs-Farthing (Fuchs (1922)) method)

Figure 6.7.1, shows the experimental set-up required for this step. 10g of finely powdered γ-ester was suspended in 150 cm^3 of ethyl acetate and brought to reflux. By bubbling phosgene into a preweighed flask containing 150

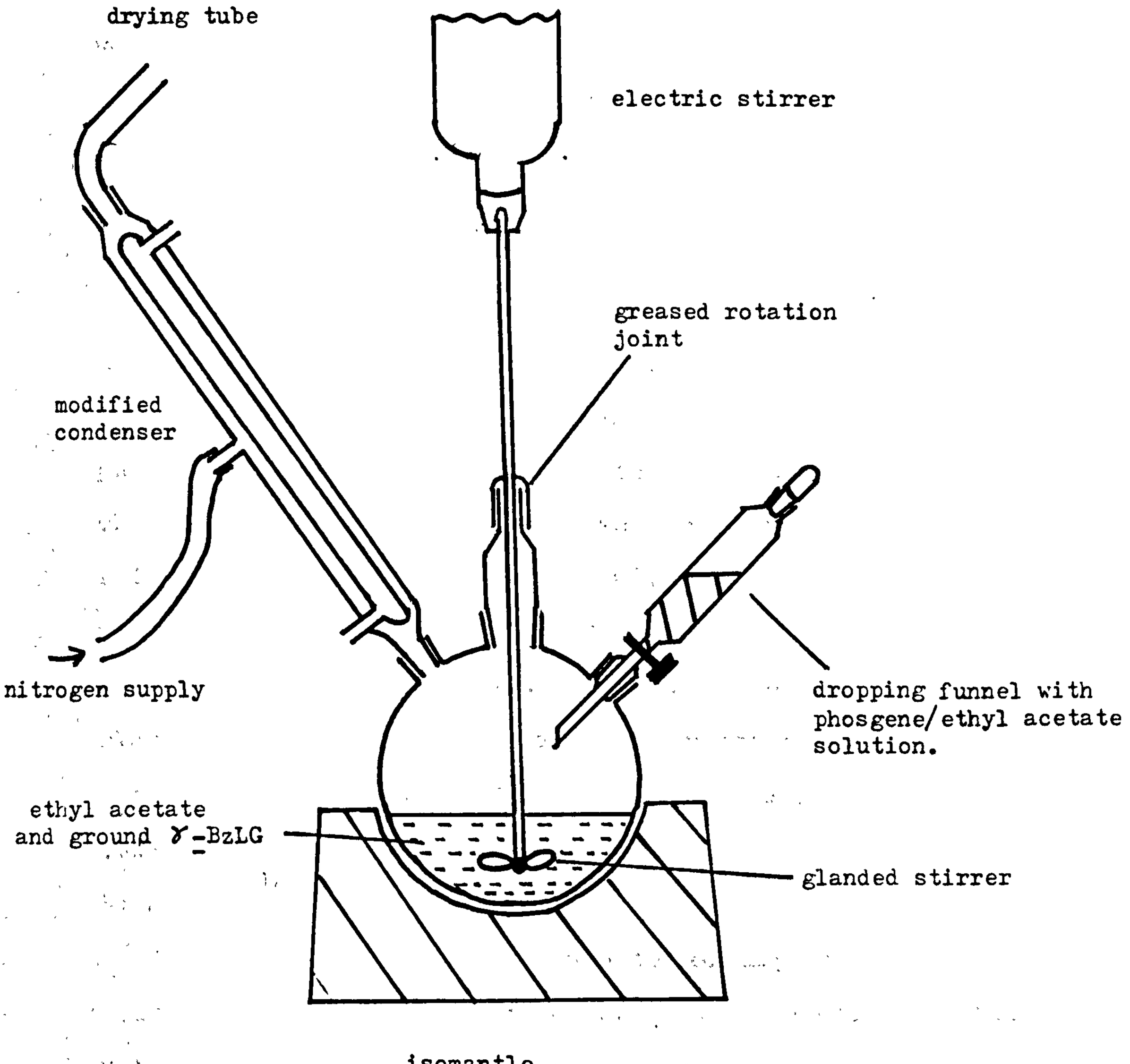

Figure 6.7.1 Apparatus for the synthesis of γ-BzLG NCA.

cm^3 of ice cold phosgene, and reweighing, a 10% w/w solution was prepared. This solution was gradually added to the refluxing system through the dropping funnel in about 10 cm^3 portions. After addition, reaction was allowed to occur for about 5 minutes, and then a stream of nitrogen was applied to flush out HCl vapour from the condenser. The addition of the phosgene solution continued until only traces of the γ-ester remained. Any excess phosgene was then removed by bubbling nitrogen directly through the reaction mixture.

The NCA was then isolated by evaporating off the ethyl acetate, and the product was recrystallised from ethyl acetate until sufficiently pure (i.e. chloride free). The purity of the NCA was checked in terms of ionisable chloride, as follows. A small sample of the NCA (0.1g) was refluxed with 1 cm^3 of 0.1M nitric acid for about two minutes and then 1 cm^3 of 0.1M silver nitrate solution was added. The NCA was deemed to be pure when the resultant cloudiness was no worse than that observed when the silver nitrate solution was added to tap water, (yield ca. 9g (81%)).

3) NCA to HMW PBzLG

5g of NCA was dissolved in 5 cm^3 of dry ethyl acetate by gentle warming. 14 cm^3 of a 0.7% (v/v) solution of tri-n-butylamine in dry dichloromethane, was then added as initiator ([M]/[I] ratio approximately 45), and the mixture refluxed for 30 minutes, before leaving at room temperature for about 12 hours. The resultant solution was like

treacle, and the PBzLG was isolated by precipitating into 500 cm^3 of methanol. The dried, filtered polymer resembled a white fibrous, asbestos-like material, (yield ca. 3.0g (60%)).

6.7.2 LMW PBzLG Samples for L.B. Studies

The same recipe as that described for preparing γ-benzyl-L-glutamate and then the NCA for the HMW PBzLG sample, was followed in the case of the LMW PBzLG samples. The corresponding yields for these intermediates were as follows:- γ-BzlG (15g(13%)); NCA (8.3g (75%)).

In total, four different LMW samples were prepared. 0.293g of ethanolamine was added to 30 cm^3 of dry (24 hours over molecular sieve), distilled DMF to make an initiator solution. 2.05g portions of NCA were then dissolved in 20 cm^3 DMF, and appropriate volumes of the initiator solution were added using a pipette. Each reaction mixture was then left overnight and the polymer product isolated by precipitation in 250 cm^3 of methanol followed by filtration and drying. The following table summarises the volumes of initiator solution, the [M]/[I] values and the yields corresponding to the four samples prepared.

Sample	Initiator solution Added/cm^3	Yield g(%)	No. of units [M]/[I]	Expected M.W.
LMW1	10	0.27(13)	5	1122
LMW2	5	0.79(39)	10	2184
LMW3	2.5	1.14(56)	20	4331
LMW4	1.75	0.91(44)	30	6148

Molecular Weights

There is no analytical data to confirm the molecular weights of either the HMW or the LMW samples (viscosity measuring equipment for determining M.W. was not available). However, the asbestos-like nature coupled with the type of polymerisation used for the HMW sample, indicate a typical weight average molecular weight of around 300,000 (or degree of polymerisation of approx. 1300), as suggested by Block (1983).

The powdery nature of the LMW samples is indicative of a lower M.W. (c.f. the HMW sample) but to what extent is not known.

Comparison of the M/I ratios of 45 and 30 in the polymerisations to make the HMW and the LMW4 samples respectively, only highlights the differing mechanistic routes probably followed (and discussed in section 1.1.2) to produce polymer samples of such vastly differing texture and physical appearance.

{Note:- polymerisations carried out by Gerber and Elias (1968) used a M/I ratio of 200 with triethylamine to obtain a sample with a molecular weight of 550,000}.

UV spectral data obtained from HMW and LMW samples dissolved in chloroform are shown in figures 6.7.2 and 6.7.3, and tabulated below.

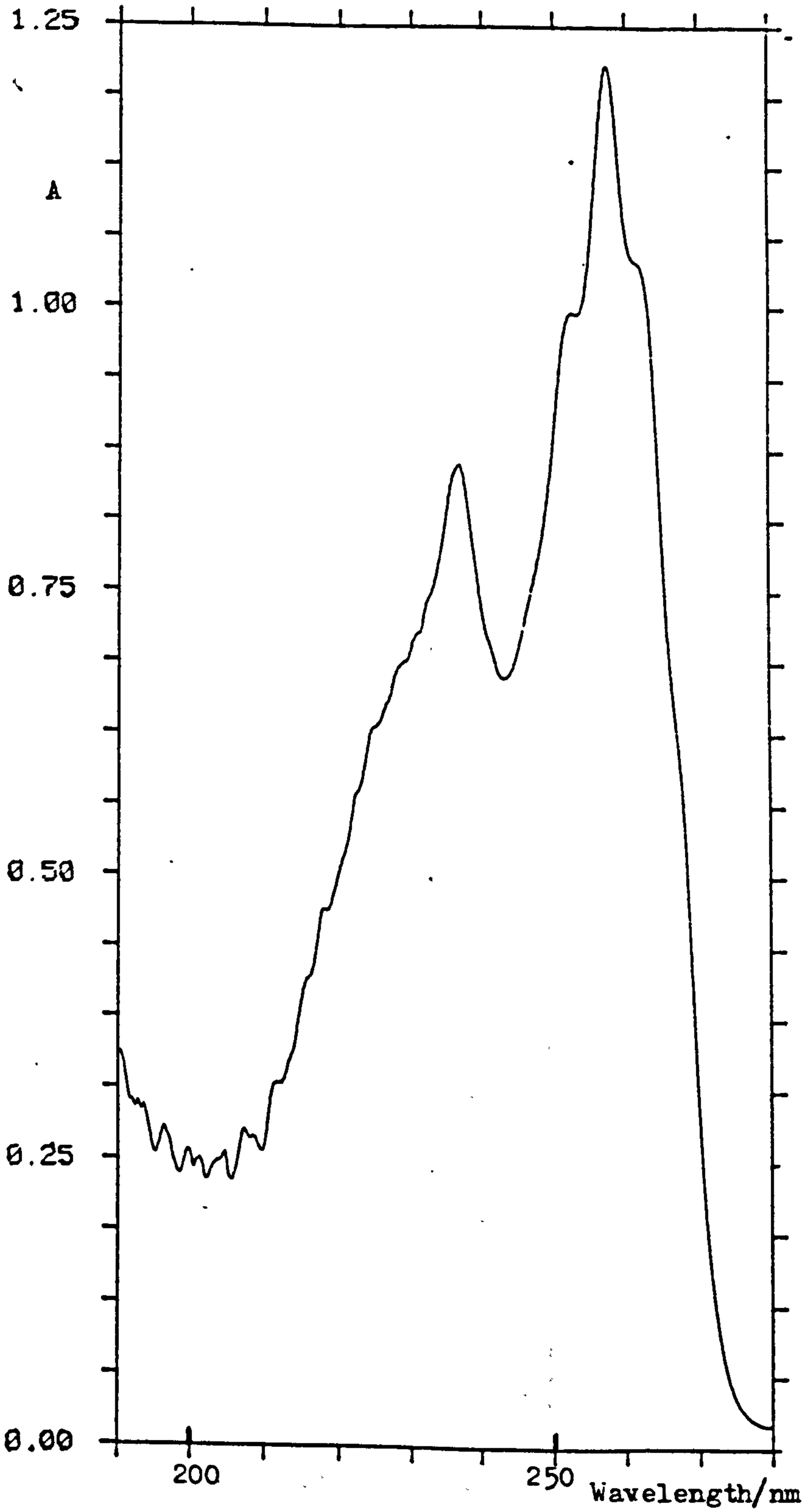

Figure 6.7.2 UV spectrum of HMW PBzLG in chloroform

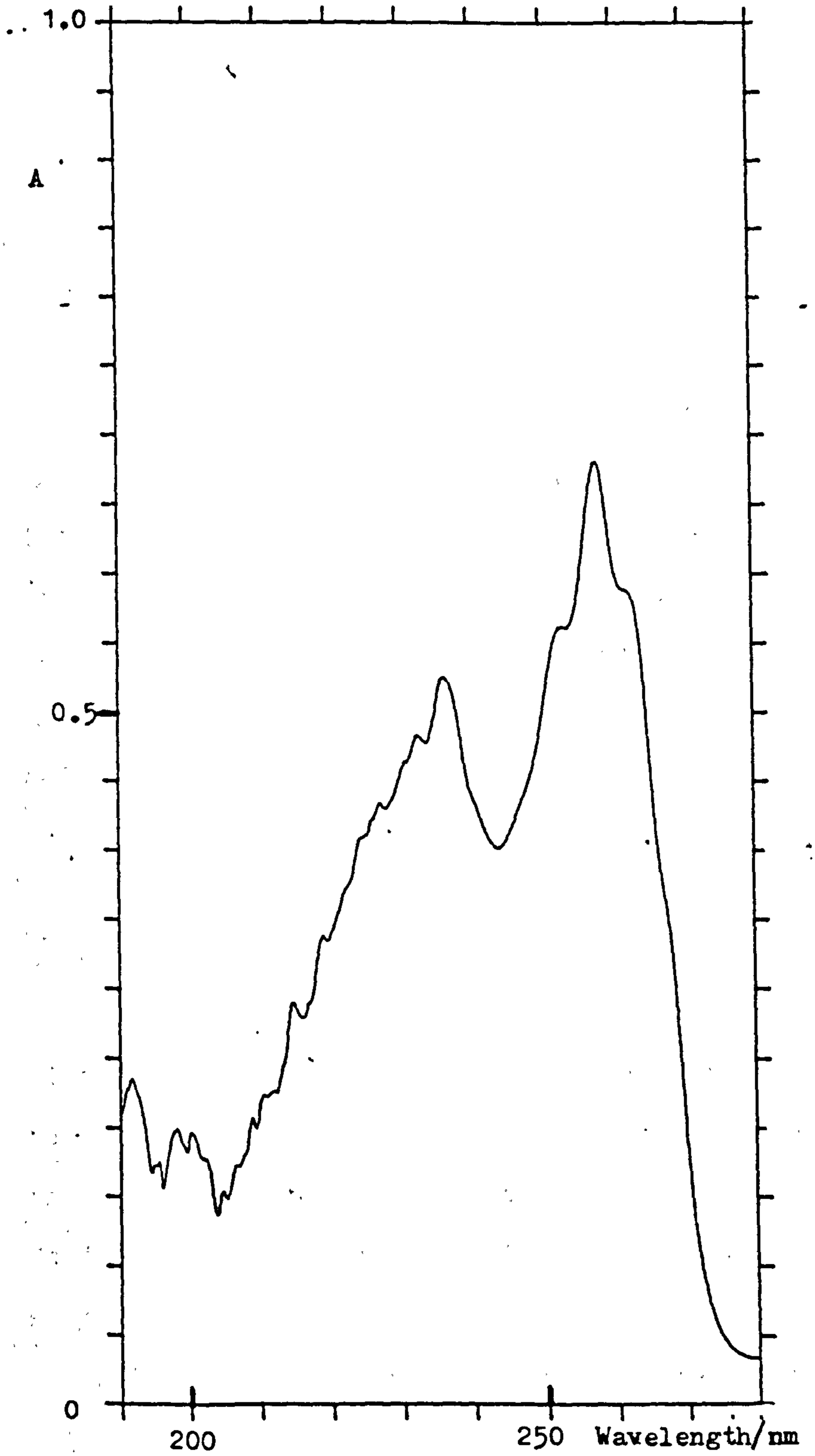

Figure 6.7.3 UV spectrum of LMW3 PBzLG sample in chloroform.

Sample	Wavelength nm	Concentration g/l	Absorbance	ε $g^{-1} \cdot l\ cm^{-1}$
LMW2	257.6	0.822	0.747	0.909
	236.4	0.822	0.586	0.713
LMW3	257.6	0.728	0.681	0.934
	236.0	0.728	0.526	0.723
LMW4	257.6	0.794	0.739	0.931
	236.4	0.794	0.576	0.725
HMW	257.6	1.357	1.215	0.895
	236.4	1.357	0.863	0.636

The comparison between figures 6.7.2 and 6.7.3 confirms the presence of the same material in both samples. Also, infrared spectra taken of films formed by evaporation from chloroform compare favourably with the spectra of PBzLG shown in the paper by Bur and Fetters (1976).

6.7.3 Side chain Modification of PBzLG

Using hexylamine, the following reaction conditions were used.

Reaction (A):-

1.02g of PBzLG was dissolved in 60 cm^3 of dioxane. 2 cm^3 of n-hexylamine was added, and the reaction temperature was maintained at 54°C for 7 days using a water bath. Product (A) was isolated by precipitation into methanol followed by filtration and drying in air, (yield ca. 1g (98%)).

Reaction (B):-

1.00g of PBzLG was dissolved in 35 cm^3 of dioxane and 35

cm^3 of n-hexylamine. The reaction was then run at 78°C for 5 days. Product (B) was found to have precipitated within the reaction mixture and was filtered off and dried, (yield 0.7g (68%)).

Product Analysis

UV spectral data is now given for solutions of PBzLG and Product (A) made up in dichloroethane.

	Concentration moles/l	Absorbance at 258 nm
Product (A)	0.00193	0.258
PBzLG	0.00193	0.264

The absorbance at 258 nm corresponds to the benzyl group of the polymer side chains. The decrease in absorbance from PBzLG to Product (A) is < 3% and implies very little replacement of the benzyl groups by the hexylamine took place during the reaction. This is why reaction (B) was undertaken.

Product (B) was found to be insoluble in all the following solvents:-

TGDM, dichloroethane, ethanol, water, ether, methanol, dilute acid, dilute NaOH, petroleum ether, ethyl acetate.

The change in conditions between reaction (A) and (B) certainly produced a marked effect on the solubility of the products in dichloroethane, which may be indicative of significant replacement of benzyl groups by n-hexylamine. However, the inability of the product (B) to dissolve in

any of the wide range of solvents mentioned (particularly the vinyl monomer), immediately made it uninteresting for further investigation.

The change in conditions from (A) to (B) may have been so extreme, that intermediate conditions may have existed which might result in products with the ideal solubility characteristics. However, further investigation would certainly have required the use of large amounts of PBzLG which was not considered practical.

6.7.4 γ-Alkyl-L-Glutamate Synthesis

i) Via copper(II) complex (see figures 1.5 and 6.7.4 for complete reaction scheme).

a) L-glutamic acid copper(II) complex copper(II) salt tetrahydrate

41.2g of copper(II) acetate monohydrate was dissolved in 750 cm^3 of water. This was added dropwise for 1.5 hours to a stirred solution of 29.4g L-glutamic acid in 750 cm^3 of water at 70°C. The resultant solution was then allowed to stand for 2 days at room temperature, after which time, a blue crystalline product (I) had precipitated and was filtered. The product was then washed with water, ethanol, and ether before drying in a vacuum oven at 50°C, (yield ca. 42g (86%)).

The product (I) was then stored, and used in small samples for the next stages.

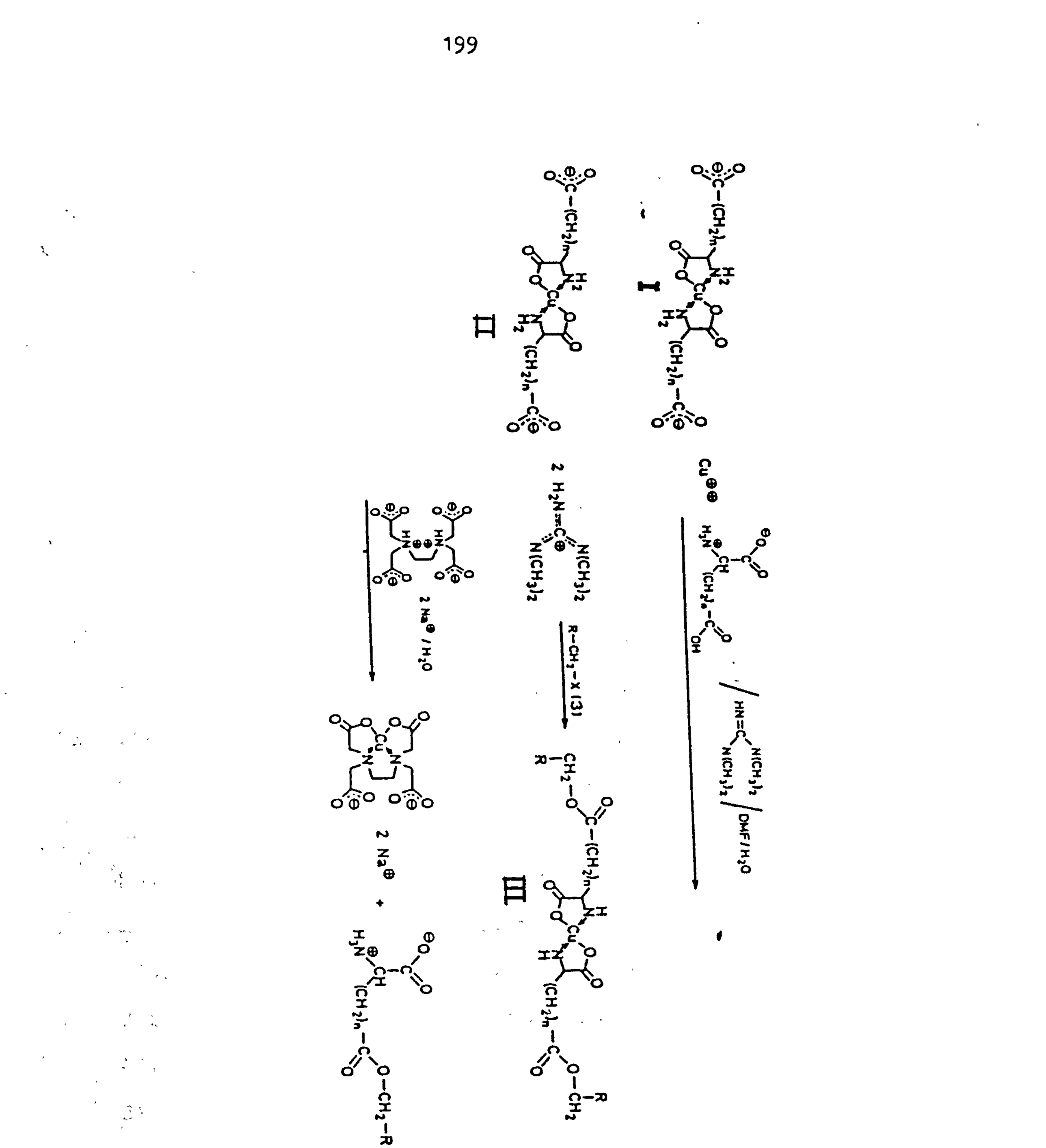

Figure 6.7.4 Reaction scheme for Cu(II) complex route.

b) L-glutamic acid copper(II) complex N,N,N',N'-tetramethyl guanidinium salts

5.48g of product (I) and 3.32g of L-glutamic acid were ground in a mortar and dispersed in 24 cm^3 of a 6:1 (v/v) DMF/water mixture. 5.5 cm^3 of N,N,N',N'-tetramethylguanidine was then slowly dripped into this mixture with stirring, followed by a prolonged stirring (2.5 hours) until dissolution of all solids was achieved. A further 16 cm^3 of DMF was then added to this blue solution, to produce the solution (II) to be used for the following alkylation step.

c) L-glutamic acid alkyl ester copper(II) complex

For each reaction with an alkyl halide, varying volumes of the solution (II) were used depending on the scale of the reaction (see following table for specific volumes).

All the alkyl halide (solid (powdered) or liquid) was added to the solution (II) and stirred for at least 48 hours. Little or no precipitation occurred at this stage for any of the alkyl halides tried, so excess acetone was added whereupon thick, blue gelatinous precipitates formed. These were then filtered to form wet cakes, of product (III).

d) alkyl-L-glutamate

The wet cakes were then added to an excess of saturated ethylenediaminetetraacetic disodium salt in water whereupon, white precipitates tended to form within a pale blue solution. The precipitates were filtered, washed with water and dried in a vacuum oven.

Code	Alkyl Halide	Quantity of Alkyl Halide	Volume of Solution/cm^3	Yield of Product/g
IOD	1-iodooctadecane	5.7g	15	5.1(a)
		15.2g	80	10.7(a)
BHD	1-bromohexadecane	14.5 cm^3	45	0.82(b)
IDD	1-iododododecane	6.3g	23	-
IMP	1-iodo-2methylpropane	2.72 cm^3	23	-

a) For the two IOD products, infrared spectra were obtained which showed no carbonyl stretching frequency, characteristic of a glutamic ester. These products were found to be unreacted 1-iodooctadecane (by comparison of infrared spectra).

b) An infrared spectrum of BHD product showed carbonyl stretches at a frequency of 1724cm^{-1}, which is characteristic of a glutamic ester.

Acid-Catalysed Esterification

The following recipe gives the general method followed to produce alkyl-L-glutamates using an acid catalysed esterification route, and applies to the list of alcohols used and given in the following table.

20g of L-glutamic acid was dissolved by stirring in a mixture of 12g of alcohol and 17g of 80% sulphuric acid at 70°C. The reaction temperature was then maintained at 70°C for 2 hours, before concentrating in a vacuum oven at the

same temperature for a further 2 hours. The concentrated reaction mixture was then poured into 200 cm^3 of ice cold water containing 22g of sodium hydrogen carbonate, producing a neutral solution and the crystalline product (translucent flakes). This was filtered and together with more crystals from the mother filtrate, was recrystallised from water.

Alcohol	Yield of product obtained
2-butanol	1-5g (3-18%)
1-butanol	1-2g (3-6%)
2-methyl-1-propanol (isobutylalcohol)	1-2g (3-6%)

Elemental analysis and m.p. were carried out on the iso-butyl and the n-butyl products as tabulated below:-

γ-ester	%			m.p./°C
	H	N	C	measured(expected)
iso-butyl	8.57	6.64	51.71	160-2 (182-183)
n-butyl	8.70	6.71	52.89	155-7 (190-191)
Theory	8.43	6.89	53.18	-

The expected m.p. values are those given in the paper by Sugai et al. (1966). Although significantly different from the measured values, it is interesting to remember that in the case of the γ-BzLG ester, the m.p. value given by Aldrich Chem. Co. was significantly different to that measured.

Infrared spectra ran on the two samples compared favourably with the spectra of a sample of ethyl-L-

glutamate that was available, and would be expected to have a similar spectrum.

6.7.5 Synthesis of Poly(alkyl-L-glutamate)

The following recipes describe the attempts to prepare poly(alkyl-L-glutamate) samples, using the γ-alkyl-L-glutamates prepared from the acid-catalysed esterification method above.

Solvent Treatment

Ethyl acetate - dried over anhydrous potassium carbonate for 24 hours, and then distilled.

Hexane/Dioxane - dried over molecular sieve for 24 hours.

Tetrahydofuran (THF) - dried over molecular sieve for 24 hours, and then distilled.

Note:- although the solid, triphosgene was used in the following reactions, it was always added to the reaction in solution, (in the same solvent as that in the reaction vessel). This allowed a similar apparatus to that shown in figure 6.7.1 to be used, (i.e. γ-BzLG NCA apparatus).

i) Poly(iso-butyl-L-glutamate)

γ-Ester to NCA Step

2-methyl-1-propyl-L-glutamate was ground up and dispersed in THF at between 40-50°C. The triphosgene solution was carefully added, and after 30 minutes, nitrogen gas was bubbled through the mixture until a clear solution resulted. The reaction mixture was then poured into hexane and the resulting suspension stored in a fridge over night. The crystalline NCA product was then filtered

and recrystallised from ethyl acetate/hexane. Two attempts were made to prepare the NCA as indicated by the following table.

γ-Ester	THF	Triphosgene	Hexane	Yield	m.p.	Expected m.p.
g	cm^3	g	cm^3	g	°C	°C
2.84	30	1.35	100	-		
10	100	4.80	300	4.5(b)	56-58	60-61
				0.7(a)	55-58	

a) The additional yield of 0.7g was obtained after reducing the final filtrate, and filtering the precipitate.

b) On recrystallising, a small sample (1g) of unpurified product was found to be insoluble in ethyl acetate, and had to be filtered off, (m.p. test - decomposed at 170°C).

NCA to polymer Step

2-methyl-1-propyl-L-glutamate NCA was dissolved in 40 cm^3 dioxane and 0.04g ethylamine was added. The reaction was then left stirring for 6 days, and a cloudy mixture formed. This was then refluxed for 1 hour, and the resultant clear solution was concentrated under vacuum and then poured into distilled water to give a flaky product. This was filtered and dried.

NCA	Dioxane	ethylamine	water	yield	expected M/I	code
g	cm^3	g	cm^3	g		
4.5	45	0.04	500	1.0 (20%)	22	PiBLG1
0.7	7	0.02	90	0.2 (25%)	7	PiBLG2

Both PiBLG samples were found to be insoluble in the

following monomers:- TGDM, TGDA (triethylene glycol dimethracrylate), and HEMA (hydroxyethylmethacrylate).

ii) Poly(n-butyl-L-glutamate)

5g of n-butyl-L-glutamate was ground and suspended in 40 cm^3 of dioxane. 2.44g of triphosgene was added, and the reaction maintained between 40-50°C for 1.5 hours. The solution was then rotary evaporated to remove the dioxane and drive off any HCl vapour present. 30 cm^3 of dioxane was then added to the remaining liquid NCA residue and 0.06g of ethylamine (M/I ca. 18) was added. After standing for 5 days, the reactants were poured into 250 cm^3 of water but no polymer precipitated.

6.8 Langmuir Blodgett Studies

6.8.1 General Aims

It was hoped, that oriented monolayers of PBzLG could be transferred onto a substrate to form multilayers with a non-centrosymmetric structure, using the L.B. technique.

To assist with this process, hydrophilic properties were added to the ends of the polymer chains as they were formed. The synthetic route used to produce these LMW samples specifically for L.B. work has already been described. The use of ethanolamine as initiator was

intended to add hydrophilic nature in the form of a hydroxy group to just one end of each polymer chain.

It was thought that a certain minimal molecular weight might exist, below which the chain is not long enough to support a helix. Some loose end component at either end of the helix would certainly be expected, and in addition, the presence of the initiator residue on the end of the chain might prevent the helix formation from starting until some distance along the polymer chain.

As a result, the preparation of different molecular weight samples was intended to alter the length of the helix attached to the hydrophilic head, to see if there was a significant effect.

In addition to the LMW samples, some HMW sample was also used, which had been prepared for earlier work and which did not contain the hydrophilic heads (having been initiated using tributylamine). Of the four LMW samples specifically prepared for L.B. work, only samples 2-4 were found to be suitable for deposition as monolayers, because sample LMW1 would not dissolve completely in chloroform.

6.8.2 Practical Details

L.B. studies were carried out using a Nima Technology L.B. trough as shown in figure 6.8.1, under clean room conditions.

The trough operated under computer control allowing parameters such as barrier speed, dipping speed etc. to be

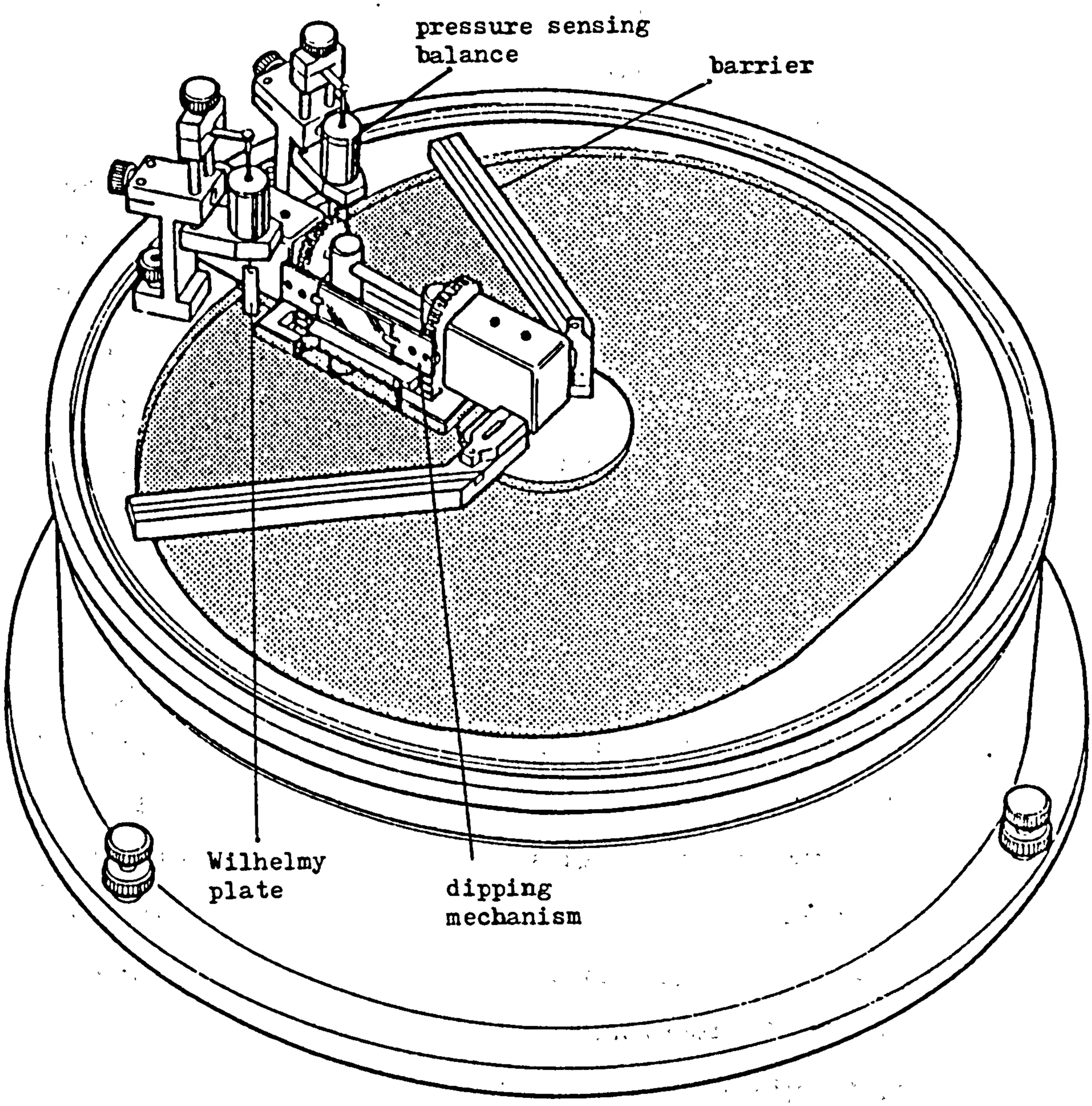

Figure 6.8.1 Nima Technology L.B. trough.

programmed in. The only other major manual task was the spreading of the monolayer solution onto the trough, using a microsyringe.

The surface pressure of the system was followed using a Wilhelmy plate method, which is described in appendix 1.

As in most L.B. studies, ultraclean, filtered water was used in the trough, and Gold Star Chloroform (Aldrich Chem. Co.) was used as the spreading solvent. (Note: dichloroethane was also tried as the spreading solvent, but the LMW sample solutions in this solvent were found to age).

Before depositing any solution of material onto the water surface of the trough, it had to be thoroughly cleaned using a suction nozzle. The surface was deemed to be cleaned when no detectable pressure change occurred for complete closure of the barrier.

Solutions of approximately 1 mg/cm^3 were always prepared at least 24 hours before use, to allow for the slow dissolution properties typical of polymers. For this particular concentration, 30-40 microlitres was found to be an ideal volume of solution to deposit on the trough, to produce a workable area of monolayer. Application of the solution was always carried out as slowly as possible, by dripping small drops of solution from as close to the surface as possible, and at as many different spots as possible. An evaporation period of 1-2 minutes was then always observed, before commencing any compression work.

6.8.3 Pressure-Area Isotherm Studies

Pressure-area isotherms were obtained for samples using various compression rates, and using a number of multiple processes involving compression followed by expansion, to test the reversibility of the isotherm. The results from these studies were important in determining if dipping with a substrate should take place.

More importantly, the input of accurate values into the computer for solution concentration, molecular weight and volume of solution deposited, would lead to quantitative analysis of the areas per molecule determined from the isotherms.

Substrate treatment

Quartz slides were used as the dipping substrate. The following process was used to clean and then treat the slides. (Throughout the cleaning process slides were always handled using tweezers and wearing rubber gloves, to prevent contamination from grease).

The slides were first wiped with acetone and then systematically cleaned using an ultrasonic bath with the following solvents, in order:-

a) chloroform; (b) isopropanol; (c) distilled water.

For hydrophobic treatment, the clean slides were placed in a solution of dimethyl-dichlorosilane overnight.

For hydrophilic treatment, the clean slides were placed in a 2 g/l NaOH solution overnight.

In either case, the treated slides were then washed with ultraclean water and dried with nitrogen.

6.8.4 Deposition Studies

The Nima trough used was designed to allow alternate layer deposition. For this work, the alternate layer deposition program within the computer was used, but only one compartment of the trough was ever covered with a monolayer. This was intended to try to impose Z- or X-type deposition.

In general, dipping was carried out at very slow speeds (10 mm/min), and at as large a surface pressure allowed by the isotherm.

Film Analysis

Analyses of the L.B. films were made using a Perkin-Elmer Lambda-7 UV spectrometer. The use of Quartz slides (rather than glass), allowed study in the 190-300 nm range, where PBzLG was known to absorb. In general for each slide, a number of spectra were taken at different points across the slide to give an idea of surface coverage. A blank, hydrophobic or hydrophilic slide was used in the reference beam.

6.8.5 L.B. Results

Pressure-Area Isotherms

General Observations

LMW samples:- table 6.8.a shows the relevant conditions applicable to the pressure-area isotherms shown in figures 6.8.2-3, where the assumed molecular weights represent those values given to the trough program to calculate the area per molecule (or per residue). The value of 219 is

used in figure 6.8.3, because it represents the molecular weight of a single monomer residue.

In general, the isotherm clearly showed two rises separated by a plateau region of constant pressure. If a compression/expansion/compression process was followed reproducibility of the lower section (i.e. 1st rise and plateau region) of the isotherm was good. However, once the second rise had been reached, the film would not expand, and maintained a constant pressure reading (very slow decay), on opening the barrier.

The pressure of the plateau region varied between 8 and 13 mN/m, not only from sample to sample but also between runs on the same sample. However, the general shape of the isotherms were unaffected.

The LMW sample isotherm did not appear to show a collapse in the second rise, and although it shows a very sharp, smooth climb in pressure, the values are in fact unreliable. In this region of the compression, the pressure sensing Wilhelmy plate was actually being moved sideways and upwards by the now solid polymer skin, and probably giving a false surface pressure reading.

However for completeness, table 6.8.b gives the extracted areas per molecule/ (or per residue) at zero pressure for both rises of the isotherms in figures 6.8.2-3.

HMW samples:- in general, the isotherms were poor in comparison to those of the LMW samples and the reproducibility from run to run was difficult. Figure 6.8.4

Table 6.8.a

Pressure-Area Conditions For:-

Figure 6.8.2;

Sample	Assumed Molecular Weight(a)	Compression Rate cm^2/min
LMW2	2184	180
LMW3	4331	180
LMW4	6148	180

Figure 6.8.3;

Sample	Monomer Residue Molecular Weight	Compression Rate cm^2/min
LMW2	219	180
LMW3	219	180
LMW4	219	180

Figure 6.8.4.

HMW	219	100

(a) Assumed molecular weight refers to the value fed into the trough program, for the particular run, and which was determined from the [M]/[I] ratio used in polymerisation step of the synthesis of the samples.

Table 6.8.b

Extracted Area per Molecule/Residue values At Zero Pressure

Figure 6.8.2 Sample

Sample	Area per Molecule/ Å^2 Isotherm Rise 1st	2nd
LMW2	190 ± 5	63 ± 3
LMW3	400 ± 5	115 ± 5
LMW4	580 ± 5	170 ± 5

Figure 6.8.3 Sample

Sample	Area per Residue/ Å^2 Isotherm Rise 1st	2nd
LMW2	19.0 ± 0.5	6 ± 0.5
LMW3	19.5 ± 0.5	6 ± 0.5
LMW4	20.5 ± 0.5	6 ± 0.5

Figure 6.8.4	HMW	23	10.5 ± 1 7.5 ± 1

PRESSURE-AREA ISOTHERM LMW PBZLG

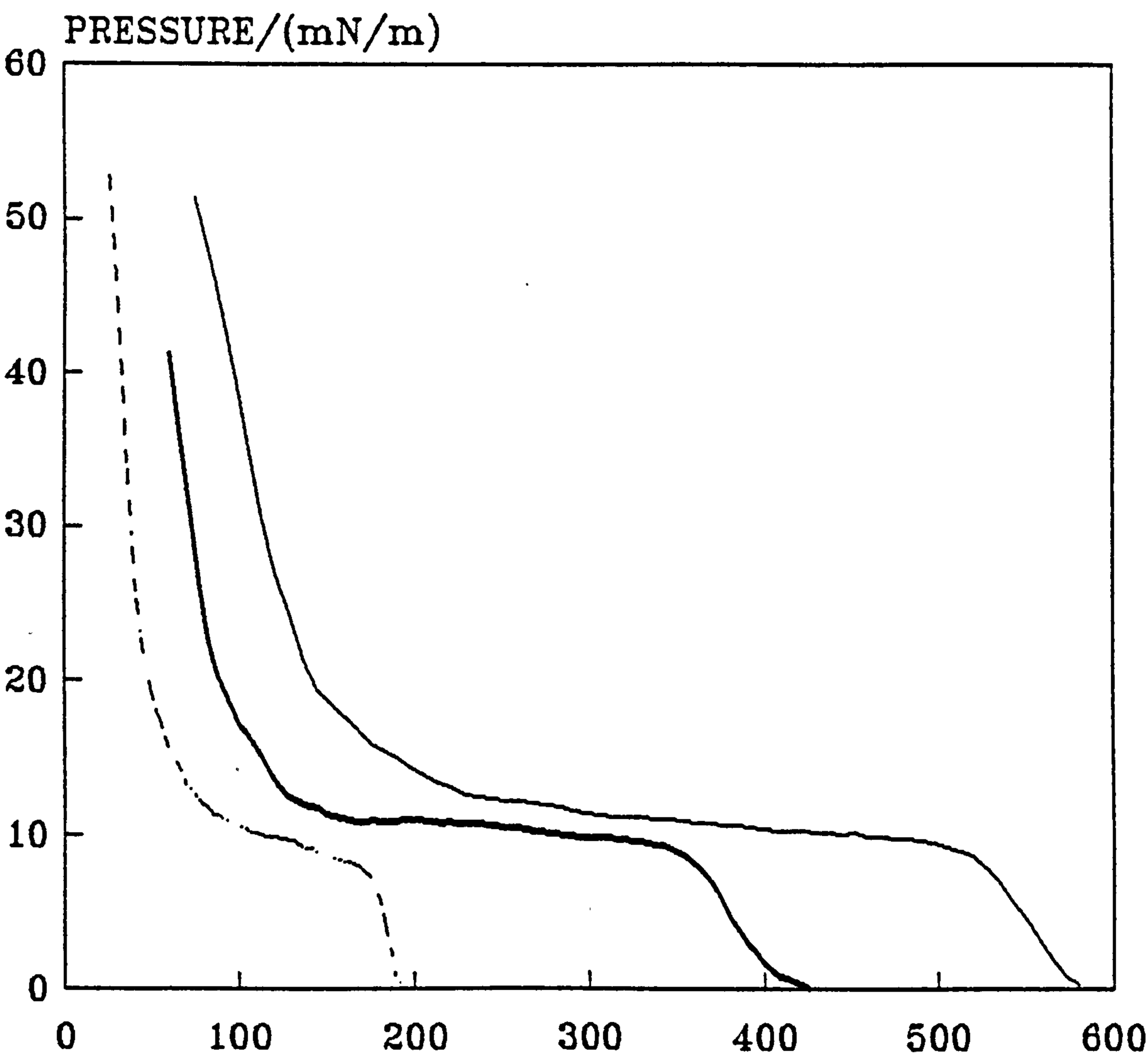

Figure 6.8.2 Pressure-area isotherms for LMW samples : using assumed molecular weights.

PRESSURE–AREA ISOTHERM
LMW PBZLG

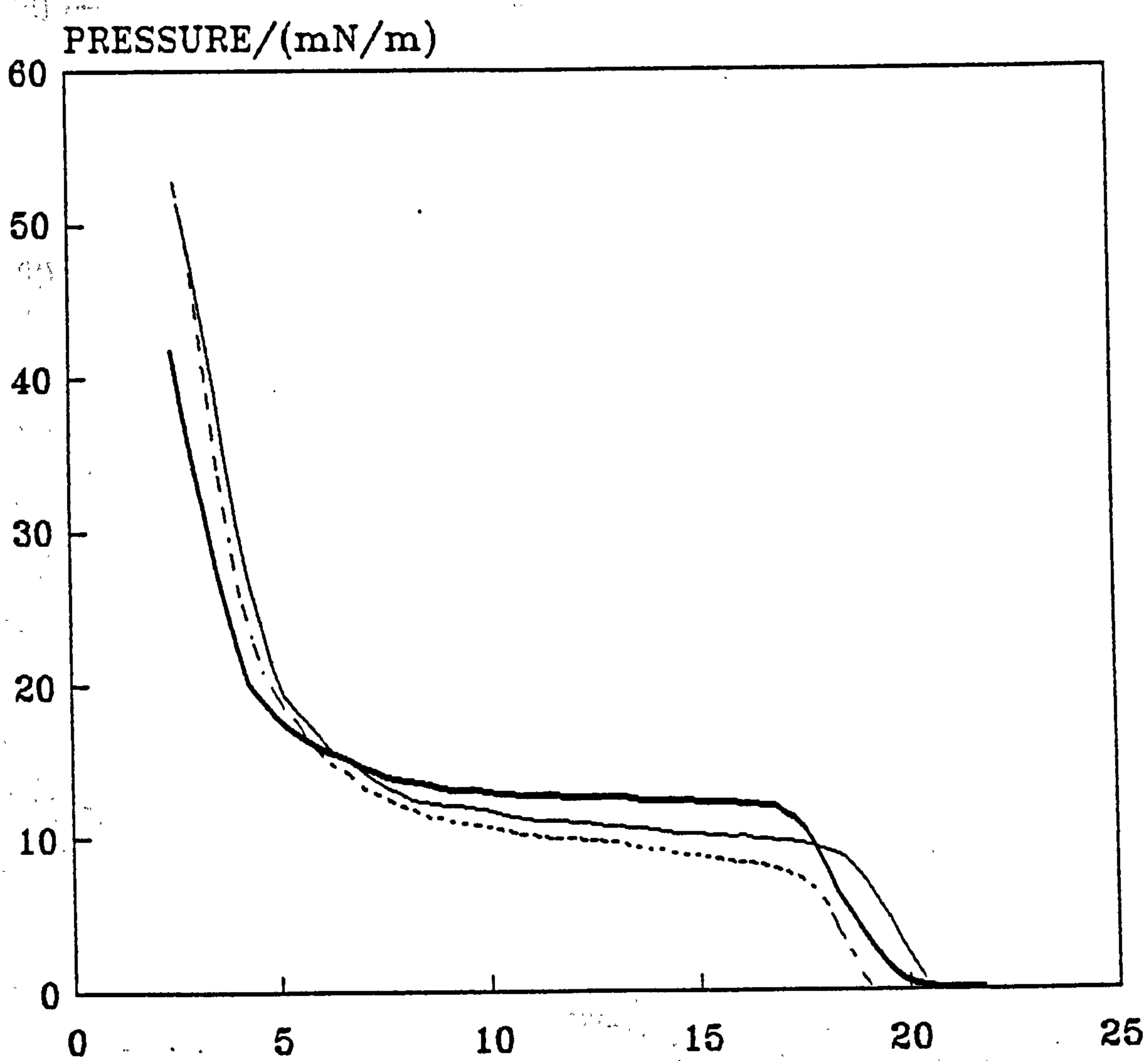

Figure 6.8.3 Pressure-area isotherms for LMW PBzLG samples using a molecular weight of 219.

PRESSURE-AREA ISOTHERM
HMW PBZLG

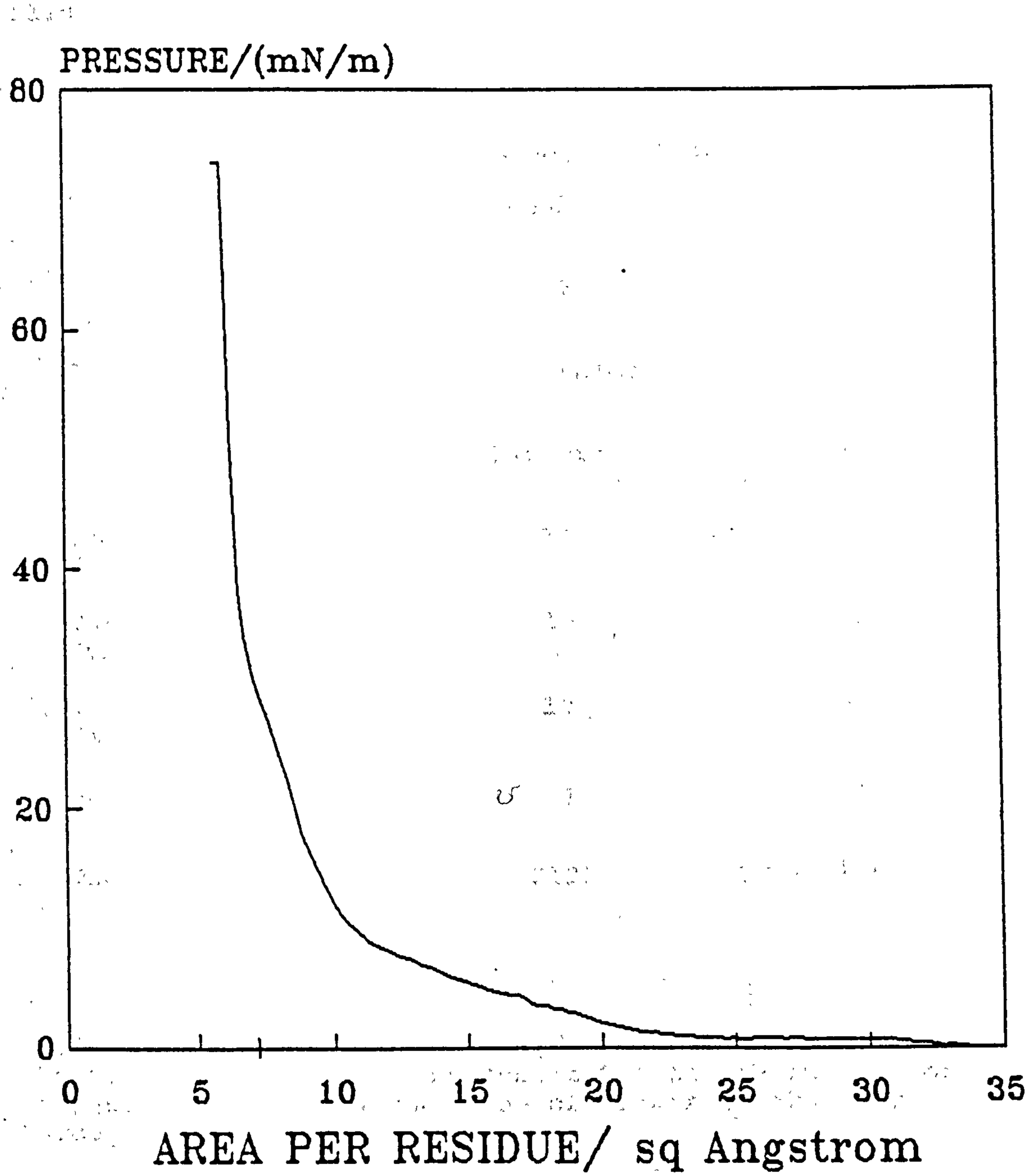

Figure 6.8.4 Pressure-area isotherm for HMW PBzLG sample using a molecular weight of 219.

Table 6.8.c

Langmuir Blodgett Deposition Conditions For a Hydrophilic Slide:-

	Figure 6.8.5a	Figure 6.8.5b
Sample	LMW3	
Concentration /mg/cm^3	1.15	0.73
Solvent	Chloroform	Chloroform
Position on Isotherm	1st Rise	1st Rise
Substrate Area /cm^3	12	12
Target Pressure /mN/m	10	8
Dipper Speed /mm/min	10	10
No. of Layers	1	3
Transfer Ratios	212%	203%:130%:143%

Note:- All transfer ratios apply to the upstroke through the Langmuir film. They represent the change in area of the trough, compared with the area of substrate that has dipped through it.

shows such an isotherm.

In the region where a plateau had been observed for the LMW samples there was not such a distinct 1st rise, more a gentle incline from 22 to 10 $\AA^2$. Here, the pressure tended to fluctuate, producing quite an uneven isotherm in some samples. A rise was then observed in a similar region to that of the second rise in the LMW sample isotherms. The films did not expand reversibly from this rise, and once compressed, could be seen to have formed a solid skin, on the surface.

L.B. Deposited Films

Transfer of material to the quartz slide was found to occur on the upstroke through a compressed monolayer, for both hydrophobic and hydrophilic slides.

Figures 6.8.5a-b show the UV spectra taken on a mono- and trilayer of the LMW3 sample, deposited under the conditions shown in table 6.8.c. The spectra are typical of all spectra taken on both the LMW and HMW samples, and are characterised by possibly two peaks between 190-200 nm and a shoulder to these peaks extending as far as 220 nm. The UV spectrum of a 10 layer deposited film is also given in figure 6.8.6.

HMW samples:- only one rise was available for deposition, in the HMW case, and this region has already been described as having poor reversible, compressional properties. Very poor surface coverage of a slide was observed for a monolayer dipped at a pressure of 18 mN/m. In fact, a detectable UV spectra could only be obtained in the central

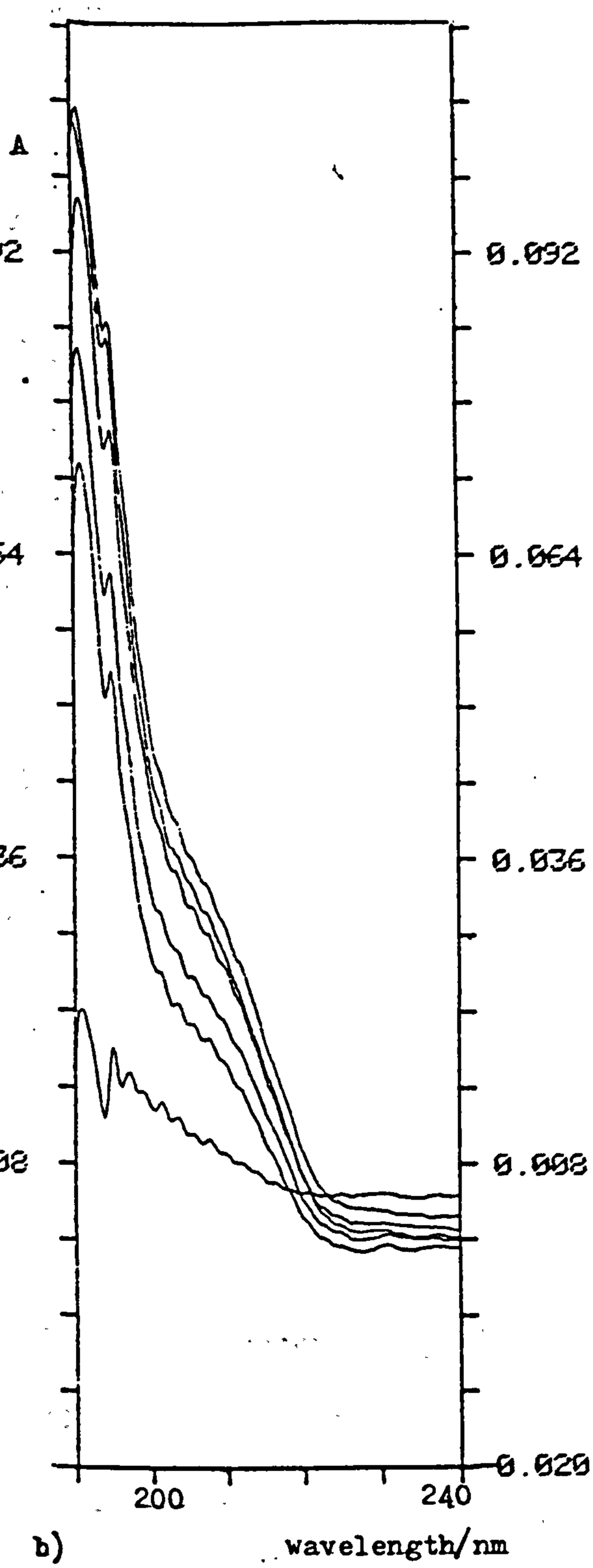

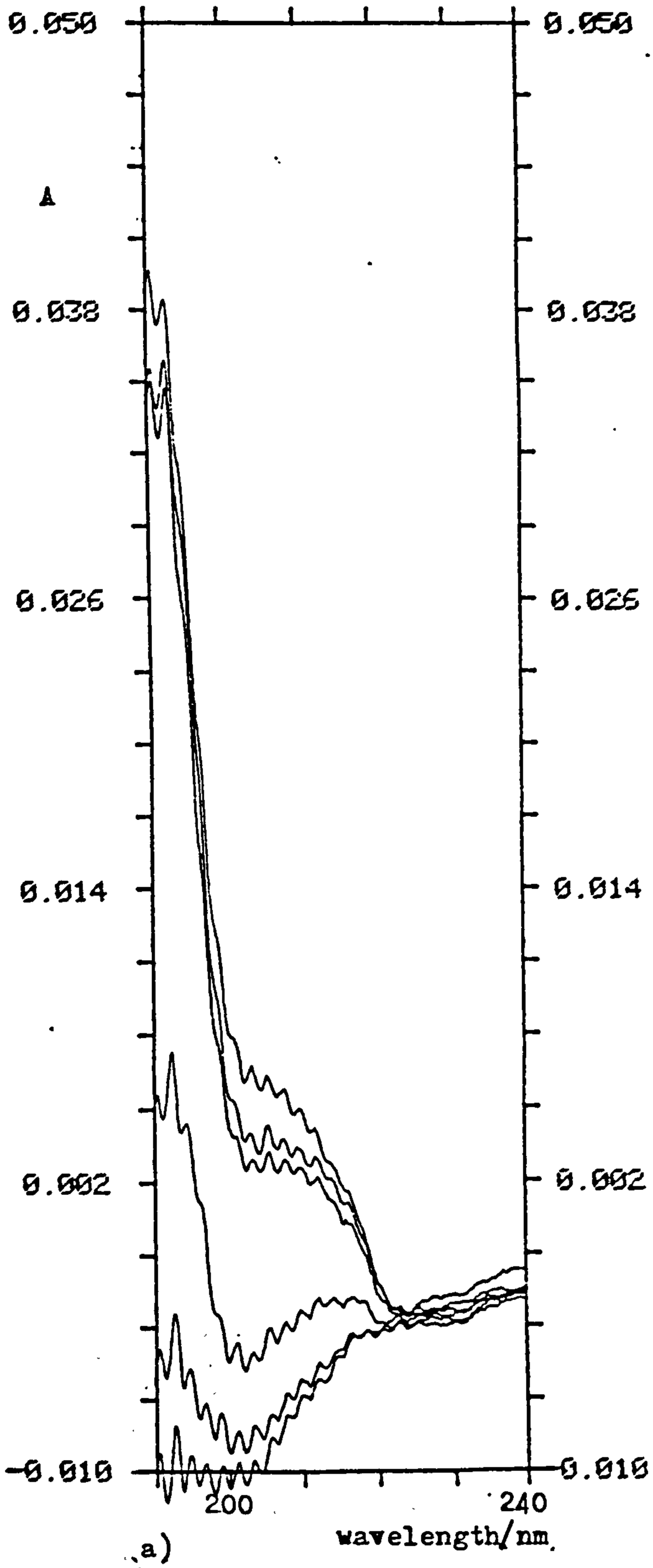

Figure 6.8.5 UV spectra of LMW3 PBzLG sample deposited as; a) a monolayer, b) a trilayer.

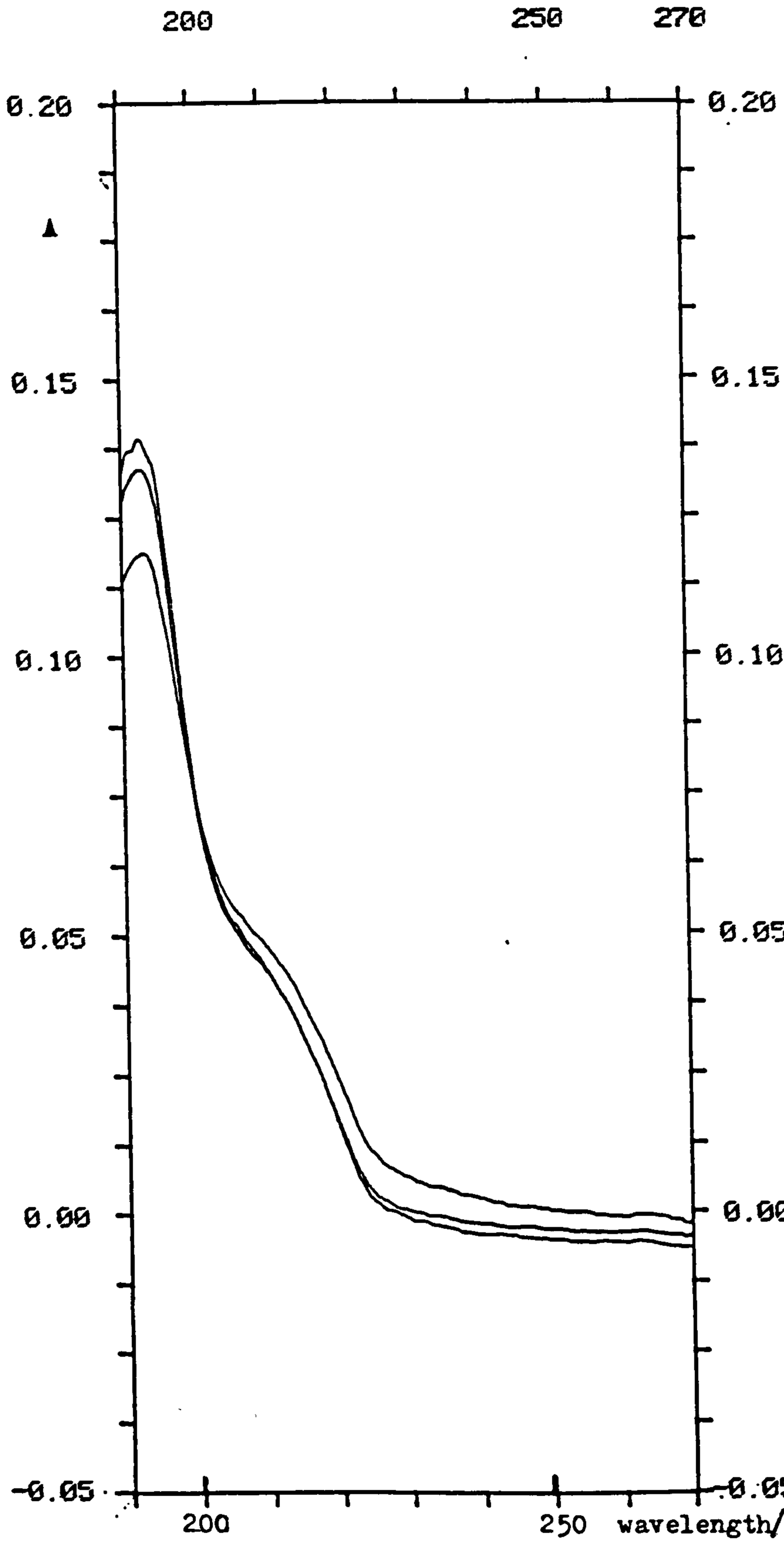

Figure 6.8.6 UV spectra of LMW3 PBzLG sample formed by deposition of ten layers.

ABSORBANCE vs No. OF LAYERS
LMW3 PBZLG

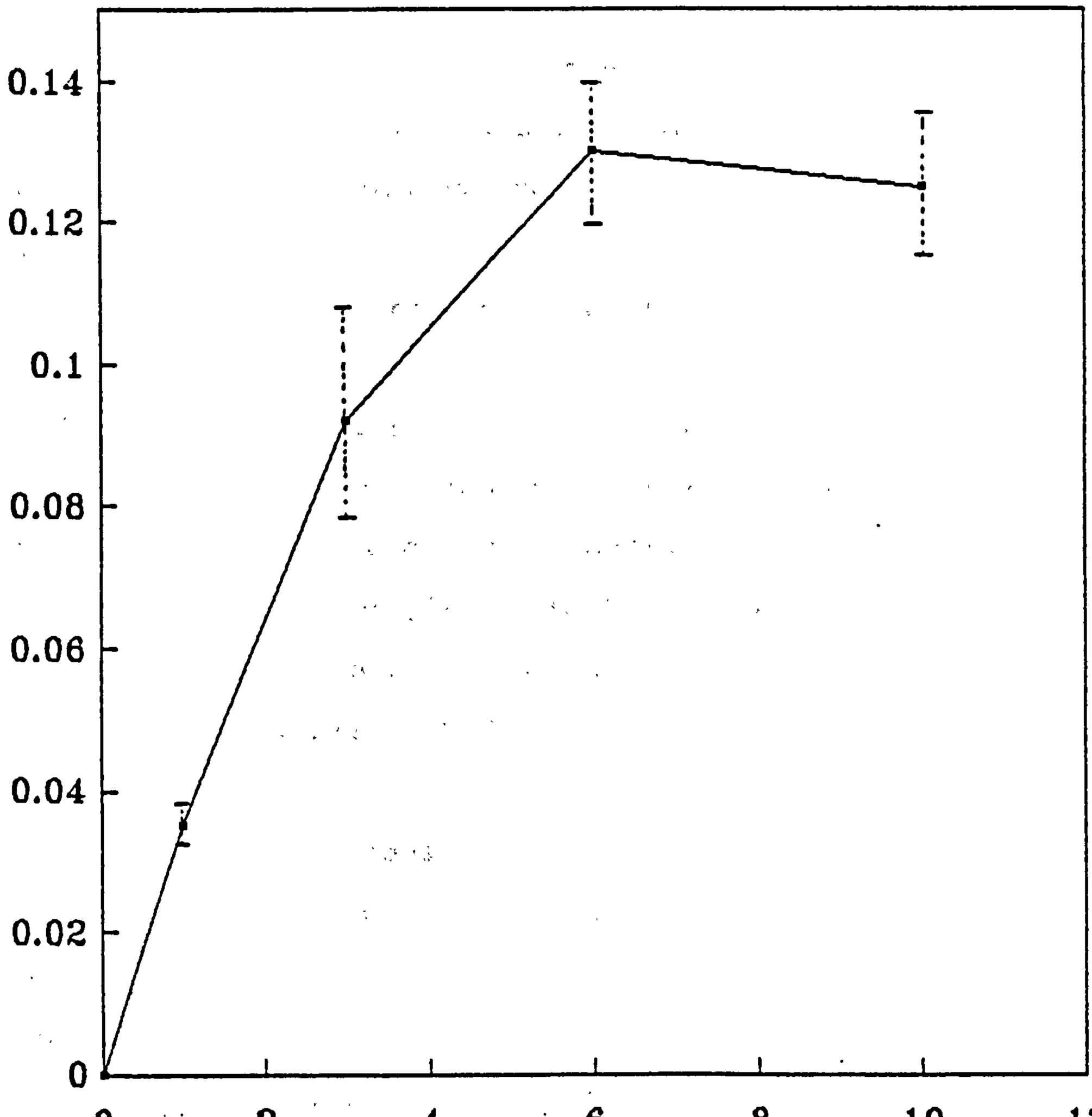

Figure 6.8.7 Plot of absorbance vs. number of deposited layers of LMW3 sample of PBzLG (at 195 nm).

region of the slide, less than 1 mm wide.

LMW samples:- in general, only the LMW samples gave reasonable even coverage of the quartz slide for the area of the slide that actually passed through the monolayer (approximately 3.5 cm wide), which lead to a characteristic absorbance of approximately 0.035 for a monolayer.

Although, isotherms for the LMW samples showed two rises, most dipping work was carried out at a pressure just below that of the plateau region, near the top of the 1st rise.

The substrate area given in table 6.8.c was only an estimate, and material may have deposited on other parts of the dipping mechanism, as well as the slide. Hence, transfer ratios can often be > 100%. However, the values given in table 6.8.c, are further proof that efficient transfer was taking place, as implied by the UV spectra. The flatter spectra shown on figures 6.8.5a-b represent the edges of the slide that did not pass through the Langmuir film.

Figure 6.8.7 shows the absorbance at 195 nm versus number of deposited layers which was obtained by depositing different multilayers of LMW3 sample, using the conditions shown in table 6.8.c.

For each point on the figure 6.8.7, a fresh quartz slide was used and the number of layers in question deposited. The absorbance value was then taken as the best reading obtained over the slide.

Of the limited dipping work carried out on the 2nd rise

of the LMW isotherms, a monolayer of LMW3 was deposited at a pressure of 11 mN/m (just above the plateau) using similar conditions to those previously used, and giving an absorbance value = 0.053 ± 0.003 at 195 nm.

6.8.6 L.B. Discussion

LMW samples:- comparing the LMW pressure-area isotherms given in figures 6.8.2-3, with those obtained from studies carried out by previous workers (section 5.4), reveals that the introduction of the hydrophilic head to the α-helical chain has not greatly effected the general shape of the isotherm. In particular, the two rises are present, separated by the plateau region.

Mention was made in section 5.4, of the observations of Shuler and Zisman (1972), who did not observe the second rise and that this was because they had allowed enough time for equilibrium to occur in the reordering of the Langmuir film during the later stages of compression. It is certain that the compression rate of 180 cm^2/min required to produce smooth isotherms in this work and which is a great deal quicker than that used for more conventional L.B. materials, would not have allowed such equilibrium to occur. The flow of the Langmuir film around the Wilhelmy plate was clearly too rapid to prevent it from being moved sideways with the flow. As far as this region of the isotherm is concerned, the Langmuir film is an irreversibly compressed film showing the viscoelastic nature characteristic of solid polymer.

The reversible nature of the isotherm in the region of the plateau and the 1st rise is worth discussion, particularly in a qualitative manner at first. The understanding of conformational state and orientation of PBzLG molecules throughout the compression process is obviously important to enable subsequent transference of the monolayers with a desired structure.

In the case of the fully expanded monolayer (i.e. below the first rise), the consensus of opinion either has the PBzLG molecules arranged as 2-D raft-like aggregates (Suzuki and Isemura (1967))) or isolated molecules. In practise, the very nature in which molecules are deposited on the surface (i.e. by syringe) is likely to produce a range of sized aggregates. In either case, it is reasonable to assume that the molecules are lying flat on the air-water interface in an α-helical conformation, although most evidence for the presence of α-helical conformation has been obtained from collapsed regions of the isotherm.

For the LMW samples in this work, the presence of the hydrophilic head may well bind one end of the molecule to the surface while the remainder of the molecule is able to lie flat on the surface.

This may have been possible because of the flexible nature of the additional two methylene groups (from the ethanolamine initiator) and the random coil nature of the end segments not incorporated into the α-helix. With such flexibility present, there is no reason to assume that the OH can overcome the forces that cause α-helical components

to lie on their side in the expanded regions of the isotherm.

Hypothetical Situation

In the ideal case of a good L.B. material, which is useful for SHG, compression of the monolayer results in a non-centrosymmetric structure. The most obvious way in which this occurs, is if the molecules are standing erect on the surface, although a tilted molecular structure would also be a non-centrosymmetric arrangement.

Note:- the term "non-centrosymmetric structure" refers to the part of the molecule that contributes to the SHG, and not necessarily the molecule as a whole. In the case of a molecule with a long hydrophobic chain, the hydrophobic chain may be perpendicular to the interface, but the polarised head may be lying flat on the surface. In the case where molecules lie flat on the surface there is a tendency for them to align antiparallel to one another, in a centrosymmetric structure.

The similarity between the isotherms of the LMW samples and those obtained by previous workers might suggest the conformations and molecular orientations during the 1st rise and the plateau region are the same in each case, regardless of the presence of the additional -OH group. The generally accepted reason for the first rise and the plateau region in previous studies has already been mentioned in section 5.4, as being caused by the close-packing of the α-helical molecules on the surface, followed by the formation of a bilayer/multilayer as molecules are

dislodged from the monolayer to alleviate the build up of pressure. In these mono-, bi- or multilayers, the α-helices are believed to be lying on their side.

Having added the hydrophilic -OH head to one end of the helix to try to induce them to stand up on compression, an alternative description might account for the isotherm, i.e. the 1st rise is still the result of closely packed helices lying on their side, whereas the pressure build-up within the monolayer is now alleviated by the molecules standing up (the cross-sectional area of the upright helix is smaller than when it is lying on its side).

In trying to take a quantitative approach for examining the isotherms, its useful to understand how the trough program calculates areas per molecule, because it can be shown that feeding the program "false" information can produce some useful results.

The program requires, the molecular weight of the PBzLG, the concentration of the depositing solution and the volume of the solution applied, to determine the number of molecules being deposited on the trough surface. The trough area is already calibrated in terms of barrier position.

For the classical L.B. material, the molecular weight is obviously well determined from the molecular structure. However, the polymer nature of the samples used in this work, immediately begs the question, what molecular weight should be used, particularly as no molecular weight determination was made on the LMW samples.

Consequently, analysis of the isotherms has been

undertaken using two molecular weights:-

i) a M.W. value calculated from the M/I ratio of the polymerisation and;

ii) a value of 219 which is the molecular weight of a single monomer residue.

In either case, a number of assumptions have been made to try and compare experimental values of areas per molecule with theoretical values:-

1) all polymer samples have a single molecular weight value, i.e. no M.W. distribution;

2) the presence of the hydrophilic head is ignored in area per molecule calculations;

3) all monomer residues are incorporated into a rigid α-helical configuration;

4) the α-helical configuration is simplified to a cylinder of cross-sectional radius = 1.473/2 (based on the average of the two interchain distances (1.519 and 1.426 nm) of a triclinic cell of PBzLG given by Block (1983)).

The length of the cylinder is dependent on the molecular weight of the molecules and can be estimated from, one spiral pitch = 0.54 nm, containing 3.6 residues (Block (1983)).

Using these values, the following estimated values ((a)-(d)) for the area per residue/or molecule, are those which should have been obtained by the trough program, if the molecules are behaving as described.

a) Area per residue for helix lying down

$$= \frac{1.473 \times 0.54}{3.6} = 0.221 \text{ nm}^2 \text{ or } 22.1 \text{ Å}^2.$$

This value is independent of molecular weight as long as the molecules are lying down.

b) Area per molecule for helix lying down

Assumed M.W.	Estimated area per molecule/ Å^2
2184	220
4331	437
6148	620

c) Area per molecule for helix standing up

= cross-sectional are of helix

= $(1.473/2)^2 \times \pi$

= 170 Å^2

This value should be independent of molecular weight, assuming the molecules are standing up, and the molecular weigh values used are correct.

d) Area per residue for helix standing up

Assumed M.W.	Area per residue/ Å^2
2184	17.0
4331	8.6
6148	6.1

The area per residue is easily calculated in this case as, helical cross-sectional area divided by the number of residues per molecular weight.

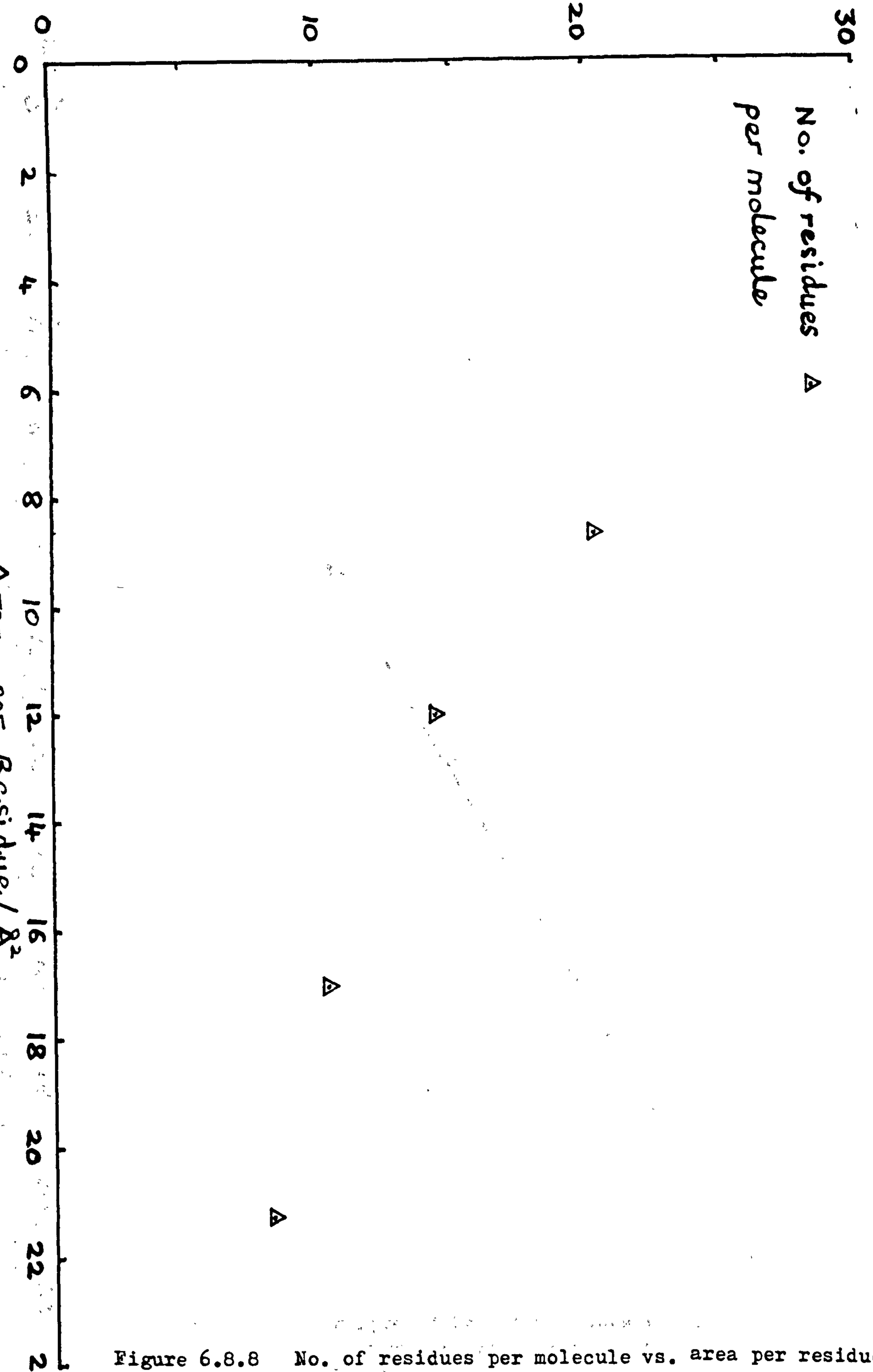

Figure 6.8.8 No. of residues per molecule vs. area per residue assuming upright helices.

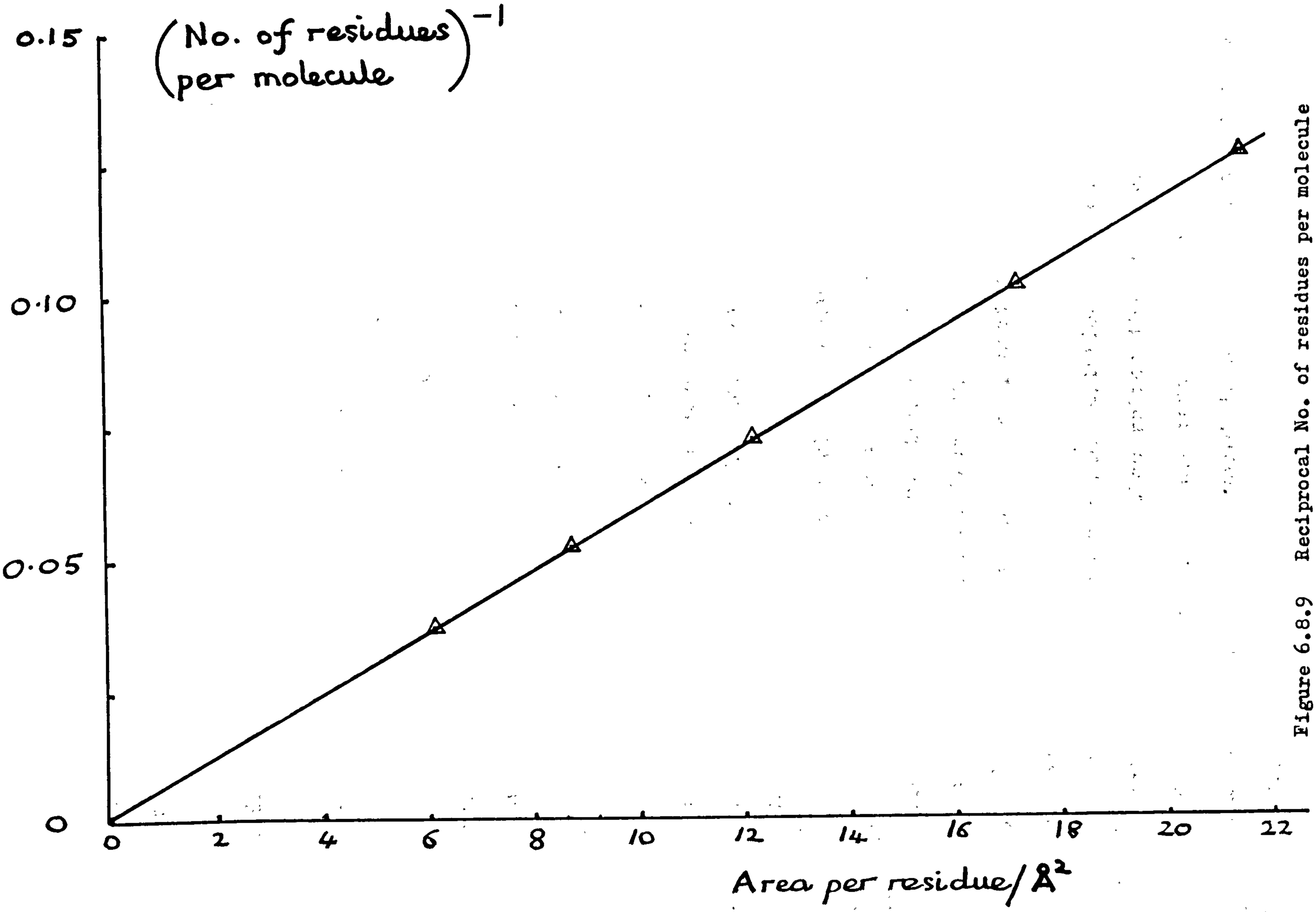

Figure 6.8.9 Reciprocal No. of residues per molecule vs. area per residue assuming upright helices.

In fact, figures 6.8.8-9 show that these calculated area per residue values are inversely proportional to the molecular weight (No. of residues per molecule).

Conclusions

The following are the possible conclusions based on values (a)-(d) and the experimental values obtained from figures 6.8.2-3 and given in table 6.8.b.

1) Figure 6.8.3 shows that the variation of area per residue throughout the isotherm is more or less identical for the three molecular weight samples. If the assumed molecular weight values are correct, this implies that the helices do not stand up (c.f. (d)).

This is also substantiated by figure 6.8.2, which should have shown identical area per molecule values for the three samples during the second rise at a value around 170 $Å^2$ (c.f. (c)).

Figures 6.8.2-3 do yield reasonable values if the molecules are assumed to be lying down throughout both rises of the isotherm. The deviation of the value 20 +/- 1 $Å^2$ per residue obtained from figure 6.8.3, from the value 22 $Å^2$ given in (a) can be accounted for by a number of reasons.

i) The spreading method from solution may result in some conglomeration of molecules rather than an even spread of individual molecules. On compression, this would not form a uniform monolayer, and would lead to a smaller area per residue.

ii) Any loss of material during compression would lower the measured value.

iii) The contribution of the hydrophilic head has not been accurately determined.

iv) The molecules might be slightly tilted, which would also reduce the measured area per residue.

Mention has been made in past work that the plateau region is possibly caused by molecules forming a bilayer. The value of 6 +/-0.5 $\AA^2$ per residue obtained for the second rise, suggests the plateau ends when a trilayer of packed helices, lying on their sides, has formed.

2) If the assumed molecular weights are not correct, the graphs (figures 6.8.8-9) may be used to determine possible molecular weights for which upright helices can be accounted for.

Assuming the helices are standing up at the 2nd rise of figure 6.8.3, a molecular weight of approximately 28 residues per molecule is associated with an area of area per residue of 6 $\AA^2$. The value of 20+/-1 $\AA^2$ which is obtained for the 1st rise could then be attributed to the molecules lying down for this part of the isotherm, which would then agree with the proposed hypothetical situation, described earlier.

(Note:- if helices are assumed to be standing up during the 1st rise, a molecular weight of 8.5 residues per molecule can be associated with the 20 $\AA^2$ per residue value, although explanation of the remainder of the isotherm then

becomes a problem).

Interestingly enough, the LMW4 sample had an intended molecular weight value of around 28 residues per molecule, and table 6.8.b, shows that this sample gives an area per molecule for the 2nd rise of 170 $Å^2$ in good agreement with (c), the cross-sectional area of the helix. When the other two samples LMW2 and LMW3 were assumed to have the same molecular weight value as LMW4 in the trough program, they too yielded a value around 170 $Å^2$ per molecule for the 2nd rise. In addition, figure 6.8.3 shows all three samples with a value of 6 $Å^2$ per residue for the 2nd rise which is in good agreement with that calculated in (d) for the molecular weight value of LMW4.

However, it is probably too much of a coincidence that the molecular weight chosen for the LMW4 sample should turnout to be the true value for the two other samples. It would imply that the intended distribution of molecular weights based on the [M]/[I] ratios for the three samples had not been successful and that identical polymer samples had been produced in each case.

Note:- the major stumbling block in trying to determine the orientation of the helices in the isotherm is that if they remain lying down, the trough program always generates the expected theoretical values for the area per molecule regardless of whether the correct molecular weight value has been used or not.

In summary, two possible explanations are available based on the experimental data.

1) The helices remain lying down throughout the compression with perhaps a slight tilt present in the molecules in the monolayer at the 1st rise. During the plateau region, the molecules are dislodged from the monolayer into a multilayer arrangement, until the area per molecule (or per residue) has reduced to one third that of the 1st rise (suggesting a trilayer formation). Formation of the trilayer is then a sufficiently rigid film to cause the pressure sensing device to move with further compression, which manifests itself as the second rise. However, it is still uncertain whether the molecular weight values expected from the [M]/[I] values are true molecular weights of the samples.

2) The helices stand up between the 1st and the 2nd rise in the plateau region, forming a monolayer which is also rigid enough to move the Wilhelmy plate. This is only true if the true molecular weight of all three samples is around 6132, (28 residues per molecule).

HMW Samples

Although the presence of the 1st rise is not so well pronounced in figure 6.8.4 for the HMW sample (c.f. LMW samples), the beginning of the gentle rise in pressure at about 23 $\AA^2$ per residues agrees well with the theoretical value of 22 $\AA^2$ already estimated for helices lying down, (i.e. (a)).

Two values of area per residue are given in table 6.8.3 for the second rise of the HMW sample because there appears to be a change in gradient (inflexion) in that area of the isotherm. The inflexion may be an artifact of the experiment, and if the steepest section is used (which yields a value of 7.5 $Å^2$), it is seen that the area of the 2nd rise is at about one third that of the 1st (i.e. trilayer formation), as suggested by the LMW sample results.

Figure 6.8.9 has already been used for LMW samples to try and determine possible orientations of the helices based on assumed molecular weight values of the samples. As far as the HMW sample is concerned, it is safe to assume that the molecular weight is well in excess of 100,000 (460 residues per molecule) based on the type of polymerisation undertaken, and the physical nature of the polymer obtained.

If the helices did stand up during the 2nd rise as is the case when figure 6.8.9 can be applied, then an area per residue of less than 0.4 $Å^2$ would be expected for a HMW sample with such a molecular weight.

Hence the value of 7.5 $Å^2$ observed, rules out this possibility of the helices standing up in the HMW case.

Reasons For L.B. deposition

Although the evidence for helices standing up erect on the surface was not proven from the pressure-area isotherms, the case for trying some L.B. deposition was

valid since detection of SHG from either a deposited monolayer or multilayer would add some credence to the idea.

Ideal L.B. work is usually carried out on steep, reversible pressure rises, which allows the compression mechanism of the trough to respond quickly to the subtle fluctuations in pressure detection of the Wilhelmy plate. This allows the deposition to occur at a constant pressure.

In view of the possible conclusions drawn from the pressure-area isotherms, the most likely place to find erect helices would appear to be towards the end of the plateau region or on the 2nd rise. In either case, the suitability for deposition work was poor, for their own particular reasons, which accounts for why very little L.B. work was carried out in these regions.

i) Although the 2nd rise was steep, it was not reversible and any pressure spikes would not be recovered by the compression mechanism of the trough.

ii) In the case of the plateau region, if the dipping pressure was set at the plateau pressure, the compression mechanism would not respond to any removal of material because there would be no apparent change in pressure.

The lst rise would appear to be the most likely place to find the helices lying on their sides, in a centrosymmetric arrangement. However, if there was any element of tilt of the molecules within the monolayer, then X- or Z-type multilayer deposition could still have generated a non-centrosymmetric structure, which may have

produced a detectable SHG signal.

Hence, the majority of L.B. deposition results given, were obtained from work carried out on the 1st rise of the LMW samples, as this offered the only viable region of the isotherm to work with.

Suitability for L.B. deposition

Figure 6.8.7 clearly demonstrates the poor multilayer forming capabilities of the LMW samples, beyond 3 or 4 layers. The loss of linearity beyond this number of layers is clearly evidence of either poor transference to the substrate or lack of adhesion to the substrate once deposited. (Note:- there was evidence of PBzLG being found on the surface of the blank side of the trough which the substrate always passed through on each deposition).

Conversely, the LMW samples were clearly good at forming even monolayers, as demonstrated by the UV spectral data.

This may be evidence of a short range effect of the treated substrate, which is able to break the interactive forces of the PBzLG molecules and the water molecules during the early depositions, but is then screened by the deposited molecules on its surface. At a certain point, an equilibrium may result between the molecules on the surface and the screening molecules on the substrate.

Interaction of PBzLG α-helical molecules at the air-water interface must involve a combination of side chain and main chain forces, which would suggest that the molecular weight (for helices lying on their side) of the

molecules might have a bearing on the ease of transference to a substrate. This .may account for the poor transference of HMW PBzLG, although the fact that the film was deposited on the 2nd rise when the Langmuir film was a compressed polymer skin may also be a contributing factor.

The problem of centrosymmetry for molecules lying on their side has been mentioned a number of times, and might explain why it is unfavourable for α-helical PBzLG molecules in particular to stand up. The driving force for the centrosymmetric structure between helical molecules lying down, is the antiparallel alignment of the dipole moments associated with neighbouring α-helices. In the specific case of the LMW samples, this antiparallel structure would be broken if the molecules stood up with their hydrophilic -OH heads attached to the surface.

Similarly, unlike a classical L.B. molecule which possesses a hydrophobic tail, a PBzLG molecule lying on its side involves hydrophilic interactions (side chain and main chain) with the air-water interface along its full length which would also need to be broken if it was to stand up.

The typical cross-sectional area of an alkyl chain on a classical L.B. molecule was earlier quoted as 22-25 $Å^2$. In comparison, the value of 170 $Å^2$ for the cross-sectional area of an α-helix may represent too large a structure to support or orientate, for the -OH hydrophilic head used in this work.

If these last two points are just considered together, one can see future work involving molecular design which

uses different hydrophilic heads and different ester side groups (with increased hydrophobic qualities).

6.9 General Conclusions

The findings of this thesis are best summarised by considering the following aspects:-

1) synthesis of the polyglutamates;

2) guest host polymer samples and PE;

3) solvent cast samples and SHG;

4) L.B. studies.

In general, poor yields of alkyl-L-glutamates prevented the synthesis of a range of polyglutamates, so only the γ-benzyl derivative (PBzLG) was prepared in significant quantities to allow its subsequent use in film/sample preparation. When considering the other synthetic routes that were attempted for the preparation of alkyl-L-glutamates, direct esterification (as used for γ-BzLG) proved to be the best method, but was still far too inefficient. In retrospect, the use of transesterification to produce PBuLG from PBzLG should have been attempted, as it may have produced at least one other polyglutamate for study, even if the method caused a reduction in molecular weight.

Poled samples prepared from the guest host polymer systems were generally poor. Allowing for phase separation which occurred when the PBzLG/vinyl monomer solutions were cured, unpoled samples were generally good and sample areas up to 12 cm^2 were possible. The inability to produce a range of poly(alkyl-L-glutamates) was the prime reason that limited the number of suitable vinyl monomer solvents available, particularly those that might have been less polar (than NVP) and more likely to withstand higher electric fields.

The lack of piezoelectric signal observed for the guest host polymer samples can be accounted for in two ways.

In the first instance, the samples may not have been poled. The high conductivity associated with NVP prevented a large field being applied. The subsequent use of a precure may have improved the quality of the films and the size of field that could be applied, but whether alignment of the helices was possible following it, is a major doubt. Similarly, if uneven polymerisation occurred across the samples as was thought, uneven poling would occur as well.

Secondly, the concentration of 10% w/w of the active polymer component may have been too dilute to produce detectable signals.

One possible improvement for this method would be to prepare the solutions inside the photopolymerisation cell. This would avoid the transference problem of the viscous polymer solutions to the cell, and would allow more concentrated solutions (if left long enough) to be prepared. The increased concentration would improve the chance of detecting PE in the cured samples, and may produce the high viscosity which may prevent phase separation.

In contrast, the use of the solvent casting method to produce samples improved the range of solvents available for PBzLG and PHIC, as it removed the necessity for a vinyl functionality. The resultant homopolymer samples showed no phase separation, and improved the chance of detecting SHG because they contained no diluting inactive polymer component.

Both PHIC and PBzLG showed detectable levels of SHG (PHIC > PBzLG), although neither is as active as some polymer systems which have been designed to have high molecular β values. Not too surprisingly, PHIC is fairly active because it is a polymeric urea (similar value to that of urea). The electron delocalisation in the urea residue of PHIC is not found in the peptide bond of PBzLG, and it would appear that the intramolecular hydrogen bonding in the α-helix does not provide any large nonlinear effect. Although a large β has been established for a PBzLG molecule (Levine and Bethea (1976)), the value per monomer residue (which is not large) must be considered as far as bulk SHG properties are concerned.

PHIC appeared to be the best system for producing the most even alignment, mainly because of the stirring effects which plagued solutions of PBzLG under field and which were incorporated into the films on evaporation. Taking into consideration these effects coupled with the biaxial suprastructure within the poled PBzLG films, inevitably light scattering will be a problem.

The problem of uneven evaporation/poling was the major factor that led to the nonuniform alignment and for future work, a spin coating/poling technique may prove to be one way forward. However, this will certainly require the use of more active materials (such as high β dopants), to ensure detectable signals are produced. In addition, the rate of evaporation will have to be controlled to allow alignment times of possibly 30 minutes to enable complete uniaxial,

nematic order to form.

The most impressive aspect of this work has been the retention with time of the SHG activity of both the polymer systems. This might overcome the problem of relaxation of aligned dipoles in thermally poled systems. The stability of the aligned system may also be beneficial to the alignment of high β additives which may or may not be attached to the polymer chains, and which may improve the level of SHG activity and other nonlinear effects. Possibly, further work using MNBA which maintained a solid solution within PBzLG, may be useful.

The inability to measure the molecular weights of the LMW samples of PBzLG prepared for the L.B. studies, meant that areas per molecule (or per residue) calculated from the pressure-area isotherms proved inconclusive when deducing possible orientations for the PBzLG helices. The samples showed poor transference beyond ten layers, so even if a non-centrosymmetric structure had been achieved by the L.B. technique, the SHG signal would have been too weak to detect.

Certainly in further work, the use of different hydrophilic heads (or even hydrophobic tails) coupled with fractionated samples of known molecular weight, would help in understanding the molecular orientation within Langmuir or L.B. films of PBzLG. However, in view of its low SHG activity, L.B. deposition work may prove impractical without the use of high β additives.

REFERENCES

AHARONI, S.M — Macromol. 12, 94, (1979).

AHARONI, S.M — J. Polym. Sci. Polym. Phys. Ed. 18, 1439, (1980a).

AHARONI, S.M — J. Polym. Sci. Polym. Phys. Ed. 18, 1303, (1980b).

AHARONI, S.M — Polymer 21, 21, (1980c).

ALLEN, S MORLEY PUGH DOCHERTY — Molecular and Polymeric Optoelectronic Materials Fundamentals and Applications Proc. SPIE 20, 682, (1986).

ALQUIE, C LEWINER — J. Revue. Phys. Appl. 20, 395, (1985).

ATKINS, P.W — Physical Chemistry, Oxford Uni. Press, (1982).

AZOZ, N CALVERT KADIM ET. AL. — Nature 344, 49, (1990).

BAMFORD, C.H BLOCK — Polyamino Acids, Polypeptides, and Proteins,(Univ. of Winconsin Press, Madison, p65, (1962).

BAMFORD, C.H BLOCK — High Polymers Vol. 26, John Wiley p687,(1972).

BAMFORD, C.H BLOCK — The Polymerisation of N-Carboxy-α-Amino Acids, Chapter 8, Comprehensive Chemical Kinetics Vol. 15, Elsevier, p583,(1976).

BETHEA, C.G — Applied Optics, 14(5), 1447, (1975).

BIRDI FASMAN — J. Polym. Sci. A1, 10, 2485, (1972).

BLOCK, H HAYES NORTH — Trans Faraday Soc. 66, 1095, (1970).

BLOCK, H — Poly(γ-Benzyl-L-glutamate) and Other Glutamic Acid Containing Polymers, ISBN 0677-05680-X, 1983 London.

BLODGETT, K.B — J. Am. Chem. Soc. 57, 1007, (1935).

BROADHURST, M.G
MALMBERG
MOPSIK
HARRIS
"Electrets, Charge Storage and Transport in Dielectrics" The Electrochemical Soc. Princetown p492, (1973).

BROUSSOUX, D
CHASTAING
ESSELIN
Le BARNEY
ET. AL
Revue Tech. Thomson-C.S.F Vol. 20-21, 151, (1989).

BRUCKNER, V
KOVACS
KOVACS
J. Chem. Soc. 15, 12, (1953).

BUCHARDS, W
Macromol. Chem. 67, 182, (1963).

BUI, L.N
SHAW
ZITELLI
IEEE Trans Sonics Ultrasonics SU-24, 331, (1971).

BUR, A.J
ROBERTS
J. Chem. Phys. 51, 406, (1969).

BUR, A.J
FETTERS
Chem. Rev. 76(6), 727, (1976).

BUR, A.J
FETTERS
Macromol. 6, 874, (1973).

CABANI, S
PACI
RIZZO
Biopolymers 15, 113, (1976).

CASPERS, J
BERLINER
RUYSSCHAERT
JAFFE
J. Coll. Interface Sci. 49(3), 433, (1974).

CURTIUS, T
J. prackt. Chem., 125, 152, (1930).

DALY, H
POCHE
Tetrahedron Lett. 29(46),5859, (1988).

DENCE, J.B
Mathmatical Techniques in Chemistry, Wiley, N.Y, p916, (1975).

DOTY, P
BRADBURY
HOLTZER
J. Am. Chem. Soc. 78,947, (1956).

DUDA, G
SCHOUTEN
ARNDT
LIESER
SCHMIDT
BUBECK
WEGNER
Thin Solid Films 159, 221, (1988).

DUKE, R.W
DUPRE
Macromol. 7(3), 374, (1974).

ELLIOT, A
AMBROSE
Farad. Soc. Disc. 9, 24, (1950).

ESSELIN, S
BARNEY
ROBIN
BROUSSOUX
DUBOIS
RAFFY
Spie. Proc. 971, 120, (1988).

FLORY, P.J
J. Polym. Sci. 49, 105, (1961).

FUCHS, F
Ber., 55, 2943,(1922).

FUJITA, H
TERAMOTO
OKITA
YAMASHITA
IKEDA
Biopolymers 4, 769, (1966).

FUKADA, E
J. Phys. Soc. Japan 10, 149, (1955).

FUKADA, E
YASUDA
J. Phys. Soc. Japan 12,1158, (1957).

FUKADA, E
Wood Sci. Technol 2, 299, (1968).

FUKADA, E
DATE
HARA
Japan. J. App. Phys. 8, 151,(1969).

FUKADA, E
TAKASHITA
Japan J. App. Phys. 10, 722, (1971a).

FUKADA, E
Progress in Polym. Sci.
2, 329, (1971b).

FUKADA, E
Advan. in Biophys. 6, 121, (1974).

FRANKLIN; B
Phil. Trans. R. Soc. 64, 445, (1774).

GABRIELLI, G
PUGGELLI
Adv. Chem. Ser. 144, 347, (1975).

GERBER, J ELIAS	Makromol. Chem. 112, 142, (1968).
GIORDMAINE, J.A	Phys. Rev. Letts. 8, 19, (1962).
GO, Y EJIRI FUKADA	Biochim. Biophys. Acta 175, 454, (1969).
HECQ, W BRASSEUR	Biopolymers 15, 1425, (1976).
CASPERS LOFFET	
VAN HEESWIJK, W.A.R EENINK FEIJEN	Synthesis p744, September (1982).
HEILMER, G.H OCKMAN BRAUNSTEIN KRAMER	Appl. Phys. Lett. 5, 229, (1964).
HILL, D.J.T CARDINAUX SCHERAGA	Biopolymers 16, 2447-67, (1977).
HOBDEN, M.V	J. App. Phys. 38(11), 4365, (1967).
HON, D	Laser Handbook ISBN 0-444-85271-9, p421-484 (1979).
IIZUKA, E	Biochim. Biophys. Acta. 175, 457, (1969).
IIZUKA, E	Biochim. Biophys. Acta. 243, 1, (1971).
IKEDA, S ISEMURA	Bull Chem. Soc. Japan 34(3),416, (1961).
ISEMURA, T HAMAGUCHI	Bull Chem. Soc. Japan, 27,125,(1954).
KATZ, H.E DIRK SCHILLING SINGER SOHN	Mater. Res. Soc. Symp. Proc. Vol. 109 Non Linear Optical Properties of Polymers, 127, Mater. Res. Soc. Pittsburgh, U.S, (1988).
KEPLER, R.G	Ann. Rev. Phys. Chem. 29, 497, (1978a).

KEPLER, R.G ANDERSON	J. App. Phys. 49(8),4490, (1978b).
KEPLER, R.G ANDERSON	CRC Crit. Rev. Solid State Mater. Sci. 9, Part 4, 399, (1980).
KIP, A.F	Fundamentals of Electricity and Magnetism, 1st. Student Ed., McGraw-Hill Kogakusha Ltd. 2nd Ed. (1969).
KOTAI, A	Acta. Chimica Acad. Sci. Hung. 54(1), 65, (1967).
KUJIJAMA, T TANAKA KUROISKI TAKAYANAGI	Chem. Lett. 11,59,(1973).
KURTZ, S.K PERRY	J. Appl. Phys. 19(8), 3798, (1968).
LANGMUIR, I	J. Am. Chem. Soc. 39, 1848, (1917).
LESLIE, T.M De MARTINO CHOE ET. AL	Mol. Cryst. Liq. Cryst. 153, 451, (1987).
LEUCHS, H	Ber., 39, 857,(1906).
LEVINE, B.F BETHEA	J. Chem. Phys. 63(6), 2666, (1975).
LEVINE, B.F BETHEA	J. Chem. Phys. 65(5), 1989, (1976).
LOCKHEAD, R.Y NORTH	J. Chem. Soc. Farad. Trans. 68(2), 1089, (1972).
LOEB, G.I	J. Coll. and Interface Sci. 26, 236, (1968a).
LOEB, G.I BAIER	J. Coll. and Interface Sci. 27, 39, (1968b).
MAKER, P.D TERHUNE NISENHOFF SAVAGE	Phys. Rev. Letts. 8, 21, (1962).
MALCOLM, B.R	Proc. Roy. Soc. London Ser. A 305, 363, (1968).

MALCOLM, B.R	J. Polym. Sci. C, 34, 87, (1971).
MALCOLM, B.R	Adv. Chem. Ser. 145, 338, (1975).
MARUTAKE, M	Bull. Kobayashi Inst. Phys. Res. 8, 239, (1958).
MEREDITH, G.R VAN DUSSEN WILLIAMS	Macromol. 15, 1385, (1982).
MINAMI, N AIKAWA SUKIGARA	Mol. Cryst. Liq. Cryst. 41(Letts.), 189, (1978).
MOORE, R.J	Honours Thesis, Liverpool Uni. (1985).
MURTHY, N.S SAMULSKI KNOX	Macromol. 19(3), 941, (1986).
NEMETHY, G SCHERAGA	Biopolymers 3,155,(1965).
NICOUD, J.F TWIEG	Non Linear Optical Properties of Organic Materials and Crystals. Vol. 2, Acad. Press, N.Y (1987).
NIX, E.L	Ferroelectrics 67, 125, (1986).
NYE, J.F	Physical Properties of Crystals: Their Representation By Tensors and Matrices. Oxford Uni. Press, New York, (1957).
OHIGASHI, H	J. App. Phys. 47, 949, (1976).
OOKUBO, N KOMATSUBARA NAKAJIMA WADA	Bioploymers 15, 929, (1976).
OUDAR, J.L	J. Chem. Phys. 67(2), 446, (1977).
PAULING, L COREY	Proc. Nat. Acad. Sci. U.S 37, 235, (1951).
PEGGION, E	Biopolymers 4, 695, (1966).
POCKELS, A	Nature 43, 437, (1891).

POWERS, J.C	Liquid Crystals and Ordered Fluids, Proc. Am. Chem. Soc. Symp. 2nd. 365, (1970).
PUGH, D MORLEY	Non Linear Optical Properties of Organic Molecules and Crystals. Vol. 1, 193, Acad. Press, N.Y, (1987).
RAYLEIGH, Lord	Proc. Soc. 47, 364, (1890).
RENTZEPIS, P.M PAO	App. Phys. Lett. 5, 156, (1964).
ROBINSON, C	Trans. Farad. Soc. 52, 571, (1956).
ROBINSON, C WARD BEEVERS	Disc. Farad. Soc. 25, 29, (1958).
ROBINSON, C	Tetrahedron 13, 219, (1961).
ROHRER, P ELIAS	Makromol. Chem., 151, 281, (1972).
SAMULSKI, T TOBOLSKY	Macromol. 1(6), 555, (1968).
SAMULSKI, T TOBOLSKY	Biopolymers 10, 1013, (1971).
SAMULSKI, T TOBOLSKI	Liq. Cryst. and Plastic Cryst. Ellis Harwood Pub. Co. 1, 175, (1974).
SCHERAGA, H.A SCOTT VANDERKOOI LEACH GIBSON OOI NEMETHY	Conformation of Biopolymers Vol. 1 Acad. Press(New York) p43, 1967.
SCHMUELI, U TRAUB ROSENHECK	J. Polym. Sci. A-2, 7, 515,(1969)
SELINA, W	M.Sc. Thesis, Cranfield Inst. of Technology, (1986).
SHASHOUA, V.E SWEENEY TIETZ	The Homopolymerisation of Monoisocyanates. J. Am. Chem. Soc. 82, 866, (1960).

SHULER, R.L
ZISMAN
Macromol. 5, 487, (1972).

SHUBNIKOV, A.V
Piezoelectric Textures, Izd-vo An SSSR (1946).

SMITH J.C
WOODY
Biopolymers 12, 2657, (1973).

SUGAI, S
KAMASHIMA
MAKINO
NOGUCHI
J. Polym. Sci. A-2, 4, 183,(1966).

SUZUKI, A
ISEMURA
Ann. Rep. Biol. Works Fac. Sci., Osaka, Uni., 15, 75, (1967).

TANAKA, H
ENDO
OKAWARA
Nippon Kagaku Kaishi 1770, (1973). [CA 80, 15398m]

TOTH, W.J
TOBOLSKY
Polym. Letts. 8, 537, (1970).

TREDGOLD, R.H
ALI-ADIB
J. Phys. D Applied Physics, 21, 1467, (1988).

TROXELL, T.C
SCHERAGA
Macromol. 4, 528 (1971).

TSUTSUI, T
TANAKA
J. Polym. Sci. Polym. Letts. Ed. 18, 17, (1980a).

TSUTSUI, T
TANAKA
Polymer 21, 1351, (1980b).

TSUTSUI, T
TANAKA
Polymer 21, 1351, (1980c).

UEMATSU, Y
UEMATSU
ACS Symp. Ser. 74, 136 (1978).

VANWART, H.E
TAYLOR
SCHERAGA
Macromol. 6, 266-73, (1973).

VITOVSKAYA M.G
TSVETKOV
Eur. Polym. J., 12, 251,(1976).

WADA, A
J. Chem. Phys. 30, 328, (1959).

WADA, A
Polyamino Acids, Polypeptides and Proteins Pub. Uni. of Winconsin Press. p131-146, (1962).

WARREN, T.C
SCHRAG
FERRY
Biopolymers 12, 1905, (1973).

WILKES, G
Polym. Letts. Ed. 10, 935, (1972a).

WILKES, G
Mol. Cryst. Liq. Cryst. 18, 165, (1972b).

WILKES, G
BAN
Polym. Sci. Technol. 1, 39, (1973).

WILLIAMS, R
J. Chem. Phys. 39, 384, (1963).

WILLIAMS, F.D
ESHAQUE
BROWN
Biopolymers 10, 753, (1971).

WILLIAMS, D.J
Angew Chem. Int. Ed. Eng. 23, 690-703, (1984).

YAMASHITA, T
YAMASHITA
Bull Chem. Soc. Japan 43, 3969, (1970).

ZIMM, B.H
BRAGG
J. Chem. Phys. 31, 526, (1959).

ZYSS, J
J. Molecular Electronics 1, 25-45, (1985).

ZYSS, J
CHEMLA
Non Linear Optical Properties of Organic Molecules and Crystals. Vol. 1, 23, Acad. Press N.Y, (1987).

Appendix 1

Piezoelectric Notation

The stress within a solid is specified by the second rank tensor σ_{ij} , where i and j equal 1, 2 or 3. The measuring of σ_{ij} is easily understood if the coordinate system is assumed to be centred in a volume element in the form of a cube which has edges of unit length parallel to the coordinate axes. The component of the force exerted on the face of the cube is specified by the second subscript j while the first subscript i, determines whether this component is a tensile or a shear stress.

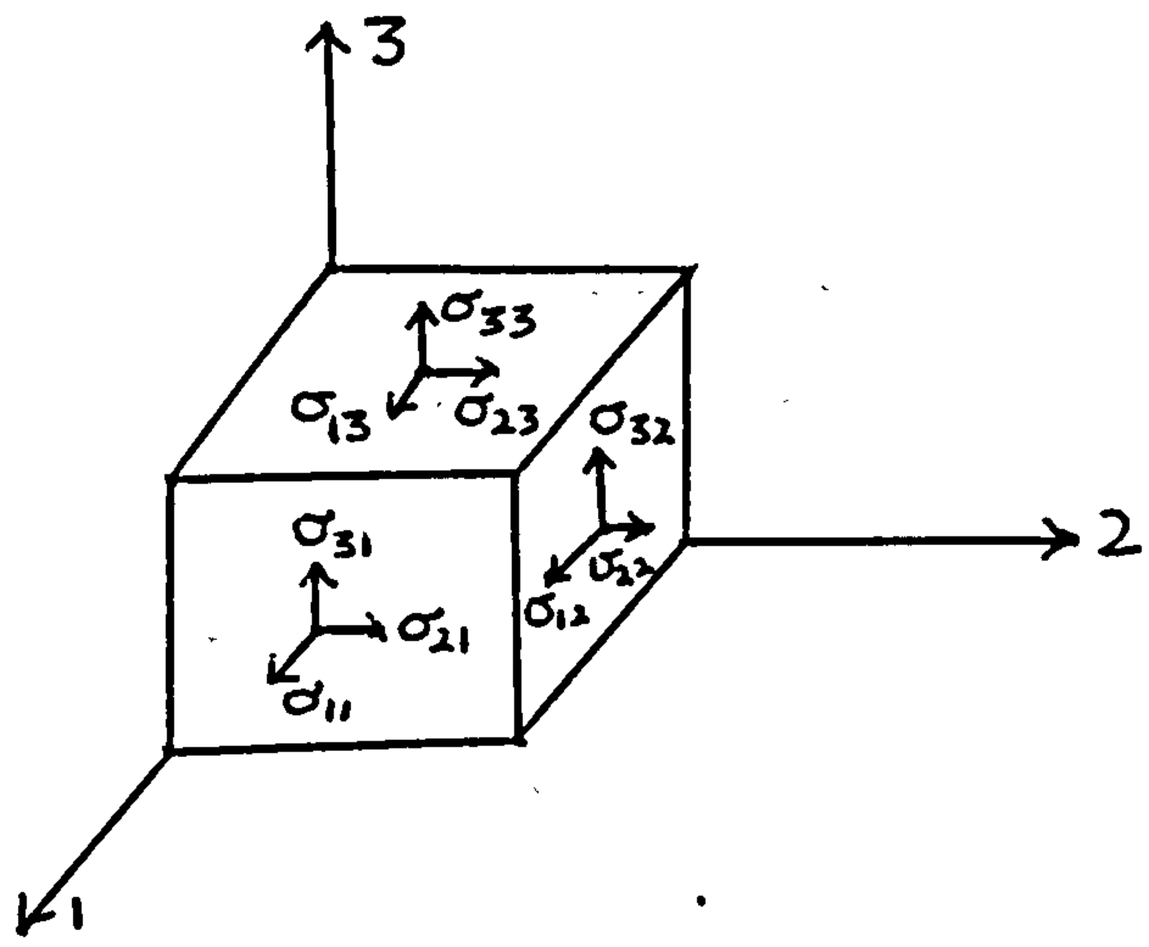

Figure app. 1, shows that σ_{11} , σ_{22} and σ_{33} are the tensile stresses, where as if $i \neq j$, σ_{ij} are said to be shear components.

In the absence of body torques, $\sigma_{ij} = \sigma_{ji}$. Symmetry of the stress tensor about the diagonal allows for a more compact description, by using the matrix notation where a single subscript replaces two.

11 = 1 23 = 4

22 = 2 31 = 5 and $\begin{vmatrix} \sigma_1 & \sigma_6 & \sigma_5 \\ \sigma_6 & \sigma_2 & \sigma_4 \\ \sigma_5 & \sigma_4 & \sigma_3 \end{vmatrix}$

33 = 3 12 = 6

The Direct Piezoelectric Effect

The direct piezoelectric effect is a linear relationship between the induced polarisation and the applied stress, as in equation 3.i, when the electric field and the temperature are held constant. Each of the 3 components of polarisation is related to each of the 9 stress components and the resultant coefficients d form a third rank tensor having 27 components.

Equation 3.i becomes:-

$$\Delta P_i = d_{ijk}\,\sigma_{jk} \qquad (B)$$

where the repeated subscripts imply the right hand side is a summation of terms. d_{ijk} are called the piezoelectric strain coefficients.

It is also possible to relate ΔP to strain, in which case the coefficients e_{ijk}, are called the piezoelectric strain coefficients.

A more compact notation now follows because of the symmetry of σ_{ij}. On expansion of equation B, terms arising from shear stress are written in pairs, i.e.

$$d_{312}\sigma_{12} + d_{321}\sigma_{21} = (d_{312} + d_{321})\sigma_{12} \qquad (c)$$

If d_{ijk} is set equal to d_{ikj}, then matrix notation results in,

$$\Delta P_i = d_{im}\,\sigma_m \qquad (D)$$

where m = 1 to 6

For m = 1 to 3, $d_{im} = d_{ijk}$

For m = 4 to 6, $d_{im} = 2d_{ijk}$

Hence, 18 coefficients provide a complete description of the linear relationship between polarisation and stress, although crystal symmetry may reduce the number of independent coefficients.

Converse Piezoelectric Effect

In this effect, a deformation of a sample is observed when an electric field is applied to it, i.e. the converse of the direct effect. In this case, the piezoelectric coefficients d^c_{im} describe a linear relationship between strain and the electric field, i.e.

$$\epsilon_m = d^c_{im} E_i$$

where ϵ = strain E = applied electric field

m = 1 to 6

Appendix 2

Langmuir Blodgett Pressure Measurement

The Whilhelmy Plate

The Whilhelmy plate is a strip of filter paper which is dipped into the air-water interface. As a result, it is pulled down by the surface tension, and the force acting on it is measured by means of an electronic balance.

If figure app. 2, shows the dimensions of the filter paper, the net force F acting down on the filter paper is

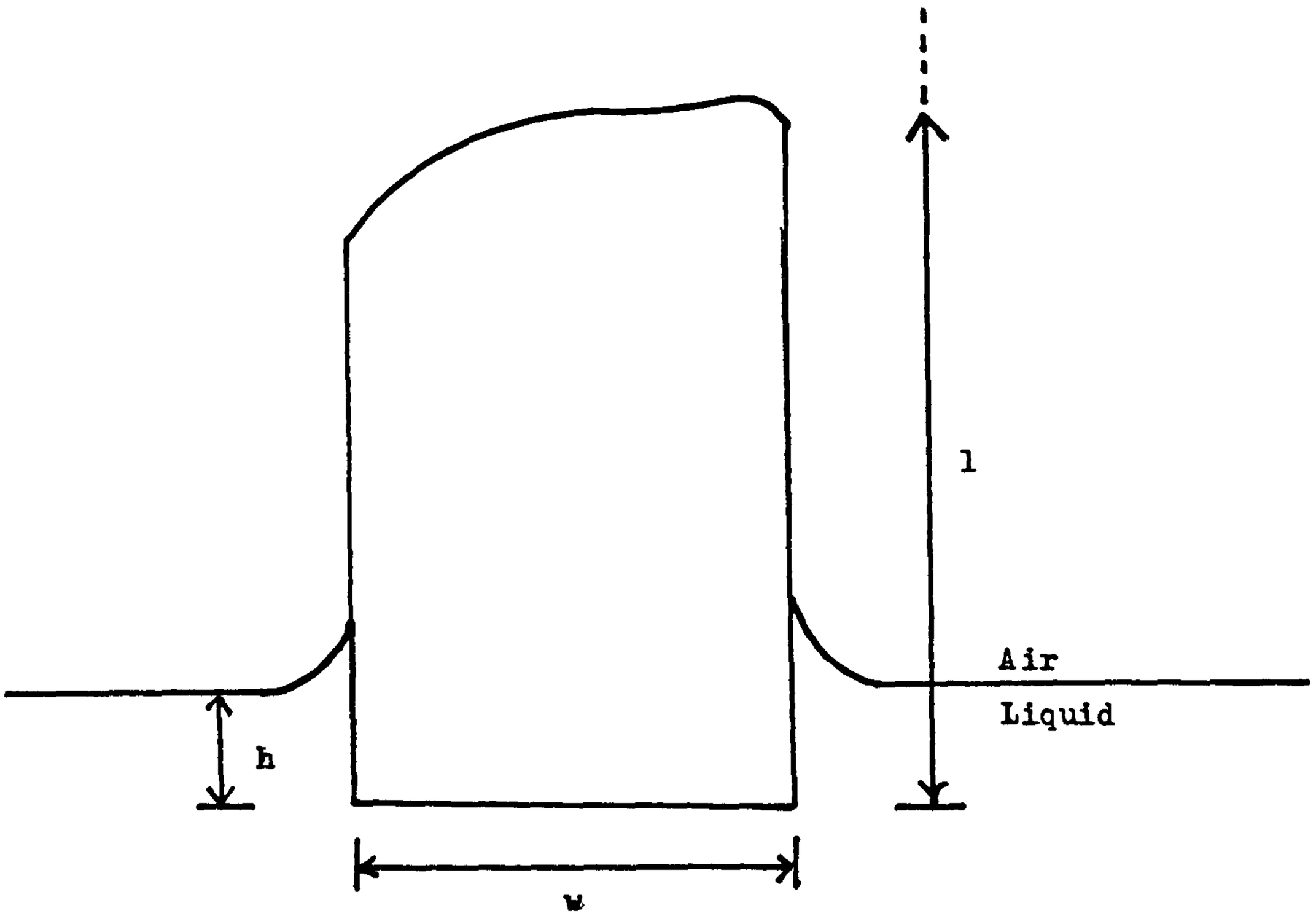

Figure App.2 The Wilhelmy Plate.

given by,

F = gravity - (buoyancy due to displaced water)

+ surface tension

$= \rho glwt - \rho' ghwt + 2\gamma(t+w)\cos\theta$

where ρ, ρ' = density of plate and subphase,

t = plate thickness,

g = acceleration due to gravity,

γ = surface tension of surfactant covered subphase,

θ = contact angle (0 for wetted filter paper).

Therefore, the difference in downward force ΔF, between pure water and the monolayer covered water is:-

$$\Delta F = 2(\gamma' - \gamma)(t+w)$$

where γ' = surface tension of pure water (72.8 mN/m).

For w = 1 cm and a negligible thickness,

$$\Delta F = 2\Delta\gamma$$

Since $\Delta\gamma = \pi$ (Surface pressure definition)

$$\Delta F = 2\pi$$

with units 1 dyne/cm or 1 mN/m.